

# Deconfined Quantum Critical Behavior of Dirac Materials

Inaugural-Dissertation  
zur Erlangung des Doktorgrades  
der Mathematisch-Naturwissenschaftlichen Fakultät  
der Universität zu Köln

*vorgelegt von*

Bernhard Maurice Daniel Rolf Ihrig

*aus*

Wickede (Ruhr)



Köln, 2021

Berichtersteller

PD. Dr. Michael Scherer  
Prof. Dr. Simon Trebst

Tag der mündlichen Prüfung: 26.04.2021

# Abstract

This thesis investigates the quantum field theoretical description of Dirac system at (deconfined) quantum critical points ([D]QCP). Using the perturbative renormalization group (RG) in higher loop orders, the critical behavior is quantitatively analyzed. In the first project, a detailed resummation of the four loop RG of the Gross-Neveu-Yukawa model is laid out for this matter. While the Landau-Ginzburg-Wilson paradigm used for this purpose proves to be very successful, exotic phase transitions beyond are treated in the remaining parts of this work. The studied quantum phase transitions describe an unexpected order-to-order transition and unveil a web of novel dualities between different theories. The second project examines the critical theory of a DQCP to the fourth loop order to address the question of transition's nature. The third project checks one of the new dualities for a system of gauged Dirac fermions. In the fourth and final project, the critical theory of a DQCP composed by fractionalized degrees of freedom is analyzed quantitatively using a series of complementary RG methods.

# Kurzzusammenfassung

Diese Arbeit beschäftigt sich mit der quantenfeldtheoretischen Beschreibung von Dirac System an (dekonfinierten) quantenkritischen Punkten ([D]QCP). Mit Hilfe der perturbativen Renormierungsgruppe (RG) in hohen Schleifenordnungen wird das kritischen Verhalten quantitativ analysiert. Im ersten Projekt wird dazu eine ausführliche Resummierung der vier Loop RG des Gross-Neveu-Yukawa Modells ausgelegt. Während sich das dafür genutzte Landau-Ginzburg-Wilson Paradigma als sehr erfolgreich beweist, werden im weiteren Teil der Arbeit exotische Phasenübergänge jenseits davon behandelt. Die untersuchten Quantenphasenübergänge beschreiben einen unerwarteten Ordnung-zu-Ordnung Übergang und eröffnen ein Netz neuartiger Dualitäten zwischen verschiedenen Theorien. Im zweiten Projekt wird die kritische Theorie eines DQCP zur vierten Schleifenordnung untersucht um auf der Frage nach der Art des Übergangs auf den Grund zu gehen. Das dritte Projekt überprüft eine der neuen Dualitäten für ein System von geeichten Dirac Fermionen. Im vierten und letzten Projekt wird die kritische Theorien eines DQCP aus fraktionalisierten Freiheitsgraden mit einer reihe komplementärer RG Methoden quantitativ untersucht.

# Contents

<b>Contents</b>	<b>iv</b>
<b>1 Introduction</b>	<b>1</b>
<b>2 Critical phenomena from the renormalization group perspective</b>	<b>5</b>
2.1 Quantum field theories in condensed matter . . . . .	5
2.2 Fundamentals of critical phenomena . . . . .	6
2.3 Concepts of the renormalization group . . . . .	10
2.3.1 General idea . . . . .	10
2.3.2 Perturbative renormalization group . . . . .	11
2.3.3 Functional renormalization group . . . . .	15
2.4 Criticality in the renormalization group . . . . .	18
2.4.1 Fixed points in the renormalization group flow . . . . .	18
2.4.2 Brief review of its success . . . . .	20
<b>3 Gross-Neveu universality in graphene and beyond</b>	<b>23</b>
3.1 Dirac fermions in graphene . . . . .	24
3.2 Effective field theory from interactions . . . . .	26
3.3 The Gross-Neveu-Yukawa model . . . . .	28
3.4 Perturbative renormalization group analysis . . . . .	29
3.4.1 Renormalization group functions . . . . .	30
3.4.2 Fixed points and critical exponents . . . . .	31
3.5 Resummation towards $d = 3$ . . . . .	32
3.5.1 Padé approximants . . . . .	32
3.5.2 Interpolations . . . . .	34
3.5.3 Borel resummation . . . . .	38
3.6 Discussion . . . . .	42
3.6.1 Graphene case ( $N = 8$ ) . . . . .	42
3.6.2 Spinless fermions on the honeycomb ( $N = 4$ ) . . . . .	43
3.6.3 Emergent supersymmetry ( $N = 1$ ) . . . . .	44
3.6.4 Other cases ( $N = 2$ and $N = 20$ ) . . . . .	45
3.7 Conclusion and Outlook . . . . .	46
<b>4 Concepts of deconfined quantum criticality</b>	<b>49</b>
4.1 Beyond the Landau-Ginzburg paradigm . . . . .	49
4.1.1 Spins on a square lattice . . . . .	50
4.1.2 Numerical findings . . . . .	51
4.2 Deconfined quantum criticality . . . . .	52
4.2.1 From Néel to VBS – and back . . . . .	52
4.2.2 Critical theory of the DQCP . . . . .	55
4.3 Conjectured web of dualities from DQCPs . . . . .	56

<b>5</b>	<b>Fixed point collision in the abelian Higgs model</b>	<b>59</b>
5.1	Motivation . . . . .	59
5.2	The abelian Higgs model . . . . .	61
5.3	Renormalization group analysis . . . . .	62
5.3.1	Fixed point collision at $n_c$ . . . . .	64
5.4	Resummation of $n_c$ . . . . .	66
5.4.1	Resummation of $(4 - \epsilon)$ expansion . . . . .	66
5.4.2	Dimensional interpolation . . . . .	67
5.5	Deconfined pseudo criticality . . . . .	69
5.5.1	Miransky scaling . . . . .	69
5.6	Discussion and Outlook . . . . .	71
<b>6</b>	<b>Deconfined criticality in the QED<sub>3</sub>-Gross-Neveu model</b>	<b>73</b>
6.1	The QED <sub>3</sub> -Gross-Neveu model . . . . .	74
6.1.1	QED <sub>3</sub> -GN model . . . . .	74
6.1.2	Gauged four-fermion theory . . . . .	75
6.1.3	Noncompact CP <sup>1</sup> model . . . . .	76
6.2	Duality conjecture . . . . .	77
6.3	Renormalization group analysis . . . . .	79
6.3.1	RG Scheme . . . . .	79
6.3.2	Beta functions . . . . .	80
6.3.3	Anomalous dimensions . . . . .	81
6.3.4	Fixed point structure . . . . .	83
6.4	Quantum critical behavior . . . . .	84
6.4.1	In the QED <sub>3</sub> -GN model . . . . .	84
6.4.2	In the gauged four-fermion model . . . . .	86
6.5	Estimates for 2+1 dimensions . . . . .	87
6.5.1	Padé approximants . . . . .	88
6.6	Comparison with duality predictions . . . . .	89
6.7	Discussion and Outlook . . . . .	90
<b>7</b>	<b>Fractionalized quantum criticality in spin-orbital liquids</b>	<b>93</b>
7.1	Fractionalized spin-orbital liquids . . . . .	93
7.2	The Gross-Neveu-SO(3) model . . . . .	95
7.3	$(4 - \epsilon)$ expansion . . . . .	96
7.3.1	Method . . . . .	96
7.3.2	Flow equations . . . . .	97
7.3.3	Critical exponents . . . . .	98
7.4	$1/N$ expansion . . . . .	99
7.4.1	Method . . . . .	100
7.4.2	Critical exponents . . . . .	102
7.5	Functional renormalization group . . . . .	104
7.5.1	Method . . . . .	104
7.5.2	Flow equations . . . . .	107
7.6	Discussion . . . . .	109

7.7 Summary and outlook . . . . .	112
<b>8 Summary &amp; Outlook</b>	<b>115</b>
<b>APPENDIX</b>	<b>117</b>
<b>A One-loop RG on Gross-Neveu-Yukawa models</b>	<b>119</b>
A.1 Gross-Neveu-Yukawa models . . . . .	119
A.2 Feynman rules & one loop diagrams . . . . .	120
A.3 Group theory for Feynman diagrams . . . . .	121
A.4 Renormalization group procedure . . . . .	123
A.4.1 Renormalization constants . . . . .	123
A.4.2 Group theoretical weights . . . . .	124
A.5 One-loop Calculations . . . . .	125
A.5.1 One-loop RG functions . . . . .	127
<b>B Tools &amp; technique</b>	<b>129</b>
B.1 Fundamentals of Feynman diagram computation . . . . .	129
B.1.1 Integration by parts . . . . .	129
B.1.2 Asymptotic expansion . . . . .	130
B.2 Tool Chain . . . . .	132
B.3 Programs for higher loops . . . . .	133
B.3.1 The Symbolic Manipulation System FORM . . . . .	133
B.3.2 Generating Feynman Diagrams with QGRAF . . . . .	133
B.3.3 Interface to Asymptotic Expansion . . . . .	134
B.3.4 IBP reduction in FORM . . . . .	136
<b>C Higher-loop RG results</b>	<b>137</b>
C.1 Chiral Ising of Gross-Neveu-Yukawa model . . . . .	137
C.1.1 Four loop RG functions . . . . .	137
C.1.2 GN critical exponents . . . . .	140
C.2 Abelian Higgs model . . . . .	140
C.2.1 Four loop RG functions . . . . .	141
C.3 QED <sub>3</sub> -Gross-Neveu model . . . . .	143
C.3.1 Further three loop RG functions . . . . .	143
C.3.2 Critical exponents for arbitrary $N$ . . . . .	144
C.4 Gross-Neveu-SO(3) model . . . . .	145
C.4.1 Epsilon expansions . . . . .	145
C.4.2 Critical exponents for $2 < d < 4$ from $1/N$ expansion . . . . .	146
<b>Bibliography</b>	<b>149</b>
<b>Acknowledgments</b>	<b>169</b>
<b>Erklärung zur Dissertation</b>	<b>171</b>

The history of critical phenomena is a story of success and inseparably linked to the achievements of quantum field theory. All the more astonishing when one considers that this required reconsidering an old and equally successful principle of theory formulation. In almost every physical theory resides the idea of an effective description for a certain length scale. No matter if it describes the behavior of quarks, the dynamics of a fluid, the motion of a mechanical pendulum or the orbits of celestial bodies, the descriptive theory gets along without references to the other scales. This decoupling of length scales establishes the foundation of physical insight all the way to quantum mechanics. For a system with a critical point marking a continuous phase transitions, however, this principle fails and it turns out to be correlated across all length scales. Even more, transitions in completely diverse systems exhibit the same universal behavior near the critical point.

The first theory on continuous phase transitions developed by Lev D. Landau [1] explains this feature as the result of a mutual symmetry, measured by an order parameter, which is spontaneously broken as soon as the system reorganizes in a certain ground state. Although this idea turned out to be correct in essence, it provided the correct result only for special cases which fulfilled the criteria added by Ginzburg [2]. At the latest with the exact calculations by Onsager [3] for the famous Ising model, it became clear that this concept needed some refinement. The till then uniform order parameters had to be elevated in the continuum limit to fields in order to capture its fluctuations. Since not only thermal fluctuations can drive a phase transition but also quantum ones, Landau's theory ultimately becomes a quantum field theory.

Quantum field theory is one of the most precise theories in physics. For its original application in high-energy physics involving the Standard Model of the fundamental interactions and beyond, it allows predictions with unprecedented accuracy. For example, the fine-structure constant  $\alpha$  computed in the Quantum Electrodynamics (QED) matches up to at least eight decimal digits [4, 5]. However, the key to this milestone lies in the development of the renormalization group, which appears utterly abstract at first sight. Since measurements of quantities such as the charge  $e$  exhibit a scale dependence of the energies used to probe in experiment, a calculation of the latter is required. This mathematically conceptional task gives rise to the renormalization group which enables us to derive an effective theory for a given scale out of another theory formulated at smaller scales. A theory that retains its form under the renormalization group is characterized by a fixed point under renormalization group transformations. Leo Kadanoff [6] and later Kenneth Wilson [7–11] realized that the implied scale invariance of these points corresponds exactly to that of a critical point. The Landau-Ginzburg-Wilson (LGW) paradigm devised out of these works has proven to be extremely successful especially for bosonic theories (see Section 2.4.2 for a brief review) and was later extended methodologically to include non-perturbative formulations as well [12]. Eventually, it is leading to even more fundamental applications in the realm of conformal field theory [13, 14]. In particular, the efforts on the computational perturbative renormalization group in high orders for theories such as quantum chromodynamics (QCD)

set the standard for many comparative studies. For fermionic systems, on the other hand, the precise quantitative determination of the critical behavior remained a long-standing challenge. In the search for critical behavior beyond the bosonic order parameter theories, systems which feature gapless fermionic excitations raised more and more attention [15]. Not the least, these challenges fostered a unification of quantum field theory and condensed matter physics [16, 17] as well as forced numerical methods such as Monte Carlo simulation to face the notorious sign problem [18–21].

In 2004, Nobel laureates Andre Geim and Konstantin Novoselov succeeded to synthesize the material graphene in the laboratory [22–24] for the first time and thus unleashed an unprecedented run on Dirac materials. Graphene owes its special properties to its two-dimensional honeycomb lattice, which makes the electrons at low energies appear like quasi-relativistic particles which entail remarkable transport properties [25–27], the applications of which seem to be far from being exhausted [28]. The phase transition from this semi-metallic ground state to one of many possible ordered states such as charge density waves, spin density waves or Kekulé valence bonds [29–31] renewed the interest of a large variety of theoretical methods [15, 21]. Among others, the perturbative loop calculations presented in this work in Chapter 3 quantitatively pushed forward the understanding of the universal quantities at the critical point. With the synthesis of slightly twisted bilayer graphene in 2018 [32, 33], another possible candidate for application and verification of this insight is under discussion [34].

Despite the successes of the LGW paradigm, some transitions seem to evade this scheme. As a prominent example serves the Kosterlitz-Thouless transition [35] in the  $2d$  XY model where the usual order parameter approach can not distinguish the different phases. But also in other low-dimensional quantum systems [36, 37], it becomes apparent that the description by one or more order parameters in the LGW paradigm may not capture unique quantum properties such as topological defects without further adjustments. However, in quantum magnets, the latter are found to contribute crucially to the nature of the transition between two ordered phases. It was found they induce emergent “deconfined” fractionalized degrees of freedom at the critical point [38–40]. A rigorous treatment of the topological details shows that, contrary to the LGW intuition, the phase transition is continuous as confirmed in several numerical simulations [41–43]. Surprisingly, the very same simulations show that the deconfined critical point also exhibits an emergent enlarged symmetry [44]. These breadcrumbs encouraged theorists to elevate of the recently developed fermionic counterpart [45–47] of the charge-vortex duality [48] to the idea of an entire web of novel dualities between both fermionic and bosonic systems [49–51]. A subset of these dualities between specific deconfined quantum critical points again involve emergent Dirac fermions. We will investigate one of these models from the renormalization group point of view in Chapter 6.

A crucial step in the derivation of a theory of the deconfined quantum critical point was to fractionalize the Néel order parameter into spinon degrees of freedom. This concept leaves the question if all sorts of quantum critical points might be affected by a fractionalization, especially when they involve a symmetry-protected topological (SPT) phase. While this was studied for bosonic (toy) models like the hard-core boson model [52, 53], fractionalization in fermionic systems was only found very recently for certain Kitaev formulations of spin-orbital liquid models [54]. The



corresponding continuum field theories again are governed by a certain type of Gross-Neveu universality where not all excitations are gapped out after the transition. We will discuss one of these models from different RG angles in Chapter 7.

## Outline

The content of this thesis was partly published or already submitted for publication. While in Chapter 2 we give a brief review on methods and the general framework, the first project presented in Chapter 3 is based on

- ▶ Bernhard Ihrig, Luminita N. Mihaila, and Michael M. Scherer. ‘Critical behavior of Dirac fermions from perturbative renormalization’. In: *Phys. Rev. B* 98 (2018). arXiv: 1806.04977

In Chapter 4, we motivate the concept of deconfined quantum criticality which sets the stage for the following chapters on the Abelian Higgs model (Chapter 5), the QED<sub>3</sub>-Gross-Neveu model (Chapter 6) and the Gross-Neveu-SO(3) model (Chapter 7) based on the following publications

- ▶ Bernhard Ihrig, Nikolai Zerf, Peter Marquard, Igor F. Herbut, and Michael M. Scherer. ‘Abelian Higgs model at four loops, fixed-point collision, and deconfined criticality’. In: *Phys. Rev. B* 100 (2019). arXiv: 1907.08140
- ▶ Bernhard Ihrig, Lukas Janssen, Luminita N. Mihaila, and Michael M. Scherer. ‘Deconfined criticality from the QED<sub>3</sub>-Gross-Neveu model at three loops’. In: *Phys. Rev. B* 98 (2018). arXiv: 1807.04958
- ▶ Shouryya Ray, Bernhard Ihrig, Daniel Kruti, John A. Gracey, Michael M. Scherer, and Lukas Janssen. ‘Fractionalized quantum criticality in spin-orbital liquids from field theory beyond the leading order’. In: *Phys. Rev. B* 103 (2021). arXiv: 2101.10335



# Critical phenomena from the renormalization group perspective

# 2

The quantum theory is one of the most successful areas of modern physics and together with statistical physics it shapes our understanding of the laws of nature. The combination of both emerged into modern quantum field theory which was originally developed to understand the standard model and therein the physics of the very essential building stones of our (known) universe. But it also finds its way into condensed matter physics. In fact, the application of QFT on the both ends of the spectrum of scales, i.e. higher energies in particle physics and low energies in condensed matter systems, is further pushed by the renormalization group method. It provides a general mathematical tool to understand how length scales interplay and in which way microscopic interactions affect the system's behavior at larger scales. Especially the latter is essential in the theory of continuous phase transitions. Their crucial feature to show fluctuations at all length scales near a critical point demands for a method beyond the usually successful study of different *decoupled* scales.

In this chapter, we will review the basic concepts and motivation of quantum field theories in condensed matter systems, the general idea of the renormalization group method, including perturbative and non-perturbative approach to it and its application to quantum phase transitions.

2.1 Quantum field theories in condensed matter .....	5
2.2 Fundamentals of critical phenomena .....	6
2.3 Concepts of the renormalization group .....	10
2.4 Criticality in the renormalization group .....	18

## 2.1 Quantum field theories in condensed matter

Quantum field theory elevates the idea of fields and wavefunctions to the quantum world and gives matter a new meaning as low energy vibrations of these fields. Indeed, it is a further generalization of quantum mechanics which in this picture emerges as the non-relativistic limit. In condensed matter theory, we can adopt this notion and introduce the fields as an effective description of reality, e.g. as spin fields in the thermodynamic limit of a solid or displacements of atoms in a lattice. The crucial point of this description is that most of the dynamics of these fields lie in the quantum regime and QFT is again the proper language to conceive their physics. But also from the statistical physics point of view QFT is relevant as the effective description of many-body quantum mechanics in the continuum limit [16].

While the quantum fields  $\mathcal{O}(x)$  (with  $x$  a point in space-time) are a vehicle of the theory, the actual physical information is completely encoded in the correlation functions

$$G^{(n)}(x_1, \dots, x_n) = \langle 0 | T \mathcal{O}(x_1) \dots \mathcal{O}(x_n) | 0 \rangle, \quad (2.1)$$

where  $|0\rangle$  describes the vacuum ground state and  $T$  denotes the time ordering. The correlators have many different interpretations depending on the QFT's purpose ranging from scattering cross-sections to energy spectra. Most interestingly throughout this thesis, they take a pivotal role in the description of a system near and at a continuous phase transitions.

1: While it usually is accredited to Richard Feynman, the foundations were laid by Gregor Wentzel [59] and Paul Dirac [60].

2: For a given action  $\mathcal{S}[\mathcal{O}]$ , the classical physics is determined by the principle of least action, demanding that  $\delta\mathcal{S}[\mathcal{O}]/\delta\mathcal{O} = 0$ . In the classical limit  $\mathcal{S}[\mathcal{O}] \gg \hbar$  it becomes clear that these are the only contributions surviving the integral in Eq. (2.2). In contrast for  $\mathcal{S}[\mathcal{O}] \sim \hbar$ , also other quantum trajectories contribute.

3: To be precise, the non-analyticity is a mathematical idealization and arises only in the *thermodynamic limit* where we assume infinite system sizes [61].

4: Second order refers to Paul Ehrenfests' classification [62] from 1933. It accounts that the second derivative of the thermodynamic potential shows the non-analyticity. The term *continuous* was coined due to the order parameters' continuous slope when tuned through the transition.

In statistical physics, the correlators are interpreted slightly different as the probability of a system to transfer between two configurations represented by the fields  $\mathcal{O}(x)$ . They are generated from the partition function which counts and weights the configurations by their "likelihood" regarding to the fundamental principle of least action. For a classical continuous system the partition function becomes an integral over the system's phase space. Richard Feynman<sup>1</sup> successfully boosted this concept to the quantum realm by allowing for quantum fluctuations in all space-time dimensions. Strictly speaking, this lifts the classical notion of the path integral to Dirac's abstract Hilbert space formulation of quantum field theory. Each possible field configuration  $\mathcal{O}(x)$  is weighted by the quantum action  $\mathcal{S}[\mathcal{O}]/\hbar$  in

$$\mathcal{Z} = \int \mathcal{D}\mathcal{O}(x) e^{i\mathcal{S}[\mathcal{O}]/\hbar} \quad (2.2)$$

where  $\hbar$  denotes the Planck constant (from hereon we set  $\hbar = 1$ ). Herein, the element  $\mathcal{D}\mathcal{O}$  defines a functional integral measure which sweeps over all possible field configurations. Indeed, the path-integral is a very powerful unification of the classical and the quantum realm<sup>2</sup>. From Eq. (2.2) the correlators are generated by extending the exponential  $\mathcal{S}[\mathcal{O}] \rightarrow \mathcal{S}[\mathcal{O}] + J \cdot \mathcal{O}$ . The dependence  $\mathcal{Z} = \mathcal{Z}[J]$  added by the additional term

$$J \cdot \mathcal{O} \equiv \int d^d x J_i(x) \mathcal{O}_i(x) \quad (2.3)$$

introduces *source* fields  $J$  and integrates over the  $d$ -dimensional space-time. By means of this term the correlators are derived as functional derivatives with respect to  $J(x)$

$$\langle \mathcal{O}_1(x_1) \dots \mathcal{O}_n(x_n) \rangle = \frac{1}{\mathcal{Z}[0]} \frac{\delta}{\delta J_1(x_1)} \dots \frac{\delta}{\delta J_n(x_n)} \mathcal{Z}[J] \Big|_{J=0}. \quad (2.4)$$

In Chapter 3, we will explore how such a QFT description for a certain system is developed in practice by considering low-energy excitations in the material graphene.

## 2.2 Fundamentals of critical phenomena

Phase transitions accompany us almost every day and yet are a challenge for theory to be fully understood. While most transitions such as from water to ice show an abrupt change of the system between two different phases, there are also phase transitions showing a gradual change and are therefore called *continuous*. From a thermodynamic point of view, a phase transition can be defined as a non-analyticity of the thermodynamic potential in the parameter space. This rather cryptic definition directly affects measurable quantities and shows that the systems' properties change drastically<sup>3</sup>.

Continuous transitions (also known as second order transitions<sup>4</sup>) show an intriguing feature that sparked an entire branch of physics known as *critical phenomena*. Close to the *critical point* separating two phases which is for example marked by a critical temperature  $T_c$ , the non-analyticity is reflected in the occurrence of power laws with a specific *critical exponent*. For instance,

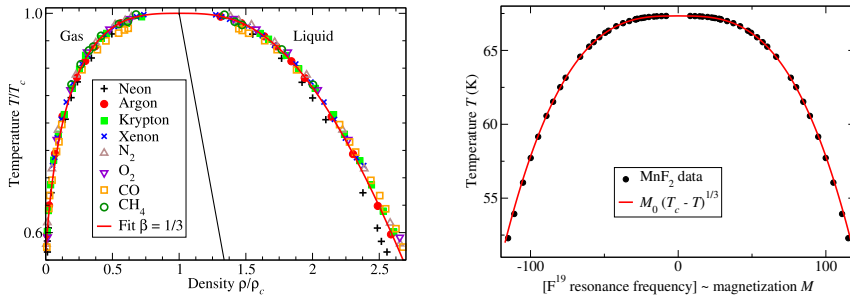


**Figure 2.1:** Critical behavior of dispart systems: (left) Liquid-gas transition for various materials. After rescaling density and temperature to their critical values, all materials show the same power law. (right) Magnetization at a paramagnet-ferromagnet transition which shows the very same power law after rescaling. (Taken from Ref. [63])

the specific heat scales like

$$C_V \sim |\Delta|^{-\alpha} \quad (2.5)$$

where  $\Delta$  measures the distance to the critical point. In thermodynamic systems, this is the reduced temperature  $t$ , i.e.  $\Delta = (T - T_c)/T_c$ . We will see later that this concept can also be extended to transitions driven by quantum fluctuations. Besides the specific heat also other quantities like the susceptibility, the compressibility or the magnetization show such a power law behavior and define additional critical exponent. Luckily, the number of exponents is very limited<sup>5</sup>.

However, the most surprising feature that attracted decades lasting attention for the this field becomes manifest if we compare the critical exponents of phase transitions in very different systems. Counter-intuitively, for some transitions we find the same set of exponents as for example shown in Fig. 2.1. Both the magnetization transition on the right as well as the liquid-gas transitions for various materials on left show the same power laws with the very same exponent  $\beta \approx 1/3$ . While this may have been expected for the group of liquid-gas transitions, the paramagnet-ferromagnet transition is apparently very different in its very nature. This phenomenon is called *universality*. Transitions that share the critical behavior are called to be in the same *universality class* which can be labeled by their unique set of critical exponents. The precise calculation of the exponents seems to be a minor detail at first but indeed it is a highly non-trivial challenge to many complementary theoretical methods and can even be understood as a benchmark for their quantitative comparison (see e.g. Section 2.4.2).

First substantial progress in the understanding of universality were made by Lev D. Landau [1] and Vitali Ginzburg [2]. Landau realized that the properties the allegedly different transitions have in common are the *spontaneously broken symmetries*<sup>6</sup> when the system changes its phase. In fact, for any symmetry breaking ground state  $|\psi\rangle$  it is possible to identify an operator  $\mathcal{O}$  with a finite expectation value

$$\phi \equiv \langle \mathcal{O} \rangle = \langle \psi | \mathcal{O} | \psi \rangle. \quad (2.6)$$

We call this expectation value *order parameter* and it measures so to speak the onset of the symmetry breaking and vanishes in symmetric phase.

The formulation of the theory in terms of a non-fluctuating *mean field*<sup>7</sup>, later extended by Vitali Ginzburg, used this observation to reinterpret the Gibbs free energy as a function of the local order parameter  $\phi(x)$ . Today, it is known

5: In fact, there are only six different exponents which are even related by non-trivial laws named after Rushbrooke, Griffiths, Fisher and Josephson [61].

6: The idea of spontaneous symmetry breaking is an extremely powerful concept which has applications to almost every area in modern physics. For a pedagogical review see Ref. [64].

7: In mean field theory, the spacial variation of the fields is omitted. While this already partially explains universal behavior it fails aside certain dimensions in which the so-called *Ginzburg-criterion* is fulfilled.

as the famous *Landau-Ginzburg energy functional*

$$E[\phi] = \int d^3x [(\nabla\phi(\mathbf{x}))^2 + m^2\phi^2 + \lambda\phi^4]. \quad (2.7)$$

In this form, constructed for an Ising transition with a  $\mathbb{Z}_2$  symmetry, only terms obeying the corresponding reflection symmetry  $\phi \rightarrow -\phi$  are allowed. The lowest gradient term accounts for nearest-neighbor interactions and suppresses short-wavelength fluctuations as wanted for the continuous transition. While the last term with positive coupling  $\lambda$  ensures stability, the most important one is the *mass*<sup>8</sup> term  $m^2\phi^2$ . It is tuned around the critical temperature  $m^2 \sim (T - T_c)$  and changes sign at the transition. Following Landaus' intuition, we can give a nice pictorial notion of spontaneous symmetry breaking by looking at the slope of the energy functional as shown in Fig. 2.2 (here for a spatially uniform field).

As long as  $T > T_c$ , the mass is positive and the energy functional of (2.7) has a unique ground state with  $\langle\phi\rangle \equiv 0$ . When tuned through the critical temperature  $m^2$  changes sign and reveals two minima with  $\langle\phi\rangle \neq 0$ . The system will have to pick one of them as its ground state and therefore spontaneously break the  $\mathbb{Z}_2$  (Ising) reflection symmetry.

While the Landau-Ginzburg theory is a phenomenological ansatz, it already lays the foundation of the field theoretical approach. In fact, Landaus observation that systems of the same universality class break the same symmetries was already right but it dismisses the role of dimensionality. His original idea was to write down an effective macroscopic theory for the transition which does not involve the microscopic details<sup>9</sup>. But on the contrary, a continuous transition is accompanied by characteristic *self-similar* structures on all length scales as shown in Fig. 2.3 again for the Ising transition (here shown in a lattice simulation [65]). No matter how we rescale the system at the critical point, it still looks the same. In terms of the order parameter operator  $\mathcal{O}$ , these structures appear when the correlation-length  $\xi$  diverges. Similar to the thermodynamic quantities we can assume a power law close to the critical point

$$\xi(\Delta) \sim |\Delta|^{-\nu}. \quad (2.8)$$

Consequently, when measuring the two-point correlations we assume the following *scaling form*

$$G(x, t) = \langle\mathcal{O}(x)\mathcal{O}(0)\rangle \sim \frac{e^{-x/\xi(\Delta)}}{x^{d-2+\eta}}. \quad (2.9)$$

Close to the transition, the correlations will therefore decay exponentially, while directly at the critical point ( $\Delta = 0$ ) the correlation function decays algebraically in a power law with dimension  $d$  and another critical exponent  $\eta$ , called the *anomalous dimension*.

The crucial point here is that a theory formulated only for one fixed length scale must fail to capture the physics of a continuous transition. Nevertheless, although at the transition the system fluctuates on all length scales, the universality shows that very different systems look the same and the microscopic details become irrelevant. These seemingly contradictory facts as well as the concept of universality itself can better be understood by studying a continuum like limit of theories. The systematic method to do

8: We call this term *mass* for historical reasons and it should not be confused with the physical mass. In fact, it can be understood as the energy gap of the spectrum at zero momentum.

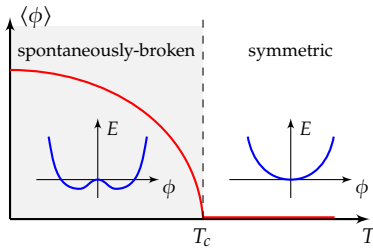


**Figure 2.2:** Order parameter and the Landau-Ginzburg energy functional. For large temperatures the system respects a certain symmetry as  $\langle\phi\rangle = 0$ . Below the critical point at  $T = T_c$ , this symmetry is broken and the ground state will collapse to one of the minima of the potential with  $\langle\phi\rangle > 0$

9: Indeed, this is a very old widely used concept in physics. Most theories are formulated for a certain length scale and ignore the others, e.g. for mathematical pendulum the motion is described only by the length of the rope with no reference to atomic or cosmic scales.

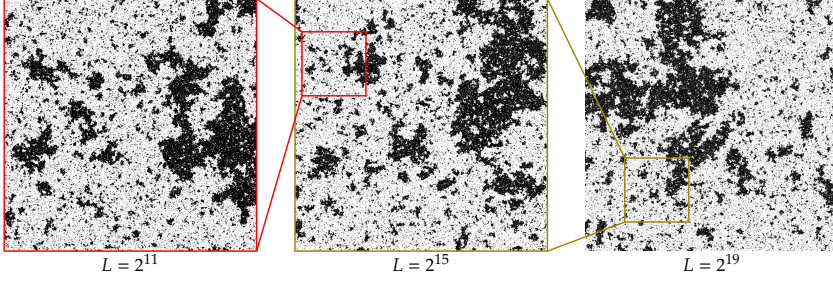


**Figure 2.3:** Ising lattice tuned to the critical temperature: At the critical point, the pattern of the Ising model shows *self-similarity*, i.e. even if zoom out as in the figures from bottom to top, the structure does not change. The crucial observation here is that a theory describing this state would have to be *scale invariant*. (Pictures taken from [65]).

this is called the *renormalization group*.

### Quantum phase transitions

The observations on critical phenomena we made so far are not limited to phase transitions driven by thermal fluctuations. In fact, there is always a competition between the thermal fluctuations and quantum fluctuations which we have not considered yet. In the Landau-Ginzburg energy functional (2.7), we account only for thermal fluctuations by allowing for spatially dependent order parameter field  $\phi(x)$  and neglect any time-dependence, assuming the system is at equilibrium. In order to generalize it to the quantum level as in Eq. (2.2) which incorporate quantum fluctuations as well, we have to allow for an imaginary-time  $\tau$  dependence of the order parameter fields

$$\mathcal{S}[\phi] = \int_0^\beta d\tau \int d^3x [\mathcal{L}_{\text{kin}}[\phi(\tau, \mathbf{x})] + (\nabla\phi(\tau, \mathbf{x}))^2 + m^2\phi^2 + \lambda\phi^4], \quad (2.10)$$

where  $\beta \sim 1/T$  (for  $k_B = 1$ ). The added term  $\mathcal{L}_{\text{kin}}$  accounts for the quantum fluctuations in the periodic imaginary-time direction. In the Matsubara formalism, we assign the frequencies  $\omega_n \sim nT$  as the field's oscillations such that  $\omega_0 = 0$  corresponds to the classical fluctuations. For finite temperature near criticality ( $m^2 \rightarrow 0$ ), the former frequencies can be integrated out and we recover the Landau-Ginzburg energy functional of Eq. (2.7) [66, 67].

However, at zero temperature this is not possible and the theory is in fact dominated by quantum fluctuations. Now the kinetic part  $\mathcal{L}_{\text{kin}}$  becomes all important and extends the correlations by a quantum imaginary “time” direction. Similar to the correlation-length  $\xi$  for the classical spatial directions in Eq. (2.8), also the correlation “time”  $\tau_c$  diverges at the critical point. Since the time-like quantum fluctuations are independent from the spatial thermal fluctuations, the power law of  $\tau_c$  reflects this anisotropy by the *dynamical critical exponent*  $z$ , i.e.

$$\tau_c(\Delta) \sim \xi^z \sim |\Delta|^{-\nu z}. \quad (2.11)$$

Whenever at low temperatures close to the critical point the energy scale of the quantum fluctuations  $\omega \sim |\Delta|^{-\nu z}$  is comparative to the energy scale of the thermal fluctuations  $\sim k_B T$ , the transition “looks” quantum critical. Therefore, upon tuning the system with respect to the quantum direction  $r = m^2$  we may find reminiscent scaling behavior but the thermal fluctuations will take over eventually [68]. This region is known as the *quantum critical fan*, as shown in Fig. 2.4. In the special case of relativistic fields, the dynamical

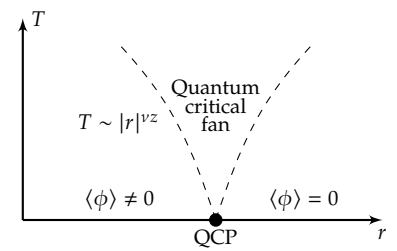


**Figure 2.4:** Principal phase diagram of systems near a quantum critical point. At temperature zero, the transitions is driven solely by quantum fluctuations. But also at finite  $T$ , the transition can be dominated by the quantum regime when the temperature is comparative to the energy scale of the quantum fluctuations, i.e.  $T \sim |r|^{\nu z}$  in the region of the so-called quantum critical fan. Here, the dynamical critical exponent  $z$  accounts for the additional imaginary time contribution to the correlation-length. (similar in Ref. [66])

critical exponent is simply  $z = 1$  which applies also for all projects throughout this thesis.

On first sight, the former discussion seems to lead to a quantum-classical mapping where the classical transitions in  $d$  dimensions map to quantum phase transitions in  $d + z$  dimensions. However, this mapping assumes that every transition can be described in the Landau order parameter picture which dismisses features special to the quantum world as e.g. topological Berry phases [39, 68]. In Chapter 4, we will discuss why this critical behavior lies *beyond* the Landau notion.

## 2.3 Concepts of the renormalization group

10: In fact, this space is infinitely dimensional and for all following discussions we already limit ourselves to subsets of it from which some are closed and others are not.

The renormalization group makes an essential abstraction important for field theories of all areas: It systemically realizes a map from the *theory space*<sup>10</sup> on itself. This renormalization group operation is sometimes called *coarse-graining*, a term which goes back to the very first ideas by Leo Kadanoff. In his seminal paper [6] on “Scaling laws for Ising models near  $T_c$ ”, he repeatedly regrouped neighboring states on a real space lattice to an effective single state. Upon this step-by-step method, it was possible to systemically reveal the self-similar structure of the system near criticality.

While this already proved to be a powerful concept, it was Kenneth Wilson who developed the modern systematic approach in momentum space [7–11], nowadays known as *Wilson RG*. Wilson realized that in momentum space the coarse-graining can be achieved by successively integrating out fast modes of a theory. He was able to unify these ideas with the renormalization group methods from high energy physics developed in the 1950s at first by Ernst Stueckelberg and André Petermann and later by Murray Gell-Mann, Francis E. Low, Richard Feynman, Julian Schwinger and Shin’ichirō Tomonaga<sup>11</sup>.

11: A long list of very intelligent people! While Gell-Mann was awarded a Nobel prize in 1969 for his contributions to elementary particle physics and Feynman, Schwinger and Tomonaga in 1965 for solving QED, it was Kenneth Wilson who was honored for developing the renormalization group with the Nobel prize in 1982 [11].

### 2.3.1 General idea

The goal of *renormalization* is to construct a macroscopic theory from microscopic degrees of freedom. While the usual approach to write down such a theory with respect to certain observations may fail, the renormalization group systematically establishes a map from all (renormalizable) microscopic theories to the macroscopic theories. This way it also allows us to understand the physics in between. Technically, we can define the renormalization group operation  $\mathcal{T}$  as a differential mapping that acts on a theory  $\mathcal{H}_\mu$  at scale  $\mu$  and tells us how it *renormalizes* to a theory at infinitesimally larger scale  $\mu + \delta\mu$

$$\mu \frac{d}{d\mu} \mathcal{H}_\mu = \mathcal{T}[\mathcal{H}_\mu]. \quad (2.12)$$

12: This condition ensures that only the theory  $\mathcal{H}_\mu$  at scale  $\mu$  is known to the renormalization and not the history of predeceasing theories. Consequently, the derivative  $\mu d_\mu = d/d \ln \mu$  accounts for this multiplicative feature that we can go back in coarse-graining. In the functional RG this observation coined the phrase *RG time*  $t = \ln \mu$ .

This is the *renormalization group equation* (RGE) where the scale  $\mu$  effectively only enters through the theory  $\mathcal{H}_\mu$ <sup>12</sup>. In order to use this rather abstract concept in practice, we deconstruct  $\mathcal{H}$  into the action  $S[\mathcal{O}]$  introduced above. Since every action of a field theory can be formulated by dynamical fields and their interactions, we describe a theory by the couplings  $g_i$  of these interaction terms and the space-time dimension  $d$  it lives in

$$\mathcal{H} \equiv \{d; g_1, g_2, \dots\}. \quad (2.13)$$



In the renormalization group, the couplings inherit an explicit scale dependence  $g_i = g_i(\mu)$  and *renormalize* under RG transformations. This scale dependence is encoded in the so-called beta function and is fixed by the RGE which in this language reads

$$\mu \frac{dg_i}{d\mu} = \frac{dg_i}{d \ln \mu} = \beta_i(d; g_1, g_2, \dots). \quad (2.14)$$

Note that the beta functions in general depend on all couplings of the theory space.

The main goal of many field theoretical RG calculations now is to compute the beta functions as precise as possible. For the purpose of this thesis, we will present two approaches: (i) the perturbative approach which requires certain conditions for the microscopic theory as we will see in the next section and (ii) the non-perturbative functional renormalization group method which overcomes these requirements but trading in its own subtleties. In the following, we will present and discuss both of them and apply them exemplarily to the  $O(N)$ -model which serves as a seminal theory with many physical interpretations. The first of them, we already mentioned as the Ising model at  $N = 1$ .

### 2.3.2 Perturbative renormalization group

A priori, we can not make any assumptions about the couplings of a theory. However, if we manage to introduce a small parameter, we can try to perform the RG analysis *perturbatively* (pRG). There are different angles to (artificially) insert such a parameter and then successively expand the beta functions in this parameter. Once this parameter is found, we also has to fix a certain *RG scheme*. In the Wilsonian RG, we mentioned above, one integrates out fast modes step-by-step in momentum shells  $k \in [\Lambda/b, \Lambda]$  ranging from the ultraviolet physics at scale  $\Lambda$  to the effective infrared behavior towards  $k \rightarrow 0$ . While this is a very intuitive approach for critical phenomena, the perturbative RG was originally developed around *the problem of infinities* in the celebrated theory of quantum electrodynamics (QED). Consequently, it became the state-of-the-art method for decades and thus is well formalized. While both approaches share the same goal in computing the beta functions of a theory, the high energy approach is apparently less intuitive but profits from the wide experience gained in computations for the standard model. Experience we can benefit from.

The method of choice for most projects throughout this thesis is the *dimensional regularization within the minimal subtraction scheme* ( $\overline{\text{MS}}$ ). Behind this complicated sounding name hides an equally complicated procedure over which entire books have been written (see e.g. Ref. [69]). In the following, we will illustrate some of the advantages and the basic ideas in terms of the prototypical Ising model which easily generalize to other theories<sup>13</sup>. At first, we generalize the Landau-Ginzburg energy functional to the free energy  $F = k_B T \mathcal{S}_{\text{Ising}}$  with the *euclidean*  $d$ -dimensional action

$$\mathcal{S}_{\text{Ising}} = \int d^d x \mathcal{L} = \int d^{d-1} x d\tau \left( \frac{1}{2} (\partial_\mu \phi_0)^2 + \frac{1}{2} m_0^2 \phi_0^2 + \frac{\lambda_0}{4!} \phi_0^4 \right), \quad (2.15)$$

13: For a detailed one-loop pRG analysis of a generalized version of Gross-Neveu-Yukawa model which will become relevant multiple times throughout this thesis, see Appendix A.

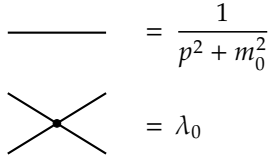


**Figure 2.5:** Feynman-rules for the  $\phi^4$ -Ising model: the propagator of the massive bosonic field  $\phi_0$  and the vertex with coupling  $\lambda_0$ .

and the corresponding derivative  $\partial_\mu = (\partial_\tau, \nabla_{d-1})$ . Note that all quantities obtained a zero index which means we have not renormalized them yet and therefore label them as *bare* because they are *scale invariant*.

Besides, we also add combinatorial factors to each term. A basic ingredient for this renormalization method are the Feynman rules for the Lagrangian to be renormalized. These can be deduced from the use of the path integral formalism. In principle, the rules stem from a perturbative expansion of the interactions which can be justified a posteriori. For the Ising model in Eq. (2.15), there are two rules for the propagator and the interaction vertex with prescriptions in momentum space shown in Fig. 2.5. The shown diagrams set the *tree-level*.

Using these rules, we can try to compute corrections to the (still) bare field  $\phi_0$  and coupling  $\lambda_0$  by allowing for virtual processes. These can be sorted by their *loop order* which accounts for the number of closed momentum integrals appearing in the process. For the Ising model, we want to compute essentially two correlators which at one loop are represented by the following diagrams

$$\langle \phi_0 \phi_0 \rangle = \text{---} + \frac{1}{2} \text{---} \text{---} + \mathcal{O}(2\text{-loop}) \tag{2.16}$$

$$\langle \phi_0^4 \rangle = \text{---} + \frac{1}{2} \text{---} \text{---} + \frac{1}{2} \text{---} \text{---} + \frac{1}{2} \text{---} \text{---} + \mathcal{O}(2\text{-loop}) \tag{2.17}$$

Besides the *tree-level* contributions from the rules themselves, there are four one-loop diagrams with loop momentum  $p$  we have to integrate over. Note that we also assigned so-called *symmetry factors*<sup>14</sup>. in front of each diagram. We have to compute only two integrals

$$\text{---} \text{---} = \lambda_0 \int \frac{d^d p}{(2\pi)^d} \frac{1}{p^2 + m_0^2} = m_0^{d-2} I_1 \tag{2.18}$$

$$\text{---} \text{---} = \lambda_0^2 \int \frac{d^d p}{(2\pi)^d} \frac{1}{(p^2 + m_0^2)^2} = \left(1 - \frac{d}{2}\right) \lambda_0^2 m_0^{d-4} I_1 \tag{2.19}$$

where by  $I_1$  we denote the result of the integral

$$I_1 = \frac{1}{(4\pi)^{d/2}} \Gamma(1 - d/2). \tag{2.20}$$

Unfortunately, this integral diverges for every  $d = 2 + 2n$ ,  $n \leq 0$  which reveals a major obstacle of the field-theoretical approach to quantum field theory. What seems as a severe problem at first sight, turns out to be a consequence of the bare and therefore unphysical quantities in the theory. The correlations of the bare fields are not the ones measured in experiment. In fact, we have to maintain the infinities by renormalizing the theory.

At first, let's gain control over the divergencies by introducing the *dimensional regularization*. By shifting the integrals dimension slightly away to  $d = 4 - \epsilon$ , we can describe the divergency in the limit  $\epsilon \rightarrow 0$ . In fact, at this stage of the analysis,  $\epsilon$  is an artificial control parameter with only one purpose: regularizing the divergence without breaking any symmetries and especially not the Lorentz-symmetry. However, it also introduces a complication for the

14: Symmetry factors in perturbative QFT can become quite complicated and basically account for the number of possibilities to attach loose ends of the vertex when drawing the diagrams. For a nice overview see Ref. [70].

coupling's mass dimension. If we want to make the calculation manifestly dimensionally correct, we therefore have to shift them by a factor proportional to the energy scale  $\mu$

$$\lambda_0 = \mu^\epsilon \lambda \quad \text{and} \quad m_0^2 = \mu^{-2} m^2. \quad (2.21)$$

We now deal with the dimensionless, *renormalized* coupling  $\lambda$  and mass  $m^2$ . A posteriori, we are also able to justify the perturbative expansion for the corrections. The (dimensional) scale dependence of the coupling  $\lambda$  is

$$0 = \frac{d\lambda_0}{d \ln \mu} = \epsilon \mu^\epsilon \lambda + \mu^\epsilon \frac{d\lambda}{d \ln \mu} \Rightarrow \frac{d\lambda}{d \ln \mu} = -\epsilon \lambda, \quad (2.22)$$

which meaning that the corrections to the renormalization of  $\lambda$  are of order  $\mathcal{O}(\epsilon\lambda)$ . For  $\epsilon \ll 1$ , this justifies the expansion of the path integral in orders of a finite coupling  $\lambda$ . However, this is only the the zero order contribution to the scale dependence of  $\lambda$  and we should now turn to refine it by allowing for the virtual processes we tried to compute above.

Practically, for the RG procedure, we reintroduce the *renormalized* fields and couplings  $\phi$ ,  $m^2$  and  $\lambda$  with so-called *renormalization group constants*  $Z_i$

$$\phi_0 = Z_\phi^{1/2} \phi, \quad m_0^2 = \mu^2 Z_m m^2, \quad \lambda_0 = \mu^\epsilon Z_\lambda \lambda. \quad (2.23)$$

For free fields (i.e. no interactions), we would expect no corrections to the renormalization. We can account for this by writing

$$Z_i = 1 + \delta Z_i \quad \forall i \in \{\phi, m^2, \lambda\}. \quad (2.24)$$

and recover the dimensional scaling of Eq. (2.21) for  $\delta Z_i = 0$ .

Inserting these definitions in the Lagrangian gives us an additional set of Feynman rules, the so-called *counter terms*. Hence, the *bare* Lagrangian  $\mathcal{L}_0$  is  $\mathcal{L}_0 = \mathcal{L}_{\text{ren}} + \mathcal{L}_{\text{ct}}$  where  $\mathcal{L}_{\text{ren}}$  is just  $\mathcal{L}_0$  upon replacing the bare fields and couplings by the renormalized ones. The counter term Lagrangian reads

$$\mathcal{L}_{\text{ct}} = \frac{1}{2} \delta Z_\phi (\partial_\mu \phi)^2 + \frac{1}{2} (\delta Z_\phi + \delta Z_m) m^2 \phi^2 + \frac{1}{4!} (\delta Z_\lambda + 2\delta Z_\phi) \lambda \phi^4. \quad (2.25)$$

This translates to very similar Feynman rules but multiplied with the respecting  $\delta Z_i$ , see Fig. 2.6. In this way, the perturbative renormalization cancels the infinities as they appear from the bare Lagrangian, i.e. order-by-order by some counter diagrams. The general idea behind is that the counter terms only cancel the unphysical divergencies, leaving only finite contributions in the corresponding correlation functions of the now fully renormalized theory. Diagrammatically, the counter terms are supposed to cancel out all divergencies at a given loop order, providing only finite correlators

$$\langle \phi^2 \rangle = \text{---} + \text{---} \otimes \text{---} + \frac{1}{2} \text{---} \circ \text{---} + \mathcal{O}(2\text{-loop}) \quad (2.26)$$

= finite +  $\mathcal{O}(2\text{-loop})$ ,

$$\langle \phi^4 \rangle = \text{---} \times \text{---} + \text{---} \otimes \text{---} + \frac{3}{2} \text{---} \cap \text{---} + \mathcal{O}(2\text{-loop}) \quad (2.27)$$

= finite +  $\mathcal{O}(2\text{-loop})$ ,

$$\text{---} \otimes \text{---} = \delta Z_\phi p^2 + \delta Z_m m^2$$

$$\text{---} \times \text{---} = \lambda (\delta Z_\lambda + 2\delta Z_\phi)$$

**Figure 2.6:** Counter term Feynman-rules for the  $\phi^4$ -Ising model: (a) the propagator counter rule  $\phi_0$  and the vertex counter rule in (b). Both involve the renormalization constants  $\delta Z_i$ .

where we summarized the three one-loop diagrams to the vertex into one as they all have the same contribution. This – in essence – is the overall perturbative approach of renormalizing a field theory. But how do we cancel the divergencies precisely?

At this point, the minimal subtraction scheme  $\overline{\text{MS}}$  comes into play. We take a step back to the divergent integrals and use the dimensional regularization at  $d = 4 - \epsilon$  dimensions. It shows that Eq. (2.20) approximates to

$$I_p(d = 4 - \epsilon) = -\frac{N_d}{\epsilon} + \mathcal{O}(\epsilon) = -\frac{1}{8\pi^2} \frac{1}{\epsilon} + \mathcal{O}(\epsilon), \quad (2.28)$$

where  $N_d = 2/((4\pi)^{d/2}\Gamma(d/2))$ . Crucially, the divergency became a  $1/\epsilon$  pole with a certain prefactor in which we are actually interested in. In the minimal subtraction scheme, the renormalization constants  $\delta Z_i$  are now chosen to cancel exactly these poles, i.e.

$$\delta Z_\phi = 0, \quad \delta Z_m = \frac{1}{8\pi^2} \frac{\lambda}{\epsilon}, \quad \delta Z_\lambda = \frac{3}{16\pi^2} \frac{\lambda}{\epsilon}. \quad (2.29)$$

This provides us with a controlled way to cancel the divergencies at every order of the perturbative expansion (also called *loop-by-loop*). Even better, it finally puts us in the position to compute the beta functions. As before for the dimensional scaling in Eq. (2.22), we use that the bare couplings have no scale dependence and obtain

$$\beta_\lambda = -\epsilon\lambda + \lambda \frac{d \ln Z_\lambda}{d \ln \mu} = -\epsilon\lambda + \frac{3}{16\pi^2} \lambda^2 + \mathcal{O}(\lambda^3). \quad (2.30)$$

Note that the renormalization constant does not explicitly depend on the scale  $\mu$  but only implicitly through the coupling  $\lambda$ . Similarly, we compute the beta function of the mass to

$$\beta_{m^2} = \left( -2 - \frac{d \ln Z_m}{d \ln \mu} \right) m^2 = \left( -2 + \frac{\lambda}{8\pi^2} + \mathcal{O}(2\text{-loop}) \right) m^2. \quad (2.31)$$

The procedure we introduced here describes how to compute the beta functions for renormalization towards the ultraviolet (UV), i.e. the scale dependence for growing  $\mu$ .

For critical phenomena, however, we are interested in the infrared behavior (IR) of a theory for larger length scales  $l$ . For this purpose, the IR-beta-functions can be recovered by connecting the energy scale  $\mu$  with the length scale  $l$  by  $\mu = \mu_0 \exp(-l)$ , i.e.  $d/d \ln \mu = -d/dl$ . Let's conclude this calculation by drawing our very first RG flow from the beta functions in Fig. 2.7. We used the IR- $\beta$ -functions and the arrows therefore point towards the infrared. Interestingly, we can already spot the so-called *Wilson-Fisher* fixed point at  $\lambda = \lambda^*$  in the flow which turns out to be essential for critical phenomena.

This concludes how we compute the beta function to one-loop order with dimensional regularization in the minimal subtraction scheme<sup>15</sup>. While this may serve as a good approximation close to the  $d = 4$ , we would need to compute higher-loop contributions to make quantitatively reliable statements. Since the perturbative RG is closed loop-order-by-loop-order,

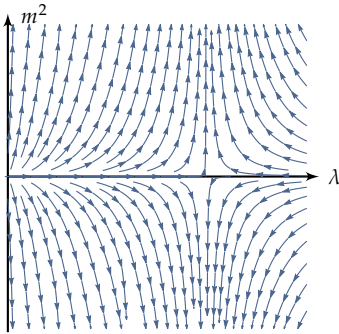


**Figure 2.7:** Perturbative renormalization group flow of the  $\phi^4$  Ising model at one loop. The direction of the flow is towards the infrared. While in the mass direction the sign of  $m^2$  separates the flow, in the  $\lambda$ -direction we see the so-called *Wilson-Fisher* fixed point.

15: There are also other regularization schemes like *cut-off regularization*, *lattice regularization* or *Pauli-Villars regularization*. The advantage of the dimensional regularization in the  $\overline{\text{MS}}$  over these schemes lies in its formalization also in higher loops which is needed for using computer algebra systems. We further address this in App. B.1.

the contributions to the beta function have the following structure

$$\beta_\lambda(\epsilon; \lambda) \sim -\epsilon\lambda + \text{[diagram]}(\lambda^2) + \text{[diagram]}(\lambda^3) + \text{[diagram]}(\lambda^4) + \dots \quad (2.32)$$

Another example for a perturbative approach is the large  $N$  or  $1/N$  expansion [71, 72]. Here the number of field components is assumed to be large and we rescale the coupling, e.g. in the case of the  $O(N)$ -model by it  $\lambda \rightarrow \lambda/\sqrt{N}$ . This limits the number of contributing diagrams dramatically by suppressing most of them by factors of  $1/N$ . The remaining RPA diagrams are calculated at arbitrary dimension  $d$ . A thorough review on this expansion can e.g. be found in Ref. [72]

In either of these perturbative methods one central question remains: Can we trust their predictions? The answer has many subtleties. First of all, the power of the epsilon expansion is to preserve the symmetries of the theory in any step of the procedure. Consequently, it provides already a good first qualitative intuition about the topology of the RG flow and its fixed points. However, extrapolating toward  $d = 3$  by naively sending  $\epsilon \rightarrow 1$  at least appears dangerous and indeed the epsilon expansions provide only asymptotic series with diverging coefficients. A quantitative finding is still possible but requires complicated resummation schemes. We will address this point in the first project in detail.

In the analysis above, we were apparently lucky that all the divergencies could be canceled out by renormalization. However, this is not a coincidence and all theories like the  $\phi^4$ -model in Eq. (2.15) can be classified as *renormalizable*, *non-renormalizable* or even *super renormalizable*. The classification is made by calculating the so-called *superficial degree of divergence* which counts the number of legs, momenta, vertices (by their type) and the dimension up to a single number. It turns out that this number is sufficient to proof (in the so-called *BPHZ theorem*<sup>16</sup>) if a theory is *perturbatively renormalizable*. Often the term “perturbative” is dropped in this context but in fact there are non-perturbative methods which can deal even with supposedly non-renormalizable theories.

### 2.3.3 Functional renormalization group

The perturbative implementation of the renormalization group in the previous Section is not the only way to calculate the scale dependence of a theory. While in Eq. (2.15) we made an explicit choice to compute the flow only for the coupling  $\lambda$  and the mass  $m^2$ , one can also take a step back and compute the flow of the *effective action* as a whole. This is known as the functional<sup>17</sup> renormalization group (FRG) [74–81]. By the effective action  $\Gamma$  we denote the Legendre transformed scale-dependent Schwinger functional. Crucially, it generates the connected one-partical irreducible diagrams we already met in the first loop order in the perturbative approach above.

For the renormalization group approach, we elevate the effective action by letting it *flow* with the momentum scale  $k$ , i.e.  $\Gamma \rightarrow \Gamma_k$ . In this way,  $\Gamma_k$  interpolates between the microscopic action  $S$  at a cut-off scale  $\Lambda$ , i.e.  $\Gamma_\Lambda = S$ , and the full effective action  $\Gamma$  after integrating out all quantum and statistical fluctuations to  $k = 0$ , i.e.  $\Gamma_0 = \Gamma$ . We can illustrate this idea as a flow diagram similar to the one we already computed, but with the major generalization

16: A quite technical proof by Bogoljubov, Paradjuk, Hepp and Zimmermann which shows that the divergencies of 1PI Feynman diagrams in a renormalizable theory can be canceled by a finite number of counter terms (see Ref. [73])

17: Sometimes also called non-perturbative RG (NPRG) or exact renormalization group (ERG). The latter term is rarely used because it raised complaints in the community due its misleading indication the method would provide the “exact” results in all its publications.

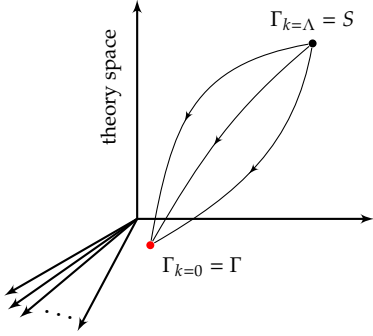


**Figure 2.8:** Schematic flow of the effective action in theory space. Starting at a microscopic action  $\Gamma_\Lambda = S$  at a cut-off scale  $\Lambda$ , the Wetterich equation describes how the effective action flows to the full effective action  $\Gamma$  in the infrared at  $k = 0$ . The different curves account for different regulators which introduce an ambiguity only at intermediate scales.

that the entire effective action flows in the infinite dimensional theory space as shown in Fig. 2.8. The equation that establishes this flow is the *Wetterich equation*

$$k\partial_k\Gamma_k = \frac{1}{2}\text{Str}\left[\frac{k\partial_k R_k}{\Gamma_k^{(2)} + R_k}\right]. \quad (2.33)$$

This involves the Hessian of the effective action  $\Gamma_k^{(2)}$  with respect to the considered fields and a so-called *regulator*  $R_k$ . The super trace  $\text{Str}$  sums over all (fermionic) field components with their respecting signs. The regulator accomplishes the crucial Wilsonian idea for the whole action at once and *freezes out* modes below a certain scale  $q$ . In this way, the renormalization of effective action is dominated by scales  $k \lesssim q$  and the successive integration of them finally establishes the flow equation. Strictly speaking, the regulator has to fulfill the following three requirements

$$(i) \quad \lim_{k \rightarrow 0} R_k(q) = 0 \quad \text{for fixed } q, \quad (2.34)$$

$$(ii) \quad \lim_{k \rightarrow \infty} R_k(q) = \infty, \quad (2.35)$$

$$(iii) \quad R_k(q) \text{ respects all global symmetries of } S. \quad (2.36)$$

The third condition is essential to not generate terms which break the symmetry. Nevertheless, by picking a certain regulator the flow becomes non-universal at intermediate scales which is depicted as a regulator-dependent “path” for the flow in theory space (represented by different paths in Fig. 2.8). Fortunately, by imposing the conditions Eq. (2.34) to (2.36), measurements of physical quantities remain untouched by this artificially introduced ambiguity. A widely used regulator in field-theoretical FRG calculations is the Litim regulator [82]  $R_k = Z_k(k^2 - q^2)\Theta(k^2 - q^2)$  where  $\Theta$  denotes the Heaviside step function and  $Z_k$  the wavefunction renormalization similar to the constant in the previous section.

Despite its innocuous appearance, the Wetterich Equation (2.33) is usually impossible to solve exactly<sup>18</sup>. Instead, we have to employ an approximation scheme either analytical or numerical. In the analytical approach the equation can be translated into an infinite tower of integro-differential equations which can be truncated at a certain order<sup>19</sup>. Since in critical phenomena we are mostly interested in the long-wavelength physics, we can usually pick the so-called *derivative expansion*. In this scheme the momentum dependence of the vertices is imposed in the beginning which limits the analysis to moderately fluctuating order parameter fields<sup>20</sup>.

Let’s illustrate the procedure by analyzing the Ising field theory again. Recall that the model has a  $\mathbb{Z}_2$  symmetry leaving any power of  $\rho = \phi^2$  invariant under the transformation  $\phi \rightarrow -\phi$ . In order to solve the flow equation we make the ansatz of a local potential  $U_k(\rho)$  which only depends on the symmetry invariant  $\rho = \phi^2$  such that the effective action reads

$$\Gamma_k = \int d^D x \left[ \frac{1}{2} Z_k (\partial_\mu \phi)^2 + U_k(\rho) \right]. \quad (2.37)$$

This is called the improved *local potential approximation* (LPA’) where the prime distinguishes the additionally wavefunction-renormalization by a scale-dependent  $Z_k$ . We skip the details of the derivation which can be

18: There are some rare examples where this actually possible, see Refs. [83, 84] and references therein.

19: The choice of a certain regulator and the truncation can be compared to the choice of a pRG scheme and its subsequent resummation. It’s not a priori safe that every regulator in every truncation will provide the same results since they confine the flow to distinct subspaces. An example of this ambiguity is shown in last project in Chapter 7

20: This again restricts the analysis to a lower dimensional sub-space of the theory space. While this is a justified approximation for many theories it might fail eventually.

found in various great reviews on the functional renormalization group such as Ref. [74, 80, 83] and directly jump ahead to the flow equation of the dimensionless potential

$$k\partial_k u_k(\rho) = -du_k(\rho) + (d-2+\eta)\rho u'_k(\rho) + l_0^d(u'_k(\rho) + 2\rho u''_k(\rho)). \quad (2.38)$$

with  $u_k$  denoting the dimensionless potential. Here, we introduced the so-called threshold function  $l_0^d$  which depends only on the regulator. For the especially interesting case  $d=3$  and the mostly used Litim-regulator the final result is

$$k\partial_k u_k(\rho) = -3u_k(\rho) + \rho u'_k(\rho) + \frac{1}{6\pi^2(1+u'_k(\rho)+2\rho u''_k(\rho))}. \quad (2.39)$$

Despite its complicated appearance we can solve this flow equation and consequently obtain the beta functions of our theory. To this end, we make the following ansatz for the potential

$$u_k(\rho) = \sum_{n=2} \frac{\lambda_n}{n!} (\rho - \kappa_k)^n. \quad (2.40)$$

In fact, this is a Taylor expansion around the potential's minimum  $\kappa_k$  of the the potential. Note, that we also allow this minimum  $\kappa_k$  to flow similar to the mass term in the perturbative renormalization group approach because it denotes the vacuum expectation value of the systems ground state. In this sense, we expanded the system in the symmetry broken phase in accordance to Fig. 2.2. Even better, if we truncate the expansion at  $n=2$ , we recover the same action<sup>21</sup> but with  $\lambda_2 = \lambda$  in comparison to Eq. (2.15). In order to get to the beta functions for the couplings  $\lambda_i$ , we now have to *truncate* the expansion at some order  $n_{\max}$ . Strictly speaking, by doing this we confine ourselves to a closed subset of theory space with a finite number of couplings. However, the truncation also introduces a regulator dependence to our beta functions which can only barely be controlled<sup>22</sup>. A local Taylor expansion of the potential is not the only way to solve Eq. (2.38). Another prominent way developed in the last decade are the application of pseudospectral methods [85] to FRG equations [86–90]. Both methods are used in the last project of this thesis in comparison, see Chapter 7. The wave-function renormalization is computed from  $Z_k$  by a projection of the hessian [74, 80] at  $q \rightarrow 0$  as

$$Z_k = \frac{(2\pi)^d}{\delta(q=0)} \lim_{q^2 \rightarrow 0} \frac{d}{dq^2} \left( \Gamma_{\phi(q), \phi(-q)}^{(2)} \right). \quad (2.41)$$

In contrast to the perturbative renormalization group, the FRG does not have a control parameter like  $\epsilon$  or  $1/N$ . This does not imply it is totally uncontrolled. However, it can treat theories beyond their renormalizable dimensions which is especially interesting for a theory of quantum gravity<sup>23</sup> [84]. Other than in the perturbative expansions, FRG results do not have to be resummed due to the non-perturbative nature of the Wetterich equation. The resummation is included is already partly included in the choice of the regulator. This advantage is the trade-off for a regulator dependency which itself is difficult to measure.

21: Of course this is not a coincidence and in fact, we are even able to recover the one-loop beta functions from our flow equation. This is possible because the Wetterich equation itself was derived from the one particle irreducible correlations [74].

22: It was shown that the Litim-regulator minimizes this dependence in most cases [82].

23: It picks up the idea by asymptotic safety proposed by Steven Weinberg where the theory flows to a finite UV fixed point. In contrast to asymptotic freedom as seen in QCD this demands for a non-perturbative method.

## 2.4 Criticality in the renormalization group

Up to this point, we introduced two ways to compute the renormalization group flow in theory space in form of the beta functions. Let's now come back to the original goal to explain universality in critical phenomena. The crucial observations of continuous transitions were the self-similar structures and that different systems show the very same critical behavior. Picking up Landau and Ginzburg's idea of an order parameter functional, the renormalization group now allows us to include also fluctuations of this parameter. This significant extension defines the so-called *Landau-Ginzburg-Wilson paradigm* (LGW).

### 2.4.1 Fixed points in the renormalization group flow

In the language of the RG the self-similarity expresses as a fixed-point under the coarse-graining. Strictly speaking, there is a theory  $\mathcal{H}^* = \{g_i^*\}$  which under repeated RG transformations remains the same

$$\mathcal{T}[\mathcal{H}^*] = 0 \quad \Rightarrow \quad \beta(\{g_i^*\}) = 0. \quad (2.42)$$

This known as the *fixed point* (FP) equation. Since the RG transformation tells us about a theory's trajectory in theory space,  $\mathcal{H}^*$  includes fluctuations on all length scales. This feature is exactly what we observe for a continuous transition and therefore  $\mathcal{H}^*$  exhibits so-called *scale invariance*. However, the existence of such fixed point is not sufficient. We also have to require certain properties for its vicinity. Remember that we formulated the QFT in terms of the order parameter fields which expectation values measure a spontaneously broken symmetry. Therefore, if the fixed point marks a critical point between those two phases it has to have exactly one axis in theory space which leads away from it under RG transformations in opposing directions. This direction is called the *critical surface* as shown in Fig. 2.9. Only in this case, the fixed point marks the border between the two described phases of the transition. We can make this requirement more precise with the help of the beta functions. Close to a fixed point  $\{g_i^*\}$  the RG flow can be linearized

$$\frac{dg_i}{d \ln \mu} = B_i^j (g_j - g_j^*) + \mathcal{O}(\{g_i\}^2), \quad (2.43)$$

with summation over  $j$  implied. The matrix  $B_i^j$  is the *stability matrix* of the fixed point and is computed from the beta functions as

$$B_i^j = \frac{\partial \beta_i}{\partial g_j}. \quad (2.44)$$

In order to find the wanted direction away from the fixed point we change to eigensystem of the stability matrix by explicitly diagonalizing it. We denote the eigendirections by the vectors<sup>24</sup>  $V_\alpha$  and the eigenvalues as  $-\theta_\alpha$ , such that

$$\mathbb{B} V_\alpha = -\theta_\alpha V_\alpha. \quad (2.45)$$

Note that we assigned an additional minus sign to the eigenvalues in our notation such that positive (negative) eigenvalues signal an infrared repulsive

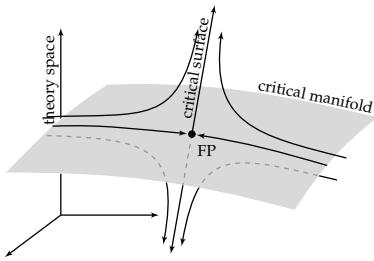


**Figure 2.9:** Depiction of the RG flow in theory space near a critical point. Once the flow hits the critical manifold it will eventually flow into the fixed point (FP). This region is sometimes also called the *basin of attraction*. If it comes only close it will get close to the FP, slow down and eventually depart to one of the phases along the critical surface.

24: Usually, we formulate the theory in a way such that least one vector  $V_\alpha$  has only one non-trivial component explicitly along the phase transition. Of course, a further analysis can show that this is not possible and operators of the original theory mix in all eigendirections.



(attractive) direction. Consequently, close to the fixed point we can integrate out Eq. (2.43). Starting at scale  $\mu_0$ , the flow takes a comprehensive form in the eigensystem as

$$g_i = g_i^* + \sum_{\alpha} C_{\alpha} V_{\alpha,i} \left( \frac{\mu_0}{\mu} \right)^{\theta_{\alpha}}, \quad (2.46)$$

where  $C_{\alpha}$  is an integration constant. The eigenvalues  $\theta_{\alpha}$  allow for a simple classification of the type of direction into three categories. We follow the renormalization group flow towards larger scales to a theory in the infrared and distinguish

- (i) *Relevant* directions with  $\text{Re } \theta_{\alpha} > 0$ : The flow in this direction leads away from the fixed point,
- (ii) *Marginal* directions with  $\text{Re } \theta_{\alpha} = 0$ : There is no flow in this direction (at least to level of precision and
- (iii) *Irrelevant* directions with  $\text{Re } \theta_{\alpha} < 0$ : The flow in this direction is attracted to the fixed point.

Irrelevant directions which lead to a fixed point define a *critical manifold*, see Fig. 2.9. Besides these categories, a direction (or better its corresponding operator) can also be *dangerously irrelevant*. In this case, either the eigenvalues dependence on this operator is non-analytic or it picks up corrections during the RG flow and turns from irrelevant in the ultraviolet to relevant at long distances in the infrared-limit<sup>25</sup>. In these terms, a fixed point, corresponding to a critical point, has to have exactly one relevant direction while the others are irrelevant. The subspace defined by the latter is often called *basin of attraction*. The only positive eigenvalue also sets the correlation-length exponent  $\nu$  since it describes how fast the RG flow departs from the fixed point to one of the phases. In this picture, the least negative and therefore irrelevant eigenvalue  $\omega$  predominantly bounds the speed of the RG flow towards the fixed point from below. Since critical behavior can only be observed when the flow settles in all irrelevant directions, this also effects the correlation length in the vicinity of the fixed point. We incorporate this behavior by refining its power law to

$$\xi \sim |\Delta|^{-\nu} (1 + A|\Delta|^{\omega} + \dots), \quad (2.47)$$

where  $A$  denotes a non-universal constant and  $\Delta$  becomes the leading distance to the fixed point in theory space. The new exponent  $\omega$  describes the *corrections to scaling* and becomes essential for the extraction of critical exponents from experiment [61].

In this elaborate discussion hides one crucial observation: not the fixed point itself determines the critical behavior but its vicinity. On top of that, it turns out to be a universal quantity because the stability matrix only depends on derivatives of the beta functions and is therefore unaffected by any re-scaling of the couplings.

While the beta functions describe how the couplings and mass renormalize under RG transformations, the wave function itself renormalizes by its renormalization constants is  $Z_{\phi}$ <sup>26</sup>. Assuming the scaling behavior of the two-point correlator in Eq. (2.9), this enables us to compute the anomalous

25: In either case, it leads to a violation of the hyperscaling relation of the critical exponents  $\alpha$ ,  $\nu$  and  $\eta$  [61].

26: In the one loop perturbative renormalization at  $d = 4 - \epsilon$  dimension the renormalization constant  $Z_{\phi} = 1 + \mathcal{O}(2\text{-loop})$ . The first non-trivial contribution enters at two loops.

dimension to

$$\eta_\phi = \left. \frac{d \ln Z_\phi}{d \ln \mu} \right|_{g_i=g_i^*}. \quad (2.48)$$

Finally, we can also give a more precise definition of universality. Since the RG operates in theory space pushing us from a microscopic theory to effective ones at larger scales any flow which hits the basin of attraction on its way will eventually flow into the fixed point and therefore share the very same critical behavior. In this way, the renormalization group allows us to group these theories into one universality class described by the fixed point and uniquely label them by the eigenvalues and the renormalization of the wavefunction in form of the anomalous dimension  $\eta$ .

### 2.4.2 Brief review of its success

The two presented renormalization group approaches to the Ising model can easily be generalized to the entire class of the seminal  $O(N)$ -model criticality. However, these are by far not the only theoretical methods to compute critical exponents and we also missed to compare the numbers with the experiment. Other complementary methods include (quantum) Monte-Carlo simulations which do not employ the RG and can make precise predictions just from simulating microscopic Hamiltonians. The trade-off is that these are often computationally expensive and if – other than for the  $O(N)$ -model – also fermions are involved, suffer from the infamous sign problem [20, 21]. In the following, we want to compare the critical exponents of the controversial [91, 92]  $O(2)$ -model where besides the theoretical computations also experimental data are available.

At the time being, the most precise numbers are achieved from the conformal bootstrap [14, 93, 94]. In this branch of conformal field theory, the scale invariance of the fixed point is elevated to a conformal field theory<sup>27</sup>. The crucial feature of any conformal field theory is that it is defined only by a finite number of so-called primary fields and their scaling dimensions which are closely related to the anomalous dimensions we introduced above. The conformal bootstrap exploits the conformal symmetry of the correlators and the invariance of different operator product expansion (OPE) channels. This way, one can formulate a set of complicated non-trivial equations. The main goal then is to solve them by a sophisticated computer aided optimization process which practically excludes more and more field theories which do not fulfill these equations. This narrows down the set of feasible field theories to small bounds on the scaling dimensions with unprecedented precision [96]. These bounds can be considered as the “final verdict” on the corresponding universality class [91]. The most recent estimates for the  $O(2)$ -model are available in Ref. [92].

In comparison, the estimates from the perturbative renormalization group were pushed to the sixth loop order with a sophisticated subsequent resummation of the epsilon expansions [97, 98]. Only this way they can compete quantitatively with the other methods. We will explore some of the used resummation techniques in the next Chapter. The non-perturbative renormalization group results (FRG) as employed in Section 2.3.3 in the LPA' are already in the vicinity of the other methods but need a refinement of the

27: Not every scale invariant field theory is conformal, but conformal invariance also implies scale invariance [13, 95].

**Table 2.1:** Table of the critical exponents of the O(2) universality class. Across the presented methods, we see a very good agreement with conformal bootstrap leading in precision [92]. Note that the FRG in the LPA' truncation provides a wrong anomalous dimension which has to be fixed by expanding in higher orders in the derivative expansion [99]. The last exponent  $\omega$  denotes the subleading exponent measuring the corrections to scaling. Unfortunately, the experimental data lies outside the conformal bootstrap bound and triggered an discussion [91].

Method	Year	$\nu$	$\eta$	$\omega$
$\epsilon$ -expansion (6-loop, Borel-resummed) [97]	2017	0.6690(10)	0.0380(6)	0.804(3)
$\epsilon$ -expansion (6-loop, Meijer-resummed) [98]	2020	0.66953	0.03824	0.80233
Functional RG (LPA'18 see Sec. 2.3.3)		0.686	0.0437	0.735
Functional RG (derivative exp. $\mathcal{O}(\partial^4)$ ) [99]	2020	0.6716(6)	0.0380(13)	0.791(8)
Monte-Carlo (hybrid Metropolis-Cluster) [101]	2019	0.67169(7)	0.03810(8)	0.789(4)
Monte-Carlo (worm-type MC) [102]	2019	0.67183(18)	0.03853(48)	0.789
Conformal bootstrap [92]	2020	0.67175(22)	0.038176(22)	0.794(8)
Experiment (lambda point in He <sup>4</sup> ) [100]	2003	0.6709(1)	–	–
Experiment (XY-Ferromag. in Gd <sub>2</sub> IFe <sub>2</sub> ) [103]	1995	0.671(24)	0.034(47)	–

derivative expansion to higher orders in  $\mathcal{O}(\partial)$ . The comprehensive study in Ref. [99] shows that this extension improves the precision significantly.

Finally, as mentioned in the beginning of this Chapter universality can be also observed experimentally. Partially triggered by the tremendous agreement of this many complementary theoretical methods, a sample of He<sup>4</sup> was brought to the space shuttle in order to study the specific heat of helium at sub-nano-Kelvin temperatures at the lambda point [100]. The vicinity of this point falls into the O(2)-universality class and we compare it with the theoretical methods in Tab. 2.1. While we can admire the astonishing agreement of different theoretical methods, it's painfully obvious that the experimental results are excluded by the conformal bootstrap bounds. This raised an on-going discussion if the experimental estimates stem from an technical or physical error. In the light of the unprecedented agreement across theoretical methods especially from the conformal bootstrap any other option seems no longer viable [91].



# Gross-Neveu universality in graphene and beyond

# 3

The remarkable success in determining the bosonic universality classes proves the quantitative precision across all methods on critical phenomena. For fermionic systems, however, the situation is much less explored. This might be also due to a long standing lack of physical motivation for corresponding quantum field theories. Lately, quantum critical points which feature besides the bosonic order parameter fluctuations also additional gapless fermion degrees of freedom, got more and more attention (for a nice recent overview see Ref. [15]). From the renormalization group point of view, one of the simplest purely fermionic QFTs is the Gross-Neveu model which was developed and studied by David Gross and André Neveu as a toy model to explain the strong interaction in quantum chromodynamics [104]. It can be understood as a two dimensional correspondent to the Nambu-Jona-Lassino model, previously proposed in the context of BCS theory for superconductivity [105]. Both models incorporate a high degree of symmetry which is emergent in the described physical systems at low energies, including relativistic and chiral invariance [106]. Similar as in the related Thirring model [107], the Lorentz invariant Grassmann fields interact via a 4-fermi term in the Lagrangian. As a prime example of a fermionic universality class, we focus in this project on the  $(2+1)d$  chiral Ising Gross-Neveu universality from the renormalization group point of view. Corresponding quantum transitions can also be realized in systems with interacting fermions such as  $\pi$ -flux or honeycomb lattices [108].

Following the works by I. Herbut [106, 109, 110], at first we go a few extra miles and motivate this class of field theories from interacting electrons in the material graphene. Due to its honeycomb lattice the low-energy spectrum provides gapless Dirac fermions which form a semi-metallic phase. We will show that short-range interactions of different kind, from on-site to next-to-nearest neighbor, trigger phase transitions to non-trivial gapped long-range orderings. We explore how these transitions can be captured and studied by semi-phenomenological quantum field theories such as the Gross-Neveu models and its ultraviolet complete siblings.

By now, the perturbative renormalization group (pRG) has been employed for up to four-loop calculations for Gross-Neveu and similar models in Refs. [111–114]. Despite these promising developments, however, no satisfactory agreement across different theoretical methods has been found for the fermionic universality classes, yet. A major obstacle from the pRG perspective, is that the obtained epsilon expansions also entail a problem known from the bosonic models: they are asymptotically divergent. This means that starting from 4-epsilon dimensions a naïve extrapolation to 2+1 dimensions is not straightforwardly promising. Fortunately, some of these difficulties can be controlled by a sophisticated resummation as discussed in the following for the chiral Ising universality class.

*The content of this Chapter's Sections 3.3 to 3.7 was published in Ref. [55] and is a result of collaboration of the author with Luminita N. Mihaila and Michael M. Scherer. The formulations and figures were kept unchanged and only updated in a few cases by new developments or for better readability. Intermediately added sentences*

3.1 Dirac fermions in graphene ..	24
3.2 Effective field theory from interactions .....	26
3.3 The Gross-Neveu-Yukawa model .....	28
3.4 Perturbative renormalization group analysis .....	29
3.5 Resummation towards $d = 3$ ..	32
3.6 Discussion .....	42
3.7 Conclusion and Outlook .....	46

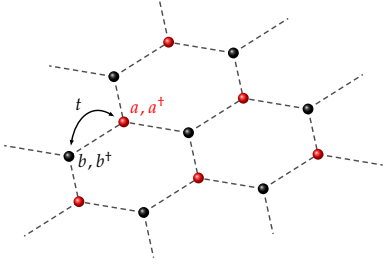


**Figure 3.1:** The honeycomb lattice of graphene can be constructed of two triangular sub-lattices (here: red and black) where electrons can hop with amplitude  $t$  between nearest neighbors.

1: Award with a Nobel prize in physics in 2010. A. K. Geim was also awarded with the infamous Ig-Nobel prize (For experiments that should never be repeated. He let a frog levitate in a strong magnetic field.) and is therefore the only one who won both prizes.

2: The existence of two dimensional materials were believed to be impossible since L. D. Landau and R. Peierls [115] (later extended by Mermin [116] and after that more generally formulated in the Mermin-Wagner-Hohenberg-theorem [117]) showed theoretically that  $2d$  crystals are thermodynamically unstable. A comprehensive answer why we still observe graphene can be found in Ref. [118].

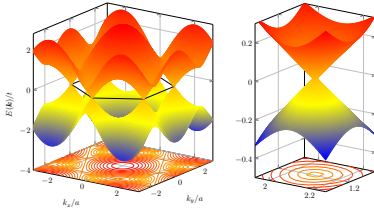


**Figure 3.2:** Dispersion of graphene from the nearest neighbor tight-binding Hamiltonian in Eq. (3.1) where the energy was normalized to the hopping amplitude  $t$ .

3: For a great and pedagogical derivation, read the lecture notes in Ref. [119] (by Nobel laureate Anthony Leggett).

are tagged by  $/*[...]*/$ . A physical motivation was added in Sections 3.1 to 3.2 for the sake of an enhanced comprehensibility.

### 3.1 Dirac fermions in graphene

The material graphene has an astonishing history and a successful academic career both as a theoretical playground as well as an experimental platform for low-dimensional condensed matter physics [25, 27]. Its possible applications range from high temperature superconductor to more recently as promising candidate in future battery technology [28].

Graphene, first fabricated by A. K. Geim and N. K. Novoselov [22, 24] in 2004<sup>1</sup>, consists of a single layer of carbon atoms which formate to honeycomb shaped lattice. The two dimensional<sup>2</sup> lattice is constructed by two triangular sub-lattices (see red and black atoms in Fig. 3.1). The tight-binding Hamiltonian reads

$$\mathcal{H}_0 = -t \sum_{\langle i,j \rangle, \sigma} \left( a_{i,\sigma}^\dagger b_{j,\sigma} + \text{h.c.} \right), \quad (3.1)$$

which accounts for hopping with amplitude  $t$  between the sub-lattices A and B (represented by creation/annihilation operators  $a_i^\dagger$  ( $b_j$ ) at site  $i$  ( $j$ )). Additionally, we allow the electrons to have spin  $\sigma \in \{\uparrow, \downarrow\}$ .

Without going through the calculations of this model in detail<sup>3</sup>, we directly jump to the full energy dispersion of the first Brillouin zone (BZ) as shown in Fig. 3.2 (left). At the corners of the hexagonal BZ, we see that the two bands touch and form isotropic *Dirac cones* as the zoom on the right in Fig. 3.2 reveals. One could expect this to be an oversimplified vintage model but at the latest, the experimental verification of gapless Dirac fermions as dominating charge carriers startet a new ‘gold rush’ [23]. From the theory perspective, the visually apparent feature of the dispersion comes along with a non-trivial mathematical structure. We can explore it by focusing on these special points of the first Brillouin zone and restrict ourselves to the low-energy excitations in the vicinity.

For charge neutral graphene the chemical potential lies exactly at the energy of the touching point and enables us to write down an effective theory by keeping only the Fourier modes near the Dirac points  $\mathbf{K}$  in the BZ, i.e. we expand the Hamiltonian for  $\mathbf{q} \simeq \mathbf{K}$

$$\begin{aligned} \mathcal{H}_{0,\mathbf{K}} &= v_F \sum_{\mathbf{q} \simeq \mathbf{K}, \sigma} \psi_{\mathbf{q} \simeq \mathbf{K}, \sigma}^\dagger \begin{pmatrix} 0 & q_x - iq_y \\ q_x + iq_y & 0 \end{pmatrix} \psi_{\mathbf{q} \simeq \mathbf{K}, \sigma} \\ &= v_F \sum_{\mathbf{q} \simeq \mathbf{K}, \sigma} \psi_{\mathbf{q} \simeq \mathbf{K}, \sigma}^\dagger [\boldsymbol{\sigma} \cdot \mathbf{q}] \psi_{\mathbf{q} \simeq \mathbf{K}, \sigma}, \end{aligned} \quad (3.2)$$

with  $\psi_{\mathbf{q} \simeq \mathbf{K}, \sigma} = (a_\sigma(\mathbf{K} + \mathbf{q}), b_\sigma(\mathbf{K} + \mathbf{q}))^T$ . The unexpected fact that we can express the Hamiltonian in terms of the Pauli matrices  $\boldsymbol{\sigma} = (\sigma_x, \sigma_y)$  is already a non-trivial feature of the low energy model. Additionally, we introduced the Fermi velocity  $v_F = 3ta/2$  which directly describes the slope of our linear dispersion. Since there are two inequivalent Dirac points  $\mathbf{K}$  and  $-\mathbf{K}$ , the total effective Hamiltonian is given by  $\mathcal{H}_{0,\mathbf{K}} + \mathcal{H}_{0,-\mathbf{K}}$  or, more conveniently, we

compose one  $4 \times 4$  matrix with the corresponding four component *spinor*

$$\Psi_{q,\sigma} \equiv (\Psi_{+, \sigma}, \Psi_{-, \sigma})^T = (a_{\mathbf{K}+q, \sigma}, b_{\mathbf{K}+q, \sigma}, a_{-\mathbf{K}+q, \sigma}, b_{-\mathbf{K}+q, \sigma})^T. \quad (3.3)$$

Note that we further implemented the notation  $q_{\pm} = (\pm q_x, q_y)$  in accordance to the local coordinate systems at the corners  $\pm \mathbf{K}$  of the Brillouin zone as shown in Fig 3.3. In case we also take the spin degree of freedom in to account, the number of components is doubled, i.e. we are left with an 8-component spinor. In the following analysis, we will call this case the  $N = 8$  *graphene case*. The full effective low energy Hamiltonian then reads

$$\begin{aligned} \mathcal{H}_{\text{eff}} &= v_F \sum_{q,\sigma} \Psi_{q,\sigma}^\dagger \left[ q_x \begin{pmatrix} \sigma_x & 0 \\ 0 & -\sigma_x \end{pmatrix} + q_y \begin{pmatrix} \sigma_y & 0 \\ 0 & \sigma_y \end{pmatrix} \right] \Psi_{q,\sigma} \\ &= v_F \sum_{q,\sigma} \Psi_{q,\sigma}^\dagger [q_x \gamma_1 + q_y \gamma_2] \Psi_{q,\sigma}. \end{aligned} \quad (3.4)$$

Here, we introduced the matrices  $\gamma_1 = \sigma_z \otimes \sigma_y$  and  $\gamma_2 = \mathbb{1}_2 \otimes \sigma_x$  which inherit the anti-commutation rule from the Pauli matrices  $\{\gamma_1, \gamma_2\} = 0$ . It turns out, that these matrices together with  $\gamma_0 = \mathbb{1}_2 \otimes \sigma_z$  in  $2 + 1$  dimensions form the *graphene* representation<sup>4</sup> of the *Clifford algebra* [109]

$$\{\gamma_\mu, \gamma_\nu\} = 2\delta_{\mu\nu} \mathbb{1}_4 \quad \text{with } \mu, \nu = 0, 1, 2. \quad (3.5)$$

This non-trivial result shows that the effective low energy theory of electrons in graphene at half filling is described by the Dirac equation [120] for massless relativistic fermions. The inherited Lorentz symmetry is a powerful, and for a lab-system unexpected, feature which explains the measured conductivity properties of graphene. The latter make this material a promising candidate for many electronic devices [28].

Before we continue our analysis by including interactions, let us analyze the symmetries of this model a bit further. First of all, there is the usual  $U(1)_{\text{ch}}$  phase-rotational symmetry  $\Psi \mapsto \Psi e^{i\theta}$  which is required by charge conservation but in this case even separately for each Dirac cone and spin. Besides, our system also shows an easy to imagine sublattice-exchange symmetry of the honeycomb lattice. It replaces red with black and vice versa in Fig. 3.1 or, on the level of the sublattice operators,  $a \leftrightarrow b$ . In the language of our spinors  $\Psi$  this transformation is in fact a  $\mathbb{Z}_2$  (Ising) reflection symmetry

$$\Psi \rightarrow (\mathbb{1}_2 \otimes \gamma_2) \Psi. \quad (3.6)$$

For book keeping, note that the system also shares a time reversal symmetry [109]. All these symmetries can be broken by a mass term proportional to the corresponding generators and open a gap at the Dirac point. We illustrate this mechanism a bit further in the next Section. At the moment, all these symmetries are preserved and we generalize to  $d$  space-time dimensions for later purpose in the proceeding LGW analysis. By casting the spinors  $\Psi$  into fermionic massless quantum fields, we obtain the following action

$$\mathcal{S}_0 = \int d^{d-1}x d\tau \bar{\Psi} (\mathbb{1}_2 \otimes \gamma_\mu) \partial_\mu \Psi, \quad (3.7)$$

where the fields  $\Psi = \Psi(x)$  are now defined in real space upon a Fourier transformation. Note that the Lorentz symmetry is expressed in the  $d$ -dimensional derivative  $\partial_\mu = (\partial_\tau, \nabla_{d-1})$ . On top of that, we summarized

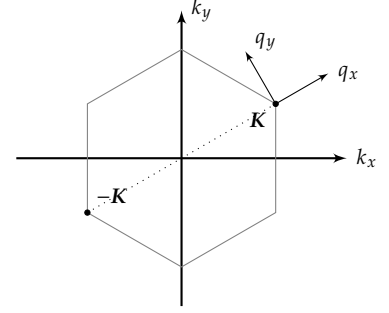


**Figure 3.3:** Brillouin zone (BZ) of the tight-binding model for graphene. At the corners of the BZ, the dispersion forms linear isotropic so-called *Dirac cones*. Since there are two inequivalent corners (here  $\pm \mathbf{K}$ ) the full effective low energy physics is composed by these two decoupled valleys. In the vicinity of point  $\pm \mathbf{K}$ , we introduced the wavevector  $q_{\pm} = (\pm q_x, q_y)$ .

4: Note, that this representation is reducible and there two further  $4 \times 4$  matrices that anticommute with all three  $\gamma_\mu$ , namely  $\gamma_3 = \sigma_x \otimes \sigma_y$  and  $\gamma_5 = \sigma_y \otimes \sigma_x$  [109].

the spinors into the 8-component vectors in the additional notation  $\bar{\Psi} = \Psi^\dagger(\mathbb{1}_2 \otimes \gamma_0)$ .

### 3.2 Effective field theory from interactions

The quasi-relativistic Dirac fermions found in the tight-binding model are a direct consequence of the lattice symmetries and accordingly endowed with the corresponding symmetries. In the sense of the LGW paradigm, we can now ask how interactions on the lattice spontaneously break these symmetries to different ordered ground states. Since the density of states vanishes at half filling, the screening of the electrons is negligibly small [106, 109, 110]. Furthermore, the  $p_z$  orbitals strongly localize at the lattice sites. In the atomic limit [106], the interactions are therefore dominated by density-density Coulomb repulsion [109]. We model these properties with the following interaction Hamiltonian

$$\mathcal{H}_{\text{int}} = \sum_{i,j,\sigma,\sigma'} n_{i,\sigma} \left[ U\delta_{ij} + \frac{e^2(1-\delta_{ij})}{4\pi|\mathbf{r}_i - \mathbf{r}_j|} \right] n_{j,\sigma'}, \quad (3.8)$$

where  $U$  denotes the on-site interaction strength,  $e$  the charge of the electrons and  $n_{i,\sigma} = \langle c_{i,\sigma}^\dagger c_{i,\sigma} \rangle$  (for  $c \in \{a, b\}$ ) the density operator at site  $\mathbf{r}_i$  with spin  $\sigma$ . At short distances, the non-local interactions will contribute the most and we can restrict ourselves to interactions up to next-to-nearest-neighbor interactions

$$\mathcal{H}_{\text{int}} \approx U \sum_i n_{i,\uparrow} n_{i,\downarrow} + V_1 \sum_{\langle i,j \rangle, \sigma, \sigma'} n_{i,\sigma} n_{j,\sigma'} + V_2 \sum_{\langle\langle i,j \rangle\rangle, \sigma, \sigma'} n_{i,\sigma} n_{j,\sigma'}. \quad (3.9)$$

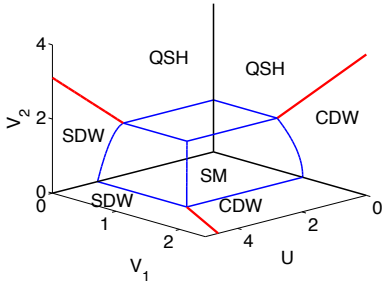


**Figure 3.4:** Mean-field phase diagram of Hubbard model on the honeycomb lattice [121].

This extended Hubbard model on the honeycomb lattice shows three phases distinct from the semi-metallic ground state, as shown in the mean field diagram from Ref. [121] in Fig. 3.4. For large on-site interaction  $U$ , the spins will order anti-ferromagnetically in a *spin density wave* (SDW), while for large nearest-neighbor interactions  $V_1$  the system favors a *charge density wave* (CDW). Tuning only  $V_2$  the system transfers to a quantum spin hall state (QSH) [121].

We depict the charge density wave order in Fig 3.5 but the ordering for a spin density wave just replaces the charge modulation by an anti-ferromagnetic spin modulation. It is easy to convince ourselves that these orderings break the sublattice symmetry (3.6) of semi-metallic graphene. A thorough analysis of all possible symmetry breaking patterns by interactions in graphene can be found in Ref. [106]. For this project, we focused on the CDW transition in particular.

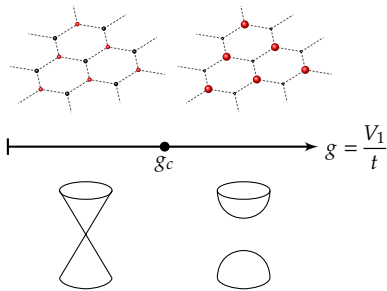


**Figure 3.5:** Interaction induced gap to the CDW phase in graphene. When the system crosses the critical ration  $g_c$  it orders to a charge density wave.

According to the mean field analysis, we only consider finite nearest-neighbor interactions  $V_1$  and realize that we can rewrite this term of the Hamiltonian in the following way

$$\mathcal{H}_{V_1} = \frac{V_1}{4} \sum_{\langle i,j \rangle, \sigma, \sigma'} [(n_{i,\sigma} + n_{j,\sigma'})^2 - (n_{i,\sigma} - n_{j,\sigma'})^2] \quad (3.10)$$

From this simple rearrangement, it is obvious that for strong interactions  $V_1 \gg t$  the system will favor a spatial modulation of the densities, i.e. the



charge density wave. We can express the two density terms by the spinors as

$$n_i + n_j = \Psi^\dagger \Psi \quad n_i - n_j = \Psi^\dagger (\mathbb{1}_2 \otimes \sigma_3) \Psi. \quad (3.11)$$

Since the terms are symmetric upon another transformation of the spinors, for the further field-theoretical analysis, it is sufficient to summarize them into one term in the action [106]. This finally brings us to the *Gross-Neveu* model with the action

$$\mathcal{S}_{\text{GN}} = \int d^{d-1}x d\tau \mathcal{L}_{\text{GN}} = \int d^{d-1}x d\tau \left( \bar{\Psi} (\mathbb{1}_2 \otimes \gamma_\mu) \partial_\mu \Psi + \frac{1}{2} g (\bar{\Psi} \Psi)^2 \right), \quad (3.12)$$

where  $g$  now denotes the coupling of the four-fermion interaction term. Originally, as mentioned in the introduction of this Chapter, David Gross and André Neveu discussed this action at length as a toy model for strong interactions in the QCD. In their seminal paper [104], they were mostly interested in a playground to study chiral symmetry breaking which in this model manifests in the following discrete chiral symmetry

$$\Psi \rightarrow \gamma_5 \Psi, \quad \bar{\Psi} \rightarrow -\bar{\Psi} \gamma_5, \quad (3.13)$$

where  $\gamma_5 = \sigma_y \otimes \sigma_y$  in the graphene representation. The Gross-Neveu model is (perturbatively) renormalizable in  $1+1$  dimension and due to its relatively simple<sup>5</sup> vertex structure it was studied in a  $d = 2 + \epsilon$  expansion up to the four loops [111]. At one-loop order the beta function of  $g$  reads

$$\beta_g = \epsilon g - (N-2) \frac{g^2}{\pi} + \mathcal{O}(g^3) \quad (3.14)$$

and shows a fixed point at  $g^* = \pi\epsilon/(N-2)$ . According to Eq. (3.13), we identify the expectation value  $\langle \bar{\Psi} \Psi \rangle$  as the system's order parameter for the chiral symmetry breaking. The fixed point corresponding to  $V_c$  in Fig. 3.5 distinguishes between two phases with  $\langle \bar{\Psi} \Psi \rangle = 0$  (semi-metallic phase) and  $\langle \bar{\Psi} \Psi \rangle \neq 0$  (the charge density wave) where the latter opens up a mass gap with  $m = \sqrt{g} \langle \bar{\Psi} \Psi \rangle$ . This is one renormalization group angle on the Gross-Neveu universality. In perturbative analysis, it was pushed recently to the fourth loop order [111] such that the critical exponents for  $N = 8$  component spinors in the  $(2 + \epsilon)$  expansion read

$$\frac{1}{\nu} = \epsilon - \frac{1}{6} \epsilon^2 - \frac{5}{72} \epsilon^3 + \frac{81\zeta_3 + 35}{216} \epsilon^4 + \mathcal{O}(\epsilon^5), \quad (3.15)$$

$$\eta_\phi = 2 - \frac{4}{3} \epsilon - \frac{7}{36} \epsilon^2 + \frac{7}{54} \epsilon^3 + \frac{1092\zeta_3 + 91}{5184} \epsilon^4 + \mathcal{O}(\epsilon^5), \quad (3.16)$$

$$\eta_\psi = \frac{7}{72} \epsilon^2 - \frac{7}{432} \epsilon^3 + \frac{7}{10368} \epsilon^4 + \mathcal{O}(\epsilon^5). \quad (3.17)$$

Again, in this notation the bosonic anomalous dimension corresponds to the charge density wave order. Expressions for general  $N$  are available in Appendix C.1.2 or Ref. [111].

Similar transitions and their properties were discussed recently. For further reading on this topic we refer to Refs. [15, 122–125] and references therein.

5: “Simple” in this context means, it is closed under RG transformations and there are no further terms and couplings generated in the RG process. For implementations of the Gross-Neveu model with terms of higher symmetry like a chiral XY or chiral Heisenberg symmetry this does not hold and in these cases a  $(2 + \epsilon)$  expansion demands a careful elaborate analysis where more than one coupling has to be taken into account.

### 3.3 The Gross-Neveu-Yukawa model

Since the order parameter in the chiral symmetry breaking towards the charge density wave is bosonic we can directly construct a semi-phenomenological model [126] for the phase transition in the spirit of the LGW paradigm as applied for the  $\phi^4$  theories. For this purpose, we consider a now fluctuating order parameter field  $\phi(x)$  with a kinetic term<sup>6</sup> and add a quartic interaction term which stabilizes the renormalization. For this work, we focus on the chiral Ising Gross-Neveu-Yukawa model which again for  $N = 8$  component spinors describes the continuous transition of graphene from the semi-metallic phase to a charge density wave as discussed above. We directly jump ahead to the Lagrangian which reads

$$\mathcal{L}_{\text{GNY}} = \bar{\psi} \not{\partial} \psi - \frac{1}{2} (\partial_\mu \phi)^2 + \frac{m^2}{2} \phi^2 + \sqrt{y} \phi \bar{\psi} \psi + \lambda \phi^4, \quad (3.18)$$

where  $y$  denotes the Yukawa coupling of the of the order parameter field  $\phi$  to the massless fermion  $\psi$ . The discrete chiral symmetry (3.13) of the Gross-Neveu model is extended to the bosonic field to

$$\psi \rightarrow \gamma_5 \psi, \quad \bar{\psi} \rightarrow -\bar{\psi} \gamma_5, \quad \phi \rightarrow -\phi. \quad (3.19)$$

*/\*In fact, the Gross-Neveu-Yukawa theory can also be derived from the Gross-Neveu model by a Hubbard-Stratonovich transformation and subsequently allowing for a canonical kinetic term as well as a quartic  $\phi^4$  interaction. The latter stabilizes the renormalization and renders the GNY model perturbatively renormalizable in  $d = 4 - \epsilon$  space-time dimensions. In this regard, the GNY model is deduced as the ultraviolet completion of the Gross-Neveu model [127], a relation which already suggests that both models not only lie in the same universality class but are even analytically linked. This statement is supported by matching the large- $N$  expansions of both theories [127] at any dimension  $d \in (2, 4)$ . A feature which puts us in an excellent position to study the universality at  $d = 2 + 1$ , i.e. exactly between the two critical dimensions of both models.*

*In the Lagrangian in Eq. (3.18) we have assumed, without further elaboration, that the bosonic order parameter field inherits the Lorentz symmetry of the Dirac fermions. Thus, we have also defined the dynamical critical exponent to be  $z = 1$ . However, it remains open whether the Lorentz symmetry is emergent. A one-loop RG calculation [128] shows that at least near 3+1 dimensions it is protected against perturbative corrections of the fermionic velocity  $v_F$  and the bosonic velocity  $v_B$  away from the speed of light  $c$ . Although these two irrelevant directions flow at different rates towards  $c$ , this implies that Lorentz Symmetry is restored in the infrared.\* /*

#### What is known about Gross-Neveu universality?

In view of the successful description of the critical behavior of the three-dimensional  $O(N)$  models, it is tempting to believe that a similar precision can also be achieved for the case of the comparatively simple three-dimensional Gross-Neveu models. Indeed, there has been promising progress in the development of the various methods, recently, suggesting that the consensual precision determination of the Gross-Neveu universality classes is within reach

6: This dynamical degree of freedom would also be generated once we run the renormalization group.

- ▶ Numerical approaches have found sign-problem free formulations for the calculation of various important quantum phase transitions of interacting Dirac fermions on the lattice [20, 21, 108, 129–135].
- ▶ The conformal bootstrap has emerged as a numerical tool to determine critical exponents for fermionic models [136–139].
- ▶ Nonperturbative field-theoretical methods like the functional renormalization group (FRG) have managed to explore sophisticated truncations schemes [81, 90, 140–143].
- ▶ The perturbative renormalization group (pRG) has seen substantial advances in computational technology and the development of suitable algorithms which facilitate the calculation of higher-loop orders.

In this Chapter, we perform a thorough analysis of resummation and interpolation techniques within the perturbative renormalization group approach to extract quantitative renormalization group predictions for the critical exponents. We show that this strategy reconciles discrepancies between the conformal bootstrap results from Ref. [139] and the pRG calculations, but not with Quantum Monte Carlo simulations. To that end, we focus on the simplest version of the Gross-Neveu-Yukawa models, i.e. the chiral Ising model [144], which in  $2 < d < 4$  lies in the same universality class as the purely fermionic Gross-Neveu model [127, 145]. Even this simplest model has a number of interesting applications. Most prominently, for  $N = 8$ , the theory describes the quantum critical point of the semimetal-to-insulator transition of spin-1/2 electrons on the graphene lattice. In the insulating phase sublattice symmetry is broken and charge density wave (CDW) order occurs [109]. The eight spinor components originate from the two sublattices of the honeycomb lattice, the two inequivalent Dirac points in the Brillouin zone and two spin projections of the spin-1/2 electrons.

Another application of the Gross-Neveu model is the case of  $N = 4$ . According to the counting of spinor components in the graphene case, this corresponds to a model of spinless fermions on the honeycomb lattice. Strong repulsive nearest-neighbor interactions also drive the spinless system through a semimetal-to-insulator transition [121]. This simplified version of graphene is accessible to a broad range of different numerical methods with reduced computational cost and therefore has been extensively studied, previously [20, 90, 112, 113, 129–131, 139, 141, 146]. For  $N = 1$ , it has been argued that in  $d = 3$  a minimal  $\mathcal{N} = 1$  superconformal theory emerges from the Gross-Neveu-Yukawa model at the quantum critical point which might be relevant at the boundary of a topological phase [146, 147].

### 3.4 Perturbative renormalization group analysis

We proceed with the perturbative renormalization group analysis of the Gross-Neveu-Yukawa model. Similar as shown for the Ising model discussed in Sec. 2.3.2, we employ a dimensional regularization in the modified minimal subtraction (MS) scheme for the renormalization group. Since, the number of diagrams in this loop expansion grows factorially, the usage of computer aided algebra is necessary and we refer to App. B.1 for a brief overview of the challenges and concepts to overcome them. While up to two loops this tool chain may seem over-engineered, only this way it was possible to push the calculation to four loops which demands the computation of 31,671

diagrams [113]. In the following, we set the stage for the actual fixed point analysis and the resummation of the epsilon expansions.

The renormalized Lagrangian can be obtained by replacing fields and couplings by their bare counterparts  $x \rightarrow x_0$  for  $x \in \{\psi, \phi, y, \lambda, m\}$  and reads

$$\mathcal{L}_{\text{GNV}} = Z_\psi \bar{\psi} \not{\partial} \psi - \frac{1}{2} Z_\phi (\partial_\mu \phi)^2 + Z_{\phi^2} \frac{m^2}{2} \phi^2 + Z_{\phi\bar{\psi}\psi} \sqrt{y} \mu^{\epsilon/2} \phi \bar{\psi} \psi + Z_{\phi^4} \lambda \mu^\epsilon \phi^4, \quad (3.20)$$

where we parameterized the energy scale of the RG flow of the couplings with  $\mu$ . Here, we introduced the wave function renormalization constants  $Z_\psi$  and  $Z_\phi$  by rescaling the fields by  $\psi_0 = \sqrt{Z_\psi} \psi$  and  $\phi_0 = \sqrt{Z_\phi} \phi$ . For the couplings and the mass term, we introduced the following renormalized quantities

$$m^2 = m_0^2 Z_\phi Z_{\phi^2}^{-1}, \quad (3.21)$$

$$y = y_0 \mu^{-\epsilon} Z_\psi^2 Z_\phi Z_{\phi\bar{\psi}\psi}^{-2}, \quad (3.22)$$

$$\lambda = \lambda_0 \mu^{-\epsilon} Z_\phi^2 Z_{\phi^4}^{-1}. \quad (3.23)$$

These relations are used to compute the RG scale dependence of the renormalized quantities by taking the derivative with respect to the scale  $\mu$ .

### 3.4.1 Renormalization group functions

The renormalization group functions are now defined from the couplings and respecting renormalization constants as the logarithmic derivative with respect to the scale  $\mu$

$$\beta_x = \frac{dx}{d \ln \mu}, \quad \text{for } x \in \{y, \lambda\}, \quad (3.24)$$

$$\gamma_x = \frac{d \ln Z_x}{d \ln \mu}, \quad \text{for } x \in \{\psi, \phi, \phi^2\}. \quad (3.25)$$

After rescaling a spherical factor from the momentum integral  $x/(8\pi^2) \rightarrow x$  for  $x \in \{y, \lambda\}$ , they take the following form

$$\beta_x = -\epsilon x + \sum_{k=1}^L \beta_x^{(kL)}, \quad \text{with } x \in \{y, \lambda\} \quad (3.26)$$

$$\gamma_x = \sum_{k=1}^L \gamma_x^{(kL)}, \quad \text{with } x \in \{\psi, \phi, \phi^2\} \quad (3.27)$$

where the latter are also often called anomalous dimensions in accordance to the scaling exponents of the fermionic and bosonic correlation functions close to the critical point. Nevertheless, the function  $\gamma_{\phi^2}$  has no such meaningful counterpart, so we will call these functions renormalization group functions to avoid any confusion. Since, the full expressions to four loop order for both beta functions and renormalization group functions become quite lengthy we present here only the one-loop contributions. In the notation, introduced

above they read

$$\beta_y^{(1L)} = (3 + N/2)y^2, \quad (3.28)$$

$$\beta_\lambda^{(1L)} = 36\lambda^2 + Ny\lambda - (N/4)y^2, \quad (3.29)$$

and

$$\gamma_\psi^{(1L)} = \frac{y}{2}, \quad \gamma_\phi^{(1L)} = 2Ny, \quad \gamma_{\phi^2}^{(1L)} = -12\lambda. \quad (3.30)$$

and refer for the full expressions to appendix C.1.1 or Ref. [113]. */\*Additionally, in Appedix A we present the one-loop pRG procedure for a generalized Gross-Neveu-Yukawa model.\**

### 3.4.2 Fixed points and critical exponents

To analyze the critical behavior, we are now looking for a stable fixed point in the beta functions. The flow diagram in Fig. 3.6 shows us that besides the trivial Gaussian fixed point and the Wilson-Fisher fixed point, there is another, non-Gaussian and fully attractive fixed point as required for a critical point. The Wilson-Fisher fixed point lies on the  $y = 0$  axis as expected and is the critical point of the  $O(N)$  models. On the level of the renormalization group functions, we can use this fixed point to perform a consistency check of our loop calculation and compare them to the findings in Ref. [97], both on the level of the epsilon expansions of the critical exponents as well as one the level of the beta functions for  $y = 0$ .

For the critical behavior of the GNY model, we concentrate on the non-Gaussian fixed point which at one loop order reads

$$(y_*, \lambda_*) = \left( \frac{\epsilon}{3 + N/2}, \frac{(3 - N/2 + s)\epsilon}{72(3 + N/2)} \right), \quad (3.31)$$

where  $s = \sqrt{9 + N(33 + N/4)}$ . The critical exponents, i.e. the (inverse) correlation length exponent  $\nu^{-1}$  and the fermionic  $\eta_\psi$  and bosonic  $\eta_\phi$  anomalous dimensions, we obtain from the renormalization group functions by evaluating them at this fixed point. Hence the anomalous dimensions are

$$\eta_\phi = \gamma_\phi(y_*, \lambda_*), \quad \eta_\psi = \gamma_\psi(y_*, \lambda_*). \quad (3.32)$$

For the inverse correlation length exponent, we apply the following relation

$$\nu^{-1} = 2 - \eta_\phi + \eta_{\phi^2}, \quad (3.33)$$

where we defined the value  $\eta_{\phi^2} = \gamma_{\phi^2}(y_*, \lambda_*)$  in the same notation as before. The resulting expressions are expanded in  $\epsilon$  where the coefficients for each critical exponent  $f_k$  of order  $\epsilon^k$  is fixed by the diagrams with  $k$  loops. Schematically, we can write the epsilon expansions of all three critical exponents to loop order  $L$  as

$$f^{\text{GN}(Y)}(\epsilon) = \sum_{k=0}^L f_k^{\text{GN}(Y)} \epsilon^k. \quad (3.34)$$

Here,  $f$  represents one of the three discussed critical exponents, i.e.  $f \in \{\nu^{-1}, \eta_\phi, \eta_\psi\}$  where each coefficient  $f_k$  is a function of the number of spinor

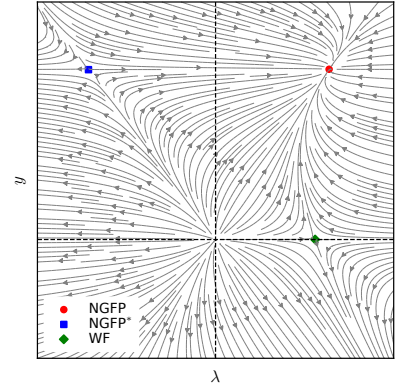


**Figure 3.6:** Renormalization group flow of the perturbatively renormalized Gross-Neveu-Yukawa model. From the one loop beta functions, we identify four fixed points (FPs). The trivial Gaussian fixed point, the Wilson-Fisher (WF) and two non-Gaussian FPs (NGFP\*). Since we search for a stable FP, the critical point is the red non-Gaussian (NGFP). WF is the critical point in the  $O(N)$ -models, but is unstable to the NGFP. In the perturbative renormalization group approach, the one loop calculation sets the topology of the RG flow and inflect it also to the higher loop orders.

components  $N$ . As indicated, this also holds accordingly for the  $(2 + \epsilon)$  expansion of the Gross-Neveu (GN) model as presented for  $N = 8$  in Eq. (3.15) to (3.17). The full expressions for expansions of the critical exponents of the GNY model in  $d = 4 - \epsilon$  can also be calculated analytically, see the ancillary files of Ref. [113] and for the GN model in  $(2 + \epsilon)$  dimensions in App. C.1.2 or in Ref. [111].

*/\*For most  $N$ , these coefficients grow at least factorially with the loop order  $k$  as you can see for example in the case of  $N = 8$  (graphene case) where the epsilon expansions read*

$$\frac{1}{\nu} \approx 2 - 0.952\epsilon + 0.007\epsilon^2 - 0.095\epsilon^3 - 0.013\epsilon^4 \quad (3.35)$$

$$\eta_\phi \approx 0.571\epsilon + 0.124\epsilon^2 - 0.028\epsilon^3 + 0.149\epsilon^4 \quad (3.36)$$

$$\eta_\psi \approx 0.071\epsilon - 0.007\epsilon^2 - 0.024\epsilon^3 + 0.018\epsilon^4. \quad (3.37)$$

*Note that the expression were approximated only to three digits for better readability. In contradiction to a usually faithful Taylor expansion, the coefficients of the higher orders in  $\epsilon$  are not decreasing<sup>7</sup> for larger  $k$ . In fact, they grow and it seems to be debatable to include them in the analysis of the critical exponents towards three dimensions if we would naively extrapolate to  $\epsilon \rightarrow 1$ .*

*This obstacle originates from the vanishing radius of convergence of the epsilon expansions which in turn is a direct consequence of the perturbative expansion in couplings before taking the path integral. Practically, we can see this problem when evaluating the critical exponents away from the expansion point at different orders in  $\epsilon$ . In Fig. 3.7, we plot the bosonic anomalous dimension  $\eta_\phi$  for different loop orders in  $\epsilon \in [0, 1]$ . It is easy to see that the values for increasing  $\epsilon$  are rapidly diverging apart, which seems to make it impossible to determine the critical exponents for large  $\epsilon$  to the interesting case  $d = 3$  ( $\epsilon = 1$ ). But not all hope is lost. In order to extract a quantitative improvement on the precision out of the higher loop orders, a resummation of these so-called asymptotic series is necessary.\* /*

7: In fact, there is an optimal order  $k_{\text{opt}}$  until which the coefficients decline. This stems from an exponential quantum ‘‘Boltzmann’’ factor for the activation energy of the classical solution [148].

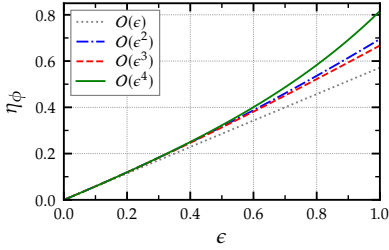


**Figure 3.7:** Naive extrapolation of the bosonic anomalous dimensions  $\eta_\phi$  for  $N = 8$  (graphene case) towards the interesting case  $d = 3$  ( $\epsilon = 1$ ).

### 3.5 Resummation towards $d = 3$

*/\*Our observation that after an initial convergence in the loop order  $k$  the coefficients start to grow for larger  $k$  is seemingly diminishing the significance of the series. Nevertheless, to benefit from the higher loop orders, we have to overcome this issue by means of a resummation. In general, distinguish between two approaches in resummation. In the first one, we focus on dealing solely with the vanishing radius of convergence and make almost no assumptions about the series structure. In the further course of this analysis, we merely assume that the critical exponents are continuous functions between  $d \in (2, 4)$ . In the second approach, we try to incorporate justified presumptions about the series coefficients, especially for large loop orders  $k \gg 1$ .\* /*

#### 3.5.1 Padé approximants

We start our resummation analysis of the chiral Ising critical exponents for general  $N$  by studying the Padé approximants which are rational functions

$$[m/n] = \frac{a_0 + a_1\epsilon + \dots + a_m\epsilon^m}{1 + b_1\epsilon + \dots + b_n\epsilon^n}. \quad (3.38)$$

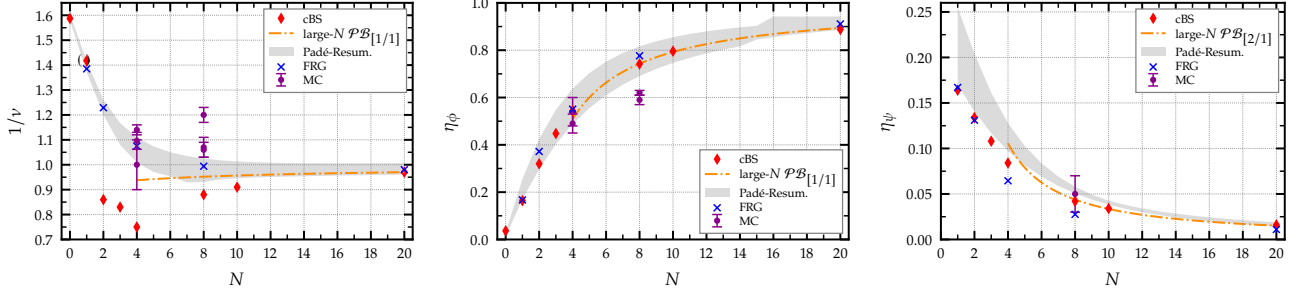


**Figure 3.8:** Chiral Ising universality in  $d = 3$ : Overview plots for the correlation-length exponent  $\nu^{-1}$  (left panel), the boson anomalous dimension  $\eta_\phi$  (medium panel) and the fermion anomalous dimension  $\eta_\psi$  (right panel) for different numbers of spinor components  $N \in [1, 20]$ . For comparison, values from Monte Carlo (MC) calculations, the functional renormalization group (FRG), and the conformal bootstrap (cBS) are also shown. For the large- $N$  results, we applied Padé-Borel resummation. (Figures from Ref. [55] updated by [150, 151])

with  $L = m + n$  where the expansion coefficients  $a_0, \dots, a_m, b_1, \dots, b_n$  are uniquely given by the condition that the series expansion of  $[m/n]$  match the original series

$$[m/n] - \sum_{k=0}^L f_k \epsilon^k = \mathcal{O}(\epsilon^{L+1}). \quad (3.39)$$

At a given order  $L$ , there are  $L + 1$  different Padé approximants and we note that it is not *a priori* clear which of them will give the most faithful estimate. Importantly, Padé approximants can be used for finding approximations to functions outside the radius of convergence  $R$  of their corresponding power series. In particular, the case  $R = 0$  is relevant in the context of the perturbative RG [148, 149]. Further, no assumption about the large-order behavior of the series coefficients is made. Systematically, we compute all  $L + 1$  possible Padé approximants for  $\nu^{-1}$ ,  $\eta_\phi$  and  $\eta_\psi$ . Evaluating them at  $\epsilon = 1$  provides us with a range of estimates which we interpret as a first rough window of confidence for their values. Note again, that at this stage we made no presumptions about the coefficients. We employ this method for the critical exponents from the  $(4 - \epsilon)$  expansion series of the GNY model at four-loop order by evaluating all  $4 + 1$  Padé approximants at  $\epsilon = 1$ , i.e. for  $d = 2 + 1$  dimensions. This provides a range of estimates for the critical exponents, which we interpret as a first rough window of confidence for their values. We show the results of this analysis as a function of  $N$  in Fig. 3.8 as the gray-shaded area. There, we have only taken into account Padé approximants which show no poles in the range  $d \in (2, 4)$ . Since this criterion is not fulfilled by all approximants for a given  $N$ , a sudden enlargement of the window may occur upon changing  $N$ . Such an example can be seen for the correlation length exponent  $\nu^{-1}$  around  $N \approx 7$ . In this case, the pole of one of the approximants is pushed out of the interval  $d \in (2, 4)$ . In the following section, when we consider two-sided Padé approximants, we will also show sequences of Padé approximants to study more carefully the convergence properties of the approximations.

For comparison, we also present the results of other methods for different  $N$  in Fig. 3.8. The functional renormalization group (FRG) [81, 90, 141] provides compatible estimates for  $\nu^{-1}$  and  $\eta_\phi$  over the whole range of  $N$ . On the other hand, the FRG values for the fermionic anomalous dimension  $\eta_\psi$  are systematically below the range we find with Padé approximants. We remark that the FRG calculations in Refs. [81, 90, 141] are based on the derivative expansion scheme and more intricate momentum dependencies

might become important for the evaluation of anomalous dimensions [152, 153]. Comparison to the conformal bootstrap results from Ref. [139] also shows very good compatibility concerning the boson anomalous dimension. Generally, the results for the fermion anomalous dimension lie between the FRG estimates and the window given by the Padé approximants. We show in the next two sections, how this discrepancy can be resolved. The conformal bootstrap results for the correlation length exponents deviate strongly from the other approaches, in particular, in the range  $2 \leq N \leq 8$ . For very small  $N$ , including the limit of the Ising universality class and the emergent SUSY limit ( $N = 1$ ), the estimates agree well with the renormalization group approaches. We note that within the conformal bootstrap method, the boson and fermion anomalous dimensions are obtained from universal bounds. The correlation length exponent estimate, however, is based on the extremal functional approach where one assumes that the theory exactly lives at the characteristic kink and subsequent extrapolation of the spectrum [139]. Therefore, it would be very interesting to obtain conformal bootstrap estimates of the correlations length exponent directly from universal bounds. From Monte Carlo simulations estimates for the Ising Gross-Neveu universality class are available for the cases  $N = 4$  and  $N = 8$ . In particular, the case  $N = 4$  was intensely studied by Monte Carlo methods [20, 129–131, 154] and the resulting estimates still varied with system size. In Fig. 3.8, we show the latest estimates for the correlation length exponent from Refs. [130, 154] for comparison, which agree quite well with the RG estimates, but not with the conformal bootstrap. For the boson anomalous dimension, the latest estimate from Ref. [130] is also in good agreement with the other approaches. For the fermionic anomalous dimension, (when compiling the paper [55]) only a value at  $N = 8$  is available [108], which with  $\eta_\psi \approx 0.38(1)$  is much larger than the estimates from the complementary methods and therefore does not appear in the range presented in the Fig. 3.8. */\*In 2020, a new comprehensive Designer-Monte-Carlo simulation [151] provides  $\eta_\psi \approx 0.05(2)$  which for the first time is in very good agreement with our and other complementary methods. We updated Fig. 3.8 and Tab. 3.1 accordingly.\** Also the  $N = 8$  estimates from Refs. [108, 155] for the correlation length exponent and the boson anomalous dimension are not in agreement with RG or the conformal bootstrap. In the left panel of Fig. 3.8, we also show the recent results from Ref. [154] for the  $N = 8$  correlation length exponent, which is much closer to our result than the one from Ref. [108]. Finally, as another perturbative method we also show the values from a large- $N$  expansion [140, 156] for  $N \geq 4$ . Note that we have resummed these series following reference [156] using the Padé-Borel method. The resulting curves are for most  $N$  deep in the shaded area of the Padé approximants.

### 3.5.2 Interpolations

In Section 3.2, we have introduced the Gross-Neveu model which is expanded in  $(2 + \epsilon)$  dimensions and in Section 3.3 the Gross-Neveu-Yukuwa model expanded  $d = 4 - \epsilon$  dimensions. Furthermore, we have seen that these models are closely related through their symmetries and symmetry-breaking patterns and universality therefore suggests that they describe the same critical point [127]. Moreover, the  $(2 + \epsilon)$  and the  $(4 - \epsilon)$  expansions can be compared to the known results from  $1/N$  expansions [157–165]. Indeed, we have confirmed that the  $(4 - \epsilon)$  expansion is fully compatible with the large- $N$



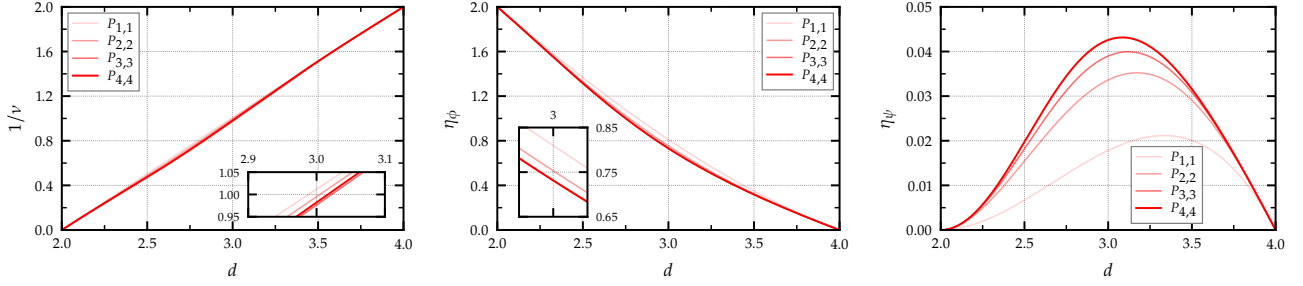


**Figure 3.9:** Order by order study of polynomial interpolation of the three critical exponents  $\nu^{-1}$  (left panel),  $\eta_\phi$  (mid panel) and  $\eta_\psi$  (right panel) between  $d \in (2, 4)$  at  $N = 8$ . We restrict ourselves to interpolations, which include the same number of loop orders in the respective critical dimensions  $d = 2$  and  $d = 4$

expansion of the Gross-Neveu model order by order, which represents a highly nontrivial check, see our Refs. [112, 113].

*/\*In the following, we combine the two expansion schemes, which are defined near their respective critical dimensions, i.e.  $d = 2$  and  $d = 4$ , into an interpolated curve.\*/\**

### Polynomial interpolation

A suitable interpolation between the two critical dimensions can be constructed by using a purely polynomial ansatz. To that end, we use both epsilon expansions for the critical exponents, simultaneously, and set up an interpolating function for the critical exponents in the interval  $d \in (2, 4)$ . More specifically, for an exponent  $f(d)$ , we choose a polynomial interpolation with polynomial  $P_{i,j}(d)$  of  $(i + j)$ -th degree, where  $i$  ( $j$ ) denotes the highest order of the epsilon expansion in  $d = 2 + \epsilon$  ( $d = 4 - \epsilon$ ) dimensions. We fix the polynomial coefficients with the expansion near the lower critical dimension and determine the first  $i + 1$  terms from the condition

$$P_{i,j}(d) = \sum_{k=0}^i f_k^{\text{GN}}(d-2)^k + \sum_{k=i+1}^{i+j+1} a_k(d-2)^k. \quad (3.40)$$

The remaining  $(j + 1)$  higher-order terms with coefficients  $a_{i+1}, \dots, a_{i+j+1}$  are then determined from the requirement that the  $j$  lowest derivatives of  $P_{i,j}(d)$  at  $d = 4$  correspond to the wpsilon expansion of the GNY model by

$$P_{i,j}^{(n)}(4) = (-1)^n n! f_n^{\text{GNY}} \quad (3.41)$$

where  $P_{i,j}^{(n)}(4)$  denotes the  $n$ -th derivative at  $d = 4$ . The resulting polynomials are then by construction  $i$ -loop ( $j$ -loop) exact near the lower (upper) critical dimension and provide a systematic estimate for the physically relevant case of three dimensions.

We show the results of this interpolation procedure, i.e.  $P_{i,i}(d)$  for  $i \in \{1, 2, 3, 4\}$  for the inverse correlation length exponent and the anomalous dimensions for the  $N = 8$  (graphene case) in Fig. 3.9. For the inverse correlation length exponent and the boson anomalous dimension, we observe a very good stability of the estimates from the interpolation procedure upon increasing the orders of the two perturbative expansions. Comparisons to other methods will be presented in the next section after we have also analysed an alternative interpolation method.

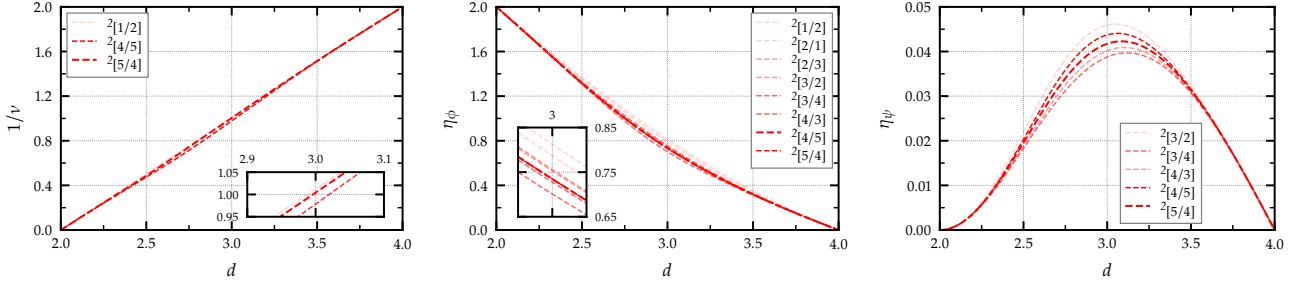


**Figure 3.10:** Order by order study of two-sided Padé approximants of the three critical exponents  $\nu^{-1}$  (left panel),  $\eta_\phi$  (mid panel) and  $\eta_\psi$  (right panel) between  $d \in (2, 4)$  at  $N = 8$ . We restrict ourselves to approximants, which include the same number of loop orders in the respective critical dimensions  $d = 2$  and  $d = 4$ . Further, we choose approximants with  $m \approx n$ .

### Two-sided Padé approximants

Another way of interpolating and also approximate the functions by a rational function, in contrast to the polynomial ansatz, is a two-sided Padé approximation. To that end, we again employ a generic Padé-approximant, cf. Eq. (3.38), and this time, we fix its coefficients such that its power series expansion near  $d = 2$  and  $d = 4$  agrees with both perturbative series in  $(2 + \epsilon)$  and the  $(4 - \epsilon)$  dimensions, respectively. Explicitly, we make the ansatz

$$2_{[m/n]}(d) = \frac{a_0 + a_1 d + \dots + a_m d^m}{1 + b_1 d + \dots + b_n d^n}, \quad (3.42)$$

and demand for the coefficients  $\{a_i\}$  and  $\{b_j\}$  to fit to the epsilon expansions. This leads to the relations

$$2_{[m/n]}^{(k)}(2) = k! f_k^{\text{GN}}, \quad (3.43)$$

$$2_{[m/n]}^{(k)}(4) = (-1)^k k! f_k^{\text{GN}^Y}, \quad (3.44)$$

with  $f_k^{\text{GN}^Y}$  being the expansion coefficient of a critical exponent at order  $k$ , cf. Eq. (3.34). In this way, the two-sided Padé approximant  $2_{[m/n]}(d)$  provides an interpolating function for a critical exponent  $f(d)$  in  $2 < d < 4$ .

We show the two-sided Padé approximants evaluated for the inverse correlation length exponent and the boson and fermion anomalous dimensions for the physically interesting case  $N = 8$  in Fig. 3.10. Moreover, we also show a sequence of two-sided Padé approximants corresponding to increasing order of the perturbative expansions which clearly shows signs of convergence towards higher orders. The two-sided Padé approximants can also have a pole in the interval  $d \in (2, 4)$  depending on the choice of  $f$  and  $N$ . In Fig. 3.10, we therefore show only the two-sided Padé approximants, which do not have a pole in  $d \in (2, 4)$  for the example  $N = 8$ . We further restrict our analysis to approximants which include the same number of loop orders at both ends, i.e. at  $d = 2$  and at  $d = 4$ . We observe a very good stability of the estimates from the two-sided Padé approximants for the three critical exponents upon increasing the orders of the expansions, even faster than in the polynomial interpolations. In particular, this also holds for the fermion anomalous dimension which vanishes in both limits, i.e. at  $d = 2$  and  $d = 4$  and is finite only in between. Finally, we remark that the series expansions for the critical exponents of the Gross-Neveu model have a pole at  $N = 2$  and therefore an extraction of estimates from the  $(2 + \epsilon)$  expansion close

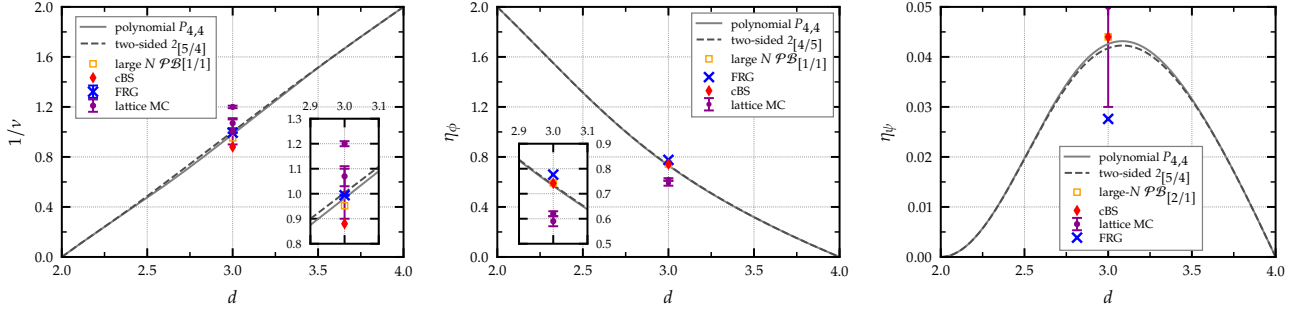


**Figure 3.11:** Interpolation of the three critical exponents  $\nu^{-1}$  (inverse correlation-length exponent, left panel),  $\eta_\phi$  (boson anomalous dimension, mid panel) and  $\eta_\psi$  (fermion anomalous dimension, right panel) between  $d \in (2, 4)$  at  $N = 8$ . The shown interpolations polynomial (red line) and two-sided Padé (dark-red dashed line) are fixed by the two epsilon-expansions at  $d = 2$  and  $d = 4$  in the first four derivatives. As a result, the asymptotic behavior is suppressed even far from these expansion points at the physical dimension  $d = 3$  and plausible values can be read off. It should also be noted that both complementary approaches for the interpolation are very close to each other and comparable to conformal bootstrap (cBS) [139], lattice Monte Carlo [108] and functional renormalization group (FRG) [90] calculations. (Figures taken from Ref. [55] and updated by [150, 151] (2020))

to or below  $N = 2$  becomes problematic. Therefore, we find that two-sided Padé approximants and other interpolation schemes cannot be faithfully applied for small  $N$ . In fact, the effects of the pole at  $N = 2$  can already be observed at  $N = 4$ .

In Fig. 3.11, we summarize our best results for the  $N = 8$  estimates from the two-sided Padé approximants as well as from the polynomial interpolation exhibiting the excellent agreement between both interpolations in the whole range  $d \in (2, 4)$ . For comparison, we also show the estimates for the critical exponents at  $d = 3$  from other methods, namely from the functional RG [90] and from the conformal bootstrap [139]. In particular, the conformal bootstrap estimates for the boson and fermion anomalous dimensions, which have been determined from universal bounds, almost perfectly match with our results. There is still a sizable difference in the estimates of the inverse correlation length exponent, which needs to be resolved in future studies. The available quantum Monte Carlo results for  $N = 8$  [108, 154] show deviations from our RG results as well as from the conformal bootstrap estimates for both, the anomalous dimensions and the correlation length exponent. It is encouraging, though, that the more recent QMC results from Ref. [154] seem to agree better than the earlier works [108, 131]. Unfortunately, in Ref. [154] only the correlation length exponent is given and the situation for the anomalous dimensions remains to be clarified. *\*A more recent study [151] was conducted in 2020 after publishing this text in Ref. [55]. The provided estimates for both anomalous dimensions show a faithful agreement with our results here. We updated the figures and Tables accordingly.\** We remark, that in the more exhaustively studied case of  $N = 4$ , it has been found that the QMC results can still be subject to some changes upon increasing the lattice size [130].

We compile our results from the two different interpolation techniques and the following resummations for  $d = 3$  as a function of  $N$  in Fig. 3.14 in the discussion section. Generally, the two interpolation procedures provide highly compatible results for  $N \gtrsim 6$  and start to deviate from each other and the other methods for  $N \lesssim 6$ . This is expected since the interpolation makes use of the series expansion in  $(2 + \epsilon)$  which exhibits poles in the critical exponents for  $N = 2$ , see Fig. 3.14. We conclude that for  $N \lesssim 6$  we cannot faithfully employ the interpolation techniques rooting in a  $(2 + \epsilon)$  expansion. In the following section, we therefore explore Borel resummation for the  $(4 - \epsilon)$  expansion to obtain improved estimates for the

Gross-Neveu universality classes at small  $N$ , in particular for smaller  $N$  where interpolation between  $(2 + \epsilon)$  and  $(4 - \epsilon)$  is difficult.

### 3.5.3 Borel resummation

A very accurate determination of critical exponents in  $d = 3$  from the  $(4 - \epsilon)$  expansion was achieved for  $O(n)$  symmetric  $\phi^4$  theories by using Borel resummation with conformal mapping [69, 148], see e.g., Ref. [97] for a recent study at six-loop order. For this resummation technique, the large-order behavior of an asymptotic series is considered, which has been computed for scalar models in the minimal subtraction scheme [166, 167]. Unfortunately, for the Yukawa models considered, here, the precise large-order behavior is not known. However, even with the knowledge of the large-order behavior as in the  $O(n)$  symmetric scalar models, resummation is a delicate issue. There, for example, the series written in terms of the coupling constant in fixed dimensions  $d = 2, 3$  is known to be Borel summable [168, 169], but the situation for the epsilon expansion remains unsettled.

Borel summability is therefore often taken as an assumption in the analysis of  $O(n)$  symmetric scalar models [170] and we will also do this, here. In the following, we also make the additional assumption that the asymptotic behavior of the GNY model is qualitatively the same as the one from the scalar models, i.e. the epsilon expansion for the critical exponents follows a formal power series with factorially increasing coefficients, i.e.

$$f_k \sim (-a)^k \Gamma(k + b + 1) \approx (-a)^k k! k^b \quad (3.45)$$

for large  $k$ . The Borel transform of such an asymptotic series  $f$  with expansion coefficients  $f_k$  is calculated as

$$\mathcal{B}_f^b(\epsilon) := \sum_{k=0}^{\infty} \frac{f_k}{\Gamma(k + b + 1)} \epsilon^k = \sum_{k=0}^{\infty} B_k^b \epsilon^k. \quad (3.46)$$

Consequently, the coefficients behave like  $B_k^b \sim (-a)^k$  for large orders  $k$  and therefore follow a geometric series which can be understood as a rational function with a pole at  $\epsilon = -1/a$ , i.e.

$$\mathcal{B}_f^b(\epsilon) \underset{k \text{ large}}{\sim} \sum_k (-a)^k \epsilon^k = \frac{1}{1 + a\epsilon}. \quad (3.47)$$

While the original series has a vanishing radius of convergence, we note that the Borel transform is analytic in a circle with  $|\epsilon| < 1/a$ . We now use the assumption that the considered series are Borel summable, i.e. that we can analytically continue the Borel transform to the positive real axis and that the Borel sum

$$\tilde{f}(\epsilon) := \int_0^{\infty} dt t^b e^{-t} \mathcal{B}_f^b(\epsilon t), \quad (3.48)$$

is convergent and gives the correct value of  $f$  for  $\epsilon = 1$ .

A perturbative expansion of the integral in Eq. (3.48) with respect to  $\epsilon$  restores the original asymptotic series. In particular, if only finitely many terms of the asymptotic series are known, the corresponding finite Borel transform in

the Borel sum merely reproduces the initial series. This can be circumvented by replacing the Borel transform in Eq. (3.48) by a nonpolynomial function which has the same power series coefficients as the Borel transform for all known terms and ideally incorporates the large-order behavior of the series. Therefore, in the next step, we analytically continue the Borel transform with a conformal transformation to the real axis, using

$$w(\epsilon) = \frac{\sqrt{1+a\epsilon}-1}{\sqrt{1+a\epsilon}+1} \Rightarrow \epsilon = \frac{4}{a} \frac{w}{(1-w)^2}. \quad (3.49)$$

This transformation preserves the origin and maps all points of the relevant positive real  $\epsilon$  axis in the unit circle, i.e.  $|w(\epsilon)| < 1$  for  $\epsilon \in [0, \infty)$ . The cut of the negative real axis  $(-\infty, -1/a)$  of the Borel transform is mapped to the unit circle in the variable  $w$ . The Borel transform in the new variable  $w$  can be found by expanding  $\mathcal{B}_f^b(\epsilon(w))$  in  $w$ , which renders the series convergent in the full integration domain of the Borel sum.

We further introduce an adjustment parameter  $\lambda$  in the Borel transform truncated at order  $L$ , cf. Refs. [97, 170],

$$\mathcal{B}_f^b(\epsilon) \approx \mathcal{B}_f^{a,b,\lambda}(\epsilon) := \left(\frac{a\epsilon(w)}{w}\right)^\lambda \sum_{k=0}^L B_k^{b,\lambda} w^k. \quad (3.50)$$

Herein, the coefficients  $B_k^{b,\lambda}$  are found by expanding the expression

$$\left(\frac{w}{a\epsilon(w)}\right)^\lambda \mathcal{B}_f^b(\epsilon(w)), \quad (3.51)$$

in a power series of  $w$ . While the Borel transform in Eq. (3.46) for finite  $L$  will diverge, this behavior is lost when introducing the conformal mapping variable as  $w$  tends to one for large  $\epsilon$ . The parametrization in Eq. (3.50) with  $\lambda \neq 0$  can be used to restore the actual large  $\epsilon$  behavior  $\sim \epsilon^\lambda$  of the Borel transform by adjusting  $\lambda$ . Since the asymptotic behavior of  $f(\epsilon)$  is unknown, we use  $\lambda$  to improve the sensitivity properties of our resummation algorithm [170], see below.

Further improvement is introduced by a homographic transformation with shifting variable  $q$

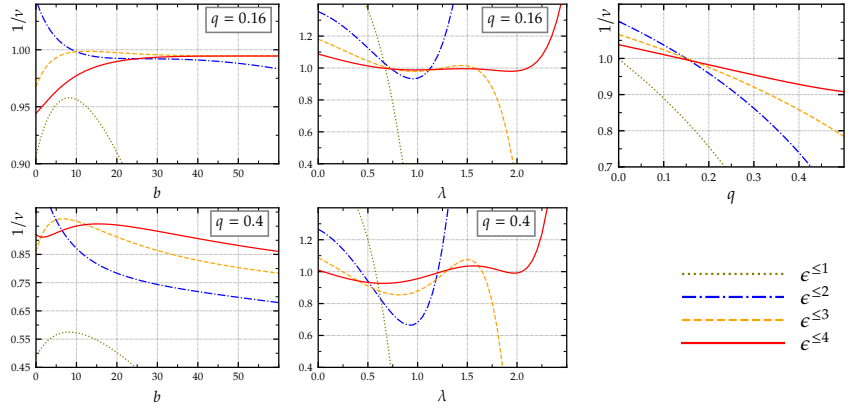
$$\epsilon = h_q(\tilde{\epsilon}) := \frac{\tilde{\epsilon}}{1+q\tilde{\epsilon}} \Rightarrow \tilde{\epsilon} = h_q^{-1}(\epsilon) = \frac{\epsilon}{1-q\epsilon}. \quad (3.52)$$

The original series is expanded in  $\tilde{\epsilon}$  and in the last step before the Borel sum transformed back by  $h_q^{-1}$ . Thus, the resummed series is determined by

$$\tilde{f}(\epsilon) \approx f_L^{a,b,\lambda,q}(\epsilon) := \int_0^\infty dt t^b e^{-t} \mathcal{B}_{f \circ h_q}^{a,b,\lambda}(h_q^{-1}(\epsilon)t). \quad (3.53)$$

The conformal mapping in the Borel transform produces poles in the Borel sum Eq. (3.48). Using the homographic transformation these poles are shifted away from the physical dimension at  $\epsilon = 1$  into a region of the integral where their diverging behavior is suppressed by  $\exp(-t)$ . This improves the stability of the numerical analysis and is essential to find an ‘‘optimized’’ parameter set.

**Figure 3.12:** Chiral Ising universality for  $d = 3, N = 8$ : Sensitivity of the Borel resummed inverse correlation-length exponent  $\nu^{-1}$  to a variation of one of the three large-order parameters  $b, \lambda$  and  $q$ . In the first row we show the change to variation of  $b$  and  $\lambda$  at the optimal  $q = 0.16$ , i.e. at the global minimum of the error estimate  $\bar{E} \equiv E_4(31.5, 0.74, 0.16) \approx 0.009$ . In this case we find plateaus with increasing spread in the loop order. For comparison, we also show the same plots at  $q = 0.4$  away from the optimum where these plateaus are lost. In the last plot we present the variation with respect to  $q$  which has no plateaus at all is only fixed by the intersection point. (Figures taken from Ref. [55])



To summarize, we introduced a resummation scheme for the asymptotic series  $f(\epsilon)$  which incorporates four parameters  $a, b, \lambda$  and  $q$  in the resummed series  $\tilde{f}(\epsilon)$  in Eq. (3.53). The resummed series would be independent of the choice of these parameters, if all orders of the expansion were known, i.e. for  $L \rightarrow \infty$ . At finite  $L$  this suggests that, for an optimized choice of resummation parameters, their variation should only induce a mild variation of the resummed  $\tilde{f}(\epsilon)$ . Consider, for example, the inverse correlation length exponent  $1/\nu$ , resummed according to Eq. (3.53). Individually changing the parameters  $b, \lambda$  and  $q$  leads to a variation of the resummed  $1/\nu$ , which we show in Fig. 3.12 for different orders in the epsilon expansion. We observe that for increasing order in epsilon, the dependence on the resummation parameters generally decreases as expected. Further, there are extended plateaus where the function  $1/\nu$  of the resummation parameters becomes rather flat, i.e. the resummed series becomes insensitive to a further variation in the corresponding parameter.

In the plots we omitted the dependence on the parameter  $a$ , cf. Eq. (3.45), which we fix to the value  $a = (3 + N/2)^{-1}$ . This is motivated by the observation that the factor  $(3 + N/2)^{-1}$  structurally appears in the RG beta functions, fixed point values and critical exponents at all available loop orders, see, e.g., Eq. (3.31). This is reminiscent of the factor  $3/(n + 8)$  appearing in the study of the scalar  $O(n)$  models, which determines  $a$  in the corresponding asymptotic behavior [171]. In our case, however, we do not have further justification to use a specific value for  $a$ . We have explicitly checked the stability of our results with respect to variations of  $a$  and we find that choosing different  $a \in (0, 1]$  only very mildly affects our results. For simplicity, we therefore proceed with the fixed choice  $a = (3 + N/2)^{-1}$ .

### Resummation algorithm

We now describe the employed resummation algorithm closely following the strategy presented in Ref. [97] and then apply it to the epsilon expansion of the GNY model. In order to find an optimized set of resummation parameters, we need a measure for the sensitivity of the summation to a parameter change. To that end, we study the variation of a function  $F$  upon changing one of its parameters  $x$  in a range  $x \in [x_0, x_0 + \Delta]$ ,

$$\mathcal{S}_x(F(x_0)) := \min_{x \in [x_0, x_0 + \Delta]} \left( \max_{x' \in [x_0, x_0 + \Delta]} |F(x) - F(x')| \right). \quad (3.54)$$

A function  $F(x)$  which only weakly varies within the plateau of length  $\Delta$  leads to a small value for  $\mathcal{S}_x$ .

Considering the example of the inverse correlation length  $1/\nu$  in Fig. 3.12 again, now, we are able to quantify the sensitivity by reading off the length  $\Delta$  of the extended plateaus. At the highest available order  $\mathcal{O}(\epsilon^4)$ , these have the spreads

$$\Delta_b \approx 40, \quad \Delta_\lambda \approx 1, \quad \Delta_q \approx 0.02, \quad (3.55)$$

which we will use in the following analysis for computing the sensitivities in Eq. (3.54). We note, that finding these plateaus without prior knowledge of the resummation parameters can be quite tedious since the parameter space is large. Here, we have performed extensive scans and in Fig. 3.12, we already show a range of parameters for  $b, \lambda$  and  $q$  which is centered around the optimized set to be determined as indicated in the caption. We want to stress at this point that the parameter  $q$  is chosen in such a way that the dependence on the parameters  $b$  and  $\lambda$  exhibits extended flat plateaus. The dependence on  $q$  itself is rather steep over the whole definition domain and we use it just as an optimization tool for the numerical analysis [172]. This is also the reason why the variation domain for  $q$  is very narrow. Note that the variation with respect to  $q$  shows no plateaus and the optimal  $q$  is fixed by the intersection point of the curves corresponding to the different loop orders, see lower left panel of Fig. 3.12.

We identify the optimal set of parameters following the method introduced in Ref. [97], i.e. making use of both the ‘‘principle of minimal sensitivity’’ and ‘‘principle of fastest convergence’’. As already extensively discussed in the literature, the errors might be underestimated if the unknown higher order corrections are much larger than the last computed ones. Such examples are known and only an explicit calculation can solve this question.

The different variations are collected in an error estimate [97],

$$\begin{aligned} E_{f,L}^{b,\lambda,q} := & \max \left\{ |f_L^{b,\lambda,q} - f_{L-1}^{b,\lambda,q}|, |f_L^{b,\lambda,q} - f_{L-2}^{b,\lambda,q}| \right\} \\ & + \max \left\{ \mathcal{S}_b \left( f_L^{b,\lambda,q} \right), \mathcal{S}_b \left( f_{L-1}^{b,\lambda,q} \right) \right\} \\ & + \mathcal{S}_\lambda \left( f_L^{b,\lambda,q} \right) + \mathcal{S}_q \left( f_L^{b,\lambda,q} \right). \end{aligned} \quad (3.56)$$

and we select the parameters in such a way that this error estimate is minimized. We also compare the sensitivities at different orders  $L$  and search for a minimum in the dependence on  $L$ .

Explicitly, we scan the parameter space in the range  $(b, \lambda, q) \in [0, 50] \times [0, 2.5] \times [0, 0.5]$  in steps of  $\delta_b = 0.5, \delta_\lambda = 0.02, \delta_q = 0.02$  and compute  $E_{f,L}^{b,\lambda,q}$  for each parameter set. We show the results of this scan for the inverse correlation length exponent  $1/\nu$  in Fig. 3.13. The global minimum  $\bar{E}$  of this scan marks the apparently best set of resummation parameters. However, this minimum is not always sharp and there are other sets of parameters which are almost equally likely. Therefore, we compute a weighted mean of all points which lie below a relative error of  $E_i/\bar{E} < 3$ . For the weights we use  $w_i = 1/E_i^2$  and plot the result as a dashed line in the parameter scans, see, e.g., in the lower panel of Fig. 3.13. From the error estimate at the minimum we compile the error for the resummation as  $3\bar{E}$ . The resulting error bars are consistent with the spread of the critical exponents around the optimum.

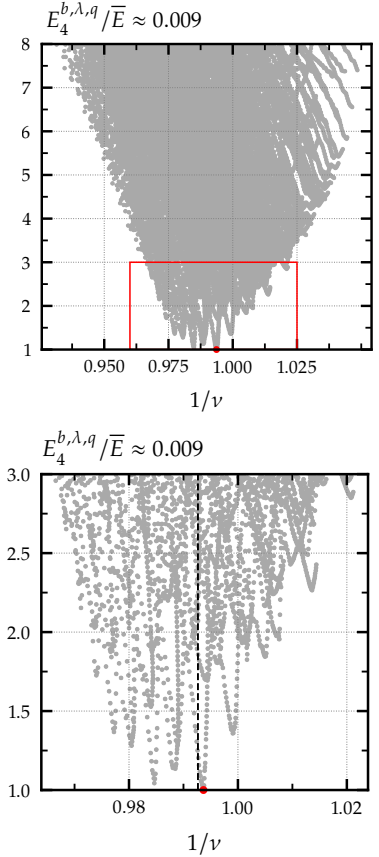


**Figure 3.13:** Chiral Ising universality in  $d = 3$ : Error estimates for the inverse correlation-length exponent  $\nu^{-1}$  at  $N = 8$ . The error axis is normalized to the smallest error in the parameters  $\bar{E} \equiv E_4(31.5, 0.74, 0.16) \approx 0.009$ . The global minimum of this parameter space (left panel) is located in an area around the value  $\nu^{-1} \approx 0.994$ , which we have zoomed in on the right panel. The weighted mean of this subspace in parameter space has  $\nu^{-1} \approx 0.993$  (dashed line). (Figures taken from Ref. [55])

We provide more detail and numerical data on the error estimates in the appendix of Ref. [55].

## 3.6 Discussion

The resummation techniques presented are now applied to several (physically motivated) cases. We start with the graphene case of  $N = 8$  component spinors which is relevant to our initial discussion.

### 3.6.1 Graphene case ( $N = 8$ )

As shown in the beginning, one of the quantum critical points that can be described by the Gross-Neveu-Yukawa model with  $N = 8$  is the semimetal-CDW transition of spin-1/2 electrons in graphene [109]. With the Borel resummation described in Sec. 3.5.3 applied to the  $(4 - \epsilon)$  expansion of the GNY model, we obtain the critical exponents  $1/\nu \approx 0.993(27)$ ,  $\eta_\phi \approx 0.704(15)$  and  $\eta_\psi \approx 0.043(12)$ . This compares very well with the perturbative RG estimates which we obtained using the combination of  $(2 + \epsilon)$  and  $(4 - \epsilon)$  expansions in terms of the two-sided Padé approximants and the polynomial interpolation Sec. 3.5.2. In particular, for the fermion anomalous dimension, the agreement is remarkable since, in this case, the one-sided Padé estimates around each critical dimension, individually, seems to significantly overestimate the value at  $d = 3$  even at order  $\mathcal{O}(\epsilon^4)$  [111, 113]. Some deviation between our different resummation approaches at the  $\lesssim 5\%$  level can be observed for the boson anomalous dimension, though. We have compiled our results for  $N = 8$  from the two-sided Padé approximants, the polynomial interpolation and the Borel resummation in Tab. 3.1. Here, to summarize all of the considerations from Secs. 3.5.1, 3.5.2 and 3.5.3, we build the simple average of the estimated critical exponents and transfer the error from the Borel resummation

$$\frac{1}{\nu} \approx 0.99(3), \quad \eta_\phi \approx 0.72(2), \quad \eta_\psi \approx 0.043(1). \quad (3.57)$$

In Tab. 3.1, we also compare to other methods and refer to the more detailed discussions of these results in Secs. 3.5.1 and 3.5.2. We would like to emphasize, again, the excellent agreement of our results for the boson and fermion anomalous dimensions with the conformal bootstrap estimates [139]. The superior agreement between two independent theoretical approaches builds

**Table 3.1:** Graphene case at  $N = 8$ : Comparison of the resummed critical exponents obtained from the resummation algorithm (Borel resummation) with the results from the polynomial interpolation, the two-sided Padé approximations (Padés) with with results from other theoretical methods. /\*Monte-Carlo[151] (2020) was added after publication\*/

$N = 8$	$\nu^{-1}$	$\eta_\phi$	$\eta_\psi$
Padés (incl. two-sided)	1.004	0.735	0.042
polynomial interpolation	0.982	0.731	0.043
Borel resummation	0.993(27)	0.704(15)	0.043(12)
large- $N$ [156, 158, 161, 162]	0.952	0.743	0.044
conformal bootstrap[139]	0.88	0.742	0.044
functional RG[90]	0.994(2)	0.7765	0.0276
Monte Carlo[108]	1.20(1)	0.62(1)	0.38(1)
Monte Carlo[156]	1.00(4)	0.754(8)	–
Monte Carlo[154]	1.07(4)	–	–
/*Monte Carlo[151] (2020)* /	1.0(1)	0.59(2)	0.05(2)



$N = 4$	$\nu^{-1}$	$\eta_\phi$	$\eta_\psi$
Padés (incl. two-sided)	0.961	0.480	0.086
polynomial interpolations	1.040	0.397	0.140
Borel resummation	1.114(33)	0.487(12)	0.102(12)
large- $N$ [158, 161, 162]	0.938	0.509	0.1056
conformal bootstrap[139]	0.76	0.544	0.084
functional RG[90]	1.075(4)	0.5506	0.0654
Monte Carlo[130]	1.14(2)	0.54(6)	–
Monte Carlo[154]	1.096(34)	–	–
Monte Carlo[20]	1.30(5)	0.45(2)	–
/*Monte Carlo[150] (2020)* /	1.06(3)	0.49(4)	–

**Table 3.2:** Spinless honeycomb fermions at  $N = 4$ : Comparison of the resummed critical exponents obtained from the resummation algorithm (Sec. V) with the results from the polynomial interpolation (Sec. IV), the two-sided Padé approximations (Sec. III) with results from other theoretical methods. /\*Monte-Carlo[150] (2020) was added after publication.\* /

a strong case for these values. At the same time, the available quantum Monte Carlo results for the anomalous dimensions at  $N = 8$  [108] show significant deviations from the pRG and conformal bootstrap results, suggesting that the QMC approach might still be affected by the finite system sizes. Surprisingly, the earliest numerical lattice studies of the chiral Ising universality class at  $N = 8$  [156] agree best with our results for the boson anomalous dimension.

We further note that there is still a sizable difference in the estimates of the inverse correlation length exponent between the different approaches which needs to be resolved in future studies. In particular, it would be very interesting to obtain conformal bootstrap estimates of the correlations length exponent directly from universal bounds.

### 3.6.2 Spinless fermions on the honeycomb ( $N = 4$ )

The universality class of the semimetal-CDW transition of spinless fermions on the honeycomb lattice is described by the  $N = 4$  GN model [106, 109]. Due to its simplicity and paradigmatic role, it has been subject to many studies, see Ref. [173] for a recent review. Within our pRG approach we have found that the two-sided Padé approximants and the polynomial interpolation presented in Sec. 3.5.2, respectively, are problematic, because the critical exponents from the  $(2 + \epsilon)$  expansion exhibit a pole at  $N = 2$ . Therefore, the dimensional interpolation in  $d \in [2, 4]$  breaks down in the vicinity of  $N = 2$  and we find that this is already shows at  $N = 4$ . For completeness, however, we also show the values for the critical exponents that we obtain from these two interpolations in Tab. 3.2 in gray fonts. The Borel resummation from Sec. 3.5.3 exclusively uses the  $(4 - \epsilon)$  expansion which is not plagued by this pole structure and, here, we obtain  $1/\nu \approx 1.114(33)$ ,  $\eta_\phi \approx 0.487(12)$  and  $\eta_\psi \approx 0.102(12)$ .

For  $N = 4$ , the agreement of the boson and fermion anomalous dimensions with the conformal bootstrap estimates from Ref. [139] is not as good as in the case  $N = 8$ , where we also had more reliable results based on the dimensional interpolation in  $d \in [2, 4]$ . Still, within the error bars extracted from the resummation procedure, the estimates deviate only on the  $\sim 10\%$  level. We would like to mention that for the anomalous dimensions, the case  $N = 4$  turns out to show the largest deviation from the conformal bootstrap results. For other  $N$ , i.e.  $N = 1, 2$  and  $N \gtrsim 6$  the agreement between these two independent methods is much better, see below. It will be interesting to see, whether this can be fully resolved by going to even higher

**Table 3.3:** Emergent SUSY at  $N = 1$ : Comparison of the resummed critical exponents obtained from the resummation algorithm (Sec. V) with the results from complementary methods: Functional Renormalization Group (FRG) and conformal bootstrap. Here, we have determined the conformal bootstrap estimate of  $1/\nu$  from the scaling relation Eq. (3.58).

$N = 1$	$\nu^{-1}$	$\eta_\phi$	$\eta_\psi$
Borel resummation	1.415(12)	0.1673(27)	0.1673(27)
conformal bootstrap[139]	1.418	0.164	0.164
functional RG[81]	1.395	0.167	0.167
functional RG[174]	1.410	0.180	0.180

loop orders. We would also like to mention that there is a series of Monte Carlo estimates for the boson anomalous dimension, i.e.  $\eta_\phi = 0.303(7)$  [129],  $\eta_\phi = 0.45(2)$  [20],  $\eta_\phi = 0.275(25)$  [131], and  $\eta_\phi = 0.54(6)$  [130]. The different results have been achieved using various Monte Carlo methods and different system sizes. The last result from Ref. [130] was obtained with the largest system size. It seems to fit very well with the conformal bootstrap result and within the  $\sim 10\%$  range also with our estimate. */\*The more recent Monte Carlo simulations in Ref. [150] narrow this window further.\** In view of the better control, we have for  $N = 8$  it would therefore be very interesting to explore this case with the same system sizes, too, and to have improved data for the fermion anomalous dimension for all cases.

The correlation-length exponent from the conformal bootstrap,  $1/\nu = 0.76$  [139], on the other hand, is very far away from all the other approaches, in particular, also from the recent Monte Carlo simulations,  $1/\nu = 1.14(2)$  [130] which agreed well for the anomalous dimension with the Borel resummed estimates from Sec. 3.5.3. Here, we note that our Borel resummed pRG estimate of  $1/\nu = 1.114(33)$  agrees very well with the Monte Carlo result from Ref. [130] as well as with another recent Monte Carlo estimate [154] where  $1/\nu = 1.096(34)$ . Unfortunately, the latter study does not provide data for the anomalous dimensions.

### 3.6.3 Emergent supersymmetry ( $N = 1$ )

The emergent supersymmetry scenario [146, 147] for the case  $N = 1$  features a supersymmetric scaling relation [174, 175] which connects the inverse correlation length exponent, dimensionality and the anomalous dimension

$$\nu^{-1} = (d - \eta)/2. \quad (3.58)$$

Note, that the anomalous dimensions of the boson and the fermion are equal in that case  $\eta = \eta_\psi = \eta_\phi$ . Eq. (3.58) therefore allows for a number of non-trivial checks for the estimates of the critical exponents. In previous works, cf. Refs. [112, 113], it has been shown that Eq. (3.58) holds exactly order by order in the epsilon expansion up to  $\mathcal{O}(\epsilon^4)$ . Moreover, the estimates for all critical exponents from simple Padé approximants already showed very good agreement with the conformal bootstrap [139] and the functional RG results [81]. Borel resummation yields the values  $1/\nu \approx 1.415(12)$ ,  $\eta_\phi \approx 0.1673(27)$  and  $\eta_\psi \approx 0.1673(27)$ . Since the anomalous dimensions of the boson and fermion coincide order by order in the epsilon expansion, also the Borel resummation provides the same values for both exponents. Further, within the error bars, the supersymmetric scaling relation, Eq. (3.58), is fulfilled as expected. Here, we obtain excellent agreement among all available theoretical approaches, see Tab. 3.3. Using the scaling relation in Eq. (3.58), we show that this agreement even holds for the inverse correlation length

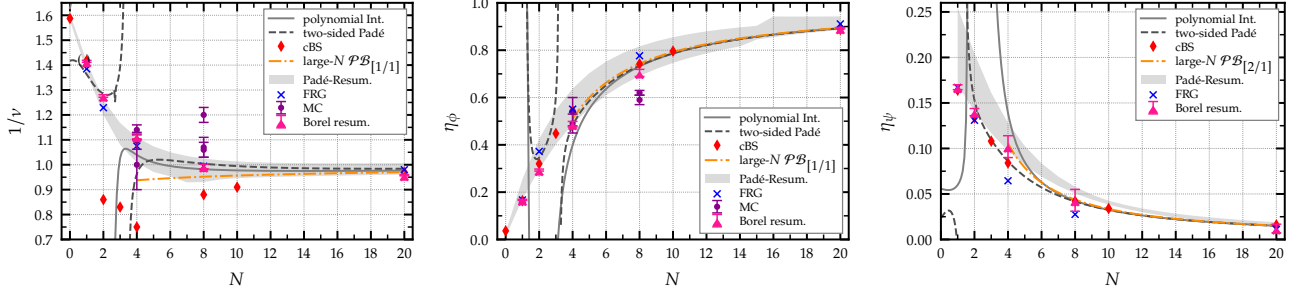


**Figure 3.14:** Chiral Ising universality in  $d = 3$ : Overview plot of the three examined  $\nu^{-1}$  (left panel), the boson anomalous dimension  $\eta_\phi$  (medium panel) and the fermion anomalous dimension  $\eta_\psi$  (right panel) for different spinor component numbers  $N \in [1, 20]$ . For comparison, the values from Monte Carlo (MC) calculations and the functional renormalization group (FRG), as well as the conformal bootstrap (cBS) were also plotted. On top of that we applied a Padé-Borel resummation on the large- $N$  expansions as in Ref. [156]. (Figure taken from Ref. [55] updated by [150, 151] (2020))

$N = 2$	$\nu^{-1}$	$\eta_\phi$	$\eta_\psi$
Borel resummation	1.276(15)	0.2934(42)	0.1400(39)
conformal bootstrap[139]	0.86	0.320	0.134
functional RG[141]	1.229	0.372	0.131

**Table 3.4:** Chiral universality at  $N = 2$ : Comparison of the resummed critical exponents obtained from the resummation algorithm (Sec. V) with the results from complementary methods: Functional Renormalization Group (FRG) and conformal bootstrap (cBS).

which, for other  $N$ , shows clear deviations. We also would like to mention that our results continuously connect to the limit  $N \rightarrow 0$  where we recover critical exponents compatible with the three-dimensional Ising model. We show this in Fig. 3.8 together with the data point from the highly accurate conformal bootstrap results [176].

### 3.6.4 Other cases ( $N = 2$ and $N = 20$ )

In addition to these cases, we compare the two additional choices  $N = 2$  and  $N = 20$ . At  $N = 2$ , no interpolation to the Gross-Neveu model in the  $(2 + \epsilon)$  expansion is possible due to the pole in the critical exponents. Other methods which provide results in this case are the conformal bootstrap and the functional RG and we compile these results for comparison in Tab. 3.4. This fits into the general picture that our anomalous dimension agree very well with the conformal bootstrap results, but the inverse correlation length agrees better with the functional RG.

Finally, we study the case  $N = 20$ , cf. Tab. 3.5, which should already be well located in the large- $N$  regime. It is accessible by all the resummation approaches we introduced in this paper and shows very good agreement between the two-sided Padé approximants, the polynomial interpolation and the Borel resummation. Moreover, it agrees excellently with the direct large- $N$  results [156], the conformal bootstrap [139] and also very well with

$N = 20$	$\nu^{-1}$	$\eta_\phi$	$\eta_\psi$
Padés (incl. two-sided)	0.9840	0.893	0.0151
polynomial interpolations	0.9763	0.893	0.0150
Borel resummation	0.9580(75)	0.893(9)	0.0120(48)
large- $N$ [158, 161, 162]	0.970	0.894	0.0152
conformal bootstrap[139]	0.97	0.888	0.016
FRG, App. [55]	0.980	0.911	0.011

**Table 3.5:** Chiral universality at  $N = 20$ : Comparison of the resummed critical exponents obtained from the resummation algorithm (Sec. V) with the results from the polynomial interpolation (Sec. III), the two-sided Padé approximants (Sec. IV) and complementary methods: Functional Renormalization Group (FRG), conformal bootstrap (cBS), Monte Carlo (MC) and large  $N$  calculations.

functional RG, which we have carried out in a simple approximation by ourselves see appendix of Ref. [55]. We expect that this level of agreement generally holds in the large- $N$  regime. This could therefore be a very good benchmark case for upcoming large-scale Monte Carlo calculations as the large- $N$  limit reduces uncertainties within the approximations required for the renormalization group methods. We have compiled an overview plot with all of our data for  $d = 3$  and comparisons for the range  $N \in [0, 20]$  in Fig. 3.14 which supports this expectation.

### 3.7 Conclusion and Outlook

We studied the universality classes of chiral Ising or Gross-Neveu(-Yukawa) models using the perturbative renormalization group up to four-loop order. Employing various resummation and interpolation techniques, in particular, dimensional interpolations between two and four dimensions as well as Borel resummation, we calculated estimates for the critical exponents.

To describe the physically interesting case of interacting electrons on graphene's honeycomb lattice which undergo a quantum phase transition towards an ordered charge density wave state, we have focused on the  $N = 8$  Gross-Neveu and Gross-Neveu-Yukawa models. We have found that all of our approaches to extract critical exponents in  $d = 2 + 1$  within the perturbative RG, i.e. the two-sided Padé approximants, the polynomial interpolation and also the Borel resummation, converge order by order towards a stable and compatible set of values, as compiled in Tab. 3.1. This is true for all the exponents that we have studied, i.e. the inverse correlation length exponent and both anomalous dimensions.

While resummation techniques for this type of theories is little explored and we cannot exclude unexpected behavior at higher orders in the loop expansion, the stability of our results still suggests they could be considered as very reasonable estimates. Moreover, for the boson and fermion anomalous dimensions at  $N = 8$ , we find excellent agreement of our results with the universal bounds provided by the conformal bootstrap method [139], which builds a strong case from independent theoretical methods for the validity of these values. The corresponding values from Quantum Monte Carlo [108, 150, 151] only partly agree for the anomalous dimensions and it will be very interesting to see whether this issue can be resolved in the future, e.g., by increasing system sizes. In particular, the fermion anomalous dimension is off by about an order of magnitude in the QMC simulations [108]. More recent simulations resolve this issue and provide estimates in agreement with our results [151]. Reconciliation with the field theoretical results may be achieved by going to larger lattice sizes as suggested from similar calculations for the case  $N = 4$  [130]. We also note that there is still a significant difference in the estimates for the inverse correlation length exponent between the perturbative RG and the conformal bootstrap. This difference is most pronounced for a range in the number of spinor components,  $2 \leq N \leq 8$ , while for larger  $N$  it disappears and all the exponents agree very well. Within the conformal bootstrap [139], in contrast to the anomalous dimensions, the correlation length exponent estimate is not obtained from universal bounds but from the extremal functional approach. It would therefore be very interesting to have conformal bootstrap estimates of the correlations length exponent directly from universal bounds, too. We have also found

very good agreement with the conformal bootstrap and the functional RG approach for the case of emergent supersymmetry,  $N = 1$ . Here, deviations across the different approaches are only found on the level of below 2%.

For the future, we identify two main directions for this line of research. Firstly, to fully establish convergence of the critical exponents within the perturbative RG approaches, loop calculations beyond fourth order are required. In view of the recent developments in computational technology and the mathematical insights into the structure of Feynman diagrams, this may be challenging but possible. Secondly, there are a number of very interesting quantum critical points of interacting Dirac fermions, which are not captured by the chiral Ising universality class. For example, superconducting or magnetic transitions of Dirac fermions exhibit critical behavior which are described by a coupling to  $U(1)$  or a  $O(3)$  order parameters, respectively. The corresponding universality classes are known as the chiral XY and chiral Heisenberg universality classes [144] and in perturbative RG are also known for higher orders [113, 114]. Moreover, for these and even more exotic transitions, there is recent QMC data [34, 125, 132–135, 177–180], which would be interesting to compare to. It can also be expected that more conformal bootstrap results will be available, soon, see, e.g., Ref. [137]. As has been the case for the chiral Ising universality class, the critical exponents of the chiral XY and chiral Heisenberg universality classes, have not been satisfactorily settled, yet. For these models, a thorough study of the critical exponents from resummation and interpolation techniques is under way. */\*For an up-to-date overview on these universality classes, see the tables in Ref. [150].\*/*

An alternative and promising approach for the quantitative characterization of the  $2 + 1$  dimensional chiral universality classes could also be the analysis of low-energy finite-size torus spectra at quantum critical points, cf. Refs. [181, 182]. Moreover, we note that it has recently been possible to observe strongly-correlated behavior and superconductivity in graphene-based systems, i.e. in twisted bilayer graphene [32, 33]. While it is currently not clear which mechanism underlies these transitions, the chiral universality classes may become relevant in this context, too. This, however, is still subject to discussion [183–187] and further experimental data and theoretical studies are required to settle the situation.



# Concepts of deconfined quantum criticality

# 4

While the Landau-Ginzburg-Wilson paradigm introduced in Chapter 2 has proven to be extremely successful in quantifying continuous (quantum) phase transitions (remember the stunning agreement for the  $O(2)$ -universality class across complementary methods in Section 2.4.2), numerical simulations for various systems [36, 40, 134, 188] hint that there could be exotic phase transitions that can not easily captured this way. In this Chapter, we want to tell the story of a certain type of these transitions which are driven by *deconfined* degrees of freedom. It's an intriguing lesson of theory-building to see how an unexpected twist in numerical simulations can open up an entire field of novel and surprisingly subtle transitions beyond the LGW paradigm [39, 40]. Its foundations lie in the discovery of topological order and especially its relevance to condensed matter systems [38]. In the ongoing discussion, it was shown that unconventional long-range-entangled states, i.e. spin-liquid states, can be stabilized in situations in which the magnetic frustration is large. Their non-local fractionalized excitations lead to fascinating new physics [53, 189] and novel fractionalized universality classes [54].

We will pave the road to the following projects by giving an partly historical overview on how especially the field of deconfined quantum critical points emerged, what its remaining questions are and which future prospects it reveals.

4.1 Beyond the Landau-Ginzburg paradigm .....	49
4.2 Deconfined quantum criticality	52
4.3 Conjectured web of dualities from DQCPs.....	56

## 4.1 Beyond the Landau-Ginzburg paradigm

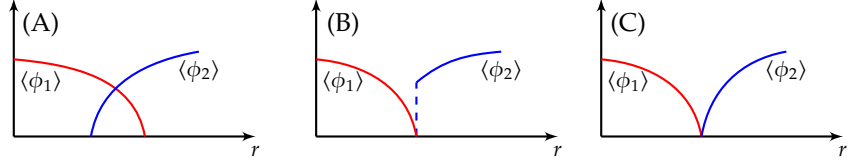
In the Landau-Ginzburg-Wilson (LGW) paradigm, we introduced in Chapter 2, the an order parameter concept plays a pivotal role. Its dynamics display both, a spontaneously broken symmetry of the ground state and the long-range properties of the system at criticality. We have seen that this notion is very successful in a vast collection of continuous phase transitions including quantum phase transitions as discussed in Sec. 2.2. The crucial feature from our persepective in these stories is the spontaneous breaking of a certain symmetry by any kind of ordering. But what if we are confronted with two symmetry breaking orders as limits of the same system and ask for the transition between them?

In the LGW language of dynamically evolving order parameters, we would search again for a functional of the free energy which incorporates the two competing orderings by independent operators, e.g.  $\phi_1$  and  $\phi_2$ . These account for the two distinct symmetry breaking orderings with  $\langle \phi_i \rangle \neq 0$ . The  $\phi^4$ -theories of Chapter 2 in mind, a simple example of such a functional could look like

$$F_L(\phi_1, \phi_2) = r_1 \phi_1^2 + \lambda_1 \phi_1^4 + r_2 \phi_2^2 + \lambda_2 \phi_2^4 + g \phi_1^2 \phi_2^2, \quad (4.1)$$

where we omitted any kinetic terms of the order parameter fields  $\phi_i$  for the moment. Here the last term with coupling  $g$  accounts for the competition of

**Figure 4.1:** Scenarios of order-to-order transition in the LGW paradigm. (A) Both orderings coexist in a crossover region. (B) One ordering is superseded by the other one in a first order transition. (C) The transition is continuous with a critical point where both orderings vanish.



1: There is a fourth, but trivial, scenario where there is a region of disorder and both order parameters vanish. However, it turns out this case is irrelevant for quantum magnets in two dimensions (see the discussion below).

2: Nevertheless, we mention the existence of multicritical points which fall in the latter scenario. In the recently discussed example in Ref. [31, 190], the broken symmetry is similar and even enhances to a higher symmetry directly at the critical point. A feature, we should keep in mind.

3: Precisely, the staggered magnetization does not commute with the Hamiltonian and it's a non-trivial finding that the Néel order for spin-1/2 survives the strong quantum fluctuations. While this was studied in Ref. [192, 193] for spin  $S \geq 1$ , we lack a rigorous proof but know from numerical studies that the ground state shows long range Néel order [194, 195].

the two orderings which are tuned by  $r_1$  and  $r_2$ . Minimizing this functional  $F_L$  leaves us with three non-trivial scenarios<sup>1</sup> as shown in Fig. 4.1

- (A) Both orderings coexist for a range of  $r_i$  where  $\langle \phi_1 \rangle \neq 0 \neq \langle \phi_2 \rangle$ . This scenario is sometimes called *crossover*.
- (B) One ordering is suddenly replaced by the other one in a first order transition.
- (C) There is a continuous transition between both orderings where  $\langle \phi_1 \rangle \rightarrow 0$  exactly when  $\langle \phi_2 \rangle$  acquires a finite value.

While in case (A) for the coexisting ordering the coupling  $g$  of our functional (4.1) simply vanishes and the situation in case (B) of a first-order transition covers nearly every non-trivial situation for  $g \neq 0$ , the continuous transition as in scenario (C) needs an unnatural fine-tuning of the  $r_i$  with the condition  $r_1 = r_2$ . Of course the latter is still possible, but in the light of our discussions so far, it seems very unlikely for a generic system with two distinct ordered ground states<sup>2</sup>.

#### 4.1.1 Spins on a square lattice

Let's turn to a practical system where the above discussion becomes important and look at spin-1/2 Heisenberg magnets. In the plain Heisenberg model, we can formulate the interaction of the spins by a simple product of their operators  $S_i$

$$H = J \sum_{\langle i,j \rangle} S_i \cdot S_j, \quad (4.2)$$

where we sum over nearest neighbors and interaction has the strength  $J > 0$ . This is known in the literature as the Heisenberg Hamiltonian [38, 191]. While the SU(2) spin symmetry is preserved by the Hamiltonian in the ground state an antiferromagnetic Néel order<sup>3</sup> is favored, as shown on the left in Fig. 4.2. It breaks the SU(2) spin symmetry but preserves the translational lattice symmetry.

What are other possible symmetry breaking ground states spin-1/2 particle can take on the square lattice? To answer this question, we induce different orderings by extending the Heisenberg Hamiltonian by another SU(2) symmetric term, e.g.

$$H = J \sum_{\langle i,j \rangle} S_i \cdot S_j - Q \sum_{\langle i,j,k,l \rangle} \left( S_i \cdot S_j - \frac{1}{4} \right) \left( S_k \cdot S_l - \frac{1}{4} \right). \quad (4.3)$$

For this second term with strength  $Q$  [41], we deliberately chose a columnar dimer ordering type encoded in  $\langle i, j, k, l \rangle$ . They refer to the corners of a plaquette, such that  $ij$  and  $kl$  form two parallel adjacent horizontal or vertical links [41]. It pushes the system to the formation of specific singlet patterns. Note that both terms still fulfill a SU(2) spin symmetry and the



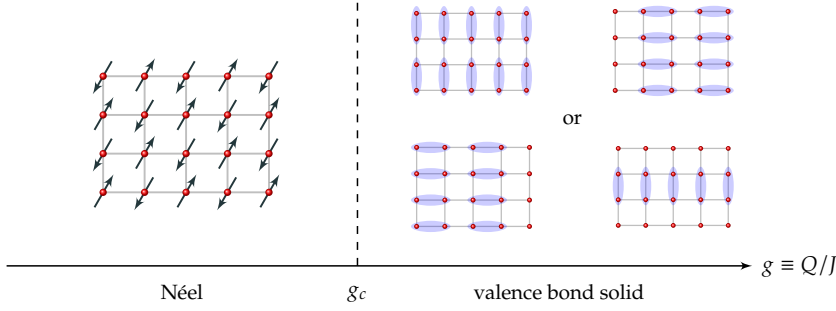


**Figure 4.2:** Cartoon of the possible symmetry breaking ground states of the  $J$ - $Q$ -model. As explained in the text, we can tune from the Néel order for  $g \ll 1$  to the VBS for  $g \gg 1$ . In the LGW paradigm, there is a  $g_c$  with most likely a first order transition between the two phases. Note that the VBS phase can take one of four orientations [200].

choice for the four spin term was made only for practical reasons in the following story. Indeed, also other  $SU(2)$  symmetric four spin term could be considered [196–198] which favor other singlet patterns while preserving the  $SU(2)$  spin symmetry without altering this story’s course [199].

Crucially, the Hamiltonian in Eq. (4.3) displays two distinct symmetry breaking orderings. For  $J \gg Q$ , the spins will again align anti-ferromagnetically to the Néel order and therefore spontaneously break the  $SU(2)$  symmetry to  $U(1)$ . Nevertheless, this transition preserves the translational lattice symmetry<sup>4</sup>. In the opposite limit, for  $J \ll Q$ , neighboring spins will form another non-trivial ordering, the so-called valence bond singlet

$$\text{valence bond} = \frac{1}{\sqrt{2}} (\uparrow\downarrow - \downarrow\uparrow) . \quad (4.4)$$

On the lattice, all the sites will pair up to one of the four feasible columnar valence bond solids (VBS) as depicted on the right side in Fig. 4.2. Most importantly, in this ground state the translational and rotational lattice symmetries are broken. On the contrary, the  $SU(2)$  spin rotational symmetry is preserved.

Our model, therefore, allows for two non-trivial ground states as limits of the ratio  $g \equiv Q/J$ . Each of them breaks completely distinct symmetries which are preserved by the other. Even better, we can tune through the transition between them by adjusting  $g$  and as we learned above the most likely nature of this transition will be the coexistence of both patterns or a first order transition.

While for classical spins one would also expect a featureless paramagnetic phase in this model, this is not possible in the quantum version. Inspired by the Lieb-Schultz-Mattis-Theorem [201] for half-integer spin system in  $1d$ , Hastings [202] proved that also for higher dimensions a generic  $SU(2)$  spin system like (4.3) will have only two possible types of ground states: (i) the ground state is gapped and degenerate (e.g. equipped with topological order or a spontaneously broken discrete symmetry) or (ii) the ground state remains gapless. The paramagnetic valence bond solid ground state falls in the first category by breaking the discrete lattice translational symmetry<sup>5</sup>. Surprisingly, the theorem by Hastings also rules out a region of disorder which one could naively expect with the classical limit in mind.

## 4.1.2 Numerical findings

The Hamiltonian in (4.3) is called  $J$ - $Q$  model [41, 42]. Similar to the class of  $J_1$ - $J_2$  models, it is especially amenable to quantum Monte-Carlo methods [204,

4: To be precise, the Néel order, i.e. staggered magnetization, is spatially uniform.

5: This line of argument is frequently used to identify quantum spin liquid phases which allegedly lack an order parameter distinguishing its ground state [203].

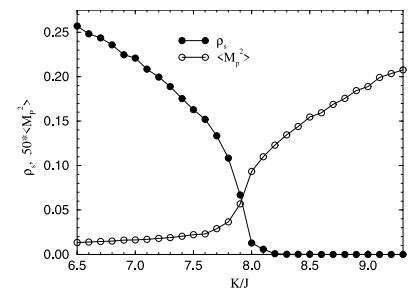


**Figure 4.3:** From [36]: Order parameters of spin stiffness  $\rho_s$  (Néel order) and a plaquette-stripe order (VBS) tuned by the ratio of their interactions strengths  $K/J$ . Surprisingly, the transition is continuous which suggests scenario (C) in Fig. 4.1.

6: The results of an extensive finite temperature quantum Monte-Carlo simulations [42] even show a ‘quantum critical fan’ (at finite  $T$ ) with a dynamical critical exponent  $z = 1$ .

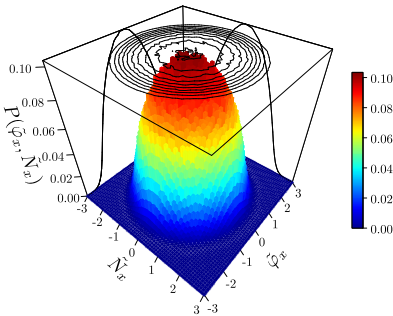


**Figure 4.4:** Emergent  $SO(5)$  symmetry at the critical point on the square lattice as seen from the joint probability distribution of both order parameters  $N$  for the Néel phase and  $(\varphi_x, \varphi_y)$  for the VBS phase. (Taken from Ref. [44]).

205]. In this light, it appears natural to approach the question above about the type of the transition between the two competing symmetry breaking orders numerically. Surprisingly, the first studies of the  $J$ - $Q$  model by Sandvik et al. [36] show an unexpected continuous transition<sup>6</sup> which suggests scenario (C) in the LGW paradigm of Fig. 4.1. Based on these findings, there remain only two explanations: (i) the continuous transition is a coincidence or (ii) the LGW paradigm fails in describing this transition. While considering only this very first observation in Ref. [36], one could argue the former. However, similar results were found for various lattice realizations [43, 198, 199, 206–211]. Even more, it was confirmed for more general  $SU(N)$  symmetric models [196, 204, 212] and in distinct numerical methods [44, 213, 214]. Beyond that, these are not the only transitions which seem to evade the LGW paradigm and there was found evidence for various similar critical points between two ordered phases [37, 134, 215].

This naturally raises the question if we have encountered an exotic class of continuous phase transitions which lies *beyond* the LGW paradigm. While the authors Ref. [36] evidently report a continuous transition, complementary studies observed an anomalous scaling behavior [216, 217] as well as a drift of the critical exponents with the system size  $L$  [43, 212]. Further, recent numerical simulations argued that the apparently strong scaling violations are a consequence from an actually *weakly first order* transition. The latter entails a reminiscent pseudo-critical behavior which could explain an anomalously large correlation-length as well as the drifting exponents [218, 219]. These contradictory observations opened a discussion about the very nature of the transition itself. We will address the intricacies of these results and their possible origin in the following Chapter.

But this is not the only unexpected observation concerning this transition. An intriguing feature which most of the numerical works share is an emergent  $SO(5)$  symmetry at the critical point [44, 199, 220, 221] as shown in Fig. 4.4. Not least, also this observation triggered the exploration of a novel web of dualities between theories which share such a critical point [50, 51]. We will elucidate this lead and its implications in Section 4.3.

## 4.2 Deconfined quantum criticality

Sparked by the numerical findings, physicists started to wonder if a continuous transition between the Néel order and the valence bond solid can occur naturally, without artificial fine-tuning. Surprisingly, it is indeed possible and the intricate subtleties of the theory behind also explain why the LGW had to fail in the first place. In the following, we want to lay out the landmarks of the derivation up to the critical theory. For a detailed and more rigorous derivation we refer to Ref. [40] and the original papers by T. Senthil, S. Sachdev and L. Balents [38, 39].

### 4.2.1 From Néel to VBS – and back

In the previous Section, we already explained that there are two possible competing orderings of spins on a square lattice: the translational invariant Néel phase and the  $SU(2)$  spin rotational invariant valence bond solid.

Crucial for the following discussion is the observation that each of them breaks the symmetry of the other phase.

Let's start our discussion in the Néel phase with the fluctuating order parameter field  $N(\mathbf{x}, \tau)$  which describes the staggered magnetization on the lattice. We skip the details of the derivation towards a field theory using spin coherent states [222] and directly write down a continuum theory at zero temperature for the order parameter field

$$\mathcal{S} = \frac{1}{2g} \int d^2x d\tau [(\nabla N)^2 + (\partial_\tau N)^2] + \mathcal{S}_B(N), \quad (4.5)$$

where  $g \sim Q/J$ . This is the *non-linear sigma model*, accompanied by a topological term  $\mathcal{S}_B$ . The first part we already saw in the very beginning of this thesis. It resembles the three-dimensional version of the Landau-Ginzburg theory<sup>7</sup>.

But the most important part of this theory is indeed the Berry phase term  $\mathcal{S}_B$ . It arises naturally from the path integral construction and measures the topological defects of the theory [222]. For a spin system, these non-trivial configurations are known as *skyrmions* and may look like the one shown in Fig. 4.5. The role of the Berry phase is to measure the appearance of the skyrmions with an integer topological winding number  $Q$  by integrating over a closed sweep of the fluctuating vector  $N(\mathbf{x}, \tau)$

$$Q = \frac{1}{4\pi} \int d^2x N \cdot \partial_x N \times \partial_y N. \quad (4.6)$$

For smooth equal-time configurations, the Berry phase will vanish and the winding number  $Q$  is conserved (in time). However, on the lattice there are events allowed which change  $Q$  in time by some integer in a *monopole event*. Precise calculations carried out by Haldane<sup>8</sup> show that the only allowed monopole events are quadrupled *hedgehogs* where the winding number jumps by  $\pm 4$  [224]. In the field theory, this can be respected by an additional term<sup>9</sup> to the Lagrangian which reads

$$\mathcal{L}_{mp} = \lambda_4((v_x^\dagger)^4 + v_x^4) \quad (4.7)$$

Here,  $\lambda_4$  denotes the monopole fugacity and the operators  $v_x^{(\pm)}$  insert monopoles of strength  $\pm 2\pi$  at  $x$  in space-time [40, 222]. In the RG, this direction turns out to be irrelevant [40]. For our derivation, the most important feature of the hedgehogs is that they preserve the  $SU(2)$  spin rotational symmetry same as the VBS phase. In fact, the quadrupling of the instantons upon proliferation will induce the  $Z_4$  structure seen in this phase. A thorough analysis supports this hint by suggesting that the operators  $v_x$  may be identified with the VBS order parameter [40, 225, 226].

For the further derivation, it turned out to be convenient to change to the *complex projective* (CP) parameterization [38, 222]. It allows to rewrite the Néel vector in fractionalized degrees of freedom

$$N = z_\alpha^* \sigma_{\alpha\beta} z_\beta. \quad (4.8)$$

The introduced spinon degrees of freedom  $\mathbf{z} = (z_1, z_2)$  are two component

7: To be precise: In order to finally arrive at the Landau-Ginzburg theory, we have to soften the length constraint of the non-linear sigma model. This is done by introducing an appropriate potential of the form  $m^2 N^2 + \lambda N^4$ .

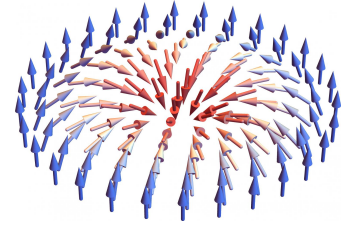


**Figure 4.5:** Depiction a skyrmion on a two dimensional lattice. Its winding number  $Q$  in this case is  $-1$ . (Taken from Ref. [223]).

8: F. Duncan M. Haldane was awarded with the Nobel prize in 2016 for his work on “*theoretical discoveries of topological phase transitions and topological phases of matter*.” together with David J. Thouless and J. Michael Kosterlitz.

9: In fact, we can write down a Lagrangian which involves all sorts of monopole insertions and not only  $\lambda_4$ . Our restriction already incorporates the findings by Haldane [224].

spin-1/2 particles which entail an all-important U(1) gauge redundancy

$$z_\alpha \rightarrow z_\alpha e^{i\theta(x,\tau)}. \quad (4.9)$$

We skip the tedious calculational details [40, 222] at this point and will arrive straight at the appealing result. The introduction of the gauge redundant spinons gives rise to a gauge field  $A_\mu$  which can be promoted to an independent degree of freedom after a Hubbard-Stratonovich transformation. Thus, the non-linear sigma model under the presented fractionalization translates into the following form

$$\mathcal{S} = \int d^2x d\tau \sum_\alpha |(\partial_\mu - iA_\mu)z_\alpha|^2 + \mathcal{S}_B. \quad (4.10)$$

Also the Berry phase term can be rewritten now in terms of the gauge field  $A_\mu$ . In fact, the winding number  $Q$  in Eq. (4.6) decodes to the flux of the gauge field at any instant of time

$$2\pi Q = \int d^2x (\partial_x A_y - \partial_y A_x). \quad (4.11)$$

Since the winding number can change only by an integer, this equation renders the gauge field  $A_\mu$  *compact*<sup>10</sup> (being an angle modulo  $2\pi$ ).

Deep in the Néel phase, the hedgehog events are very costly and therefore absent. However, at the critical point they start to proliferate and eventually destroy the Néel order [38, 40]. Above, we already mentioned that the Berry phase term only allows for quadrupled instantons and it turns out that upon their proliferation the system will ultimately take the  $\mathbb{Z}_4$  structured VBS order. This means the topological defects of the Néel phase described by the Berry phase term carry the quantum numbers of the VBS order and thus the phase transition is expected to be continuous. We will make this statement more precise in the next Section. But first, let's try to approach the critical point also from the VBS ordered phase where the situation turns out to be more intuitive.

*From the VBS phase.*

We start the discussion on the same track but on the other end of the road deep in the VBS phase. Here, a natural phenomenological candidate for a theory is the XY model with quartic anisotropy which accounts for the  $\mathbb{Z}_4$  order and its fluctuations. The discrete symmetry group  $\mathbb{Z}_4$  in this context means that the bonds can have four different orientations on the lattice as shown in Fig. 4.2 on the right. The multiple orientations on the same lattice are separated by domain walls. Similar to the hedgehog events in Néel phase, these topological defects of the VBS order become crucial at the transition [200].

A special case is the  $\mathbb{Z}_4$  vortex, where all four different orientations come together at one point forming a swirl of domain walls as shown in Fig. 4.6. Surprisingly, this situation will always leave one untangled spin-1/2 in its center carrying already the Néel quantum number. This gives us already a first hint how a spin degree of freedom as apparent in the Néel phase can come into play. But how do these swirls spark and why do not they destroy the VBS order outside the critical point?

10: Having the usual definition of a gauge field for a magnetic field  $\mathbf{B} = \nabla \times \mathbf{A}$  in mind, the crucial difference to the gauge fields known from electrodynamics is that the equation above would admit magnetic monopoles with  $\nabla \cdot \mathbf{B} \neq 0$  at the core of a hedgehog event. This gives us a more intuitive notion why the gauge field has to be compact.

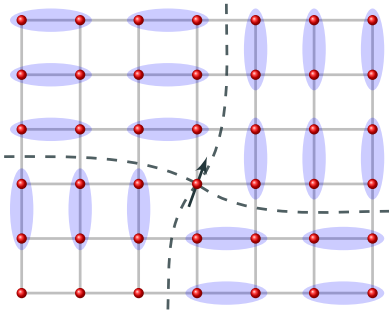


**Figure 4.6:**  $\mathbb{Z}_4$  vortex in the VBS phase: When the four different orientations of the VBS order meet they create a swirl of domain walls with an untangled spin-1/2 at the site at its center.

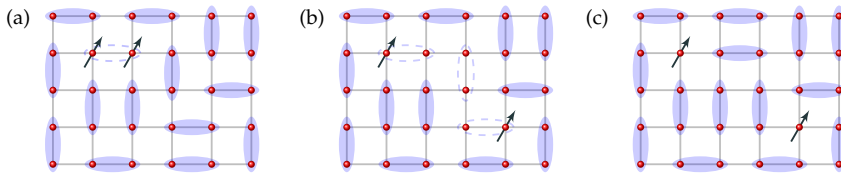


**Figure 4.7:** Cartoon of deconfinement in the VBS phase. (a) Starting in the VBS a spin-1 excitation creates two spin-1/2 spinons which are metaphorically *glued* together by a topological term (b). Driving these spinons apart costs energy and confines them. At the critical point (c) the spinons get *liberated* and proliferate.

Recall that the valence bond consists of a super-position of neighboring spin-1/2 states as written in Eq. (4.4), i.e. we can think of them as being composed by the very same fractionalized spinons  $z_\alpha$ . If we now break up a valence bond singlet to a spin-1 excitation, we are left with two spinons next to each other as shown in Fig. 4.7 (a). Pulling them apart will create a line of defects and therefore cost energy proportional to the length of the line. Consequently, deep in the VBS, the spinons will be *confined* and do not exist as free excitations [200]. Note also that by this procedure we create two  $\mathbb{Z}_4$  vortices (vortex and antivortex) with opposite charge in the gauged picture we drew above. For the case of the XY model (without the spin structure), it can be explicitly shown that the quartic anisotropy, which makes up the *glue* between the spin-1 fragments, becomes dangerously irrelevant<sup>11</sup> at the critical point [227]. This results in the emergence of a non-compact gauge theory same as in the explanation above when starting in the Néel phase. The spinons in this picture are no longer bound, become *deconfined* and proliferate. The explicit mapping for the XY model is known as the charge-vortex duality [48, 228].

11: This means it is relevant in the XY phase and only irrelevant at the critical point. How this is possible we will elucidate in the following section.

### 4.2.2 Critical theory of the DQCP

We now turn to the critical point alone. In the above discussion, we have seen that the topological defects of each phase carry the seeds of the other. We also learned that while in principle feasible these defects are confined. Only at the critical point, they condensate to finally render the transition continuous. Precisely, the two competing order parameters have long-ranged statistical interactions mediated by the topological defects what ultimately explains why a macroscopic theory in the LGW paradigm with only *local* order parameters had to fail.

The critical theory can best understood by applying these findings on the fractionalized spinon formulation in Eq. (4.10). Here the Néel phase is captured by a kinetic term of the spinons, while the VBS ordering is hidden in the Berry phase term  $S_B$ . This model is known as the *compact*  $\text{CP}^1$  model due to the compact gauge field and the  $N = 2$  spinon components<sup>12</sup>. A detailed analysis, we spare here, shows that both the compactness as well as the Berry phase are relevant perturbations and we can not drop them individually [40, 222]. However, for  $N = 1$ , we know about the charge-vortex duality. In the renormalization group language, it tells us that at the critical point neglecting both becomes a *dangerously irrelevant* perturbation. Thereby, dropping both terms simultaneously is safe only at the critical point. A similar result can be found for  $N \rightarrow \infty$  by a saddle-point approximation [229]<sup>13</sup>. By continuity [38, 230], it is now expected this feature holds also for  $N = 2$  as present here. It implies lifting the compactness and the Berry phase at the same time is, in fact, a *dangerously irrelevant* perturbation at the critical point. A conjecture which might not be true and we will shed some light on

12: Strictly speaking, it is a special case of the compact  $\text{CP}^{N-1}$  model with a  $N$ -component scalar.

13: Precisely, Murthy and Sachdev show that for large  $N$  the  $q = 4$  hedgehog monopole events we identified above as the driving defects at the transition are strongly irrelevant in  $d = 3$  dimensions.

this in Chapter 5. Upon softening the length constraint on the spinons, we obtain *at the critical point* the non-compact  $CP^1$  (NCCP<sup>1</sup>) model

$$\mathcal{S}_{\text{NCCP}^1} = \int d^2x d\tau \left[ \sum_{\alpha=1,2} |(\partial_\mu - iA_\mu)z_\alpha|^2 + r|z_\alpha|^2 + \lambda |z_\alpha^* z_\alpha|^2 + \frac{1}{4e^2} F_{\mu\nu} F^{\mu\nu} \right]. \quad (4.12)$$

Here, the gauge field promotes to a *non-compact* one and couples minimally to the spinons by a standard Maxwell term with the field strength tensor  $F_{\mu\nu} = \partial_\mu A_\nu - \partial_\nu A_\mu$ . While the original theory has no dynamical gauge degree of freedom, it will be generated under RG transformations and we can take it into account already from the beginning.

For  $r < 0$ , the expectation value of the spinon field  $\langle z_\alpha \rangle \neq 0$  and consequently  $\langle N \rangle \neq 0$ , i.e. the system is in the Néel phase. For  $r > 0$ , however, we obtain  $\langle z_\alpha \rangle = 0$  which on first glance seems not to capture the VBS phase. This is because the NCCP<sup>1</sup> model does not include a term for the monopole fugacity anymore. We neglected this term because perturbations in the  $\lambda_4$  direction were found irrelevant at the critical point.

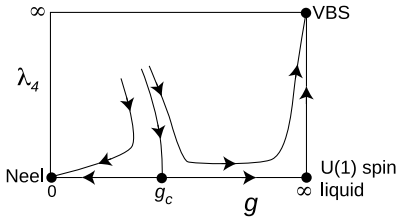


**Figure 4.8:** Schematic RG flow of spin-1/2 quadratic lattice. The NCCP<sup>1</sup> model does not include the monopole fugacity  $\lambda_4$  which is anyhow a (dangerously) irrelevant perturbation at the critical point. However, if tuned through the critical point at  $g_c$ , the system will flow to a U(1) spin-liquid state at intermediate scales before finally terminating in the VBS phase. (Taken from Ref. [39]).

In the RG flow of the spin-1/2 square lattice, the corresponding  $\lambda_4$  direction is attracted to the critical point at  $g = g_c$ , cf. Fig. 4.8. In this picture, the NCCP<sup>1</sup> model describes the flow only on the axis for  $\lambda_4 = 0$ . If we tune the flow from the Néel phase (with  $r < 0$  in the NCCP<sup>1</sup> model) through  $g_c$ , it will flow towards a U(1) spin liquid phase. However, this fixed point is *unstable* to perturbations in the  $\lambda_4$  direction. Consequently, RG transformations will terminate in the infrared at the VBS phase fixed point with  $\lambda_4 \rightarrow \infty$ .

In conclusion, at a deconfined quantum critical point the transition is governed by fractionalized spinon degrees of freedom which are “confined” in either of the adjacent ordered phases. While the field theory at the critical point alone, the NCCP<sup>1</sup> model, looks apparently like a harmless abelian version of the  $\phi^4$ -theory, it is still a strongly coupled theory. Crucially, the existence of the critical point described by the action in Eq. (4.12) is based on a continuity argument between the large- $N$  limit and the  $N = 1$  case as we mentioned before. This subtle intricacy provides an analytical RG angle on the discussion raised by the unsettled numerical results (see Sec. 4.1.2). We will partly address this discussion in the next Chapter.

### 4.3 Conjectured web of dualities from DQCPs

A duality connects in principal equivalent descriptions of the same theory (or certain aspects of it) and therefore not only resolve ambiguous theoretical formulations but can also serve as powerful tool for revealing its underlying fundamental structures which in case of condensed matter systems are encoded in the conformal invariant quantum field theories describing the critical point. In general, dualities can be categorized in *weak* and *strong* formulations [51]. A weak duality connects two descriptions of the same physical system by two theories which therefore share the same local operators and global symmetries. The prime example of dualities in field theory, the charge-vortex duality [48], for instance is a *weak* duality. It states that the superfluid-Mott-insulator transition is equally described by interacting *charges*<sup>14</sup> or vortices coupled to a U(1) gauge field. Both descriptions capture

14: In the literature, the charge-vortex duality is sometimes coined *particle-vortex* which in the authors’ opinion is a less ambiguous phrasing.

the same universal long-wavelength physics and describe the same critical point [48, 228, 231]. A *strong* duality supposes that the critical point is described by a certain conformal field theory (CFT). Each theory with a continuum Lagrangian that flows under RG in to this infrared CFT may be connected by relevant perturbations. This is a much more powerful concept which provides dual descriptions of both sides of the corresponding phase transition. Numerical simulations [232] suggest that the charge-vortex duality may even be a strong one.

In the derivation of the deconfined quantum critical theory on the square lattice, we made already use of the charge-vortex duality or to be more precise of the consequent self-duality of the easy plane NCCP<sup>1</sup> model [40, 233]. While this duality connects theories in the bosonic sector only, the idea inspired a search for a fermionic counterpart. Initiated by ideas of D. T. Son on the Dirac theory of the half-filled Landau level [234], it was proposed that the theory of a free massless fermion is dual to Dirac fermions coupled to a U(1) gauge field [45–47]. While this can be indeed understood as the fermionic counterpart to the charge-vortex duality it remains entirely in the fermionic sector.

However, there were also found early indications for a boson-fermion duality at the critical point which suggests the equivalence between  $(2 + 1)d$  quantum electrodynamics (QED<sub>3</sub>) and an easy-plane version of the CP<sup>1</sup> sigma model<sup>15</sup> at criticality [235]. Together with the fermion-fermion dualities, these findings triggered the conjecture of partly ‘bosonized’ fermion-boson dualities [49, 236]. Even better, a comprehensive web of dualities between  $2 + 1d$  theories from both gauged fermionic and bosonic sector was spanned [50]. While some of the proposed (conjectured) dualities can be explicitly derived within a lattice formulation [237], advancing established supersymmetric dualities [238] or at least verified in the large- $N$  limit [239], most of them still lack a rigorous proof or at least convincing consistency checks. A subsection or “miniweb” [51] of this novel dualities focuses on deconfined quantum critical points. The intriguing emergent SO(5) symmetry (see Fig. 4.4) in this context was proposed to be a consequence of a strong duality between the SU(2) symmetric NCCP<sup>1</sup> model and a strongly coupled version of the QED<sub>3</sub> theory coined QED<sub>3</sub>-Gross-Neveu model. We will look into this model and its conjectured scaling relations from the perturbative renormalization group point of view in Chapter 6.

15: Numerical evidence for this duality has been purported very recently as well [210, 215].





# Fixed point collision in the abelian Higgs model

# 5

The theory of the deconfined quantum phase transition of spin-1/2 particles on a square lattice involves some subtleties and pitfalls. Nevertheless, the theory we developed directly at the critical point, the NCCP<sup>1</sup> model, is surprisingly unfashionable. Although it is a strongly correlated field theory, at first glance it appears innocuous and more like the big gauge-redundant brother of the well known  $\phi^4$ -theory which we discussed in Chapter 2. One might naively assume a renormalization group analysis is not too much of a challenge. However, this assessment quickly turns out to be too simple, at least from the RG perspective. Rather, the features of the theory as we will describe them in the following, as well as the perturbative renormalizability, force us to discuss the generalized Abelian Higgs model instead of the NCCP<sup>1</sup> model.

*The content of this Chapter was published in Ref. [56] and is a result of collaboration of the author with Nikolai Zerf, Peter Marquard, Igor F. Herbut and Michael M. Scherer. The formulations and figures were kept unchanged and only slightly updated or re-arranged or for better readability. Intermediately added sentences are tagged by /\*[...]\*/.*

## 5.1 Motivation

The abelian Higgs (AH) model is one of the most fundamental field theories in both condensed matter and particle physics. It serves as the prime textbook example for the superconducting transition and the Anderson-Higgs mechanism [17, 61, 69, 240]<sup>1</sup>. The AH model features a complex scalar field coupled to a fluctuating U(1) gauge field, and it displays two distinct phases separated by a sharp transition: the symmetric phase and the phase with spontaneously broken symmetry. In the context of superconductors, the symmetric phase is related to the normal metallic state and the spontaneously broken phase to the superconducting Meissner state. As discussed in Chapter 4, the three-dimensional AH model with a single complex scalar, the charge-vortex duality links this transition to the continuous transition of the XY model [48, 228]. Moreover, this statement is backed up by numerical simulations of lattice versions of both models which confirm the conjectured mapping, and also suggest a continuous transition [48, 232, 245].

However, the field-theoretical analysis of the AH model including its generalized version with  $n$  complex scalars has turned out to be surprisingly subtle. The subtlety originates in the presence of fluctuating complex scalars and other fluctuating massless modes – here, coming from the gauge fields. Such a scenario is generic and also arises in quantum phase transitions of electronic systems. Indeed, in the AH model, the determination of the nature of transition as a function of  $n$ , i.e. the question of whether it is discontinuous or continuous, is a long-standing problem in the theory of critical phenomena [48, 228, 232, 245–255]. In mean-field approximation, for example, the  $n = 1$  transition is found to be discontinuous. This is further supported by renormalization group (RG) calculations at one-loop order

5.1 Motivation .....	59
5.2 The abelian Higgs model ....	61
5.3 Renormalization group analysis .....	62
5.4 Resummation of $n_c$ .....	66
5.5 Deconfined pseudo criticality	69
5.6 Discussion and Outlook .....	71

1: To honor its many discoverers appropriately it should always be referred to as the Anderson-Englert-Brout-Higgs-Guralnik-Hagen-Kibble mechanism [241–244], of course.

and in  $4 - \epsilon$  dimensions, which only for a very large value of  $n > n_c \sim 183$  show a critical point [246]. The next-to-leading order loop expansion, on the other hand, shows a dramatic reduction of the critical  $n_c$ , but due to the large magnitude of this correction, it remains rather inconclusive [249, 250] and has led to the belief that a perturbative RG is not well-suited for the question at hand. Nevertheless, with the sophisticated tools we are well suited to fill this long-standing void by performing a perturbative RG calculation to four-loop order and in the parameter  $\epsilon = 4 - d$ , primarily to provide an improved estimate for the critical number of complex scalars  $n_c$  above which the transition becomes continuous.

In fact, the  $n$ -component extension of the AH model is not only a playground for theoretical methods, but has is closely related to the  $\text{NCCP}^{n-1}$  models [40]. It is expected to have the same critical behavior also for the case of  $n = 2$  we found as the describing field theory in the deconfined quantum criticality context, see Eq. (4.12) [38–40, 204, 233]. On top of that, similar scenarios have been devised for  $n = 3, 4$  [206, 212] and can possibly be generalized to even higher  $n$ . To make this point clear, in the derivation of the  $\text{NCCP}^1$  model, the existence of a critical point which analytically continues from the large- $n$  results was only conjectured [38, 230]. In this light, we come back to the numerical findings, we already mentioned in Section 4.1.2. Our main concern are the doubts from recent numerical analyses [218, 219] whether the transition indeed is a continuous one in studied the spin models. In Ref. [218], the authors argue instead for a weakly first order transition but still confirm the emergent symmetry predicted by the DQCP scenario. Absence of a continuous transition with the scaling dimensions as found in Monte Carlo simulations is further supported by bounds from symmetry-enhanced conformal field theories [94, 256] which would suggest a contradictory non-unitary <sup>2</sup> conformal field theory at the critical point. These combined results suggest that the DQCP scenario is more subtle than initially expected from basic arguments.

2: In the “reply” on these findings in Ref. [198], the authors interpret the conformal bootstrap bounds as a hint for a second relevant field and conjecture it destabilizes the DQCP by topological defects.

The finding that similar scaling properties and violations are present in a variety of models suggests that the numerically observed phenomenology is not uniquely tied to a particular lattice realization and also not exclusively explicable by a fourfold anisotropy of the valence bond solid order parameter [196, 207, 208, 213, 214, 218, 219, 257]. Rather, it can be expected to be related to a general mechanism which is tied to universal physics described by an effective theory at the phase transition, i.e. the AH model.

In fact, weakly first-order transitions naturally appear in complex conformal field theories [50, 218, 219, 258] where a RG fixed point is complex-valued and, if imaginary parts are small, the complex fixed point slows down and controls the RG flow of real and unitary gapped physical theories. Such behavior naturally occurs in models where two RG fixed points collide, annihilate and move into the complex plane [259–265], e.g., the AH model below  $n_c$ .

These observations suggest that the  $n_c$  of the three-dimensional  $n$ -component AH model should be above but still near  $n = 2, 3, 4$ , to be compatible with the numerical findings. Through the explicit higher-loop RG analysis presented in this work, we provide the quantitative background for this scenario. Furthermore, we note that the special point of  $n = 1$ , which exhibits a continuous transition, is not continuously connected to the critical point at large  $n > n_c$  [218].

## 5.2 The abelian Higgs model

The  $n$ -component abelian Higgs model is also known as scalar quantum electrodynamics (QED) and is defined in  $d$ -dimensional euclidean space(time) by the Lagrangian

$$\mathcal{L} = |D_\mu \phi|^2 + \frac{1}{4} F_{\mu\nu}^2 + r|\phi|^2 + \lambda(|\phi|^2)^2. \quad (5.1)$$

Here,  $\phi = (\phi_1, \dots, \phi_n)$  describes the  $n$ -component complex scalar field with mass term  $r$  and quartic interaction  $\lambda$ . It is minimally coupled to the dynamical non-compact  $U(1)$  gauge field  $A_\mu$  via the covariant derivative  $D_\mu = \partial_\mu - ieA_\mu$  with charge  $e$  and indices  $\mu, \nu$  run from 0 to  $d - 1$ . Common summation convention over repeated indices is implied. The gauge field comes with the field strength tensor  $F_{\mu\nu} = \partial_\mu A_\nu - \partial_\nu A_\mu$  and we add a gauge fixing term  $\mathcal{L}_{\text{gf}} = -\frac{1}{2\xi}(\partial_\mu A_\mu)^2$  where  $\xi$  denotes the gauge fixing parameter.

For the case of a single complex scalar field,  $n = 1$  and in three spatial dimensions, the model is paradigmatically used to describe the superconducting transition [266] and also the nematic-to-smectic transition in liquid crystals [246]. Generally, the scalar mass parameter  $r$  can be considered as the tuning parameter of the transition towards, e.g., the superconducting state where the amplitude fluctuations of  $\phi$  become massive and – if the charge is finite  $e \neq 0$  – the phase fluctuations of  $\phi$  can be completely absorbed into the gauge field which becomes massive, too. This is the abelian and simplest version of the Higgs mechanism.

### Relation to the $CP^{n-1}$ model

In Ch. 4, we already learned that there is a close relation between the  $NCCP^{n-1}$  model (with the same universality as the AH model) and the  $CP^{n-1}$  model with the following action

$$\mathcal{S}_{CP^{n-1}} = \frac{1}{2t} \int d^d x \left( \partial_\mu \bar{\phi}_i^a \partial_\mu \phi_i^a + (\bar{\phi}_i^a \partial_\mu \phi_i^a)(\bar{\phi}_i^b \partial_\mu \phi_i^b) \right) \quad (5.2)$$

Note, that the fields are constraint by  $\sum_{a=1}^n \bar{\phi}_i^a \phi_i^a = \delta_{ij}$  [267, 268]. In terms of the renormalization group functions we can further establish this relation by considering the non-linear sigma model (nl $\sigma$ m) defined on the Grassmannian manifold of  $U(n)/[U(n-p) \times U(p)]$ . In fact for  $p = 1$ , the symmetric space is isomorphic to  $CP^{n-1}$  [269], i.e. the models share the same universality class. The beta function  $\beta_t$  for general  $p$  was computed in  $d = 2 + \epsilon$  to four-loop order [269–271]. and features an IR-unstable fixed point  $\beta_t(t_c) = 0$  reading

$$t_c = \frac{\epsilon}{n} - \frac{2\epsilon^2}{n} + \frac{3(n-4)}{2n^3} \epsilon^3 - \frac{(2n^2 - 51n + 126)}{6n^4} \epsilon^4 + \mathcal{O}(\epsilon^5), \quad (5.3)$$

which is real valued for all  $n > 0$ . Consequently, the associated correlation-length exponent  $1/\nu$  is

$$\frac{1}{\nu} = \epsilon + \frac{2}{n} \epsilon^2 + \frac{(3n-4)}{n^2} \epsilon^3 + \left( \frac{11}{n^3} - \frac{9}{2n^2} + \frac{1}{n} \right) \epsilon^4 + \mathcal{O}(\epsilon^5). \quad (5.4)$$

A further connection can be drawn between the above NL $\sigma$ M with target space  $U(n)/[U(n-p) \times U(p)]$  and a  $SU(p) \times U(1)$  gauge theory with Lagrangian [268, 272]

$$\mathcal{L} = |D_\mu \phi_a|^2 + \frac{F^2}{4} + \frac{G^2}{4} + \lambda(\bar{\phi}_a \phi_a)^2 + \gamma(\bar{\phi}_a \phi_b)(\bar{\phi}_b \phi_a). \quad (5.5)$$

Here,  $D_\mu = \partial_\mu - ieA_\mu - igB_\mu$  is the covariant derivative and  $F^2$  ( $G^2$ ) are kinetic terms for the  $U(1)$  ( $SU(p)$ ) gauge fields  $A_\mu$  ( $B_\mu$ ). Eq. (5.5) represents a generalization of the AH model and its beta functions can be deduced from it upon replacing  $n \rightarrow pn$  supplemented by the beta function for the  $SU(p)$  gauge field [268]. For  $p = 1$  we recover the AH model beta functions. The large- $n$  expansion for Eq. (5.5) gives correlation-length exponent [272]

$$\nu = \frac{1}{d-2} \left( 1 + \frac{2(d^2-d) \sin(d\pi/2) \Gamma(d-1)p}{\pi n \Gamma^2(d/2)} \right),$$

and anomalous dimension

$$\eta = \frac{p}{2n} \left( \frac{2(d-4) \sin(\pi d/2) \Gamma(d-1)}{\pi d \Gamma^2(d/2)} \right) \left( 1 - \frac{4(d-1)^2}{4-d} \right).$$

As a check, we will expand the critical exponents of the AH model to first order in  $1/n$ . An order-by-order agreement in  $\epsilon$  corroborates the evidence that both theories lie in the same universality class for large  $n$ .

### 5.3 Renormalization group analysis

The AH model has an upper critical dimension of  $d_c^+ = 4$  where the charge and the quartic coupling,  $g_i \in \{g_1 = \alpha = e^2, g_2 = \lambda\}$ , become marginal simultaneously, i.e. it is perturbatively renormalizable in  $d \leq d_c^+$ . Here, we present a perturbative renormalization group analysis in  $4 - \epsilon$  dimensions using dimensional regularization (DREG) and the modified minimal subtraction scheme ( $\overline{\text{MS}}$ ) to four-loop order. To that end, we introduce the bare Lagrangian, which is the one from Eq. (5.1) with fields and couplings replaced by their bare counterparts, i.e.  $x \mapsto x_0$  and  $x \in \{\phi, A_\mu, e, r, \lambda, \xi\}$ . Then, the renormalized Lagrangian reads

$$\mathcal{L}' = Z_\phi |D_\mu \phi|^2 + Z_{\phi^2} r \mu^2 |\phi|^2 + Z_{\phi^4} \lambda \mu^\epsilon (|\phi|^2)^2 + \frac{Z_A}{4} F_{\mu\nu}^2 - \frac{1}{2\xi} (\partial_\mu A_\mu)^2. \quad (5.6)$$

with  $D_\mu \phi = (\partial_\mu - ie\mu^{\epsilon/2} A_\mu)\phi$  and  $\mu$  defines the energy scale parametrizing the renormalization group flow. Here, we have introduced explicit  $\mu$  dependencies to rescale the dimensionless couplings in  $(4 - \epsilon)$  dimensions as well as the wavefunction renormalizations  $Z_\phi$  and  $Z_A$  to relate the bare and the renormalized Lagrangian through  $\phi_0 = \sqrt{Z_\phi} \phi$  and  $A_{0,\mu} = \sqrt{Z_A} A_\mu$ . Accordingly, the bare and the renormalized bosonic mass terms are related by  $r = r_0 \mu^{-2} Z_\phi Z_{\phi^2}^{-1}$  and we obtain the following relations between the bare and the renormalized couplings

$$\alpha = e_0^2 \mu^{-\epsilon} Z_A, \quad \lambda = \lambda_0 \mu^{-\epsilon} Z_\phi^2 Z_{\phi^4}^{-1}. \quad (5.7)$$

For completeness, we note that the flow of the gauge-fixing parameter is encoded in the relation  $\xi = \xi_0 Z_A^{-1}$ . In Fig. 5.1, we show the different types of

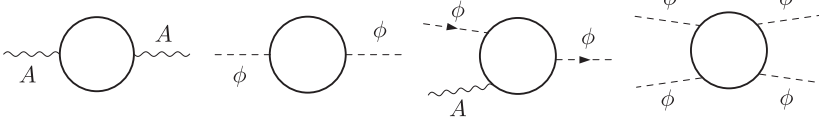


**Figure 5.1:** The four types of diagrams, we have to compute in the perturbative renormalization group procedure. Wiggly lines represent the gauge field  $A_\mu$  and dashed the bosonic field  $\phi$ . Each diagram corresponds to the renormalization of the its correlator  $\langle A_\mu A_\nu \rangle$ ,  $\langle \phi^* \phi \rangle$ ,  $\langle \phi^* A_\mu \phi \rangle$  and  $\langle |\phi|^4 \rangle$

diagrams necessary to compute. In total, we computed 1,908,140 diagrams. The calculation of the renormalization constants  $Z_x$  with  $x \in \{\phi, \phi^2, \phi^4, A\}$  at four-loop order is performed by using an automated protocol which is described in Appendix B as well as in the appendix of the original publication [56].

From the renormalization constants, we can construct the renormalization group beta functions which are defined as the logarithmic derivatives of the dimensionless renormalized couplings  $\{g_1 = \alpha = e^2, g_2 = \lambda\}$  with respect to  $b = \mu^{-1}$ . Schematically, the beta functions have the form

$$\beta_i = \frac{dg_i}{d \ln b} = \epsilon g_i + \sum_k \beta_i^{(k\ell)}, \quad (5.8)$$

where the index  $k$  indicates the loop order. Explicitly, we obtain for the gauge coupling  $\alpha$ ,

$$\beta_\alpha^{(1\ell)} = -\frac{n}{3} \alpha^2, \quad (5.9)$$

$$\beta_\alpha^{(2\ell)} = -2n \alpha^3, \quad (5.10)$$

$$\beta_\alpha^{(3\ell)} = \left(\frac{49}{72} n^2 - \frac{29}{8} n\right) \alpha^4 - \frac{n^2+n}{2} \alpha^3 \lambda + \frac{n^2+n}{8} \alpha^2 \lambda^2. \quad (5.11)$$

The beta functions for the quartic self-interaction coupling  $\lambda$  up to three-loop order are given accordingly as

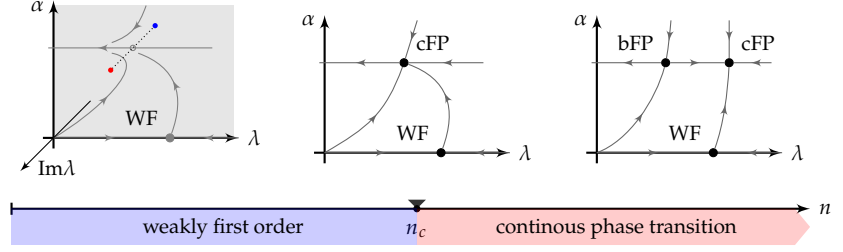
$$\beta_\lambda^{(1\ell)} = -6\alpha^2 + 6\alpha\lambda - (n+4)\lambda^2, \quad (5.12)$$

$$\beta_\lambda^{(2\ell)} = \left(\frac{14}{3}n + 30\right) \alpha^3 - \left(\frac{71}{6}n + \frac{29}{2}\right) \alpha^2 \lambda - (4n+10)\alpha\lambda^2 + \left(\frac{9}{2}n + \frac{21}{2}\right) \lambda^3,$$

$$\begin{aligned} \beta_\lambda^{(3\ell)} = & \left(-\frac{7}{18}n^2 + \left[\frac{203}{8} - 27\zeta_3\right]n + \frac{367}{8} - 45\zeta_3\right) \alpha^4 \\ & + \left(-\frac{5}{216}n^2 + \left[18\zeta_3 - \frac{989}{8}\right]n - \frac{889}{4} - 54\zeta_3\right) \alpha^3 \lambda \\ & + \left(\frac{43}{16}n^2 + \left[18\zeta_3 + \frac{1749}{16}\right]n + \frac{1093}{8} + 126\zeta_3\right) \alpha^2 \lambda^2 \\ & + \left(-\frac{33}{16}n^2 + \left[-15\zeta_3 - \frac{461}{16}\right]n - \frac{185}{4} - 33\zeta_3\right) \lambda^4 \\ & + \left(\left[\frac{25}{2} - 6\zeta_3\right]n + \frac{29}{2} + 6\zeta_3\right) \alpha \lambda^3, \end{aligned} \quad (5.13)$$

where  $\zeta_3 = \zeta(3)$  denotes the Riemann  $\zeta$ -function. The four loop contributions are presented in Appendix C.2. Note that the beta functions are gauge parameter independent as expected. Further, the expressions are in full agreement to the two-loop results [61, 247]. Also, in the limit  $\alpha \rightarrow 0$  we recover the beta functions of the purely bosonic  $2n$ -vector model up to four-loop order [148]. For completeness, we list the beta function of the gauge fixing parameter in Appendix C.2 as well. Note that we also provide the field anomalous dimensions there.

**Figure 5.2:** Renormalization group flow and fixed point annihilation in the Abelian Higgs model. The perturbative computations suggest that above a critical number of scalar components  $n_c$  an IR-attractive charged FP exists. At  $n_c$  this collides with the bicritical FP so that they annihilate and disappear in the complex plane of the quartic coupling. At  $n_c$ , the transition switches from continuous to weakly first order.



### 5.3.1 Fixed point collision at $n_c$

*/\*In Section 2.4, we showed that the critical behavior of a theory in the renormalization group approach is encoded in the stability matrix  $B_{ij}$  of a fixed point  $\{g_i^*\}$  (FP). Recall that the eigenvalues  $\theta_i$  and eigenvectors  $\mathbf{v}_i$  of  $B_{ij}$  determine the critical exponents and the corresponding directions. Positive eigenvalues describe relevant and negative ones irrelevant directions. A vanishing eigenvalue means the RG flow in this direction becomes marginal.\*/\**

When two FP solutions coincide, the flow between them is marginal, implying that the stability matrix has a vanishing eigenvalue, i.e. the determinant vanishes,

$$\det(B_{ij})|_{\{g_i^*\}} = 0, \quad (5.14)$$

providing an additional condition to the fixed point equations in Eq. (2.42). We use Eq. (5.14) and the condition of a vanishing eigenvalue,  $\theta_i = 0$  for some  $i$ , as a criterion for the appearance of a fixed point collision for both, the abelian Higgs model in  $(4 - \epsilon)$  dimensions as well as the non-linear sigma model in  $(2 + \epsilon)$  dimensions, see below.

At one-loop order, the beta functions read

$$\beta_\alpha^{(1\ell)} = -\frac{n}{3}\alpha^2, \quad \beta_\lambda^{(1\ell)} = -6\alpha^2 + 6\alpha\lambda - (n+4)\lambda^2. \quad (5.15)$$

This set of beta functions features four fixed points (FP) where  $\epsilon$ , i.e.  $\beta_i(\alpha^*, \lambda^*) = 0$  and scaling may emerge. In  $d = 4 - \epsilon$ , one FP is the trivial Gaussian fixed point,  $\alpha^* = \lambda^* = 0$ , and another one is the Wilson-Fisher fixed point of the scalar  $O(2n)$  model,  $\alpha^* = 0, \lambda^* = \epsilon/(n+4) + \mathcal{O}(\epsilon^2)$ .

The two remaining non-trivial non-Gaussian fixed points have identical FP coordinate of the gauge coupling,  $\alpha^* = 3\epsilon/n + \mathcal{O}(\epsilon^2)$ . There are two corresponding FP solutions for the quartic interaction,

$$\lambda_\pm^* = \frac{3(18 + n \pm \sqrt{s})}{2n(n+4)}\epsilon + \mathcal{O}(\epsilon^2), \quad (5.16)$$

where  $s = n^2 - 180n - 540$ . We refer to  $(\alpha^*, \lambda_+^*)$  as the charged FP and to  $(\alpha^*, \lambda_-^*)$  as the bicritical FP. The charged FP is irrelevant in both directions, i.e. represents a stable FP. The bicritical FP is unstable to perturbations in the quartic coupling.

The fixed points have a strong dependence on the number of field components  $n$ , in particular, the quartic coupling only provides real-valued solutions above a certain critical  $n > n_c$ , when the radicand  $s$  of the square root in Eq. (5.16) is positive. At  $n = n_c$  the two fixed points collide and, for  $n < n_c$ ,

drift into the complex plane. The one-loop analysis predicts that this happens for values of

$$n_{c,0} = 6(15 + 4\sqrt{15}) \approx 182.95. \quad (5.17)$$

Consequently, for  $n \geq n_c$  there is a continuous transition while below it is expected to become first-order [246]. Note that we neglected an unphysical negative solution  $n_{c,-} = 6(15 - 4\sqrt{15}) + \mathcal{O}(\epsilon) \approx -2.952 + \mathcal{O}(\epsilon)$ . At the next order around the negative solution  $n_{c,-}$ , we find it to become even more negative  $n_{c,-} \approx -2.952(1 + 1.62323\epsilon + \mathcal{O}(\epsilon^2))$ .

In the previous section, we considered the fixed points of the AH model at one-loop level and found that two fixed points collide and disappear in the complex plane when tuning the number of scalar components  $n$ . The critical number  $n_c$  below which the fixed points disappear in the complex plane was computed by analyzing the imaginary part of the quartic coupling's charged FP coordinate. Here, we compute corrections to this value at higher orders.

We use Eqs. (2.42) and (5.14) to calculate the fixed point collision point  $n_c$  in the parameter  $n$  at higher orders in the epsilon expansion to obtain the series expansion

$$n_c \approx n_{c,0} + n_{c,1}\epsilon + n_{c,2}\epsilon^2 + n_{c,3}\epsilon^3 + \mathcal{O}(\epsilon^4), \quad (5.18)$$

with  $n_{c,0}$  from Eq. (5.17) and we find

$$n_{c,1} = -\frac{9}{70} (317\sqrt{15} + 1265), \quad (5.19)$$

$$n_{c,2} = \frac{53396968 + 25893277\sqrt{\frac{3}{5}}}{768320} + \frac{27981 - 22872\sqrt{\frac{3}{5}}}{245} \zeta_3, \quad (5.20)$$

$$n_{c,3} = \frac{197218191162096 - 49532015359609\sqrt{15}}{189744307200} + \frac{1251897}{490} \zeta_5 - \frac{492241}{49\sqrt{15}} \zeta_5 \\ + \frac{(9327 - 7624\sqrt{\frac{3}{5}})}{9800} \pi^4 + \frac{(5103190199\sqrt{15} - 17908675920)}{50421000} \zeta_3, \quad (5.21)$$

where, again,  $\zeta_3 = \zeta(3)$  and  $\zeta_5 = \zeta(5)$  denote the Riemann  $\zeta$  function. Numerical evaluation then provides the approximate expression

$$n_c \approx n_{c,0}(1 - 1.752\epsilon + 0.798\epsilon^2 + 0.362\epsilon^3) + \mathcal{O}(\epsilon^4). \quad (5.22)$$

This series expansion exceeds previous estimates by two orders in  $\epsilon$ . Since the coefficients in the series of Eq. (5.18) are still decreasing in magnitude, we provide direct evaluation for  $\epsilon = 1$ , see Fig. 5.3. In the following, we will explore resummation of the series.

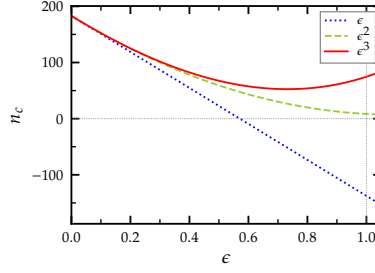


**Figure 5.3:** Direct evaluation of the epsilon expansion in Eq. (5.18) for the critical number of components  $n_c$  at different orders in  $\epsilon$ .

Order	$\epsilon = 1$
$\epsilon^0$	182.95
$\epsilon^1$	-137.54
$\epsilon^2$	8.42
$\epsilon^3$	74.69

## 5.4 Resummation of $n_c$

The expansions from perturbative RG calculations are asymptotic series. Consequently, obtaining reliable estimates for  $n_c$  at  $d = 3$  requires resummation. Whether or not such resummation yields reliable results depends on the underlying model, the order of the expansion and the knowledge about the large-order behavior. We begin with a Padé-(Borel)-resummation of the actual epsilon expansion and then move on to more sophisticated and equally hypothetical interpolation to two dimensions. Application of the Borel resummation scheme as shown in Chapter 3 was not fruitful and we refer for details on this to the appendix in our publication [56].

### 5.4.1 Resummation of $(4 - \epsilon)$ expansion

**Table 5.1:** Padé and Padé-Borel approximants of the epsilon expansion evaluated at  $d = 3$  ( $\epsilon = 1$ ). The Padé-Borel [2/1] is not available due to a singularity in the integral of the Borel sum.

$[m/n]$	Padé	Padé-Borel
[0/1]	66.48	89.11
[0/2]	36.42	66.78
[1/1]	-37.25	-46.53
[0/3]	25.27	58.42
[2/1]	129.81	-
[1/2]	1.81	-13.65

At first, we explore three resummation schemes for the series in  $(4 - \epsilon)$  dimensions, i.e. 1. Padé approximants, 2. Padé-Borel approximants and 3. Borel resummation. The employed schemes presented here are conventional and we use standard notation, e.g., for the Padé approximants  $[m/n]$ . Explicit definitions are provided in the appendix of Ref. [56]. We display the available Padé and Padé-Borel approximants order by order in Fig. 5.4 and in Tab. 5.1. The Borel resummation scheme including the corresponding set of resummation parameters is introduced in the appendix of Ref. [56] and we merely state the results here. Optimization through variation of the resummation parameters according to the principle of minimal sensitivity and the principle of fastest convergence yields a negative weighted mean value for  $n_c(\epsilon = 1)$  with a huge error of  $n_c(\epsilon = 1) \approx -52 \pm 45$ . In the present case, we find that the three methods do not allow us to extract a precise numerical result for  $n_c(\epsilon = 1)$  and estimates are scattered over a rather large range.

The main conclusion drawn from this one-sided resummation analysis is therefore merely that  $n_c(\epsilon = 1)$  lies significantly below the leading-order

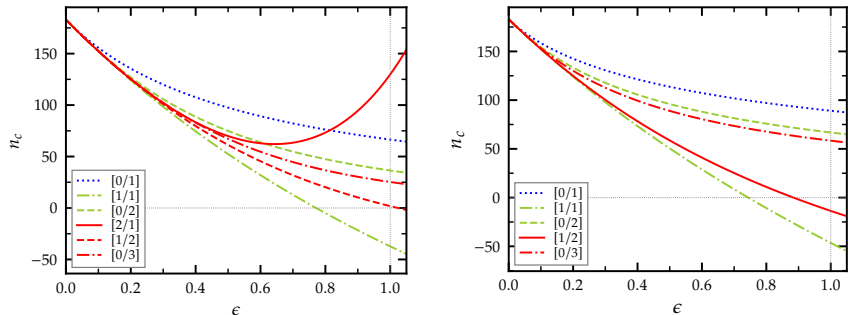


**Figure 5.4:** Resummed epsilon expansion for the critical number of components  $n_c$ . Left panel: Padé approximants. Right panel: Padé-Borel approximants. (Adapted from Ref. [56])



result of  $n_{c,0} \approx 183$ .

## 5.4.2 Dimensional interpolation

In view of the high order series for  $n_c$  in  $\epsilon$ , we would like to obtain a better estimate on  $n_c(\epsilon = 1)$  than the one from the resummations explored in the previous section. This is possible through an interpolation between two and four dimensions and by additionally including the assumption of  $n_c(d = 2 + \epsilon) = a\epsilon$ , with unknown coefficient  $a > 0$ . /\*Assuming a continuous function for  $n_c(d)$  we can hope to find it somewhere in the gray shaded area of Fig. 5.5 in  $d \in (2, 4)$ . Above the line we then would expect a continuous transition and below a weakly first order one. Note that with  $n = 1$  at  $d = 3$  we know the transition has to be continuous because of the charge-vortex duality [48] but this point does not necessarily lie in the large- $n$  interpolation. Before we carry out the explicit interpolations between two and four dimensions, we briefly review the arguments leading to that conjecture.\* /

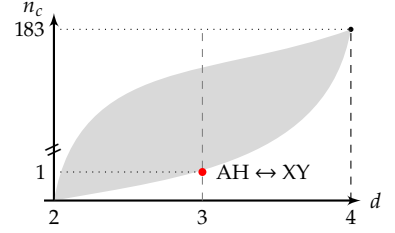


**Figure 5.5:** Schematic plot of  $n_c(d)$ . When we fix it at  $n_c(d = 2 + \epsilon) = a\epsilon$  with  $a > 0$ , the curve will hopefully lie in the gray shaded area. Note that the point with  $n = 1$  at  $d = 3$  is known to be a continuous transition from the charge-vortex duality [48].

### Nonlinear $\sigma$ model in $(2 + \epsilon)$ dimensions

The first item is suggested from studying the nonlinear sigma model in  $(2 + \epsilon)$  dimensions, e.g., in the  $CP^{n-1}$  formulation [267, 268] as we laid out in Sec. 5.2. Practically, this connection is exhibited by comparing their critical exponents with the large- $n$  result expanded in the respective dimension which turn out to be identical. We find that, the large- $n$  inverse correlation-length exponent expanded around  $d = 2 + \epsilon$  agrees with the exponent from the  $CP^{n-1}$  model to all available orders in  $\epsilon$ . Therefore, the two expansions near two and four dimensions in the respective models can be employed to provide for a continuous interpolation of the same renormalization group fixed points in the plane  $(n, d)$  for large enough  $n > n_c(d)$ .

In the  $CP^{n-1}$  model  $n_c(d \rightarrow 2) \rightarrow 0$  [267, 268]. Moreover in  $d = 2 + \epsilon$ , the beta function of the model coupling  $t$  features a real valued fixed-point solution  $t^*$  for all  $n > 0$ , which for small  $\epsilon$  is  $t^* = \epsilon/n + \mathcal{O}(\epsilon^2)$ . Therefore, a fixed-point collision is expected to be exhibited in the symmetry-allowed higher-derivative terms of the non-linear sigma model. For example, the RG scaling of the canonically least irrelevant higher-derivative terms, i.e. the four-derivative terms, is found to be  $y_4 = -2 + \epsilon + 4t^*$  at one-loop order. A fixed-point collision would now be indicated by a vanishing of  $y_4$ , i.e. when the scaling becomes marginal, cf. Eq. (5.14), which at that order yields  $n_c(d = 2 + \epsilon) = 2\epsilon + \mathcal{O}(\epsilon^2)$ .

At this point a word of caution seems in order. Concerning a possible fluctuation-induced fixed-point destabilization due to the RG relevance of terms with an even larger number of derivatives in nonlinear sigma and related models, there has been an extended discussion in the literature, e.g., Refs. [273–275], which we here will not attempt to resolve. Instead, we take on a pragmatic approach by assuming that near two dimensions the first fluctuation-induced relevant direction comes from the least irrelevant canonical terms, which is the four-derivative term. Moreover, since  $t^*$  is of  $\mathcal{O}(1)$  at that point and therefore not small, the corrections to the leading-order behavior of  $y_4$  cannot be expected to be small either. We therefore refrain from fixing the coefficient of the epsilon expansion of  $n_c(d + \epsilon)$  and just

3: The scaling of higher-derivative terms is found to be  $y = 2 - 2k + \epsilon + 2k(k - 1)t^*$  for terms  $2k$  derivatives, cf. Ref. [273].

write  $n_c(d = 2 + \epsilon) = a\epsilon$ , with unknown coefficient  $a > 0$  as stated above, see also Ref. [218].

### Interpolation

A suitable interpolation between the two critical dimensions can now be constructed by using a polynomial ansatz as we employed it already in Chapter 3. To that end, we use both epsilon expansions for  $n_c$ , simultaneously, and set up an interpolating function in the interval  $d \in [2, 4]$ . More specifically, we choose a polynomial interpolation with polynomial  $P_{i,j}(d)$  of degree  $i + j$ , where  $i$  ( $j$ ) denotes the highest order of the epsilon expansion in  $d = 2 + \epsilon$  ( $d = 4 - \epsilon$ ) dimensions, i.e.  $i = 1$  and  $j \in \{1, 2, 3, 4\}$ . We fix the polynomial coefficients of the first  $i + 1$  terms with the expansion near the lower critical dimension. The remaining  $j + 1$  higher-order coefficients are then determined from the requirement that the  $j$  lowest derivatives of  $P_{i,j}(d)$  at  $d = 4$  correspond to the  $(4 - \epsilon)$ -expansion. The resulting polynomials are then by construction  $i$ -loop exact near the lower critical dimension and  $(j$ -loop) exact near the upper critical dimension. From this calculation, we obtain interpolating functions for general coefficient  $a$ , i.e.  $P_{1,1}(d = 3) \approx 11.35 + 0.25a$ ,  $P_{1,2}(d = 3) \approx 2.023 + 0.125a$ ,  $P_{1,3}(d = 3) \approx 17.86 + 0.0625a$ , exhibiting that the dependence on the coefficient  $a$  is rather weak.

In Ref. [218] the additional conjecture that  $n_c(d)$  increases monotonically, i.e.  $n'_c(d) > 0$ , has been put forward, however, without further justification. Here, we briefly discuss the impact of this assumption: while  $P_{1,3}(d)$  increases monotonically for  $0 < a \lesssim 80$ ,  $P_{1,1}(d)$  requires  $10 \lesssim a \lesssim 200$  and  $P_{1,2}(d)$  is never monotonous for  $2 < d < 4$ . We show the results for the polynomial interpolation as a function of  $d$  in the left panel of Fig. 5.6 and compiled their estimates at  $d = 3$  in Tab. 5.2.

Following the same reasoning, we can set up two-sided Padé approximants  $2_{[m/n]}(d)$ , cf. the right panel of Fig. 5.6 and Chapter 3 for definitions. Tentatively, setting  $a = 1$ , we observe that increasing the order in  $2_{[m/n]}(3)$  from  $m + n = 3$  to  $m + n = 5$  decreases the range spanned by the estimates for  $n_c(d = 3)$  order by order. This behavior is even more pronounced upon disregarding the values which belong to non-monotonous interpolations, i.e. dropping the values for  $2[3/1]$  and  $2[4/1]$ .

We use the highest order,  $m + n = 5$ , including the non-monotonous  $2[4/1]$ , to calculate the average and error

$$n_c(d = 3) \approx 12.2 \pm 3.9. \quad (5.23)$$

This is our best estimate based on the above reasoning. We have also studied the dependence on the parameter  $a$  and find that, within an extended range of  $a \in [0.2, 5]$ , this estimate varies mildly, see in the appendix of Ref. [56].

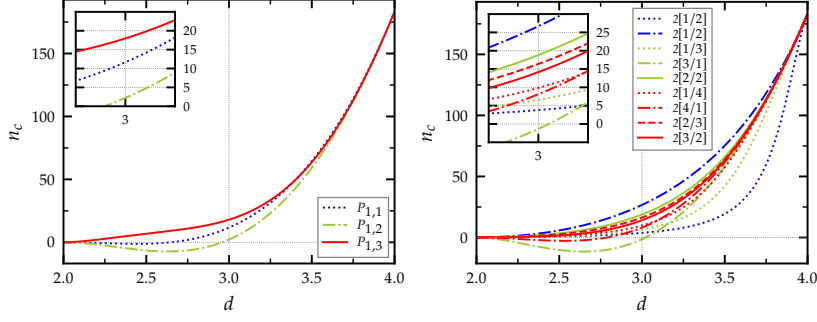


**Figure 5.6:** Left panel: Estimates from polynomial interpolation for the critical number of components  $n_c(d)$  for  $a = 1$ . Right panel: same for two-sided Padé approximants. (Adapted from Ref. [56])

## 5.5 Deconfined pseudo criticality

*/\*Since the  $n$ -component abelian Higgs model has been argued to describe the universal properties of the Néel–valence-bond-solid transition as we laid out in Chapter 4, we may also comment on the on-going discussion of the recent numerical simulations we mentioned earlier from the renormalization group perspective. Especially the strong violations of scaling which was accounted to a weakly first order transition with an anomalously large correlation length and drifting critical exponents could possibly explained by walking of the RG flow and the caused Miransky scaling.\* /*

### 5.5.1 Miransky scaling

The behavior described above may be due to emergent walking behavior that appears when two fixed points have just been annihilated and vanished into the complex plane, e.g., just as it happens in the AH model below  $n_c$ . Here, we briefly recap the underlying reasoning using the beta functions at one-loop order, cf. Eqs. (5.15). At that order for the gauge coupling the fixed point value  $\alpha_* = 3\epsilon/n$  can be acquired for any choice of  $n \leq n_c$ . Further, the gauge coupling is irrelevant and we therefore can replace  $\alpha = \alpha_*$  in the beta function for the quartic coupling  $\lambda$ , to obtain

$$\left. \frac{d\lambda}{d \ln b} \right|_{\alpha_*} = \left( 1 + \frac{18}{n} \right) \epsilon \lambda - (n+4)\lambda^2 - \frac{54}{n^2} \epsilon^2. \quad (5.24)$$

This flow equation can be integrated yielding

$$\ln \left( \frac{b_{\text{IR}}}{b_{\text{UV}}} \right) = \frac{-2n}{\epsilon \sqrt{-s}} \arctan \left( \frac{2n(4+n)\lambda - (18+n)\epsilon}{\epsilon \sqrt{-s}} \right) \Big|_{\lambda_{\text{UV}}}^{\lambda_{\text{IR}}},$$

with  $s = n^2 - 180n - 540$ , again. For  $n \lesssim n_c$ , where  $s < 0$  and  $|s| \ll 1$ , the flow of  $\lambda$  proceeds as follows:  $\lambda$  starts at some positive value, goes through a walking regime and eventually diverges towards negative values. Therefore, in the infrared and the ultraviolet, the argument of the arctan is always large, i.e. we can use  $\lim_{x \rightarrow \pm\infty} \arctan x = \pm\pi/2$ . Arbitrarily choosing  $b_{\text{UV}} = 1$  and renaming  $b_{\text{IR}} = L_{\text{IR}}$ , we obtain the exponentially large infrared length scale [218, 261, 262]

$$L_{\text{IR}}(n) \simeq \exp(\pi f(n)), \quad \text{where } f(n) = \frac{2n}{\epsilon \sqrt{-s}}, \quad (5.25)$$

which is also referred to as Miransky scaling. Note that including the running of the infrared-attractive gauge coupling yields power-law corrections to

**Table 5.2:** Estimates from polynomial interpolation and two-sided Padé approximation for the critical number of components  $n_c$  at  $d = 3$  dimensions for  $a = 1$ . The values which belong to a non-monotonous interpolating function  $n_c(d)$  for  $d \in [2, 4]$  are printed in italics.

	polyn. Int.	Two-sided Padé	
$P_{1,1}$	11.60	2[2/1]	26.62
		2[1/2]	3.77
$P_{1,2}$	2.15	2[2/2]	18.76
		2[1/3]	6.56
		2[3/1]	-1.40
$P_{1,3}$	17.92	2[2/3]	16.32
		2[3/2]	14.11
		2[1/4]	9.80
		2[4/1]	8.06

this behavior [276]. Further, higher-loop contributions will generally modify the function  $f(n)$ .

Now, approaching  $n_c$  from below, this correlation length grows exponentially to diverge at  $n_c$ . Therefore, to obtain a large correlation length, one needs to be close to  $n_c$ , which at one-loop order, Eq. (5.25), is  $n_{c,0} \sim 183$ . Generically, small changes in  $n \lesssim n_c$  induce a large hierarchy in length scales, for example at  $\epsilon = 1$ ,  $L_{\text{IR}}(180)/L_{\text{IR}}(179) \sim 833$  or  $L_{\text{IR}}(179)/L_{\text{IR}}(178) \sim 97$  which, however, decreases rapidly when  $n$  moves away from  $n_c$ . In case,  $n$  is further away from  $n_c$ , the correlation length is, of course, exponentially suppressed.

Including higher-loop contributions into this reasoning will significantly change the quantitative aspects of this behavior, but not its qualitative features. For this work, we refrain from providing a corresponding quantitative analysis, since this would require an appropriate resummation of the underlying higher-loop beta functions. We postpone such an analysis to the future and describe the underlying qualitative implications, instead.

### Hierarchy of length scales

In numerical simulations of deconfined quantum transitions, similar scaling violations have been observed for various lattice models [196, 207, 208, 213, 214, 257] and, notably, also for a range of values for  $n$ , i.e.  $n = 2, 3, 4$  [206, 212]. Here, based on our four-loop calculations and the interpolating functions from Sec. 3, we will explore whether such scaling violations for  $n = 2, 3, 4$  can be consistently be ascribed to the pseudo-critical or walking behavior related to Miransky scaling, cf. Eq. (5.25), in the three-dimensional AH model. First, we note that our estimate of  $n_c(3) \approx 12.2 \pm 3.9$ , Eq. (5.23), tentatively supports the scenario that  $n_c(3)$  is of comparable order as the physically relevant  $n = 2, 3, 4$ . Uncertainties in this determination are still large and it is therefore conceivable that the true  $n_c(3)$  is closer to  $n = 2, 3, 4$ . The following reasoning, however, will not rely on the precise number  $n_c(3)$ , but on the behavior of the interpolating function  $n_c(d)$  for  $d \in [2, 4]$  as exhibited in Fig. 5.6.

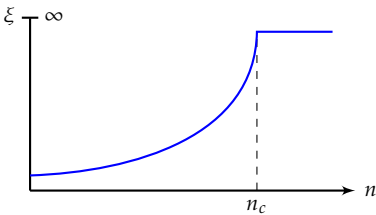


**Figure 5.7:** Depiction of the Miransky scaling below the fixed point collision. Towards but below  $n_c$ , the correlation-length  $\xi$  grows exponentially leading to a strong hierarchy of length scales close to  $n_c$ . Above  $n_c$ , the fixed point exists and we can observe critical behavior with  $\xi = \infty$ .

The essential feature of the infrared length scale as given by the Miransky scaling, Eq. (5.25), is that the length scale diverges when approaching  $n_c$  from below as shown in Fig. 5.7. This is related to the singularity in the argument  $f(n)$  appearing in the exponential at  $n_c$ . Sufficiently close to  $n_c$ , the slope of  $L_{\text{IR}}(n)$  diverges, too, and small variations of  $n$  are expected to lead to large changes in  $L_{\text{IR}}(n)$ . This behavior is generic unless the function  $f(n)$  is exceptionally flat just before it develops the singularity, e.g., like an inverse step function  $\Theta^{-1}(n_c - n)$ . Whereas, we cannot quantitatively determine the function  $f(n)$  from our present analysis, our interpolating functions for  $n_c(d)$ , cf. Fig. 5.6, do not provide indications for such exceptionally flat behavior. We therefore expect that near  $n_c$  a change of  $n \rightarrow n \pm 1$  significantly impacts the correlation length due to its exponential behavior. On the other hand, if  $n$  is further away from  $n_c$ , it is exponentially suppressed and the pseudo-critical or walking regime where, approximate scaling can be observed, should be small.

We conclude that, generically, a substantial hierarchy of characteristic correlation lengths can be expected for different values of  $n$ . In particular, if the true  $n_c(3)$  lies close enough to  $n = 2, 3, 4$ , we predict that the three cases

should exhibit this large hierarchy of length scales, which can be probed in numerical simulations by comparing the correlation lengths for  $n = 2, 3, 4$ .

## 5.6 Discussion and Outlook

We have delivered a study of the  $n$ -component AH model at four loops and in  $(4 - \epsilon)$  dimensions and analysed the critical number of complex scalars  $n_c$ , below which a fixed-point collision appears and the phase transition turns from second to first order. Based on a series of assumptions on the topology of the RG flow between two and four dimensions, we have obtained a smooth interpolating function  $n_c(d)$  and our best estimate for the three-dimensional case yields  $n_c(3) \approx 12.2 \pm 3.9$ . Slightly below  $n_c$  weakly first order behavior occurs with a correlation length which is governed by Miransky scaling, i.e. it is exponentially suppressed upon increasing the distance to the point of fixed-point collision.

Due to this exponential dependence, even small variations of  $n$  are expected to induce substantial changes in the correlation length unless the argument appearing in the exponential is an exceptionally flat function of  $n$ . We do not find indications of such behavior and therefore predict a large hierarchy of correlation lengths for different  $n$ , if  $n_c(3)$  is near these values. This is relevant to the results from different lattice studies of the corresponding deconfined phase transitions for  $n = 2, 3, 4$  and we expect that indications of this hierarchy of length scales can be measured in numerical simulations.

In the future, it will be interesting to extract more quantitative estimates for the merging line  $d_c(n)$  employing appropriate resummations of the beta functions [277]. */\*A potential prospect could be offered by non-perturbative RG as explored in Refs. [253–255, 278]. These works either find a vanishing  $n_c$  at three dimensions [253, 254] or a strong regulator dependence [255] when using the modified Ward-Takahashi identities [83]. A conclusive answer to this question from the RG perspective is therefore still pending.\* /*



# Deconfined criticality in the QED<sub>3</sub>-Gross-Neveu model

# 6

The conjectured web of dualities we discussed in Chapter 4 also involves the duality between the SU(2) symmetric noncompact CP<sup>1</sup> model, describing the Néel-VBS deconfined QCP, and the QED<sub>3</sub>-Gross-Neveu (QED<sub>3</sub>-GN) model [50]. This latter theory consists of 2+1d gapless Dirac fermions that are charged under a U(1) gauge field as in QED<sub>3</sub>, but are additionally coupled to a critical Gross-Neveu scalar field. The duality implies an emergent SO(5) symmetry at the deconfined QCP [50], which rotates components of the Néel and VBS order parameters into each other. Such an emergent symmetry had in fact been observed numerically earlier [44] as well as confirmed in more recent simulations [199, 220, 221]. Although having passed a number of consistency checks [50], it should be emphasized that this fermion-boson duality, just as most of the other new duality relations in 2+1 dimensions, lacks a formal proof. In particular, it is at present unclear, whether the strong version of the duality holds, implying that the two theories flow to the same renormalization group (RG) fixed point and describe the same infrared physics, or only a weaker version applies, stating that the two theories “live in the same Hilbert space,”. In the later, they have the same local operators, the same symmetries, and the same anomalies (if any) [50]. Assuming the strong version of the duality, however, implies a number of nontrivial scaling relations between the CP<sup>1</sup> and QED<sub>3</sub>-GN models, as well as new pertinent scaling relations entirely within the QED<sub>3</sub>-GN model itself. These scaling relations allow to test the duality conjecture on a quantitative level and, eventually, to answer the question which version of the duality applies.

Recently, it has been shown that the QED<sub>3</sub>-GN model exhibits an infrared stable RG fixed point, the existence of which is a prerequisite for the proposed (strong version of the) duality to hold [279]. This can be established within a suitable generalization of the model to noninteger space-time dimension  $d$  with  $2 < d < 4$ . This theory has an upper critical space-time dimension of  $d_c^+ = 4$ , enabling one to compute the critical behavior within a controlled epsilon expansion in  $d = 4 - \epsilon$  dimensions. Here, we extend the previous one-loop analysis [279] to the three-loop order and compute the scaling dimensions of various operators to compare with the predictions from the duality. Moreover, we establish the previously conjectured [279] equivalence of the QED<sub>3</sub>-GN model with a gauged fermionic theory in which the boson-mediated scalar interaction is replaced by a corresponding critical four-fermion interaction. This fermionic theory is amenable to a  $1/N$  expansion in fixed dimension  $2 < d < 4$ , which allows us to demonstrate order by order in a double expansion in both  $\epsilon$  and  $1/N$  the explicit equivalence of the ultraviolet stable fixed point in this theory with the infrared stable fixed point of the QED<sub>3</sub>-GN model. This puts the asserted equivalence of these gauge theories on the same level as the known ultraviolet-infrared correspondence between the usual ungauged Gross-Neveu and Gross-Neveu-Yukawa models [127, 156] which connection we exploited in the first project in Chapter 3.

*The content of this Chapter was published in Ref. [57] and is a result of collaboration of the author with Lukas Janssen, Luminita N. Mihaila and Michael M. Scherer. The formulations and figures were kept unchanged and only slightly updated or*

6.1 The QED <sub>3</sub> -Gross-Neveu model	74
6.2 Duality conjecture .....	77
6.3 Renormalization group analysis .....	79
6.4 Quantum critical behavior ...	84
6.5 Estimates for 2+1 dimensions	87
6.6 Comparison with duality predictions.....	89
6.7 Discussion and Outlook .....	90

*re-arranged or for better readability. Intermediately added sentences are tagged by /\*[...]\*/*

## 6.1 The QED<sub>3</sub>-Gross-Neveu model

*/\*In this Section, we introduce the two relevant U(1)-gauged fermionic models for the dual description of the deconfined quantum critical point, i.e., the QED<sub>3</sub>-GN model and the corresponding gauged four-fermion model. Especially, the QED<sub>3</sub>-GN model appears familiar since it can also be understood as the partially gauge-invariant big brother of the chiral Ising Gross-Neveu-Yukawa model, we extensively discussed in Chapter 3. Nevertheless, the gauge degree of freedom turns out to be not only a minor subtlety but elevates the model to a new universality class with its own challenges.\*/*

### 6.1.1 QED<sub>3</sub>-GN model

The QED<sub>3</sub>-GN model is defined in  $d = 2+1$  Euclidean space-time dimensions by the Lagrangian [50]

$$\mathcal{L} = \bar{\psi}_i(\not{D} + g\phi)\psi_i + \frac{1}{4}F_{\mu\nu}^2 + \frac{1}{2}\phi(r - \partial_\mu^2)\phi + \lambda\phi^4, \quad (6.1)$$

with  $\psi_i$  and  $\bar{\psi}_i$  being  $2N$  flavors of two-component gapless Dirac spinors,  $i = 1, \dots, 2N$ , which interact with each other through the real scalar field  $\phi$ . Here, we have abbreviated the covariant derivative  $\not{D} \equiv (\partial_\mu - ieA_\mu)\sigma_\mu$ , with the  $2 \times 2$  matrices  $\sigma_\mu$  serving as a two-dimensional representation of the Clifford algebra,  $\{\sigma_\mu, \sigma_\nu\} = 2\delta_{\mu\nu}\mathbf{1}$ . The summation convention over repeated indices is implicitly assumed.  $F_{\mu\nu} = \partial_\mu A_\nu - \partial_\nu A_\mu$  is the field strength tensor of the U(1) gauge field  $A_\mu$ ,  $\mu, \nu \in \{0, 1, 2\}$ . In our calculations, we will also add a gauge-fixing term

$$\mathcal{L}_{\text{gf}} = -\frac{1}{2\xi}(\partial_\mu A_\mu)^2, \quad (6.2)$$

to the Lagrangian with gauge fixing parameter  $\xi$ , allowing us to check the gauge invariance of our results. In addition to the U(1) gauge symmetry, the theory satisfies an SU(2N) flavor symmetry and a set of discrete symmetries such as parity, charge conjugation, and time reversal. Under the latter, the scalar field  $\phi$  maps to  $-\phi$ . The scalar mass parameter  $r$  can be used as a tuning parameter for a symmetry-breaking phase transition at some critical  $r_c$ . For  $r < r_c$ ,  $\phi$  acquires a vacuum expectation value,  $\langle\phi\rangle \propto \langle\bar{\psi}_i\psi_i\rangle \neq 0$ , signaling the spontaneous breaking of time-reversal symmetry and the dynamical generation of a fermion mass.

A lattice realization of this ordered state is given by the quantum anomalous Hall state with spontaneously generated microscopic currents, a gapped bulk spectrum, and topologically protected chiral edge states [280]. The gauge symmetry as well as the flavor symmetry remain intact across this transition. In Eq. (6.1), the charge  $e$ , the Yukawa coupling  $g$ , as well as the bosonic selfinteraction  $\lambda$  become simultaneously marginal at the upper critical dimension  $d_c^+ = 4$ , suggesting that the critical point may be approached within a standard  $\epsilon$  expansion in  $d = 4 - \epsilon$  space-time dimensions.



In order to generalize the theory to arbitrary dimension  $2 < d < 4$ , we first combine the  $2N$  flavors of two-component spinors into  $N$  flavors of four-component spinors [281]

$$\Psi_a \equiv \begin{pmatrix} \psi_a \\ \psi_{a+N} \end{pmatrix} \quad \text{and} \quad \bar{\Psi}_a \equiv (\bar{\psi}_a, -\bar{\psi}_{a+N}), \quad (6.3)$$

with  $a = 1, \dots, N$ . The Dirac kinetic term then becomes  $\bar{\Psi}_a \partial_\mu \gamma_\mu \Psi_a$  with  $\gamma_\mu = \sigma_z \otimes \sigma_\mu$ , where  $\sigma_z$  denotes the diagonal  $2 \times 2$  Pauli matrix.  $\gamma_\mu$  serves as four-dimensional *reducible* representation of the Clifford algebra. The Yukawa interaction reads  $\phi \bar{\Psi}_a \gamma_{35} \Psi_a$  with  $\gamma_{35} = i\gamma_3 \gamma_5 = \sigma_z \otimes \mathbb{1}$ . Here,  $\gamma_3$  and  $\gamma_5$  are the two ‘‘left-over’’ gamma matrices, which anticommute with each other as well as with  $\gamma_0, \gamma_1$ , and  $\gamma_2$  [106, 282]. It is important to note that  $\gamma_{35}$  squares to one and commutes with the fermion propagator  $G_\Psi(p) = -i\delta_{ab}\not{p}/p^2$  in  $d = 3$ . The above theory with the full  $SU(2N)$  flavor symmetry therefore has the same loop expansion as a corresponding theory with a smaller symmetry of only  $SU(N) \times SU(N) \times U(1)$ , in which the Yukawa interaction is replaced by the simple scalar interaction involving only the identity operator

$$\phi \bar{\Psi}_a \gamma_{35} \Psi_a \mapsto \phi \bar{\Psi}_a \mathbb{1} \Psi_a. \quad (6.4)$$

This is because in any nonvanishing closed fermion loop, the bilinear operator  $\gamma_{35}$  occurs always twice and may thence in all diagrams be replaced by  $\mathbb{1}$  from the outset. The critical behavior determined by, e.g., the critical exponents  $\eta_\phi$  and  $\nu$ , of these two theories should therefore coincide to all orders in the perturbative expansion. We note, however, that subleading exponents, such as the corrections-to-scaling exponent  $\omega$ , corresponding to irrelevant operators, might deviate, cf. Ref. [281].

A generalization of  $\gamma_{35}$  to noninteger dimensions can be obtained by noting that  $\gamma_{35} = -\frac{i}{3!}\epsilon_{\mu\nu\rho}\gamma_\mu\gamma_\nu\gamma_\rho = -i\gamma_{[\mu}\gamma_\nu\gamma_\rho]}$ , where the square brackets denote complete antisymmetrization. The last form is a well-defined expression also in noninteger dimension [283], however, this expression does not preserve the commutation relation between  $\gamma_{35}$  and  $G_\Psi$  in  $d \neq 3$ . In  $d = 4$ , e.g., one obtains  $\gamma_{35} \rightarrow \gamma_\mu\gamma_5$ , which neither commutes nor anticommutes with  $G_\Psi$ . By contrast, the naive generalization of the  $SU(N) \times SU(N) \times U(1)$ -symmetric theory, which keeps the simple scalar Yukawa term  $\bar{\Psi}_a \Psi_a$  in all dimensions  $2 < d < 4$ , does retain this crucial property of the loop expansion in a trivial way,  $[G_\Psi, \mathbb{1}] = 0$ . In this work, we therefore advocate the use of this latter theory to approach the critical behavior of the QED<sub>3</sub>-GN model within an  $\epsilon$  expansion around the upper critical space-time dimension of  $d_c^+ = 4$ .

### 6.1.2 Gauged four-fermion theory

In Ref. [279], it was suggested that the infrared stable fixed point in the critical QED<sub>3</sub>-GN model can be equivalently understood as an ultraviolet stable fixed point of a gauged four-fermion model with Lagrangian

$$\mathcal{L}_{4\text{-fermi}} = \bar{\Psi}_a \not{D} \Psi_a + \frac{1}{4} F_{\mu\nu}^2 + \frac{g^2}{2r} (\bar{\Psi}_a \Psi_a)^2. \quad (6.5)$$

This is reminiscent of the correspondence between the infrared fixed point in the critical Gross-Neveu-Yukawa model and the ultraviolet fixed point of the fermionic Gross-Neveu model [127, 156]. The correspondence can be made

plausible by means of a Hubbard-Stratonovich transformation, where the quartic interaction is replaced by a Yukawa coupling to an order-parameter field  $\phi$ , yielding the effective fermion-boson Lagrangian

$$\mathcal{L}'_{4\text{-fermi}} = \bar{\Psi}_a (\not{D} + g\phi) \Psi_a + \frac{1}{4} F_{\mu\nu}^2 + \frac{r}{2} \phi^2, \quad (6.6)$$

which is equivalent to Eq. (6.1) up to the presence of the gradient term  $\propto \partial^2 \phi^2$ , the boson self-interaction  $\propto \lambda \phi^4$  and the previously discussed difference in flavor symmetry. Within the  $1/N$  expansion, the model (6.5) has been shown to possess a critical fixed point in all dimensions  $2 < d < 4$  [284–286]. Below, we collect additional evidence that the theories defined by Eqs. (6.1) and (6.5) lie in the same universality class upon a double expansion in both  $1/N$  and  $\epsilon = 4 - d$ . In fact, we carry out this expansion up to linear order in  $1/N$  and cubic order in  $\epsilon$  and show that the exponents  $\eta_\phi$  and  $\nu$  precisely coincide order by order in the calculation.

### 6.1.3 Noncompact CP<sup>1</sup> model

As part of the web of dualities we laid out in Sec. 4.3, the bosonic theory that has been proposed [50] to be dual to the QED<sub>3</sub>-GN model is the CP<sup>1</sup> sigma model describing two complex fields  $z_\alpha$ ,  $\alpha = 1, 2$ . They satisfy the length constraint  $\sum_\alpha |z_\alpha|^2 = 1$ , and interact via a noncompact U(1) gauge field  $b_\mu$ . The Lagrangian can be written as

$$\mathcal{L}_{\text{CP}^1} = \frac{1}{\kappa} \sum_\alpha |(\partial_\mu - ib_\mu)z_\alpha|^2, \quad (6.7)$$

with the coupling constant  $\kappa$ , which is marginal for  $d = 2$  and perturbatively irrelevant for  $d > 2$ . In order to employ a controlled expansion in fixed  $d = 2 + 1$ , the above Lagrangian can be generalized to the CP <sup>$N_b - 1$</sup>  model by allowing an arbitrary number  $N_b$  of components of  $z$ ,  $\alpha = 1, \dots, N_b$ . At large  $N_b$ , the model can be shown to possess a quantum critical point at finite  $\kappa = \kappa_c$ , separating an ordered phase for  $\kappa < \kappa_c$  from a disordered phase for  $\kappa > \kappa_c$ . The critical exponents have been computed up to the linear order in  $1/N_b$  [246, 287, 288], yielding the correlation-length exponent  $\nu$  as

$$1/\nu_{\text{CP}^1} = 1 + \frac{48}{\pi^2 N_b} + \mathcal{O}(1/N_b^2) \quad (6.8)$$

and the anomalous dimension  $\eta_z$  as

$$\eta_z = -\frac{4(3 + 2\xi)}{\pi^2 N_b} + \mathcal{O}(1/N_b^2). \quad (6.9)$$

Note that  $\eta_z$  depends on the gauge-fixing parameter  $\xi$ , while  $\nu$  is gauge independent. The case relevant for the deconfined critical point between Néel and VBS orders on the square lattice is given by  $N_b = 2$ . The “spinon fields”  $z = (z_1, z_2)^T$  then describe the fractionalized quasiparticles at the transition point, and the Néel order parameter is  $\mathbf{N} = z^\dagger \boldsymbol{\sigma} z$ . Here,  $\boldsymbol{\sigma}$  stands for the three-dimensional vector of Pauli matrices. The anomalous dimension of the Néel order parameter is given by  $\eta_{\text{Néel}} = 1 + 2\eta_z + 2\eta_{z^\dagger \boldsymbol{\sigma} z}$ , where  $\eta_{z^\dagger \boldsymbol{\sigma} z}$  denotes the anomalous dimension of the vertex  $z^\dagger \boldsymbol{\sigma} z$ . To the linear order in

$1/N_b$ , it reads

$$\eta_{\text{Néel}} = 1 - \frac{32}{\pi^2 N_b} + \mathcal{O}(1/N_b^2), \quad (6.10)$$

in which the gauge dependence has dropped out, as expected [288]. The coefficient of the leading-order correction  $\propto 1/N_b$  is large, and higher-order calculations are necessary to yield an estimate for the case of  $N_b = 2$ . The VBS order parameter is given by the instanton operator  $\mathcal{M}_b$ , which creates a monopole in the gauge field  $b_\mu$  with lowest finite topological charge. The scaling dimension of  $\mathcal{M}_b$  has been computed up to next-to-leading order in the  $1/N_b$  expansion [289], yielding the VBS anomalous dimension

$$\eta_{\text{VBS}} = 0.249N_b - 0.237 + \mathcal{O}(1/N_b), \quad (6.11)$$

which is well consistent with numerical results for various  $N_b$  [204].

## 6.2 Duality conjecture

Let us review the conjectured duality between the  $\text{CP}^1$  model and the  $N = 1$  QED<sub>3</sub>-GN model in 2+1 dimensions [50]. On the bosonic side, the two real components of the complex VBS order parameter  $\mathcal{M}_b$  and the three components of the Néel order parameter  $\mathbf{N}$  can be combined into a 5-tuplet,

$$\mathbf{n}_{\text{CP}^1} = (2\Re\mathcal{M}_b, 2\Im\mathcal{M}_b, z^\dagger\sigma_x z, z^\dagger\sigma_y z, z^\dagger\sigma_z z). \quad (6.12)$$

Here, the first two components of  $\mathbf{n}_{\text{CP}^1}$  transform into each other under the global U(1) symmetry, while the last three components transform as a 3-vector under the SU(2) spin symmetry.

On the fermionic side, a monopole in the gauge field  $A_\mu$  created by the operator  $\mathcal{M}_A$  induces a zero mode for each of the two Dirac fermions, with one of it filled as a consequence of the Atiyah-Singer index theorem [290]. This allows to construct a 5-tuplet in the QED<sub>3</sub>-GN model with  $N = 1$  as

$$\mathbf{n}_{\text{QED}_3\text{-GN}} = [\Re(\psi_1^\dagger\mathcal{M}_A), -\Im(\psi_1^\dagger\mathcal{M}_A), \Re(\psi_2^\dagger\mathcal{M}_A), \Im(\psi_2^\dagger\mathcal{M}_A), \phi]. \quad (6.13)$$

The  $N = 1$  QED<sub>3</sub>-GN model has an explicit SU(4) symmetry in 2+1 dimensions, under which the first four components of  $\mathbf{n}_{\text{QED}_3\text{-GN}}$  are rotated into each other.

The proposed strong version of the duality now implies that  $\mathbf{n}_{\text{CP}^1}$  and  $\mathbf{n}_{\text{QED}_3\text{-GN}}$  are dual to each other when both  $\text{CP}^1$  and QED<sub>3</sub>-GN models are tuned to their respective critical points,

$$\mathbf{n}_{\text{CP}^1}(\kappa \rightarrow \kappa_c) \sim \mathbf{n}_{\text{QED}_3\text{-GN}}(r \rightarrow r_c). \quad (6.14)$$

We emphasize that the duality is expected to hold only precisely in  $d = 2 + 1$  dimensions and for two flavors of two-component Dirac spinors on the QED<sub>3</sub>-GN side (corresponding to  $N = 1$  in our notation). The duality immediately implies an emergent SO(5) symmetry in both models at criticality, since any component of  $\mathbf{n}_{\text{CP}^1}$  and  $\mathbf{n}_{\text{QED}_3\text{-GN}}$ , respectively can be rotated into each other by applying the symmetry transformation of the respective dual theory. If the duality holds, it would therefore explain the emergent SO(5) observed

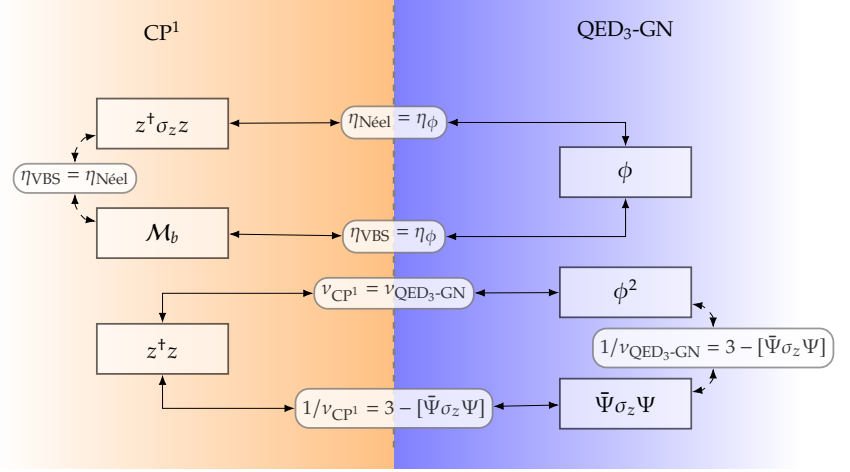


**Figure 6.1:** Summary of conjectured duality relations among and within the CP<sup>1</sup> and QED<sub>3</sub>-GN models. The duality relation within the  $N = 1$  QED<sub>3</sub>-GN model is emphasized by the thicker red arrow and will be subject to investigation here.

numerically at the deconfined critical point [44]. It also implies that the scaling dimensions of all components of  $\mathbf{n}_{\text{CP}^1}$  and  $\mathbf{n}_{\text{QED}_3\text{-GN}}$  coincide. For instance,  $[\mathcal{M}_b] = [z^\dagger \sigma_z z]$ , from which we obtain

$$\eta_{\text{VBS}} = \eta_{\text{N\acute{e}el}}, \quad (6.15)$$

which is consistent with the numerics [218]. Also,  $z^\dagger \sigma_z z \sim \phi$  implies that the anomalous dimensions of the CP<sup>1</sup> and QED<sub>3</sub>-GN models coincide at criticality,

$$\eta_{\text{N\acute{e}el}} = \eta_\phi. \quad (6.16)$$

Moreover, from the SO(5) vectors  $\mathbf{n}_{\text{CP}^1}$  and  $\mathbf{n}_{\text{QED}_3\text{-GN}}$  we can construct traceless second-rank tensor operators

$$X^{(2)} = \mathbf{n} \mathbf{n}^T - \frac{1}{5}(\mathbf{n})^2 \mathbb{1}_5, \quad (6.17)$$

with the duality implying

$$X_{\text{CP}^1}^{(2)}(\kappa \rightarrow \kappa_c) \sim X_{\text{QED}_3\text{-GN}}^{(2)}(r \rightarrow r_c). \quad (6.18)$$

Note that  $X_{\text{CP}^1}^{(2)}$  involves the operators  $\mathcal{M}_b^\dagger \mathcal{M}_b$  and  $N^2$ , which tune through the N\acute{e}el-VBS transition, while  $X_{\text{QED}_3\text{-GN}}^{(2)}$  involves  $\phi^2$ , which tunes through the time-reversal-symmetry-breaking transition in the QED<sub>3</sub>-GN model. We therefore have that  $[\mathcal{M}_b^\dagger \mathcal{M}_b] = [N^2] = [\phi^2]$ , and the correlation-length exponents must coincide as a consequence of the duality,

$$v_{\text{CP}^1} = v_{\text{QED}_3\text{-GN}}. \quad (6.19)$$

Even more interestingly, the fermion bilinear  $\bar{\psi} \sigma_z \psi = \bar{\psi}_1 \psi_1 - \bar{\psi}_2 \psi_2$  can be understood to also correspond to an element of  $X_{\text{QED}_3\text{-GN}}^{(2)}$  [50], yielding

$$[\bar{\psi} \sigma_z \psi] = 3 - 1/v_{\text{QED}_3\text{-GN}} \quad (6.20)$$

at the critical point of the 2+1 dimensional QED<sub>3</sub>-GN model. Eq. (6.20) represents an especially powerful implication of the duality, as it relates the scaling dimensions of different operators of the *same* model to each other, and can thus be fully checked within a standalone QED<sub>3</sub>-GN calculation [50]. The duality between the CP<sup>1</sup> and QED<sub>3</sub>-GN models and the implications for

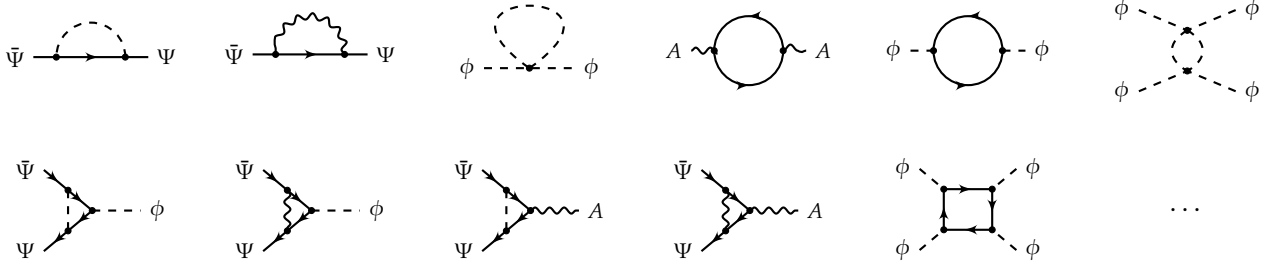


**Figure 6.2:** One-loop diagrams of the QED<sub>3</sub>-GN model. The solid arrowed line denotes the fermionic field  $\Psi$ , the dashed line the bosonic field  $\phi$  and the snake line the gauge field  $A$ . In total there are 18 diagrams (we omitted diagrams of the  $\phi^4$ -vertex which just have an anti-clockwise running fermion or interchanged external legs).

the critical behaviors are summarized in Fig. 6.1. In the following, we will compute the critical behavior of the QED<sub>3</sub>-GN model with a particular focus on this scaling relation as a nontrivial check of the conjectured duality.

## 6.3 Renormalization group analysis

In principle we employ the same setup for the three-loop renormalization group analysis in  $d = 4 - \epsilon$  space-time dimensions as in the projects before. In this section, we want to lay out a few technicalities and further present the full set of  $\beta$ - and  $\gamma$ -renormalization group functions up to three-loop order before we carry on with the critical behavior in the epsilon expansion.

### 6.3.1 RG Scheme

The bare Lagrangian is defined by Eq. (6.1) upon replacing the fields and couplings by their bare counterparts, i.e.  $\Psi \mapsto \Psi_0$ ,  $\phi \mapsto \phi_0$ ,  $A_\mu \mapsto A_{0,\mu}$ ,  $e \mapsto e_0$ ,  $g \mapsto g_0$ ,  $\lambda \mapsto \lambda_0$ ,  $\xi \mapsto \xi_0$ . The renormalized Lagrangian is then introduced as

$$\begin{aligned} \mathcal{L}' = & Z_\Psi \bar{\Psi}_a \not{\partial} \Psi_a - i Z_{A\bar{\Psi}\Psi} e \mu^{\epsilon/2} A \bar{\Psi}_a \Psi_a \frac{Z_A}{4} F_{\mu\nu}^2 + \frac{Z_\phi}{2} (\partial_\mu \phi)^2 \\ & + Z_{\phi^2} \frac{r}{2} \mu^2 \phi^2 + Z_{\phi\bar{\Psi}\Psi} g \mu^{\epsilon/2} \phi \bar{\Psi}_a \Psi_a + Z_{\phi^4} \lambda \mu^\epsilon \phi^4, \end{aligned} \quad (6.21)$$

where  $\mu$  again defines the effective energy scale parametrizing the RG flow. We have defined the wavefunction renormalizations  $Z_\Psi$ ,  $Z_\phi$ , and  $Z_A$ , which relate the bare and the renormalized Lagrangian upon the field rescalings  $\Psi_0 = \sqrt{Z_\Psi} \Psi$ ,  $\phi_0 = \sqrt{Z_\phi} \phi$ , and  $A_{0,\mu} = \sqrt{Z_A} A_\mu$ . The explicit  $\mu$  dependencies in the above Lagrangian arise from the introduction of dimensionless couplings. Demanding that the coefficient in front of the mass term remains invariant under the RG requires  $r = r_0 \mu^{-2} Z_\phi Z_\Psi^{-1}$ . The dimensionless couplings are then related to the bare couplings as

$$\alpha = e_0^2 \mu^{-\epsilon} Z_\Psi^2 Z_A Z_{A\bar{\Psi}\Psi}^{-2}, \quad (6.22)$$

$$y = g_0^2 \mu^{-\epsilon} Z_\Psi^2 Z_\phi Z_{\phi\bar{\Psi}\Psi}^{-2}, \quad (6.23)$$

$$\lambda = \lambda_0 \mu^{-\epsilon} Z_\phi^2 Z_{\phi^4}^{-1}. \quad (6.24)$$

**Table 6.1:** Number of diagrams to compute in dimensional regularization to the third loop order.

Type	1 $\ell$	2 $\ell$	3 $\ell$
$\langle \bar{\Psi}\Psi \rangle$	2	13	177
$\langle \phi^2 \rangle$	2	9	99
$\langle A_\mu A_\nu \rangle$	1	6	83
$\langle \phi \bar{\Psi}\Psi \rangle$	2	38	876
$\langle A_\mu \bar{\Psi}\Psi \rangle$	2	37	844
$\langle \phi^4 \rangle$	9	153	4248
Total	18	256	6327

In the above equations, we have introduced the dimensionless parameters  $\alpha \equiv e^2$  and  $y \equiv g^2$ , where we have implicitly used the fact that the RG flow must be symmetric under sign changes of  $e$  and/or  $g$ .

We calculate the renormalization factors  $Z_x$  up to the three-loop order for  $x \in \{\Psi, \phi, A, \phi^2, \phi\bar{\Psi}\Psi, A\bar{\Psi}\Psi, \phi^4\}$  near the upper critical dimension by employing dimensional regularization and the modified minimal subtraction scheme (MS) using a chain of computer algebra tools described in Appendix B. For the first loop order, the diagrams are shown in Fig. 6.2. Note that we omitted diagrams which are variations of the shown upon interchanging external legs. Up to three-loop order, the complete number of diagrams is sizable as shown in Tab. 6.1 for the different types of diagrams corresponding to the respective renormalization group factor  $Z_x$ .

### 6.3.2 Beta functions

The beta functions for couplings  $x \in \{\alpha, y, \lambda\}$  and the gauge fixing parameter  $\xi$  are defined as before as the logarithmic derivatives with respect to  $\mu$  as

$$\beta_x = \frac{dx}{d \ln \mu}. \quad (6.25)$$

We use rescaled couplings  $x/(8\pi)^2 \mapsto x$  for  $x \in \{\alpha, y, \lambda\}$ . To three-loop order the  $\beta$ -functions can then be written in the form

$$\beta_x = -\epsilon x + \beta_x^{(1L)} + \beta_x^{(2L)} + \beta_x^{(3L)}, \quad (6.26)$$

where we have defined the functions  $\beta_x^{(iL)}$  to collect the contributions of the  $i$ th loop order to the coupling  $x \in \{\alpha, y, \lambda\}$ .

Up to the three-loop order, the beta function of the gauge coupling  $\alpha$  reads

$$\beta_\alpha^{(1L)} = \frac{4}{3}N\alpha^2, \quad (6.27)$$

$$\beta_\alpha^{(2L)} = 2N\alpha^3 - Ny\alpha^2, \quad (6.28)$$

$$\beta_\alpha^{(3L)} = -\frac{\alpha^2 N}{36} [2\alpha^2(22N + 9) - 9(7N + 6)y^2 + 27\alpha y]. \quad (6.29)$$

The beta function for the Yukawa coupling  $y$  is given by

$$\beta_y^{(1L)} = (3 + 2N)y^2 - 6\alpha y, \quad (6.30)$$

$$\beta_y^{(2L)} = 24\lambda^2 y - \left(\frac{9}{8} + 6N\right) y^3 - 24\lambda y^2 + (12 + 5N)y^2\alpha + \frac{1}{6}(20N - 9)y\alpha^2, \quad (6.31)$$

$$\begin{aligned} \beta_y^{(3L)} = & \frac{1}{16} y^2 [192\alpha\lambda + \alpha^2(-64N^2 + 98N + 327) + 48\lambda^2(91 - 30N)] \\ & + \frac{1}{64} [2N(112N + 67) - 697] y^4 - \frac{1}{4} y^3 [\alpha(79N + 174) - 72\lambda(5N + 7)] \\ & + \frac{3}{4} \zeta_3 y [-32\alpha^3 N + (18N + 19)y^3 + 4\alpha(4N + 3)y^2 - 12\alpha^2(6N + 7)y] \\ & - 216\lambda^3 y + \frac{1}{108} \alpha^3 [4N(70N + 621) - 3483] y. \end{aligned} \quad (6.32)$$

$\zeta_z = \zeta(z)$  denotes Riemann's zeta function. The beta function of the scalar interaction with coupling  $\lambda$  reads

$$\begin{aligned}\beta_\lambda^{(1L)} &= 36\lambda^2 - Ny^2 + 4Ny\lambda, \\ \beta_\lambda^{(2L)} &= (10\alpha\lambda - 72\lambda^2 + 4y^2 - 2\alpha y + 7\lambda y) Ny - 816\lambda^3, \\ \beta_\lambda^{(3L)} &= 31320\lambda^4 - \frac{1}{8}N^2y(64\alpha^2\lambda + 157y^3 - 868\lambda y^2 - 116\alpha^2y + 864\lambda^2y) \\ &\quad - 3\zeta_3 \{Ny[-12\alpha\lambda(\alpha + 12\lambda) + 4y^3 + 4y(\alpha^2 + 19\alpha\lambda - 81\lambda^2) \\ &\quad + y^2(39\lambda - 8\alpha)] - 6912\lambda^4\} + \frac{y}{32}N[8\lambda(6192\lambda^2 - 119\alpha^2 - 1836\alpha\lambda) \\ &\quad + 5y^3 - 2y^2(44\alpha + 4395\lambda) + 4y(131\alpha^2 + 1302\alpha\lambda + 4332\lambda^2)].\end{aligned}\quad (6.34)$$

Note that the beta functions are gauge independent as expected and we use this as a sanity check on our calculations. Further, the above expressions fully agree with the QED beta functions [291–293] in the limit of  $y \rightarrow 0$  and  $\lambda \rightarrow 0$ . Also, we recover the beta functions of the Ising Gross-Neveu-Yukawa model for  $\alpha \rightarrow 0$  [112, 113] and the scalar  $\phi^4$  theory with Ising symmetry [148]. Moreover, Eqs. (6.27), (6.30), (6.33) are consistent with the one-loop result from Ref. [279]. For completeness, the beta function of the gauge fixing parameter is listed in Appendix C.3.

### 6.3.3 Anomalous dimensions

The field anomalous dimensions  $\gamma_x$  are defined by  $\gamma_x = \frac{d \ln Z_x}{d \ln \mu}$  for  $x \in \{\Psi, A, \phi, \phi^2\}$  and at three-loop order, they can be expanded as

$$\gamma_x = \gamma_x^{(1L)} + \gamma_x^{(2L)} + \gamma_x^{(3L)}. \quad (6.35)$$

Explicitly, the boson anomalous dimension is given by

$$\gamma_\phi^{(1L)} = 2Ny, \quad (6.36)$$

$$\gamma_\phi^{(2L)} = -\frac{5}{2}Ny(y - 2\alpha) + 24\lambda^2, \quad (6.37)$$

$$\begin{aligned}\gamma_\phi^{(3L)} &= \frac{1}{4}N^2y(25y^2 - 16\alpha^2) - 216\lambda^3 + \frac{1}{32}Ny[21y^2 - 84y\alpha - 476\alpha^2 + 960y\lambda \\ &\quad - 2880\lambda^2] + \frac{3}{2}Ny(y^2 - 4y\alpha + 12\alpha^2)\zeta_3.\end{aligned}\quad (6.38)$$

Note that  $\gamma_\phi$  involves no explicit dependence on the gauge-fixing parameter  $\xi$ , which is consistent with the fact that the scalar-field anomalous dimension determines the exponent in the anomalous power law of the two-point correlator at criticality.

The exponent  $\nu$ , governing the divergence of the correlation length, can be

computed from the renormalization of the mass term, which reads

$$\gamma_{\phi^2}^{(1L)} = -12\lambda \quad (6.39)$$

$$\gamma_{\phi^2}^{(2L)} = -2Ny^2 + 24Ny\lambda + 144\lambda^2 \quad (6.40)$$

$$\begin{aligned} \gamma_{\phi^2}^{(3L)} &= 36Ny^3 - 28Ny^2\alpha - 4N^2y^2(4y - 9\lambda) \\ &\quad - \frac{33}{2}Ny^2\lambda + 153Ny\alpha\lambda - 288Ny\lambda^2 - 6264\lambda^3 \\ &\quad - 12Ny [y^2 - 3y(\alpha - 5\lambda) + 12\alpha\lambda] \zeta_3. \end{aligned} \quad (6.41)$$

The anomalous dimensions for the fermion and the gauge boson are given in the appendix for completeness. Again, we have checked that these expressions are fully compatible with the known expressions from QED [291, 292], the Ising Gross-Neveu-Yukawa model [112, 113], the scalar  $\phi^4$  theory with Ising symmetry [148] and the one-loop results from Ref. [279] in the appropriate limits.

We are also interested in the scaling dimension of the flavor-symmetry-breaking bilinear

$$\bar{\psi}_i(\sigma_z \otimes \mathbb{1}_N)_{ij}\psi_j \mapsto \bar{\Psi}_a(\sigma_z \otimes \mathbb{1}_2)\Psi_a \equiv \bar{\Psi}\sigma_z\Psi. \quad (6.42)$$

Here  $\sigma_z \otimes \mathbb{1}_2 = \gamma_{35}$  in our representation of the  $2+1d$  Clifford algebra. A natural generalization to  $d = 4 - \epsilon$  can be obtained by assuming an even number  $N$  of four-component spinors, allowing us to construct an  $8 \times 8$  operator  $\Gamma_{35} = \Gamma_{35}^{-1}$  that commutes with the fermion propagator,  $[G_\Psi \otimes \mathbb{1}_2, \Gamma_{35}] = 0$ . The results for odd  $N$  are obtained by analytical continuation. If the CP<sup>1</sup>-QED<sub>3</sub>-GN duality holds, the scaling dimensions of  $[\bar{\Psi}\sigma_z\Psi]$  and  $\phi^2$  coincide for  $d = 2 + 1$  and  $N = 1$  at the critical fixed point, leading to a nontrivial scaling relation (cf. Sec. 6.2).

To calculate the scaling dimension of the bilinear in Eq. (6.42), we introduce an additional term  $h\bar{\Psi}\sigma_z\Psi$ , where  $h$  serves as an infinitesimal background field that couples linearly to the flavor-symmetry-breaking bilinear. To leading order in  $h$ , we obtain

$$\gamma_{\bar{\Psi}\sigma_z\Psi}^{(1L)} = 3\alpha - \frac{3}{2}y \quad (6.43)$$

$$\gamma_{\bar{\Psi}\sigma_z\Psi}^{(2L)} = \frac{1}{12}\alpha^2(9 - 20N) + \frac{7}{4}Ny^2 + \frac{9}{16}y^2 - 6\alpha y \quad (6.44)$$

$$\begin{aligned} \gamma_{\bar{\Psi}\sigma_z\Psi}^{(3L)} &= \frac{1}{216}\alpha^3(-280N^2 - 2484N + 3483) + \frac{87\alpha y^2}{4} \\ &\quad + \frac{1}{128}(176N^2 - 604N + 697)y^3 + \frac{137}{16}\alpha Ny^2 \\ &\quad - \frac{3}{8}\zeta_3(12y^2(\alpha + 2\alpha N) - 32\alpha^3N + 19y^3 - 84\alpha^2y) \\ &\quad + \frac{3}{32}y(464\lambda^2 + \alpha^2(80N - 109)) - 30\lambda y^2. \end{aligned} \quad (6.45)$$

Finally, we note that Eq. (6.43) agrees with the previous one-loop result from Ref. [279]. We have also checked that it is consistent with the QED limit [283, 294] up to three loops.



### 6.3.4 Fixed point structure

At one-loop the QED<sub>3</sub>-GN model was already analyzed in Ref. [279] and the RG flow as shown in Fig. 6.3 exhibits several fixed points. In this work, we build up on these findings and extend the determination of the RG fixed points order by order in the epsilon expansion. To the leading order, we find a unique infrared stable fixed point at

$$(\alpha_*, y_*, \lambda_*) = \left( \frac{3}{4N}, \frac{2N+9}{2N(3+2N)}, \frac{-2N^2-15N+s}{72N(3+2N)} \right) \epsilon + \mathcal{O}(\epsilon^2), \quad (6.46)$$

where

$$s \equiv \sqrt{4N^4 + 204N^3 + 1521N^2 + 2916N}, \quad (6.47)$$

in agreement with the previous result [279]. The higher-order terms suppressed in the above equation are straightforwardly computed by making use of the beta functions (6.27)–(6.34), but we do not display them for general  $N$  here for notational simplicity. At  $N = 1$  we obtain to the third loop order

$$\begin{aligned} \alpha_* &= \frac{3}{4}\epsilon - \frac{9}{40}\epsilon^2 + \frac{430\sqrt{4645}-101630}{48000}\epsilon^3 + \mathcal{O}(\epsilon^4) \\ &\approx 0.75\epsilon - 0.225\epsilon^2 - 1.50674\epsilon^3 + \mathcal{O}(\epsilon^4) \end{aligned} \quad (6.48)$$

$$\begin{aligned} y_* &= \frac{11}{10}\epsilon + \frac{86\sqrt{4645}-10741}{5400}\epsilon^2 + \left( \frac{13263\zeta_3}{2500} + \frac{271988639}{19440000} - \frac{389515313}{388800\sqrt{4645}} \right) \epsilon^3 + \mathcal{O}(\epsilon^4) \\ &\approx 1.1\epsilon - 0.903655\epsilon^2 + 5.66874\epsilon^3 + \mathcal{O}(\epsilon^4) \end{aligned} \quad (6.49)$$

$$\begin{aligned} \lambda_* &= \frac{(\sqrt{4645}-17)}{360}\epsilon + \left( \frac{14471}{32400} - \frac{308027}{6480\sqrt{4645}} \right) \epsilon^2 \\ &+ \left[ \frac{66888(78285599\sqrt{4645}-6406570729)}{50332551120000}\zeta_3 + \frac{1814042581409\sqrt{4645}-132453179835199}{50332551120000} \right] \epsilon^3 + \mathcal{O}(\epsilon^4) \\ &\approx 0.142095\epsilon - 0.250827\epsilon^2 + 1.53577\epsilon^3 + \mathcal{O}(\epsilon^4). \end{aligned} \quad (6.50)$$

We note that the three-loop coefficients are large, signaling the divergent behavior of the series at finite  $\epsilon \sim \mathcal{O}(1)$ . For general  $N$ , the series read

$$x_*(N, \epsilon) = \sum_{k=1}^3 x_*^{(kL)}(N) \epsilon^k, \quad (6.51)$$

with  $x_* \in \{\alpha_*, y_*, \lambda_*\}$  and expansion coefficients  $x_*^{(1L)}$ ,  $x_*^{(2L)}$ , and  $x_*^{(3L)}$  at one-, two-, and three-loop order, respectively. The dependence of the expansion coefficients as a function of  $N$  is shown in Fig. 6.4. Note that the higher-loop corrections become small for large  $N$  in all three cases.

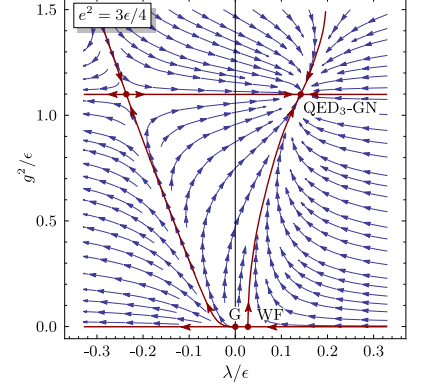


**Figure 6.3:** RG flow of the QED<sub>3</sub>-GN model in  $(4 - \epsilon)$  dimensions at the one-loop fixed point gauge coupling  $\alpha^* = (\epsilon^*)^2 = 3\epsilon/4$ . The critical behavior is governed by the infrared stable fixed point (QED<sub>3</sub>-GN). Taken from Ref. [279].

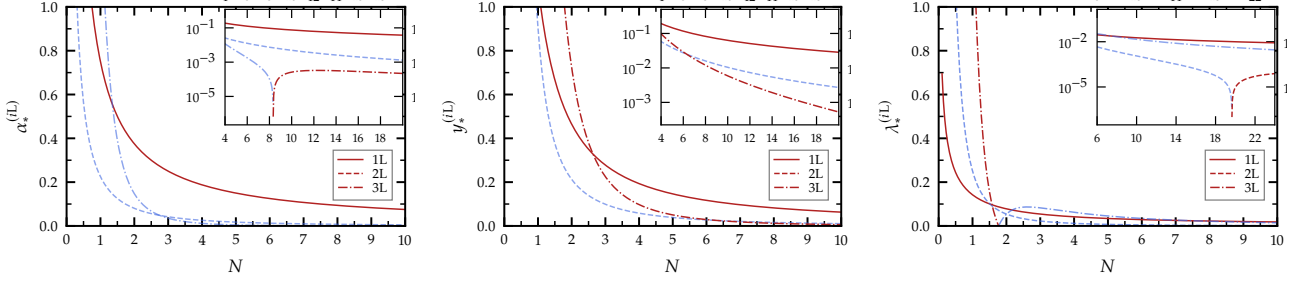


**Figure 6.4:** Expansion coefficients  $x_*^{(kL)}$  from  $k$ -loop order of the expansion of the fixed-point values  $x_* = \alpha_*$  (left panel),  $y_*$  (middle panel), and  $\lambda_*$  (right panel) as a function of  $N$ . The coefficients are large for small  $N$ , but satisfy a hierarchy  $|x_*^{(3L)}| < |x_*^{(2L)}| < |x_*^{(1L)}|$  at large  $N$ . Darker red (lighter blue) lines denote positive (negative) coefficients.

## 6.4 Quantum critical behavior

Here, we discuss the critical behavior of the QED<sub>3</sub>-GN model, which can be extracted from the  $\epsilon$ -expansion, i.e. we provide the series expansions for the inverse correlation length exponent, the boson anomalous dimension and the fermion bilinear  $\bar{\Psi}\sigma_z\Psi$  up to order  $\mathcal{O}(\epsilon^3)$ . For comparison, we also give the corresponding expressions at one-loop order for the four-fermion model and explicitly establish the correspondence between both models in a combined epsilon and  $1/N$  expansion.

### 6.4.1 In the QED<sub>3</sub>-GN model

When the QED<sub>3</sub>-GN model is tuned to criticality, the couplings  $\alpha$ ,  $y$ , and  $\lambda$  flow to the infrared stable fixed point and the system becomes scale invariant. Right at the critical point, the two-point correlation function  $G_\phi(p) = \langle \phi(-p)\phi(p) \rangle$  satisfies a power law  $G_\phi(p) \propto 1/p^{2-\eta_\phi}$ , where the critical exponent  $\eta_\phi$  is given by the anomalous dimension at the fixed point,

$$\eta_\phi = \gamma_\phi(\alpha_*, y_*, \lambda_*). \quad (6.52)$$

The gauge-field anomalous dimension  $\eta_A$  is similarly given by  $\eta_A = \gamma_A(\alpha_*, y_*, \lambda_*)$  and governs the power law of the gauge-field propagator  $G_A(p) \propto 1/p^{2-\eta_A}$  at the critical point. Near criticality, the correlation length  $\xi_c$  diverges with exponent  $\nu$  as  $\xi_c \propto |\delta r_0|^{-\nu}$ , where  $\delta r_0$  measures the distance to the critical point. The correlation-length exponent is obtained from the flow of the dimensionless mass parameter  $\beta_r = (-2 + \gamma_\phi - \gamma_{\phi^2})r$  as

$$\nu^{-1} = 2 - \eta_\phi + \gamma_{\phi^2}(\alpha_*, y_*, \lambda_*). \quad (6.53)$$

We also compute the scaling dimension of the flavor-symmetry-breaking bilinear, which, according to the proposed duality [50], is related to  $\nu$ ,

$$[\bar{\Psi}\sigma_z\Psi] = d - 1 - \eta_{\bar{\Psi}\sigma_z\Psi} \quad (6.54)$$

where  $\eta_{\bar{\Psi}\sigma_z\Psi} = \gamma_{\bar{\Psi}\sigma_z\Psi}(\alpha_*, y_*, \lambda_*)$ .

We have computed the scaling dimensions and the critical exponents for all  $N$  to the third order in  $\epsilon = 4 - d$ , see appendix. Here, we display the result for the situation of one four-component spinor  $\Psi$ , which is the case relevant

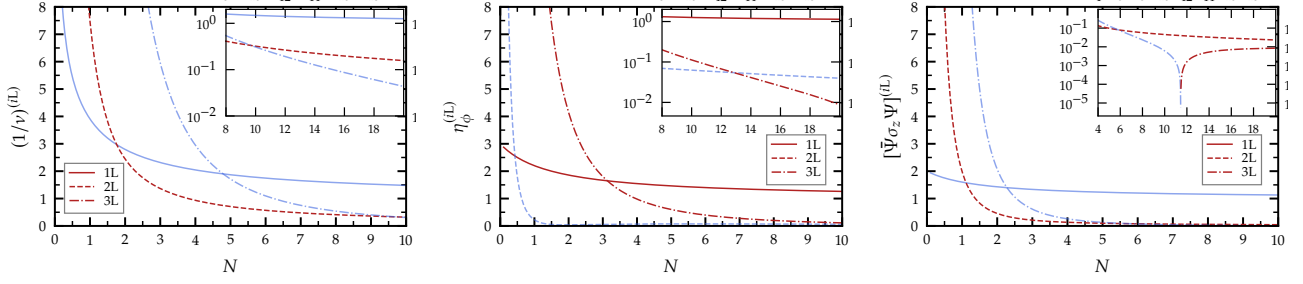


**Figure 6.5:** Expansion coefficients of the inverse correlation-length exponent  $1/\nu$  (left), the order-parameter anomalous dimension  $\eta_\phi$  (middle), and the scaling dimension of the flavor-symmetry-breaking bilinear  $[\bar{\Psi}\sigma_z\Psi]$  (right) as a function of  $N$ . Darker red (lighter blue) lines denote positive (negative) coefficients. The higher-loop corrections are again large for  $N = 1$ , but become small for large  $N$ .

for the duality conjecture. For the scalar-field anomalous dimension  $\eta_\phi$  and the correlation-length exponent  $\nu$  we find for  $N = 1$ :

$$\begin{aligned} \eta_\phi &= \frac{11}{5}\epsilon + \frac{(23\sqrt{4645}-1768)}{900}\epsilon^2 + \left(\frac{91497}{5000}\zeta_3 + \frac{818567}{60000} - \frac{383489}{300\sqrt{4645}}\right)\epsilon^3 \\ &\approx 2.2\epsilon - 0.222725\epsilon^2 + 16.8838\epsilon^3 + \mathcal{O}(\epsilon^4) \end{aligned} \quad (6.55)$$

and

$$\begin{aligned} \nu^{-1} &= 2 - \frac{(\sqrt{4645}+49)}{30}\epsilon + \left(\frac{33311}{54\sqrt{4645}} - \frac{853}{540}\right)\epsilon^2 + \left(\frac{39308173}{27000\sqrt{4645}} - \frac{5931383}{67500}\right)\zeta_3\epsilon^3 \\ &\quad + \left(\frac{39127961}{2430000} - \frac{1646143919039}{902988000\sqrt{4645}}\right)\epsilon^3 \\ &\approx 2 - 3.90514\epsilon + 7.47146\epsilon^2 - 90.5962\epsilon^3 + \mathcal{O}(\epsilon^4) \end{aligned} \quad (6.56)$$

We expect hyperscaling to hold at the critical point. The other exponents  $\alpha$ ,  $\beta$ ,  $\gamma$ , and  $\delta$  can hence be obtained from the usual scaling laws [66].

In order to compare with the  $1/N$  expansion of the gauged four-fermion model, it is useful to also compute the exponents  $\eta_\phi$  and  $1/\nu$  in the limit of large  $N$ . We find

$$\eta_\phi = \left(1 + \frac{3}{N} - \frac{9}{2N^2}\right)\epsilon - \left(\frac{1}{N} - \frac{39}{8N^2}\right)\epsilon^2 - \left(\frac{3}{4N} - \frac{816\zeta_3-413}{32N^2}\right)\epsilon^3 + \mathcal{O}(1/N^3, \epsilon^4) \quad (6.57)$$

and

$$\begin{aligned} \nu^{-1} &= 2 - \left(1 + \frac{6}{N} - \frac{63}{2N^2}\right)\epsilon + \left(\frac{7}{2N} - \frac{207}{8N^2}\right)\epsilon^2 \\ &\quad + \left(\frac{1}{N} - \frac{45\zeta_3}{N^2} + \frac{629}{32N^2}\right)\epsilon^3 + \mathcal{O}(1/N^3, \epsilon^4). \end{aligned} \quad (6.58)$$

The scaling dimension of the flavor-symmetry-breaking bilinear reads for  $N = 1$

$$\begin{aligned} [\bar{\Psi}\sigma_z\Psi] &= 3 - \frac{8}{5}\epsilon + \frac{(43\sqrt{4645}+646)}{1800}\epsilon^2 + \left(\frac{51393}{10000}\zeta_3 - \frac{22196749}{3240000} - \frac{37077727}{32400\sqrt{4645}}\right)\epsilon^3 \\ &\approx 3 - 1.6\epsilon + 1.987\epsilon^2 - 17.46\epsilon^3 + \mathcal{O}(\epsilon^4) \end{aligned} \quad (6.59)$$

whereas in the large- $N$  limit we obtain

$$\begin{aligned} [\bar{\Psi}\sigma_z\Psi] &= 3 + \left(-1 - \frac{3}{2N} + \frac{9}{4N^2}\right)\epsilon + \left(\frac{1}{2N} - \frac{15}{16N^2}\right)\epsilon^2 \\ &\quad + \left(\frac{3}{8N} + \frac{1-216\zeta(3)}{64N^2}\right)\epsilon^3 + \mathcal{O}(1/N^3, \epsilon^4). \end{aligned} \quad (6.60)$$

For the gauge-field anomalous dimension  $\eta_A$  we find

$$\eta_A = \epsilon + \mathcal{O}(\epsilon^4), \quad (6.61)$$

for all  $N$ , which is consistent with the Ward identity associated with the U(1) gauge symmetry, requiring  $Z_\Psi = Z_A\bar{\Psi}\Psi$  in the renormalized Lagrangian, Eq. (6.21). This result provides another nontrivial crosscheck of our calculations. The power law of the gauge-field propagator at criticality thus reads  $G_A(p) \propto 1/p$  exactly, in agreement with the situation in plain QED<sub>3</sub> [295–297].

We show the expansion coefficients as a function of  $N$  for the inverse correlation-length exponent, the order-parameter anomalous dimension and the scaling dimension of the flavor-symmetry-breaking bilinear in Fig. 6.5. The figure demonstrates that only for large enough  $N$  the higher-loop corrections become small. For small  $N$ , the series expansions of these other exponents, in contrast to  $\eta_A$ , exhibit a sizable growth in magnitude, with the three-loop terms for  $N = 1$  being significantly larger than the leading-order terms. This is in analogy to the notorious situation in multi-loop calculations of the standard bosonic O( $N$ ) models [148]. The determination of estimates for scaling dimensions of operators in three dimensions therefore requires a suitable resummation scheme. Due to the lack of knowledge on the large-order behavior of the series, here, we employ simple Padé approximants.

#### 6.4.2 In the gauged four-fermion model

Here, we compare the exponents  $\eta_\phi$  and  $\nu$  of the QED<sub>3</sub>-GN model with those of the gauged four-fermion model in Eq. (6.5). The scaling dimensions of the latter model have been computed before within the  $1/N$  expansion for all space-time dimensions  $2 < d < 4$  [284–286]. At the critical point, the scalar-field propagator in real space satisfies the power law  $G_\phi(x) \propto (1/x_\mu^2)^a$  with exponent [285]

$$a = 1 + \frac{(d-1)\Gamma(d-1)}{2[\Gamma(d/2)]^3\Gamma(\frac{4-d}{2})} \frac{1}{N} + \mathcal{O}(1/N^2), \quad (6.62)$$

where  $\Gamma(\cdot)$  denotes the Gamma function. From the exponent  $a$ , we obtain the anomalous dimension  $\eta_\phi$  as

$$\eta_\phi = 4 - d + \frac{(d-1)\Gamma(d-1)}{[\Gamma(d/2)]^3\Gamma(\frac{4-d}{2})} \frac{1}{N} + \mathcal{O}(1/N^2) = 1 + \frac{16}{\pi^2 N} + \mathcal{O}(1/N^2), \quad (6.63)$$

where the second line correspond to the physical case of  $d = 3$ . We note that the  $\mathcal{O}(1/N)$  correction in  $\eta_\phi$  is *positive*, indicating an unusually large anomalous dimension  $\eta_\phi > 1$ , at least as long as  $N$  is large. This is in contrast to the situation in the (ungauged) Gross-Neveu model [159, 162], but consistent with our result in the QED<sub>3</sub>-GN model, see Eq. (6.57).

Near, but not right at, the critical point, the scaling of the propagator receives corrections according to

$$G_\phi(x) \propto \frac{1}{(x_\mu^2)^a} \left[ 1 + c (x_\mu^2)^b + \dots \right], \quad (6.64)$$

where  $x \equiv \sqrt{x_\mu^2}$ ,  $c$  a constant (with respect to  $x$ ), and the ellipsis denotes higher-order terms that vanish upon approaching the critical point. From the above equation, we can read off the scaling form of the correlation length  $\xi_c \propto |\delta r_0|^{-\nu}$  with  $\nu = 1/(2b)$ .

Using the result of Ref. [285] for the exponent  $b$ , we find

$$\nu^{-1} = d - 2 - \frac{\Gamma(d+1)}{2\Gamma\left(\frac{4-d}{2}\right)\Gamma\left(\frac{d}{2}\right)^3} \frac{1}{N} + \mathcal{O}(1/N^2), \quad (6.65)$$

$$= 1 - \frac{24}{\pi^2 N} + \mathcal{O}(1/N^2), \quad (6.66)$$

where the second line corresponds again to  $d = 3$ . Expanding the above  $1/N$  series for  $\eta_\phi$  and  $\nu$  further in  $\epsilon = 4 - d$  allows us to make contact with the exponents of the QED<sub>3</sub>-GN model. We find

$$\eta_\phi = \left(1 + \frac{3}{N}\right)\epsilon - \frac{\epsilon^2}{N} - \frac{3\epsilon^3}{4N} + \mathcal{O}(1/N^2, \epsilon^4). \quad (6.67)$$

and

$$\frac{1}{\nu} = 2 - \left(1 + \frac{6}{N}\right)\epsilon + \frac{7\epsilon^2}{2N} + \frac{\epsilon^3}{N} + \mathcal{O}\left(\frac{1}{N^2}, \epsilon^4\right). \quad (6.68)$$

Both Eqs. (6.67) and (6.68) precisely agree with the corresponding Eqs. (6.57) and (6.58) in the QED<sub>3</sub>-GN model. This constitutes yet another useful cross-check of our calculations. Even more importantly, this result demonstrates the equivalence between the QED<sub>3</sub>-GN model and the gauged four-fermion model at criticality, at least in the regime where both  $1/N$  and epsilon expansions are under perturbative control. Put differently, here we have explicitly verified the naive expectation that the presence or absence of the gradient term  $\propto \partial^2 \phi^2$  and/or the scalar selfinteraction  $\propto \phi^4$  in the QED<sub>3</sub>-GN Lagrangian [Eq. (6.1)] does not change the universality class of the critical system.

## 6.5 Estimates for 2+1 dimensions

As is usually the case in a perturbative calculation below the upper critical dimension, the resulting series are (at best) asymptotic and diverge upon naively extrapolating to  $\epsilon = 1$ . This problem can often be overcome with the help of a suitable resummation scheme, which is a particularly promising approach if the high-order coefficients can be estimated within, e.g., a strong-coupling expansion [148]. Due to the limited knowledge of the strong-coupling behavior in the present fermionic theories, here we constrain ourselves to a simple Padé approximation. A comparison with Padé-Borel resummed estimates is deferred to the appendix of the original

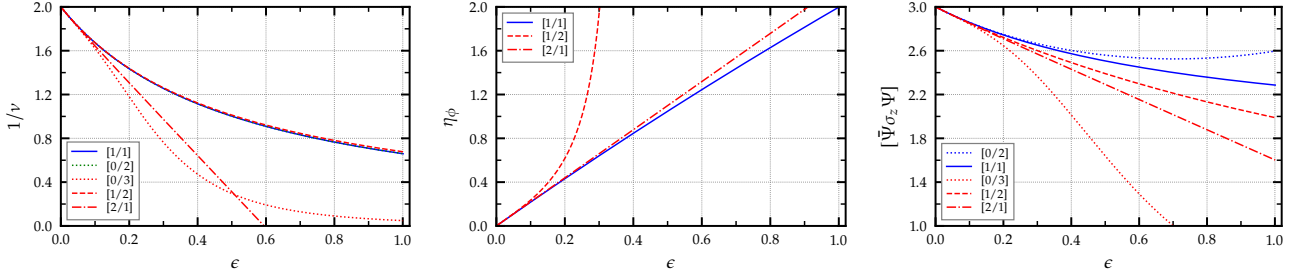


**Figure 6.6:** Padé approximants of the inverse correlation-length exponent  $1/\nu$  (left panel), the boson anomalous dimension  $\eta_\phi$  (mid panel) and the bilinear  $[\bar{\Psi}\sigma_z\Psi]$  (right panel) at  $N = 1$ . Note that, e.g., the  $[1/2]$  approximant of the boson anomalous dimension  $\eta_\phi$  has a pole in  $\epsilon \in [0, 1]$  and has therefore been omitted in Tab. 6.2.

**Table 6.2:** Padé-approximated estimates for the inverse correlation-length exponent  $1/\nu$ , the boson anomalous dimension  $\eta_\phi$  and the fermion bilinear scaling dimension  $[\bar{\Psi}\sigma_z\Psi]$  in the  $N = 1$  QED<sub>3</sub>-GN model in  $D = 2 + 1$  space-time dimensions from two- and three-loop epsilon expansion. Values, for which the approximant has a pole in  $\epsilon \in [0, 1]$  or is not defined, have been omitted (denoted by “–”). Estimates from  $[0/3]$  strongly deviate from all other Padé approximants and are hence not displayed.

Order	$[m/n]$	$1/\nu$	$\eta_\phi$	$[\bar{\Psi}\sigma_z\Psi]$
$\epsilon^2$	$[0/2]$	0.6602	–	2.5964
	$[1/1]$	0.6595	1.9978	2.2863
$\epsilon^3$	$[1/2]$	0.6774	–	1.9894
	$[2/1]$	–	2.1971	1.6030

publication [57]. At this point, we only note that these yield a larger spread for the inverse correlation-length than the simple Padé approximants.

### 6.5.1 Padé approximants

The Padé approximant for a series expansion  $f(\epsilon) = \sum_{k=0}^L f_k \epsilon^k$  truncated at order  $L$  is a rational function

$$[m/n] = \frac{a_0 + a_1\epsilon + \dots + a_m\epsilon^m}{1 + b_1\epsilon + \dots + b_n\epsilon^n}. \quad (6.69)$$

The results for the correlation-length exponent  $\nu$ , the order-parameter anomalous dimension  $\eta_\phi$ , and the scaling dimension of the flavor-symmetry-breaking bilinear  $[\bar{\Psi}\sigma_z\Psi]$  for different Padé approximants are given for the case of  $N = 1$  in Tab. 6.2 for  $\epsilon = 1$  (corresponding to  $d = 2 + 1$ ) and in Fig. 6.6 as a function of  $\epsilon \in [0, 1]$ .

A few remarks are in order:

- (1) The deviation between the different Padé estimates is not small, in particular for the fermion bilinear. This may point to an inherent strong-coupling nature of the problem, indicated by the large fixed-point values at finite  $\epsilon$  for  $N = 1$ , see Eqs. (6.48)–(6.50). The issue dissolves for larger  $N$ , for which the loop corrections become small.
- (2) The order-parameter anomalous dimension is significantly larger than in the ungauged Gross-Neveu and Gross-Neveu-Yukawa models, for which  $\eta_\phi^{\text{GN}} \lesssim 1$  [55, 113]. Our result that  $\eta_\phi^{\text{QED}_3\text{-GN}} > 1$  in the QED<sub>3</sub>-GN models is consistent with the findings at large  $N$ , cf. Eq. (6.63).
- (3) The Padé approximation predicts an anomalous dimension of the order of two. Hyperscaling then requires the susceptibility exponent  $\gamma$  to (nearly) vanish. An unusual situation would occur if  $\eta_\phi$  turned

out to be larger than two, leading to a negative  $\gamma$  and a vanishing susceptibility at the quantum critical point.

## 6.6 Comparison with duality predictions

We aim to compare our results for the critical behavior of the QED<sub>3</sub>-GN model involving two two-component Dirac fermions (corresponding to  $N = 1$  in our notation) with the predictions from the conjectured duality with the CP<sup>1</sup> model. We take the mean values for  $1/\nu$ ,  $\eta_\phi$ , and  $[\bar{\Psi}\sigma_z\Psi]$ , respectively, from the different Padé approximants shown in Tab. 6.2 as our best guesses for the critical exponents in  $d = 2 + 1$ , and the largest deviation among the different Padé results as an estimate for the order of the confidence interval. Let us focus on the scaling relation (6.20) that follows from the assumption of emergent SO(5) symmetry at the deconfined critical point. This nontrivial relation allows to compare scaling dimensions fully within the QED<sub>3</sub>-GN model. For the left-hand-side of the relation, we find

$$[\bar{\Psi}\sigma_z\Psi] \approx 2.12(50), \quad (6.70)$$

which, according to the duality conjecture, should coincide with the right-hand-side

$$3 - 1/\nu \approx 2.33(1). \quad (6.71)$$

We note that in view of the quickly growing series coefficients for  $1/\nu$  the spread is likely to be accidentally small. In any case, these estimates are consistent with the duality prediction.

We should emphasize, however, that our estimates do not agree with the exponents measured in the simulations of the spin systems that are believed to possess a deconfined critical point [41–43, 207, 211, 218], see Table 6.3. In particular, the anomalous dimensions  $\eta_{\text{Néel}} \approx \eta_{\text{VBS}}$  in these bosonic systems (although already being an order of magnitude larger than in the usual Heisenberg or XY universality classes) are significantly below one, while both the epsilon expansion of the QED<sub>3</sub>-GN model in  $d = 4 - \epsilon$  and the  $1/N$  expansion of the corresponding four-fermion model in fixed  $d = 2 + 1$  find a

CP <sup>1</sup>	QED <sub>3</sub> -GN ( $N = 1$ )
$\eta_{\text{Néel}} \approx 0.26(3)$ [41]	$\eta_\phi \approx 2.1(1)$ [this work]
$\approx 0.35(3)$ [42]	$\approx 1.3(9)$ [279]
$\approx 0.30(5)$ [207]	
$\approx 0.22$ [254]	
$\approx 0.259(6)$ [218]	
$\eta_{\text{VBS}} \approx 0.28(8)$ [207]	
$\approx 0.25(3)$ [218]	
$3 - 1/\nu \approx 1.72(5)$ [41]	$3 - 1/\nu \approx 2.33(1)$ [this work]
$\approx 1.53(9)$ [42]	$\approx 2.7(4)$ [279]
$\approx 1.15(19)$ [207]	
$\approx 1.21$ [254]	$[\bar{\Psi}\sigma_z\Psi] \approx 2.12(50)$ [this work]
$\approx 1$ [218]	$\approx 1.8(5)$ [279]
$\approx 0.76(4)$ [43]	$\approx 1.98(8)$ [298]
$\approx 0.802(2)$ [211]	

**Table 6.3:** Comparison of critical exponents in 2+1 dimensions for the Néel-VBS deconfined critical point described by the non-compact CP<sup>1</sup> model and the conjectured dual QED<sub>3</sub>-GN model for  $N = 1$ . (Updated by Ref. [211] (2020) and Ref. [298] (2018). Note that the four loop epsilon expansions allow no conclusive estimates for the anomalous dimension and the inverse correlation-length due to its strong asymptotic behavior [298]).

value for  $\eta_\phi^{\text{QED}_3\text{-GN}}$  that is significantly above one. Similarly, the correlation-length exponent  $\nu_{\text{CP}^1}$  in the spin systems appears to be smaller than one, while we find  $\nu_{\text{QED}_3\text{-GN}} \approx 1.50(2) > 1$ , in qualitative agreement with the  $1/N$  expansion of the four-fermion model [Eq. (6.66)]. This discrepancy may be interpreted within one of the following three possible scenarios:

- (A) The strong version of the CP<sup>1</sup>-QED<sub>3</sub>-GN duality may not hold for the infrared physics and, in this case, the apparent consistency between Eqs. (6.70) and (6.71) would be accidental.
- (B) While the perturbative approach to the QED<sub>3</sub>-GN model approximately sustains the duality relation within the model as reflected by Eqs. (6.70) and (6.71), it might not be well-suited to provide reliable absolute estimates for the critical exponents. In that case, non-perturbative approaches, e.g., the functional renormalization group or the conformal bootstrap, could help to check the conjectured duality on the level of critical exponents and scaling relations.
- (C) The deconfined critical point may really be only a pseudocritical point corresponding to a critical fixed point that has disappeared from the real coupling space as a consequence of a collision and annihilation with another fixed point. If indeed existent, any other fixed point would be located outside the perturbative regime for  $\epsilon \ll 1$  and can only approach the QED<sub>3</sub>-GN fixed point at some finite  $\epsilon > 0$ . Such a fixed-point annihilation scenario is known to occur in various gauge theories both in  $2+1d$  and  $3+1d$  [246, 261, 262, 264, 296, 299–301], and has recently been entertained also in the context of deconfined criticality in the spin models [50, 218]. In this scenario, SO(5) would only emerge as an approximate symmetry near a weakly-first-order phase transition with an exponentially large, but finite correlation length  $\xi_c$  [219]. The CP<sup>1</sup>-QED<sub>3</sub>-GN duality would then only hold at length scales  $\ell \lesssim \xi_c$  in the simulations, and the exponents computed here for the QED<sub>3</sub>-GN model would not apply to this pseudocritical regime, but would in fact characterize the nonunitary SO(5)-symmetric fixed point located at complex coupling.

## 6.7 Discussion and Outlook

We have determined the critical behavior of the QED<sub>3</sub>-GN model within a three-loop epsilon expansion around the upper critical space-time dimension of  $d_c^+ = 4$ . Within this expansion, the model exhibits a unique infrared stable fixed point corresponding to a continuous phase transition at which a time-reversal symmetry broken fermion mass term is spontaneously generated. In analogy to the ungauged Gross-Neveu and Gross-Neveu-Yukawa models [127], the infrared fixed point of the QED<sub>3</sub>-GN model can be equivalently understood as an ultraviolet fixed point of a corresponding gauged four-fermion theory, the critical behavior of the latter is amenable to a  $1/N$  expansion [285]. We have explicitly verified this infrared-ultraviolet correspondence by demonstrating that the critical exponents coincide order by order (up to the order we calculated) within a  $(1/N, \epsilon)$  double expansion.

Most interestingly, our estimates for the critical behavior of the  $2+1d$  QED<sub>3</sub>-GN universality class for the case of two flavors of two-component Dirac fermions (corresponding to  $N = 1$  in our notation) are consistent with a nontrivial scaling relation that follows from emergent SO(5) symmetry



implied by the proposed duality between the QED<sub>3</sub>-GN and noncompact CP<sup>1</sup> models [50]. If this agreement persists in future calculations that will narrow down our uncertainty interval, it would constitute a strong indication for emergent SO(5) symmetry at the  $N = 1$  QED<sub>3</sub>-GN fixed point. Our results, on the other hand, are not compatible with the most recent simulation results for the deconfined critical point in the spin models [43, 44], and we have given a possible interpretation of this discrepancy in terms of the previously proposed [44, 50, 219] pseudocriticality scenario.

For future work, it would be interesting to study the possible existence of other fixed points that might collide and annihilate with the QED<sub>3</sub>-GN fixed point at some space-time dimension between  $d = 3$  and  $d = 4 - \epsilon$ . As a complementary approach, it would be desirable to test whether the time-reversal-symmetry-breaking transition in the QED<sub>3</sub>-GN model is continuous or (weakly) first order, e.g., within a numerical simulation of a suitable lattice model. Furthermore, to increase the precision, a more systematic study of different resummation techniques is necessary and left to future work. It could possibly involve other non-polynomial approximants, using e.g. hypergeometric functions [302].

*/\*After this work was published, in Ref. [298] a comprehensive four loop pRG analysis was published. Unfortunately, the epsilon expansion keep their strong asymptotic behavior and the authors only provide a reasonable estimate for the bilinear at  $d = 3$  and  $N = 1$ . This may be interpreted as another hint for a strongly coupled problem which has to be treated beyond perturbative methods. Additionally, in Ref. [303] the authors revisit the large- $N$  RG analysis and argue that previous epsilon and large- $N$  expansions are missing the analysis of so-called Aslamazov-Larkin diagrams. These arise from the tensor structure of the gamma matrices at three dimensions, exactly where the duality was conjectured to hold. Indeed, the modified large- $N$  boson anomalous dimensions is in better agreement with the Néel-VBS transition than our epsilon expansion. Nevertheless, the inverse correlation-length exponent  $1/\nu$  still does not fit. We updated Tab. 6.3 accordingly.*

*Recently, the QED<sub>3</sub>-Gross-Neveu-XY model with a two component bosonic field was studied extensively as the critical theory for another confinement transition from gapless QED<sub>3</sub> to a VBS phase [304–306]. Furthermore also a chiral Heisenberg version, the QED<sub>3</sub>-O(3) model, was discussed as model for a Néel-to-algebraic spin liquid transition [307]. It will be interesting to extend those studies and further symmetry classes of QED<sub>3</sub>-GN model in possible applications. A nice overview of the current knowledge is given in Ref. [15].\*/*



# Fractionalized quantum criticality in spin-orbital liquids

# 7

In the analysis of “conventional” phase transitions, the LGW paradigm has proven to be extremely successful. However, as we saw in Chapter 4 in the derivation of the deconfined phase transitions of quantum magnets in two spatial dimensions, the absence of an easy to identify order parameter in systems with symmetry-protected topological (SPT) phases leaves behind many loose ends to understand. The search for other transitions involving intrinsic topological order and to understand their universal properties at the unconventional quantum critical points pose an on-going challenge and might reveal a deeper understanding of long-range entanglement structures such as in the deconfined quantum criticality scenario. A crucial step in the derivation of Chapter 4 was the fractionalization of the Néel order parameter which also introduced the gauge degrees of freedom which turned out to be emergent exclusively at the critical point. In this scenario the fractionalized degrees of freedom not only linked the topological term intrinsically to the valence bond solid (through an intermediate U(1)-spin liquid phase) but more importantly governed the critical behavior. In fact, this is an example for a *fractionalized* quantum critical point.

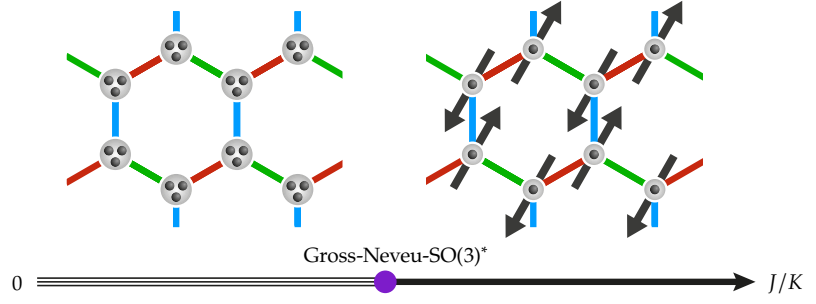
Since there are also other systems hosting topological order, it remains open to understand systematically how the criticality changes if governed by (a subset) of fractionalized degrees of freedom. While this question was addressed in a range of bosonic models, such as a (toy) model of hard-core bosons with a fractionalized XY\* [52] critical point and also subsequent generalizations to Ising and O(N) models, it was only very recently found also in spin-orbital liquids featuring emergent gapless Majorana fermions [54]. Here, the low-energy fermion excitations arise from fractionalization of the microscopic spin and orbital degrees of freedom. Spin-orbital models hence realize a fractionalized counterpart of the Gross-Neveu-type transitions we discussed in Chapter 3, dubbed Gross-Neveu\*.

## 7.1 Fractionalized spin-orbital liquids

In the Gross-Neveu transitions, studied so far, all Dirac cones become simultaneously gapped out in the long-range-ordered phase. In the case of a continuous-symmetry breaking, this leaves behind the bosonic Goldstone modes alone as low-energy excitations. If only a discrete symmetry is broken, it leads to a full gap in the spectrum of the ordered phase. The fractionalized Gross-Neveu\* transitions differ from the ordinary Gross-Neveu transitions in the universal finite-size spectrum [308]. However, in contrast to the situation in the fractionalized bosonic universality classes [52, 309], at a Gross-Neveu\* transition, *two* independent universal exponents, such as the order-parameter anomalous dimension  $\eta_\phi$  and the correlation-length exponent  $\nu$ , feature the same values as in the transition’s ordinary counterpart. As a consequence of the hyperscaling relations, this then implies that also the exponents  $\alpha$ ,  $\beta$ ,  $\gamma$  and  $\delta$  in a fractionalized Gross-Neveu\* universality classes agree with those of the corresponding ordinary Gross-Neveu universality class. Starting point for the model in Ref. [54] is a spin-orbital model with a

7.1 Fractionalized spin-orbital liquids .....	93
7.2 The Gross-Neveu-SO(3) model	95
7.3 $(4 - \epsilon)$ expansion .....	96
7.4 $1/N$ expansion .....	99
7.5 Functional renormalization group .....	104
7.6 Discussion .....	109
7.7 Summary and outlook .....	112

**Figure 7.1:** Schematic phase diagram of the fractionalized spin-orbital liquid. For  $K \ll J$ , the model in Eq. (7.1) realizes a Dirac semi-metal ground state with three gapless excitations (see also the corresponding Gross-Neveu-SO(3) model in Fig. 7.2). For  $J \ll K$ , the system will order anti-ferromagnetically as shown on the right and therefore spontaneously break the SO(3) symmetry. (Adapted from Ref. [54]).



1: In Ref. [54], the authors also discuss the case of an even number of  $\nu_M$  on a square lattice. In this case the fractionalized critical point is found to be governed by the chiral Ising Gross-Neveu universality which we studied extensively in Chapter 3.

bond-dependent Kitaev interaction [310] and an odd number  $\nu_M$  of itinerant Majorana fermions on the honeycomb lattice<sup>1</sup>. We are particularly interested in the transition between a symmetric  $\mathbb{Z}_2$  quantum spin-orbital liquid on the honeycomb lattice and a symmetry-broken phase, in which the spins order anti-ferromagnetically, while the orbital degrees of freedom remain disordered [54]. On the lattice, the model in Ref. [54] is composed by a biquadratic Heisenberg-spin and Kitaev orbital interaction with strength  $K$  and an anti-ferromagnetic Heisenberg interaction term  $J$

$$\mathcal{H} = \mathcal{H}_K + \mathcal{H}_J = -K \sum_{\langle ij \rangle_\gamma} \sigma_i \cdot \sigma_j \otimes \tau_i^\gamma \tau_j^\gamma + J \sum_{\langle ij \rangle} \sigma_i \cdot \sigma_j \otimes \mathbb{1}_i \mathbb{1}_j, \quad (7.1)$$

where  $\gamma = 1, 2, 3$  refers to the three inequivalent bonds. Crucial for this model is that the spin degrees of freedom  $\sigma = (\sigma_x, \sigma_y, \sigma_z)$  are present in both terms while the orbital degrees of freedom  $\tau$  only couple to them by the Kitaev term  $H_K$ . For this reason, the latter exhibits  $\mathbb{Z}_2$ -gauged Majorana fermions leading to a SO(3) symmetry. In this sense, the  $\mathbb{Z}_2$  quantum spin-orbital liquid can be understood as a generalization of Kitaev's quantum spin liquid [310], in which the number of Majorana fermions that couples to the  $\mathbb{Z}_2$  gauge field is tripled [311]. For  $K \gg J$ , the model realizes a Dirac semi-metal ground state with  $N = 3$  (i.e.  $\nu_M = 3$ ) gapless excitations as shown on the left in Fig. 7.1. On the other end, for  $J \gg K$  the system is expected to order anti-ferromagnetically and therefore spontaneously breaking the SO(3) to a residual  $\text{SO}(2) \times \mathbb{Z}_2$  symmetry leaving two out of the three Dirac cones gapped out, while the third one remains gapless (i.e.  $\nu_M = 1$ ). This partially gapped phase can be understood as a spin-1 antiferromagnet [54].

*The content of this Chapter was published in Ref. [58]. Intermediately added sentences are tagged by /\*[...]\*/. Each section presents a different advanced renormalization group methods contributed by Shoryya Ray and Lukas Janssen (Sec. 7.5), Daniel Kruti (Sec. 7.5 [pseudospectral methods]), John A. Gracey (Sec. 7.4) and BI and Michael M. Scherer (Sec. 7.3).*

In this work, we focus on the corresponding family of Gross-Neveu transitions, at which the fermion spectrum is only partially gapped out. In particular, we study the critical behavior of the Gross-Neveu-SO(3) universality class. This universality class describes a transition between a symmetric Dirac semimetal phase featuring SO(3) symmetry and  $N$  gapless Dirac fermions, where  $N$  is an integer multiple of three, and a long-range-ordered phase, in which SO(3) is spontaneously broken and  $2N/3$  Dirac cones are gapped out. Importantly,  $N/3$  Dirac cones remain gapless throughout the ordered phase, as illustrated in Fig. 7.2.

The purpose of this work is to provide refined estimates for the critical exponents characterizing the (2+1)-dimensional Gross-Neveu-SO(3) univer-

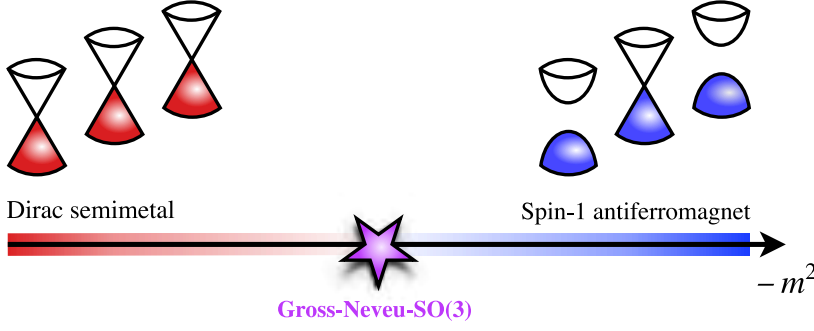


**Figure 7.2:** Quantum phase diagram of the  $(2+1)$ -dimensional Gross-Neveu-SO(3) model as function of tuning parameter  $m^2$ . The theory exhibits a quantum critical point between a Dirac semimetal and a long-range-ordered phase in which two Dirac cones acquire a mass gap, while one remains gapless, as depicted in the insets. In this work, we provide improved estimates for the universal exponents  $1/\nu$ ,  $\eta_\phi$ , and  $\eta_\psi$ , characterizing this universality class. (Adapted from Ref. [58])

sality class. To this end, we compare the results of three complementary advanced field-theoretical approaches. We use a chain of computer-algebra tools developed in the context of high-energy physics (see Appendix B) to determine the critical behavior within an  $\epsilon$  expansion around the upper critical space-time dimension of four at three-loop order. Further, by solving the Schwinger-Dyson equations directly at the critical point [71, 72, 157, 312], we compute the correlation-length exponent  $\nu$  and the order-parameter anomalous dimensions  $\eta_\phi$  at order  $\mathcal{O}(1/N^2)$  in the large- $N$  expansion; the fermion anomalous dimension  $\eta_\psi$  is determined at order  $\mathcal{O}(1/N^3)$  by making use of the large- $N$  conformal bootstrap technique [72, 162, 163, 313, 314]. Finally, by employing the functional renormalization group (FRG) in the derivative-expansion scheme, we compute the critical behavior of the Gross-Neveu-SO(3) universality class at the level of the improved local potential approximation (LPA').

## 7.2 The Gross-Neveu-SO(3) model

The continuum field theory describing the Gross-Neveu-SO(3) universality class is given by the action  $\mathcal{S} = \int d^d x \mathcal{L}$  with [54]

$$\mathcal{L} = \bar{\psi} \gamma^\mu \partial_\mu \psi + \frac{1}{2} \phi_a \left( -\partial_\mu^2 + m^2 \right) \phi_a + \lambda (\phi_a \phi_a)^2 - g \phi_a \bar{\psi} (\mathbb{1}_{2N/3} \otimes L_a) \psi \quad (7.2)$$

in  $d$  Euclidean space-time dimensions. Here, we have assumed the summation convention over repeated indices  $\mu = 0, \dots, d-1$  and  $a = 1, 2, 3$ . We use conventions in which the Dirac matrices  $\gamma_\mu$  form a  $2N$ -dimensional representation of the Clifford algebra,  $\{\gamma^\mu, \gamma^\nu\} = 2\delta^{\mu\nu} \mathbb{1}_{2N}$ , such that  $N$  corresponds to the number of two-component fermion flavors. The spinor  $\psi$  and its Dirac conjugate  $\bar{\psi} \equiv \psi^\dagger \gamma^0$  have  $2N$  components each. The interaction Lagrangian comprises the SO(3)-counterpart of the Heisenberg-Yukawa interaction [106, 140], parameterized by its Yukawa coupling  $g$ , and a quartic boson self-interaction with coupling  $\lambda$ . As in the standard Gross-Neveu-Yukawa models [315], the Dirac matrices commute with the Yukawa vertex operator,  $[\gamma^\mu, \mathbb{1}_{2N/3} \otimes L_a] = 0$ . The  $3 \times 3$  matrices  $L_a$  are generators of SO(3) in the fundamental representation, corresponding to spin 1. The order-parameter field  $\phi_a$  is a scalar under space-time rotations, but transforms as a vector under SO(3). In  $d = 2$  and  $d = 3$  space-time dimensions, this requires that  $N$  is a multiple of three, whereas in  $d = 4$ ,  $N$  would need to be a multiple of six in any physical realization. However, in what follows, it will prove to be useful to compute the critical behavior for general  $2 < d < 4$

2: We note that subleading exponents, such as  $\omega$ , corresponding to the corrections to scaling, may depend on whether the theory is defined in terms of  $N$  flavors of two-component fermions or  $N/2$  flavors of four-component fermions, see Ref. [281].

and arbitrary  $0 \leq N \leq \infty$ , allowing one to analytically continue also to noninteger values of both  $d$  and  $N$ . As Aslamazov-Larkin diagrams vanish for the ungauged Gross-Neveu models [303], the critical exponents  $\nu$ ,  $\eta_\phi$ , and  $\eta_\psi$  do not depend on whether the theory is defined in terms of reducible or suitable copies of irreducible fermion flavors<sup>2</sup>. The physical case realized in the spin-orbital models [54] corresponds to  $N = 3$  and  $d = 3$ .

The zero-temperature phase diagram of the Gross-Neveu-SO(3) model as a function of the tuning parameter  $m^2$  can be understood on the level of mean-field theory, see Fig. 7.2. In this case, the fluctuations of the order parameter  $\phi_a$  are neglected. Formally, this corresponds to the strict limit  $N \rightarrow \infty$ . For  $m^2 > 0$ , the ground state is symmetric and the spectrum consists of  $N$  gapless Dirac cones. For  $m^2 < 0$ , the order parameter field acquires a finite vacuum expectation value  $\langle \phi_a \rangle \neq 0$  and the SO(3) flavor symmetry is spontaneously broken. However, since  $L_a$  has a zero eigenvalue, only  $2N/3$  of the Dirac cones acquire a mass gap, while the remaining  $N/3$  Dirac cones remain gapless throughout the long-range-ordered phase. In this work, we demonstrate that the mean-field picture remains qualitatively correct for finite values of  $N$ , but the corresponding critical exponents characterizing the universality class receive sizable corrections to their mean-field values.

### 7.3 (4 - $\epsilon$ ) expansion

The field theory defined in Eq. (7.2) has an upper critical space-time dimension  $d_{\text{up}} = 4$ , where both, the Yukawa coupling  $g$  and the quartic bosonic self-interaction  $\lambda$ , become simultaneously marginal. This allows for a controlled expansion in  $d = 4 - \epsilon$  dimensions. In this section, we report our calculation of the renormalization group functions at three-loop order. Further, we extract the correlation-length exponent  $\nu$ , the boson anomalous dimension  $\eta_\phi$ , and the fermion anomalous dimension  $\eta_\psi$  at order  $\mathcal{O}(\epsilon^3)$ .

#### 7.3.1 Method

We define the bare Lagrangian upon replacing fields and couplings in Eq. (7.2) by their bare counterparts  $\psi \mapsto \psi_0$ ,  $\phi_a \mapsto \phi_{a,0}$ ,  $g \mapsto g_0$  and  $\lambda \mapsto \lambda_0$ . The renormalized Lagrangian reads

$$\begin{aligned} \mathcal{L} = & Z_\psi \bar{\psi} \gamma^\mu \partial_\mu \psi - Z_{\phi \bar{\psi} \psi} g \mu^{\epsilon/2} \phi_a \bar{\psi} (\mathbb{1}_{2N/3} \otimes L_a) \psi \\ & + \frac{Z_\phi}{2} (\partial_\mu \phi_a)^2 + \frac{Z_{\phi^2}}{2} m^2 \phi_a \phi_a + Z_{\phi^4} \lambda \mu^\epsilon (\phi_a \phi_a)^2, \end{aligned} \quad (7.3)$$

with the renormalization constants  $Z_\psi$ ,  $Z_\phi$ ,  $Z_{\phi \bar{\psi} \psi}$ ,  $Z_{\phi^2}$ , and  $Z_{\phi^4}$ . The kinetic terms in the renormalized and bare Lagrangian can be related to each other upon identifying  $\psi_0 = \sqrt{Z_\psi} \psi$  and  $\phi_0 = \sqrt{Z_\phi} \phi$ . The energy scale  $\mu$  parametrizes the renormalization group flow. It is introduced upon shifting the couplings  $g^2 \mapsto \mu^\epsilon g^2$  and  $\lambda \mapsto \mu^\epsilon \lambda$  after the integration over  $(4 - \epsilon)$ -dimensional spacetime. The renormalized mass and the renormalized

couplings are then related to the corresponding bare quantities as

$$m^2 = m_0^2 Z_\phi Z_\phi^{-1}, \quad (7.4)$$

$$g^2 = g_0^2 \mu^{-\epsilon} Z_\psi^2 Z_\phi Z_\phi^{-2} Z_{\phi\bar{\psi}\psi}, \quad (7.5)$$

$$\lambda = \lambda_0 \mu^{-\epsilon} Z_\phi^2 Z_\phi^{-1}. \quad (7.6)$$

In the following, we compute all renormalization constants up to three-loop order. To that end, as in the previous projects we employ  $\overline{\text{MS}}$  dimensional regularization and the modified minimal subtraction scheme ( $\overline{\text{MS}}$ ). For the Gross-Neveu-SO(3) model this amounts to the evaluation 1,815 Feynman diagrams. For the sophisticated chain of computer algebra tools originally developed for loop calculations in high-energy physics we again refer to Appendix B. Furthermore in Appendix A, we present the one-loop RG on a generalized Gross-Neveu-Yukawa model.

### 7.3.2 Flow equations

The beta functions for the squared Yukawa coupling  $g^2$  and the quartic scalar coupling  $\lambda$  are defined as

$$\beta_{g^2} = \frac{dg^2}{d \ln \mu}, \quad \beta_\lambda = \frac{d\lambda}{d \ln \mu}. \quad (7.7)$$

It is convenient to further rescale the couplings as  $g^2/(8\pi^2) \mapsto g^2$  and  $\lambda/(8\pi^2) \mapsto \lambda$ , such that the  $\beta$  functions at three loop order read

$$\begin{aligned} \beta_{g^2} = & -\epsilon g^2 + \frac{2}{3}(N+6)g^4 - \frac{1}{2}g^2 [(7+6N)g^4 + 80g^2\lambda - 80\lambda^2] \\ & + 10g^6\lambda(5N+24) + 10g^4\lambda^2(48-5N) - 440g^2\lambda^3 \\ & + 6\zeta_3 g^8(N+3) + \frac{1}{8}g^8(6N^2+37N-118), \end{aligned} \quad (7.8)$$

$$\begin{aligned} \beta_\lambda = & -\epsilon\lambda + 44\lambda^2 - \frac{1}{3}g^2N(g^2-4\lambda) + \frac{1}{3}g^2N(5g^4+4g^2\lambda-88\lambda^2) - 1104\lambda^3 \\ & + \frac{1}{72} \left\{ -3g^8N(66N+19) + 2g^6\lambda N(562N-4761) \right. \\ & - 48g^4\lambda^2N(22N-521) + 49632g^2\lambda^3N + 3469248\lambda^4 \\ & \left. - 36\zeta_3 [g^4N(7g^4+120g^2\lambda-792\lambda^2) - 56832\lambda^4] \right\}. \end{aligned} \quad (7.9)$$

Here,  $\zeta_s = \zeta(s)$  is the Riemann zeta function. We have sorted the terms in Eqs. (7.8) and (7.9) such that the first lines show the tree level and one-loop contributions, the second lines show the two-loop contributions, and the remaining lines show the three-loop contributions. The wavefunction renormalization functions  $\gamma_\phi$  and  $\gamma_\psi$  are defined as  $\gamma_{\phi/\psi} = d \ln Z_{\phi/\psi} / (d \ln \mu)$ . At three-loop order they read

$$\begin{aligned} \gamma_\phi = & \frac{2}{3}Ng^2 + 40\lambda^2 - \frac{4}{3}Ng^4 + \frac{41g^6N^2}{36} \\ & + \frac{g^2}{24}N(21g^4 + 400g^2\lambda - 1200\lambda^2) - 440\lambda^3, \end{aligned} \quad (7.10)$$

$$\gamma_\psi = g^2 - \frac{2N+1}{4}g^4 - \frac{g^2}{48} [g^4(4N^2-84N-9) - 960g^2\lambda + 2640\lambda^2]. \quad (7.11)$$

Finally, we consider the mass renormalization function as  $\gamma_{\phi^2} = d \ln Z_{\phi^2} / (d \ln \mu)$ , which at three-loop order reads

$$\begin{aligned} \gamma_{\phi^2} = & -20\lambda - \frac{2}{3}Ng^4 + \frac{40}{3}Ng^2\lambda + 240\lambda^2 + \frac{61}{3}Ng^6 - 2\zeta_3Ng^4(g^2 + 50\lambda) \\ & - \frac{130}{3}Ng^4\lambda - 160Ng^2\lambda^2 - \frac{4}{9}N^2g^4(7g^2 - 15\lambda) - 12920\lambda^3. \end{aligned} \quad (7.12)$$

The corresponding  $\beta$  function for the bosonic mass is then computed from the dimensionless mass  $\tilde{m}^2 = \mu^{-2}m^2$  as

$$\beta_{\tilde{m}^2} = (-2 + \gamma_{\phi} - \gamma_{\phi^2})\tilde{m}^2. \quad (7.13)$$

We note that in the limit  $g^2 \rightarrow 0$ , we recover the three-loop results for the O(3)-symmetric real scalar  $\phi^4$  theory [97].

### 7.3.3 Critical exponents

The above  $\beta$  functions feature several renormalization group fixed points, i.e., couplings  $g_{\star}^2$  and  $\lambda_{\star}$  at which the flow vanishes,  $\beta_{g^2}(g_{\star}^2, \lambda_{\star}) = \beta_{\lambda}(g_{\star}^2, \lambda_{\star}) = 0$ . At the fixed points, the system becomes scale invariant, giving rise to quantum critical behavior. We find that the Gaussian fixed point at  $(g_{\star}^2, \lambda_{\star}) = (0, 0)$  and the purely bosonic Wilson-Fisher fixed point  $(g_{\star}^2, \lambda_{\star}) = (0, \lambda_{\star})$  are characterized by two and one relevant directions within the critical plane  $\tilde{m}^2 = 0$ , respectively. They are thus unstable and cannot be accessed in a system with a single control parameter without fine tuning. We further find a pair of interacting fixed points at finite  $g_{\star}^2 \neq 0$ , one of which is fully infrared stable. To the leading order, the corresponding critical couplings are

$$(g_{\star}^2, \lambda_{\star}) = \left( \frac{3}{2(N+6)}, \frac{\sqrt{N^2+120N+36}-N+6}{88(N+6)} \right) \epsilon + \mathcal{O}(\epsilon^2), \quad (7.14)$$

in agreement with the previous calculation [54]. The corresponding higher-order contributions up to  $\mathcal{O}(\epsilon^3)$  are lengthy but straightforward expressions that can be obtained from Eqs. (7.8) and (7.9) analytically, and will be used in the following.

The critical behavior is determined by the renormalization group flow at and near the stable fixed point. The anomalous dimensions are given by the wavefunction renormalization functions  $\gamma_{\psi}$  and  $\gamma_{\phi}$  at the fixed point,

$$\eta_{\psi} = \gamma_{\psi}(g_{\star}^2, \lambda_{\star}), \quad \eta_{\phi} = \gamma_{\phi}(g_{\star}^2, \lambda_{\star}). \quad (7.15)$$

The inverse of the correlation-length exponent is extracted from the flow of the bosonic mass, which acts as tuning parameter,

$$\frac{1}{\nu} = \left. \frac{d\beta_{\tilde{m}^2}}{d\tilde{m}^2} \right|_{(g_{\star}^2, \lambda_{\star})} = 2 - \eta_{\phi} + \eta_{\phi^2}. \quad (7.16)$$

The full expressions for general  $N$  are given in Appendix C.4. Electronic versions of the exponents are also available as Supplemental Material for download, see [58] for further instructions. For  $N = 3$ , which corresponds to



the situation relevant for the spin-orbital models [54], the exponents read

$$\begin{aligned} \frac{1}{\nu} &= 2 - \frac{5\sqrt{5}+9}{22}\epsilon + \frac{937\sqrt{5}-3182}{31944}\epsilon^2 \\ &\quad + \frac{264(576665-306864\sqrt{5})\zeta_3+5132520\sqrt{5}-113996279}{834888384\sqrt{5}}\epsilon^3 + \mathcal{O}(\epsilon^4) \\ &\approx 2 - 0.917\epsilon - 0.0340\epsilon^2 - 0.0735\epsilon^3 + \mathcal{O}(\epsilon^4), \end{aligned} \quad (7.17)$$

$$\begin{aligned} \eta_\phi &= \frac{1}{3}\epsilon + \frac{80\sqrt{5}+89}{2904}\epsilon^2 - \frac{351384\zeta_3+66393\sqrt{5}-357226}{6324912}\epsilon^3 + \mathcal{O}(\epsilon^4) \\ &\approx 0.333\epsilon + 0.0922\epsilon^2 - 0.0338\epsilon^3 + \mathcal{O}(\epsilon^4), \end{aligned} \quad (7.18)$$

$$\begin{aligned} \eta_\psi &= \frac{1}{6}\epsilon + \frac{105\sqrt{5}+79}{8712}\epsilon^2 - \frac{234256\zeta_3+72458\sqrt{5}-187711}{8433216}\epsilon^3 + \mathcal{O}(\epsilon^4) \\ &\approx 0.167\epsilon + 0.0360\epsilon^2 - 0.0303\epsilon^3 + \mathcal{O}(\epsilon^4). \end{aligned} \quad (7.19)$$

We note that the above expansions are asymptotic series with vanishing radius of convergence. It is reassuring, however, that the coefficients of the two- and three-loop corrections are still small compared to the one-loop values. For comparison with the large- $N$  expansion, we also state the expressions we have obtained upon further expanding the general  $(4 - \epsilon)$ -expansion results in  $1/N$ . We obtain

$$\begin{aligned} \frac{1}{\nu} &= 2 - \epsilon - \left[9\epsilon - \frac{39}{4}\epsilon^2 + \frac{9}{16}\epsilon^3\right] \frac{1}{N} \\ &\quad + \left[459\epsilon - \frac{5895}{8}\epsilon^2 + \frac{27}{32}(153 - 184\zeta_3)\epsilon^3\right] \frac{1}{N^2} + \mathcal{O}(\epsilon^4, 1/N^3), \end{aligned} \quad (7.20)$$

$$\begin{aligned} \eta_\phi &= \epsilon + \left[-6\epsilon + \frac{15}{4}\epsilon^2 + \frac{21}{16}\epsilon^3\right] \frac{1}{N} \\ &\quad + \left[36\epsilon - \frac{261}{8}\epsilon^2 - \frac{9}{32}(72\zeta_3 + 95)\epsilon^3\right] \frac{1}{N^2} + \mathcal{O}(\epsilon^4, 1/N^3), \end{aligned} \quad (7.21)$$

$$\begin{aligned} \eta_\psi &= \left[\frac{3}{2}\epsilon - \frac{9}{8}\epsilon^2 - \frac{9}{32}\epsilon^3\right] \frac{1}{N} + \left[-9\epsilon + \frac{369}{16}\epsilon^2 - \frac{513}{64}\epsilon^3\right] \frac{1}{N^2} \\ &\quad + \left[54\epsilon - \frac{4023}{16}\epsilon^2 + \frac{243}{32}(33 - 4\zeta_3)\epsilon^3\right] \frac{1}{N^3} + \mathcal{O}(\epsilon^4, 1/N^4). \end{aligned} \quad (7.22)$$

For any fixed  $N$ , we extract estimates for the physical dimension  $\epsilon = 1$  by employing standard Padé approximants

$$[m/n] = \frac{a_0 + a_1\epsilon + \dots + a_m\epsilon^m}{1 + b_1\epsilon + \dots + b_n\epsilon^n}, \quad (7.23)$$

with  $m, n \in \{0, 1, 2, 3\}$  and  $m + n = 3$ . The coefficients  $a_0, \dots, a_m$  and  $b_1, \dots, b_n$  are obtained from matching the Taylor series of  $[m/n]$  order by order with the  $\epsilon$  expansions. The discussion of the resulting estimates for  $1/\nu$ ,  $\eta_\phi$ , and  $\eta_\psi$  for different values of  $N$  is deferred to Section 7.6.

## 7.4 $1/N$ expansion

In the limit of a large number of fermion flavors  $N \rightarrow \infty$ , the fluctuations of the order-parameter field  $\phi_n$  freeze out, which allows us to compute the critical exponents in arbitrary  $2 < d < 4$  in a systematic expansion in powers of  $1/N$  and is the topic of this section.

### 7.4.1 Method

To achieve this, we have applied the large- $N$  critical point method developed in Refs. [71, 312, 314] for the scalar  $O(N)$  model and later extended to the Gross-Neveu universality class in Refs. [157, 159–163]. As the latter formalism has already been applied to variations of the Gross-Neveu model, we will highlight only the key differences here. Indeed given the strong overlap with the Gross-Neveu-SU(2) (= chiral Heisenberg) model that the present SO(3) study is similar to, we refer the reader to Ref. [72] for the finer details of the technique.

One of the first steps is to recognize that the Lagrangian that serves as the basis for the method of Refs. [71, 312, 314] is that of the universal theory that resides at the stable fixed point in all dimensions  $2 < D < 4$ . It is a simpler version of Eq. (7.2) in that only the fermion kinetic term and the three-point vertex are the essential ones needed to define the canonical dimensions of the fields at the fixed point, together with a quadratic term in the boson field. Specifically,

$$\mathcal{L}_{\text{univ}} = \bar{\psi} \not{\partial} \psi - \phi_a \bar{\psi} (\mathbb{1}_{2N/3} \otimes L_a) \psi + \frac{1}{2} \phi_a \phi_a, \quad (7.24)$$

where  $\not{\partial} \equiv \gamma^\mu \partial_\mu$  with  $\gamma^\mu$  again being  $(2N) \times (2N)$  Dirac matrices, such that the spinors  $\psi$  and  $\bar{\psi}$  have  $2N$  components, as in the original Lagrangian [Eq. (7.2)]. The scalar  $\phi_a$  has been rescaled since at criticality the perturbative coupling constant is fixed and does not run. The quartic interaction present in Eq. (7.2) is required in four dimensions to ensure renormalizability. Its contribution in  $\mathcal{L}_{\text{univ}}$  is automatically accounted for through closed fermion loop diagrams with four external boson fields [316]. The other main aspect of the setup concerns the algebra of the SO(3) generators  $L_a$ , which satisfy the relation

$$(L_a)_{ij}(L_a)_{kl} = \delta_{il}\delta_{jk} - \delta_{ik}\delta_{jl}. \quad (7.25)$$

We have used this in determining the group-theory factors associated with the Feynman diagrams that contribute to the large- $N$  formalism.

In general the method of Refs. [71, 312, 314] entails analyzing the behavior of various Schwinger-Dyson equations in the approach to criticality. At the stable fixed point, the propagators of the fields have a simple scaling behavior where the exponent of the propagator corresponds to the full scaling dimension. Specifically, in coordinate space the propagators take the asymptotic forms

$$\psi(x) \sim \frac{A \not{x}}{(x^2)^\alpha} [1 + A'(x^2)^\lambda], \quad (7.26)$$

$$\phi(x) \sim \frac{B}{(x^2)^\beta} [1 + B'(x^2)^\lambda], \quad (7.27)$$

where we have used the name of the field as a shorthand for the propagator at criticality, with the scaling exponents

$$\alpha = \mu + \frac{1}{2}\eta_\psi, \quad \beta = 1 - \eta_\psi - \chi, \quad (7.28)$$

and we have introduced  $\mu \equiv d/2$ . Here,  $\eta_\psi$  is the fermion anomalous dimension, which has been computed to three loops at criticality in the previous section. The anomalous dimension of the boson-fermion vertex is

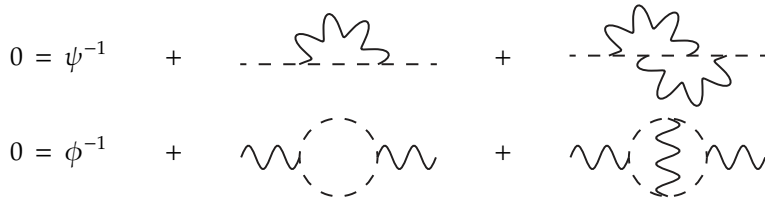


**Figure 7.3:** Skeleton Schwinger-Dyson two-point functions used to determine  $\eta_\psi$  at  $\mathcal{O}(1/N^2)$ . Dashed inner lines correspond to critical fermion propagators [Eq. (7.26)] and wiggly inner lines correspond to critical boson propagators [Eq. (7.27)].

denoted by  $\chi$  so that

$$\eta_\phi = 4 - 2\mu - 2\eta_\psi - 2\chi. \tag{7.29}$$

In addition to these leading exponents, each propagator includes a correction term involving the exponent  $\lambda$ . At criticality, this exponent corresponds to the correlation-length exponent as  $1/\nu = 2\lambda$ . The canonical dimension of  $\lambda$  is  $(\mu - 1)$ . The quantities  $A, B$ , as well as  $A'$  and  $B'$  are  $x$ -independent amplitudes. The first two always appear in the combination  $A^2B$ , but this plays an intermediate role in deriving exponents. The first terms of the respective equations in Fig. 7.3 represent the asymptotic scaling forms of the two-point functions and have been given in Ref. [157]. They are derived from Eqs. (7.26) and (7.27) and have a similar scaling form to these although  $A$  and  $B$  occur in the denominator.

### Skeleton Schwinger-Dyson equations

To determine the anomalous dimensions of the two fields, one focuses on the two-point Schwinger-Dyson equations shown in Fig. 7.3, as well the three-point vertex function, for which the first correction is depicted in Fig. 7.4. For both the two- and three-point functions the contributing diagrams are computed with the asymptotic propagators, Eqs. (7.26) and (7.27). As the power of the leading term of each propagator includes the nonzero anomalous dimensions of Eq. (7.28), then there are no self-energy corrections on the contributing diagrams in order to avoid double counting. By evaluating the diagrams and solving the equations of Fig. 7.3 self-consistently, eliminating the product  $A^2B$  in the process, one obtains an expression for  $\eta_\psi$  at  $\mathcal{O}(1/N^2)$ . The value of  $\chi$  at  $\mathcal{O}(1/N)$  is required for this to ensure that no  $\ln(x^2)$  terms remain after renormalization. This value for  $\chi$  is deduced from the scaling behavior of the diagram of Fig. 7.4. Moreover, this produces  $\eta_\phi$  at  $\mathcal{O}(1/N)$  as a corollary from Eq. (7.29). For the next order of  $\chi$ , one extends the critical-point evaluation of the higher-order diagrams to the three-point function, which are given by the decorations of the leading-order diagram of Fig. 7.4 with vertex corrections, as well as the non-planar and three-loop diagrams shown in Fig. 7.5. This produces  $\chi$  and hence  $\eta_\phi$  at  $\mathcal{O}(1/N^2)$ .

Once we have established the anomalous dimensions of the fields at  $\mathcal{O}(1/N^2)$ , the correction to scaling terms in Eqs. (7.26) and (7.27) can be included in order to determine  $1/\nu$  via the determination of  $\lambda$ . Since the correction terms involve  $(x^2)^\lambda$ , then the two-point Schwinger-Dyson consistency equation contains terms of different dimensions. These split into terms which are independent of the correction to scaling amplitudes,  $A'$  and  $B'$ , and those that are not. It is the latter ones that determine  $\lambda$  to  $\mathcal{O}(1/N^2)$  [312], since a consistency equation can be formed from the  $2 \times 2$  matrix defined by the

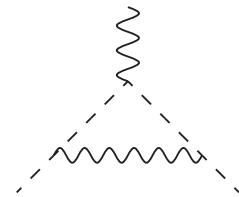
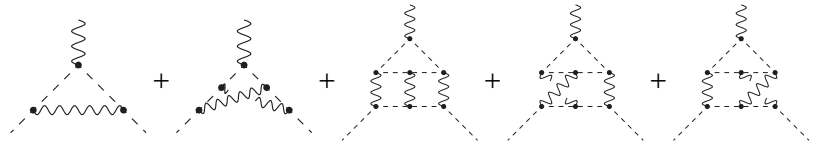


**Figure 7.4:** Leading-order skeleton Schwinger-Dyson three-point function used to determine  $\chi$  at  $\mathcal{O}(1/N)$ .

**Figure 7.5:** Diagrams contributing to large- $N$  conformal bootstrap formalism to deduce  $\eta_\psi$  at  $\mathcal{O}(1/N^3)$ . Black dots refer to Polyakov conformal triangles, see Ref. [72] for details.



coefficients of  $A'$  and  $B'$  in each equation of Fig. 7.3. Finding the solution to the equation formed by setting the determinant of this matrix to zero defines the consistency equation. For the Gross-Neveu universality classes there is a known complication in that while all the propagators of the diagrams of Fig. 7.3 include the correction terms, extra diagrams are needed due to the same reordering that arises in the original Gross-Neveu- $\mathbb{Z}_2$  (= chiral Ising) model [157, 160, 161, 163]. This necessitates the inclusion of the higher-order Feynman diagram as given in Fig. 4 of Ref. [72], but with the appropriate group factor for the present model.

### Large- $N$ conformal bootstrap technique

Finally, we have been able to apply what is termed the large- $N$  conformal bootstrap technique to compute the  $\mathcal{O}(1/N^3)$  term of  $\eta_\psi$ . This method was originally developed for the  $O(N)$  scalar model in Ref. [314] using the early work of Refs. [313, 317, 318]. It was subsequently extended to the Gross-Neveu- $\mathbb{Z}_2$  universality class in Refs. [159, 162, 163] and more recently for the Gross-Neveu-SU(2) (= chiral Heisenberg) model in Ref. [72]. We refer readers to that later article for more details of the large- $N$  conformal bootstrap technique for the present context. However, it is worth noting some of the key aspects of the approach. Rather than focusing on the skeleton Schwinger-Dyson two-point functions, the underlying self-consistency equations that ultimately produce  $\eta_\psi$  at  $\mathcal{O}(1/N^3)$  are derived from the vertex functions. By contrast to the two-point function approach, one is in effect performing perturbation theory in the vertex anomalous dimension  $\chi$ . The relevant diagrams are given in Fig. 7.5. Again, while there is no dressing on the propagators, there are no vertex corrections unlike the diagrams in Fig. 7.3. Instead, the contributions that underlie the vertex structure are subsumed into the black dots, which denote Polyakov conformal triangles. These are designed in such a way that the sum of the critical exponents of the propagators connected to the vertex is  $(2\mu + 1)$ . This value means that all the scalar-fermion vertices are unique in the sense of conformal integration [157, 160, 161, 163]. So it is possible to evaluate all the diagrams to the necessary order to determine  $\eta_\psi$  at  $\mathcal{O}(1/N^3)$ .

### 7.4.2 Critical exponents

Having summarized the large- $N$  critical point formalism, we are now in a position to discuss the results. Expressions in general space-time dimensions  $2 < d < 4$  for all the exponents we have determined are presented in Appendix C.4 and electronically as supplemental material to Ref. [58]. However, the epsilon expansion of the large- $N$  expressions must agree with the explicit three-loop exponents derived from the renormalization group functions at the stable fixed point. Therefore, if we expand each of  $\eta_\psi$ ,  $\eta_\phi$ , and  $1/\nu$  around  $d = 4 - \epsilon$ , we find

$$\begin{aligned} \frac{1}{\nu} &= 2 - \epsilon + \left[ -9\epsilon + \frac{39}{4}\epsilon^2 - \frac{9}{16}\epsilon^3 - \frac{9}{64}(1 + 16\zeta_3)\epsilon^4 + \frac{3}{256}(208\zeta_3 - 144\zeta_4 - 3)\epsilon^5 \right] \frac{1}{N} \\ &+ \left[ 459\epsilon - \frac{5895}{8}\epsilon^2 + \frac{27}{32}(153 - 184\zeta_3)\epsilon^3 + \frac{27}{64}(320\zeta_5 - 276\zeta_4 + 1376\zeta_3 + 203)\epsilon^4 \right. \\ &\left. + \frac{9}{1792}(4795 - 90496\zeta_5 + 6720\zeta_3^2 - 123984\zeta_3 + 33600\zeta_6 + 86688\zeta_4)\epsilon^5 \right] \frac{1}{N^2} + \mathcal{O}(\epsilon^6, 1/N^3), \end{aligned} \quad (7.30)$$

$$\begin{aligned} \eta_\phi &= \epsilon + \left[ -6\epsilon + \frac{15}{4}\epsilon^2 + \frac{21}{16}\epsilon^3 + \frac{3}{64}(11 - 32\zeta_3)\epsilon^4 + \frac{3}{256}(80\zeta_3 - 96\zeta_4 + 19)\epsilon^5 \right] \frac{1}{N} \\ &+ \left[ 36\epsilon - \frac{261}{8}\epsilon^2 - \frac{9}{32}(72\zeta_3 + 95)\epsilon^3 + \frac{9}{64}(472\zeta_3 - 108\zeta_4 + 45)\epsilon^4 + \frac{9}{256}(97 - 288\zeta_5 + 1416\zeta_4 - 1248\zeta_3)\epsilon^5 \right] \frac{1}{N^2} \\ &+ \mathcal{O}(\epsilon^6, 1/N^3), \end{aligned} \quad (7.31)$$

$$\begin{aligned} \eta_\psi &= \left[ \frac{3}{2}\epsilon - \frac{9}{8}\epsilon^2 - \frac{9}{32}\epsilon^3 + \frac{3}{128}(16\zeta_3 - 3)\epsilon^4 + \frac{9}{512}(16\zeta_4 - 16\zeta_3 - 1)\epsilon^5 \right] \frac{1}{N} \\ &+ \left[ -9\epsilon + \frac{369}{16}\epsilon^2 - \frac{513}{64}\epsilon^3 - \frac{9}{128}(128\zeta_3 + 69)\epsilon^4 + \frac{9}{512}(1008\zeta_3 - 384\zeta_4 - 89)\epsilon^5 \right] \frac{1}{N^2} \\ &+ \left[ 54\epsilon - \frac{4023}{16}\epsilon^2 + \frac{243}{32}(33 - 4\zeta_3)\epsilon^3 + \frac{27}{256}(2184\zeta_3 - 216\zeta_4 + 493)\epsilon^4 + \frac{27}{1024}(6552\zeta_4 - 576\zeta_5 - 20024\zeta_3 - 2375)\epsilon^5 \right] \frac{1}{N^3} \\ &+ \mathcal{O}(\epsilon^6, 1/N^4). \end{aligned} \quad (7.32)$$

All terms to  $\mathcal{O}(\epsilon^3)$  agree exactly with Eqs. (7.20)–(7.22), which is a highly non-trivial check on our  $d$ -dimensional expressions. In the above equations, we have included additional terms to  $\mathcal{O}(\epsilon^5)$  to provide checks for future higher-loop computations.

With this check of the  $d$ -dimensional exponents satisfied, we can now deduce their values in the  $1/N$  expansion in fixed  $d = 2 + 1$  space-time dimensions. We find

$$\begin{aligned} \frac{1}{\nu} &= 1 - \frac{16}{\pi^2 N} + \frac{324\pi^2 + 2624}{3\pi^4 N^2} + \mathcal{O}(1/N^3) \\ &\approx 1 - \frac{1.62114}{N} + \frac{19.92200}{N^2} + \mathcal{O}(1/N^3), \end{aligned} \quad (7.33)$$

$$\begin{aligned} \eta_\phi &= 1 - \frac{20}{\pi^2 N} + \frac{2(81\pi^2 - 1028)}{3\pi^4 N^2} + \mathcal{O}(1/N^3) \\ &\approx 1 - \frac{2.02642}{N} + \frac{1.56428}{N^2} + \mathcal{O}(1/N^3), \end{aligned} \quad (7.34)$$

$$\begin{aligned} \eta_\psi &= \frac{4}{\pi^2 N} + \frac{304}{3\pi^4 N^2} + \frac{972\pi^2 \ln(2) + 255\pi^2 - 10206\zeta_3 - 3796}{9\pi^6 N^3} + \mathcal{O}(1/N^4) \\ &\approx \frac{0.40528}{N} + \frac{1.04029}{N^2} - \frac{0.79721}{N^3} + \mathcal{O}(1/N^4). \end{aligned} \quad (7.35)$$

In effect, three terms in the expansion of each exponent are available, but involve different powers of  $1/N$ . We note that the leading two terms of  $1/\nu$  and the leading terms of  $\eta_\phi$  and  $\eta_\psi$  are the same as those of the Gross-Neveu-SU(2) model [72]. However, the  $\mathcal{O}(1/N^2)$  term of  $1/\nu$  is nearly twice that of its SU(2) counterpart and the coefficients of the subsequent terms of  $\eta_\phi$  and  $\eta_\psi$  are also significantly larger here, with the exception of the  $\mathcal{O}(1/N^2)$  term in  $\eta_\phi$ .

For extrapolating the large- $N$  series to finite  $N$ , we again use Padé approximants

$$[m/n] = \frac{a_0 + a_1 N^{-1} + \dots + a_m N^{-m}}{1 + b_1 N^{-1} + \dots + b_n N^{-n}}, \quad (7.36)$$

where now  $m, n \in \{0, 1, 2\}$  ( $m, n \in \{0, 1, 2, 3\}$ ) and  $m + n = 2$  ( $m + n = 3$ ) for  $1/\nu$  and  $\eta_\phi$  ( $\eta_\psi$ ). The numerical estimates for different values of  $N$  are discussed in Sec. 7.6.

## 7.5 Functional renormalization group

Finally, as the physical case of interest  $d = 2 + 1$  and  $N = 3$  lies outside the regimes in which the epsilon and  $1/N$  expansions are fully controlled, we also employ the FRG as a complementary approach to estimate the critical exponents.

### 7.5.1 Method

*/\*In this Section, we present the technical details for the FRG calculation. Our starting point is the Wetterich equation in Eq. (2.33). For the effective action we introduce  $\Phi$  which corresponds to a collective field variable, which comprises all individual fields contained in the theory.\** Hence, in the Gross-Neveu-SO(3) case, we have  $\Phi = (\phi_a, \psi, \bar{\psi})$ .

$$\Gamma_k^{(2)} = \frac{\overrightarrow{\delta}}{\delta\Phi^\top} \Gamma_k \frac{\overleftarrow{\delta}}{\delta\Phi}, \quad (7.37)$$

and the supertrace operator  $\text{STr}$  extends the usual trace by accounting for Fermi-Dirac statistics thus:

$$\text{STr} \begin{pmatrix} B & * & * \\ * & F_1 & * \\ * & * & F_2 \end{pmatrix} = \text{Tr} B - \text{Tr} \begin{pmatrix} F_1 & * \\ * & F_2 \end{pmatrix}. \quad (7.38)$$

See Refs. [74, 76, 77, 83] for introductory expositions on the method, and Refs. [78, 79, 84] for reviews on applications to interacting many-body systems. The Wetterich equation itself is exact, but generically not exactly soluble.

In the absence of a small control parameter for the physical case of  $N = 3$  and  $d = 3$ , here we pursue an ansatz in the spirit of a derivative expansion of the effective average action,

$$\Gamma_k = \int d^d x \left[ Z_{\psi,k} \bar{\psi} \gamma^\mu \partial_\mu \psi + \frac{1}{2} Z_{\phi,k} (\partial_\mu \phi_a)^2 - g_k \phi_a \bar{\psi} (\mathbb{1} \otimes L_a) \psi + U_k(\varrho) \right], \quad (7.39)$$

where we have introduced the SO(3)-invariant  $\varrho = \frac{1}{2} \phi_a \phi_a$ . General field-dependence of renormalization group functions is allowed only in the effective average bosonic potential  $U_k$ , which is assumed to carry no explicit momentum dependence. Pure fermionic interactions, such as four-fermion terms, that may be generated in the nonperturbative regime, are neglected. The next-to-leading order contributions come from the kinetic terms, whose scale-dependences are approximated by field-independent renormalization constants  $Z_{\phi,k}$ ; all higher-order terms in the gradient expansion are neglected. This truncation of the effective average action is commonly referred to as ‘‘improved local potential approximation’’ (LPA’). It has been proven to yield reliable results in a number of similar Gross-Neveu-Yukawa-type models [30,

31, 126, 140, 188, 300, 319–323]. Extensions of this approximation for the present class of models have been discussed in Refs. [90, 141, 142, 324]. A final approximation entails choosing a suitable ansatz for the effective average potential. Here, we employ two different expansion techniques. We have verified that our numerical results from the two approaches converge to the same values within the error bars.

### Taylor expansion of effective potential

A simple ansatz is a truncated Taylor expansion

$$U_k(\varrho) = \sum_{i=1}^{n/2} \frac{1}{i!} \lambda_{i,k} \varrho^i, \quad (7.40)$$

where we have assumed that the fixed point is located in the symmetric regime, such that the minimum of the potential is at  $\varrho = 0$ . If this assumption is violated at the fixed point, i.e.,  $U'(0) < 0$ , an alternative expansion

$$U_k(\varrho) = \sum_{i=2}^{n/2} \frac{1}{i!} \hat{\lambda}_{i,k} (\varrho - \varrho_{0,k})^i \quad (7.41)$$

is more expedient; this is called the spontaneously symmetry broken (SSB) regime. In the above,  $\varrho_{0,k}$  is the (scale-dependent) location of the minimum of  $U_k(\varrho)$ . It is related to the vacuum expectation value (VEV) of the order parameter by  $\rho_{0,0} = \frac{1}{2} \langle \phi_a \rangle^2$ . Note that the linear term in the Taylor expansion is absent, since  $\partial U(\varrho) / \partial \phi_a = \phi_a U'(\varrho)$ , and hence  $U'(\varrho_0) = 0$  if  $\varrho_0 \neq 0$  is a local minimum.

For practical computations, the ansatz (7.40) is truncated at some finite order  $n \in 2\mathbb{N}$ . This defines the so-called LPA $n'$ . The validity of this polynomial truncation can be checked *a posteriori* by verifying convergence of the results upon increasing  $n$ . The expansion of the effective potential introduces a plethora of coupling constants, of which  $\lambda_1 = m^2 > 0$  is proportional to the squared boson mass and  $\lambda_2 = 4!\lambda$  is the quartic boson self-coupling. Inclusion of the higher-order couplings  $\lambda_{i>2}$  is a minimal way to incorporate nonperturbative corrections in space-time dimensions  $d < 4$ , in addition to the effects from the nonperturbative propagator, cf. Eq. (2.33).

The flow of the bosonic self-couplings are determined from the flow of  $U_k(\varrho)$  by differentiating successively with respect to  $\varrho$ . In the symmetric regime, this is straightforward to implement:

$$\partial_t \lambda_i = [(\partial_\varrho)^i \partial_t U_k(\varrho)]_{\varrho \rightarrow 0} \quad (i \in \mathbb{N}_{\geq 1}). \quad (7.42)$$

The corresponding system of equations in the SSB regime is given by

$$\partial_t \hat{\lambda}_i = [(\partial_\varrho)^i \partial_t U(\varrho)]_{\varrho \rightarrow \varrho_0} + \hat{\lambda}_{i+1} \partial_t \varrho_0 \quad (i \in \mathbb{N}_{\geq 2}), \quad (7.43)$$

and has to be supplemented by a flow equation for the VEV:

$$\partial_t \varrho_0 = -\frac{1}{\hat{\lambda}_2} [ \partial_\varrho \partial_t U(\varrho) ]_{\varrho \rightarrow \varrho_0}. \quad (7.44)$$

The latter follows from  $U'(\varrho_0) = 0$  in the SSB regime [321].

### Pseudospectral decomposition of effective potential

In the context of the present work, we aim at systematically comparing the results from different quantum-field-theoretical methods between two and four dimensions. In particular, towards two dimensions, we have to be careful about a possible breakdown of the convergence of a local expansion in the effective potential. This is related to the canonical dimensionality of the operators or couplings in the local expansion, i.e. the terms  $\propto \lambda_i \varrho^i$ . More specifically, the canonical dimension  $[\cdot]$  of the bosonic field  $\phi$  is given by  $[\phi] = (d - 2)/2$ , i.e. the dimension of the operator  $\varrho^i$  is  $(d - 2)i$ . Therefore, the corresponding coupling  $\lambda_i$  scales as  $[\lambda_i] = d - (d - 2)i$ . Lowering the dimension towards  $d = 2$  means that more and more couplings with higher  $i$  become canonically relevant until they all have the same canonical dimension of two in  $d = 2$ . Depending on the model and the specific fixed point, this behavior can severely limit the reliability of a finite-order local expansion in the bosonic operators.

In lieu of a local Taylor expansion for the effective potential, non-local expansion schemes can be advantageous in terms of tractability, accuracy, and fast convergence. An approximation scheme that has been explored in the context of FRG fixed-point- and flow equations, is based on pseudospectral methods [85]. Importantly, these methods facilitate, e.g., an efficient and high-precision resolution of global aspects of the effective potential including the correct description of a model's asymptotic behavior [86–90, 142, 325, 326].

In the present case of the fixed point equation for the effective potential, we need to find an approximate solution to an ordinary differential equation in one variable, which is defined on the domain  $\mathbb{R}^+$ . To that end, we can expand the effective potential, i.e.  $U(\varrho)$ , into a series of Chebyshev polynomials, where the domain of  $U(\varrho)$  is decomposed into two subdomains, i.e.  $[0, \varrho_m]$  and  $[\varrho_m, \infty)$ . The expansion then reads

$$U(\varrho) \approx \begin{cases} \sum_{i=0}^{n_T} t_i T_i\left(\frac{2\varrho}{\varrho_m} - 1\right), & \varrho \leq \varrho_m, \\ U_\infty(\varrho) \sum_{i=0}^{n_R} r_i R_i(\varrho - \varrho_m), & \varrho \geq \varrho_m. \end{cases} \quad (7.45)$$

Here, the  $T_i(x)$  are the Chebyshev polynomials of the first kind and the  $R_i(x) = T_i\left(\frac{x-L}{x+L}\right)$  are rational Chebyshev polynomials with a free parameter  $L$ , which parametrizes the compactification in the argument  $x$ . Further,  $U_\infty(\varrho)$  is the leading asymptotic behavior of the effective potential for large field arguments, i.e.  $\varrho \rightarrow \infty$ , which we obtain from the dimensional scaling terms in the flow equation. The matching point  $\varrho_m$  separates the subdomains and is another free parameter that has to be chosen large enough such that the minimum of the effective potential appears for  $\varrho = \varrho_0 < \varrho_m$ . We can use  $L$  and  $\varrho_m$  to optimize numerical convergence. The values of the effective potential and its derivatives for all field arguments  $\varrho$  are straightforwardly obtained by employing efficient recursive algorithms [85]. In fact, we only need a relatively small number of expansion coefficients  $t_i$  and  $r_i$  due to fast convergence of the series.

For the determination of the coefficients  $t_i$  and  $r_i$  in the Chebyshev expansion, we use the collocation method, i.e. we insert the ansatz in Eq. (7.45) into the flow Eq. (2.33) and evaluate it on a given set of collocation points. The collocation points are chosen to be the nodes of the highest Chebyshev



polynomials in the respective domain and we add the origin, i.e.  $\varrho = 0$ . Finally, to accomplish smoothness, we implement matching conditions for the values of the effective potential and its derivatives at  $\varrho_m$ . The resulting set of algebraic equations is then solved with the Newton-Raphson method. In practice, we actually expand the derivative of the dimensionless effective potential  $u'(\varrho)$  along these lines, we optimize  $L$  and  $\varrho_m$  as well as the number of collocation points until we reach convergence in our numerical results. For the present model, we observe numerical convergence of the first four significant digits already starting at  $n_T = n_R = 9$  and, as a sanity check, we have increased the number of collocation points up to 18 in each subdomain for selected cases.

The anomalous dimensions of the quantum critical point are then obtained directly from the fixed-point solution of  $u'(\varrho)$  using the FRG flow equations specified in the next section. To obtain the inverse correlation length exponent, we use the pseudospectral expansion from the first subdomain, i.e.  $\varrho < \varrho_m$ , rewriting it as a local expansion around its minimum. With the latter expansion, we then calculate the stability matrix and extract the eigenvalues at the fixed-point potential. The largest positive eigenvalue is the inverse correlation length exponent.

## 7.5.2 Flow equations

For convenience, we introduce dimensionless versions of renormalized couplings and the effective potential, to wit:

$$\tilde{g}^2 = Z_{\phi,k}^{-1} Z_{\psi,k}^{-2} k^{d-4} g_k^2, \quad u(\tilde{\varrho}) = k^{-d} U_k(Z_{\phi,k}^{-1} k^{d-2} \tilde{\varrho}), \quad (7.46)$$

where  $\tilde{\varrho} = Z_{\phi,k}^{-1} k^{d-2} \varrho$  (and likewise for the VEV  $\varrho_0$ ) and we have suppressed the indices indicating the scale dependence for simplicity. In the following, we shall work solely with dimensionless quantities, and leave the ‘‘tilde’’ implicit. Furthermore, we define the bosonic and fermionic anomalous dimensions in usual fashion,  $\eta_{\phi,k} = -\partial_t Z_{\phi,k} / Z_{\phi,k}$  and  $\eta_{\psi,k} = -\partial_t Z_{\psi,k} / Z_{\psi,k}$ . The FRG flow equations can be derived by inserting the ansatz (7.39) into the Wetterich equation (2.33) and comparing coefficients. In particular, evaluating for constant  $\phi_a = (0, 0, \sqrt{2\varrho})$  yields the flow equation for the effective potential

$$\begin{aligned} \partial_t u(\varrho) = & -du(\varrho) + (d-2 + \eta_\phi)\varrho u'(\varrho) \\ & + 2v_d \ell_0^{(B),d} (u'(\varrho) + 2\varrho u''(\varrho); \eta_\phi) \\ & + 4v_d \ell_0^{(B),d} (u'(\varrho); \eta_\phi) \\ & - 4v_d \left[ \frac{2N}{3} \ell_0^{(F),d} (2\varrho g^2; \eta_\psi) + \frac{N}{3} \ell_0^{(F),d} (0; \eta_\psi) \right]. \end{aligned} \quad (7.47)$$

The factor  $v_d := [2^{d+1} \pi^{d/2} \Gamma(d/2)]^{-1}$  arises from integration over the surface of the sphere in  $d$ -dimensional Fourier space. The threshold functions  $\ell_0^{(B),d}$  and  $\ell_0^{(F),d}$  involve the remaining radial integration and encode the details of the regularization scheme, see Ref. [74] for formal definitions. While the first line of Eq. (7.47) represents the tree-level flow, the second and third line arise from the fluctuations of the one Higgs mode with mass  $2\varrho u''(\varrho)$  and the two Goldstone modes respectively, in full agreement with the Gross-Neveu-SU(2) case [140]. In the fermion bubble contribution (last

line), the first term corresponds to the  $2N/3$  gapped modes with mass  $2\rho g^2$ , and the second term to the  $N/3$  modes that remain gapless in the presence of a constant background  $\rho$ .

The definition of the Yukawa coupling is actually ambiguous in the SSB regime, as in general the fermions couple differently to Higgs and Goldstone modes. Assuming the coupling to the Goldstone modes (due to their masslessness) to be the one primarily important for critical behavior [140, 324], we determine the flow of the Yukawa coupling by projecting onto  $\phi_1 \bar{\psi}(L_1 \otimes \mathbb{1}_2)\psi$  and obtain

$$\begin{aligned} \partial_t g^2 = & (d - 4 + \eta_\phi + 2\eta_\psi)g^2 + 8v_d \ell_{11}^{(\text{FB}),d}(2\rho_0 g^2, u'_0; \eta_\psi, \eta_\phi)g^4 \\ & - 16v_d \rho_0 u''_0 \ell_{111}^{(\text{FBB}),d}(2\rho_0 g^2, u'_0, u'_0 + 2\rho_0 u''_0; \eta_\psi, \eta_\phi)g^4. \end{aligned} \quad (7.48)$$

Likewise, comparison of coefficients for the kinetic terms gives the anomalous dimensions,

$$\eta_\phi = \frac{32Nv_d}{3d} m_4^{(\text{F}),d}(2\rho_0 g^2; \eta_\psi)g^2 + \frac{16v_d}{d} m_{22}^{(\text{B}),d}(u'_0, u'_0 + 2\rho_0 u''_0; \eta_\phi)\rho_0 u''_0{}^2 \quad (7.49)$$

$$\begin{aligned} \eta_\psi = & \frac{16v_d}{3d} \left[ m_{12}^{(\text{FB}),d}(0, u'_0; \eta_\psi, \eta_\phi) + m_{12}^{(\text{FB}),d}(2\rho_0 g^2, u'_0; \eta_\psi, \eta_\phi) \right. \\ & \left. + m_{12}^{(\text{FB}),d}(2\rho_0 g^2, u'_0 + 2\rho_0 u''_0; \eta_\psi, \eta_\phi) \right] g^2. \end{aligned} \quad (7.50)$$

Here,  $\ell_{11}^{(\text{FB}),d}$ ,  $m_4^{(\text{F}),d}$ ,  $m_{22}^{(\text{B}),d}$  and  $m_{12}^{(\text{FB}),d}$  are further threshold functions defined in Ref. [74].

In this work, we use a linear cutoff, which satisfies an optimization criterion [82], as well as a sharp cutoff [324] for comparison. For these regulators, the threshold functions are known analytically, see, e.g., the appendix of Ref. [324] for an overview.

As a consistency check, we derive, in the limit of small  $\epsilon = 4 - d$ , the one-loop flow equations of Ref. [54]. Since the latter employed Wilsonian RG with a sharp cutoff, we need to insert<sup>3</sup> the threshold functions corresponding to the sharp cutoff in the flow equations (7.47)–(7.50). We assume the fixed-point effective potential lies in the symmetric regime. Assuming furthermore that fixed-point couplings  $g_\star^2 = \mathcal{O}(\epsilon)$ ,  $\lambda_{n,\star} = \mathcal{O}(\epsilon^{n-1})$  are parametrically small, we may neglect all higher-order couplings  $\lambda_{i>2}$  in the flow of the effective potential above (i.e., we work in LPA4'). Thus,

$$\partial_t \lambda_1 = (-2 + \eta_\phi)\lambda_1 - 10v_d \frac{\lambda_2}{1 + \lambda_1} + \frac{16}{3}v_d N g^2, \quad (7.51)$$

$$\partial_t \lambda_2 = (-\epsilon + 2\eta_\phi)\lambda_2 + 22v_d \frac{\lambda_2^2}{(1 + \lambda_1)^2} - \frac{32}{3}v_d N g^4, \quad (7.52)$$

and

$$\partial_t g^2 = (-\epsilon + \eta_\phi + 2\eta_\psi)g^2 + 8v_d \frac{g^4}{1 + \lambda_1}, \quad (7.53)$$

with  $\eta_\phi = \frac{32}{3} \frac{v_d}{d} N g^2$  and  $\eta_\psi = 16 \frac{v_d}{d} g^2 / (1 + \lambda_1)^2$ . We then rescale the couplings  $\lambda_2 \rightarrow \lambda_2 / (4v_d)$  and  $g^2 \rightarrow g^2 / (4v_d)$  and take into account that  $v_d = \frac{1}{32\pi^2} + \mathcal{O}(\epsilon)$ . Upon identifying  $\lambda_1 \equiv m^2$  and  $\lambda_2 \equiv 4!\lambda$ , Eqs. (7.51)–(7.53) coincide precisely with the one-loop flow equations given in Ref. [54].

3: The flow equations are non-universal (i.e., dependent on cutoff scheme), so care must be taken when comparing results for fixed-point couplings, and flow equations *a fortiori*, obtained using different methods (this would be true even if we could employ the respective methods exactly). The exponents, on the other hand, are universal and hence scheme-independent. In fact, the loop expansion near the upper critical dimension is universal order by order. We have checked explicitly that the exponents using the linear cutoff agree to  $\mathcal{O}(\epsilon)$  with the sharp cutoff result.

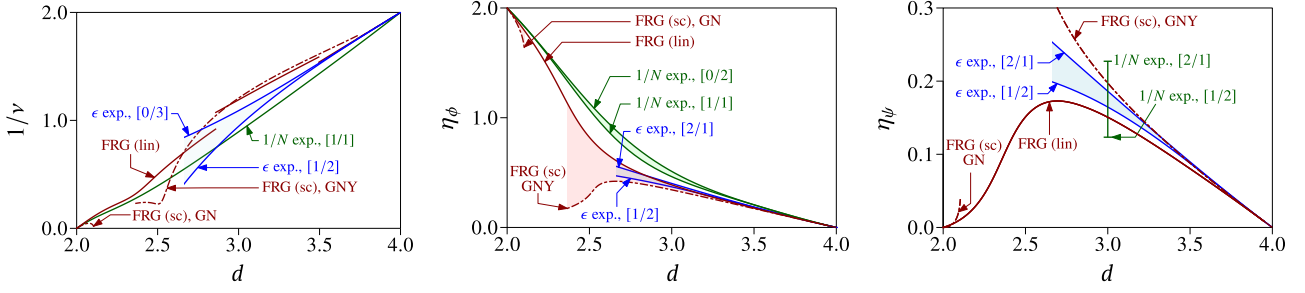


**Figure 7.6:** Critical exponents of the Gross-Neveu-SO(3) universality class as a function of space-time dimension  $d$  for  $N = 3$  flavors of two-component Dirac fermions from three-loop  $(4 - \epsilon)$  expansion, second-order  $1/N$  expansion (third-order for  $\eta_\psi$ ), and FRG in LPA16' using linear (lin) and sharp (sc) regulators.  $[m/n]$  correspond to different Padé approximants.

A fixed point of the FRG flow equations is given by  $\partial_t g^2 = 0$  and  $\partial_t u(\varrho) = 0$  for all  $\varrho > 0$ . Employing the polynomial expansion of the average potential yields  $(n + 2)/2$  coupled nonlinear equations for the  $(n + 2)/2$  couplings  $(g^2, \lambda_1, \dots, \lambda_{n/2})$  or  $(g^2, \varrho_0, \hat{\lambda}_2, \dots, \hat{\lambda}_{n/2})$  depending on regime. In an arbitrary fixed space-time dimensions  $2 < d < 4$ , these equations can be solved iteratively [140]. For our numerical results, we use the linear cutoff, which satisfies an optimization criterion [82], as well as a sharp cutoff [324] for comparison. In both cases, the threshold functions are known analytically, see, e.g., the appendix of Ref. [140] for an overview. In  $d = 3$ , we always find a unique fixed point that is characterized by a single relevant direction in the renormalization group sense. Upon increasing the dimension towards  $d \nearrow 4$ , this fixed point is adiabatically connected to the infrared stable fixed point of the one-loop flow in the  $(4 - \epsilon)$  expansion. We discuss the corresponding critical exponents in the following section, together with the results of the other two approaches.

## 7.6 Discussion

The quantum critical point is characterized by a set of universal exponents. In this work, we focus on the leading exponents  $\nu$  and  $\eta_\phi$ , as well as the fermion anomalous dimension  $\eta_\psi$ . Here, the exponent  $\nu$  determines the divergence of the correlation length  $\xi$  upon approaching the quantum critical point, while the boson and fermion anomalous dimensions  $\eta_\phi$  and  $\eta_\psi$  govern the scaling forms of the respective correlators. We emphasize that the fermionic correlator is not gauge invariant in the spin-orbital models and therefore  $\eta_\psi$  does not correspond to an observable quantity in this setting. However, as the Gross-Neveu-SO(3) universality may in principle also be realized in a model of interacting fermions, in which case  $\eta_\psi$  is measurable, we also

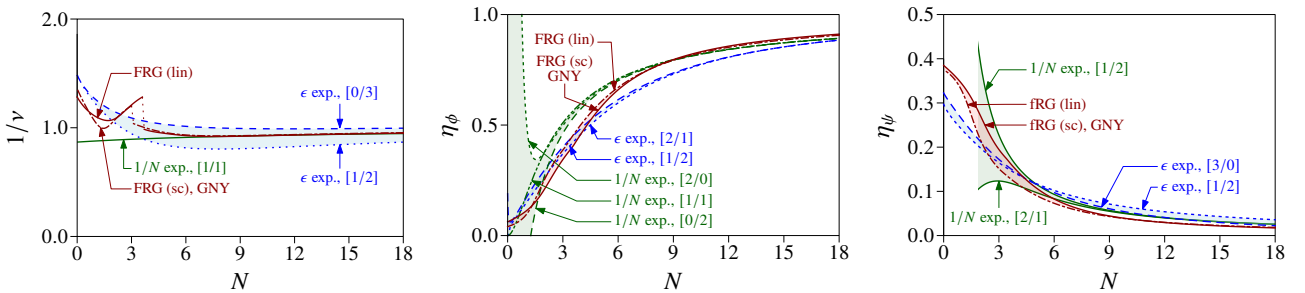


**Figure 7.7:** Same as Fig. 7.6, but as a function of two-component Dirac fermion flavors  $N$  in fixed space-time dimension  $d = 3$ .

**Table 7.1:** Critical exponents for the Gross-Neveu-SO(3) universality class for  $N = 3$  flavors of two-component fermions in  $d = 2 + 1$  space-time dimensions as relevant for the spin-orbital model on the honeycomb lattice [54] from three-loop  $(4 - \epsilon)$  expansion, second-order  $1/N$  expansion (third-order for  $\eta_\psi$ ), and functional renormalization group.  $[m/n]$  correspond to different Padé approximants. For the  $(4 - \epsilon)$ -expansion results ( $1/N$ -expansion results), we have refrained from showing approximants that exhibit a singularity in  $d \in (2, 4)$  [in  $N \in (0, \infty)$ ], marked with “sing.”; those that do not exist are marked “n.-e.”. A dash (—) signifies that the approximant either entails the computation of terms which go beyond the scope of this work, or (conversely) does not exhaust all the terms computed in the preceding sections. For the FRG results, we have employed the LPAN’ approximation with  $n \leq 16$  for the linear regulator and  $n \leq 28$  for the sharp regulator. The error bars correspond to the uncertainty in the extrapolation to  $n \rightarrow \infty$ .

$N = 3$			$1/\nu$	$\eta_\phi$	$\eta_\psi$	
$4 - \epsilon$ expansion	[2/1]	sing.	0.36989	0.18622		
	[1/2]	0.94472	0.40086	0.16458		
	[3/0]	0.97516	0.39181	0.17234		
	[0/3]	1.09000	n.-e.	n.-e.		
	$1/N$ expansion	[1/1]	0.89397	0.46276	—	
		[2/0]	sing.	0.49833	—	
		[0/2]	sing.	0.51074	n.-e.	
		[2/1]	—	—	0.22716	
		[1/2]	—	—	0.12337	
		[3/0]	—	—	0.22116	
[0/3]		—	—	n.-e.		
FRG	Taylor	linear	1.1901(10)	0.38781(6)	0.15068(8)	
		sharp	1.209(4)	0.3434(5)	0.1966(6)	
	pseudospectral	linear	1.18974	0.38781	0.15072	
		sharp	1.20465	0.34340	0.19649	

discuss this quantity here. Subleading quantities that control the corrections to scaling upon approaching the quantum critical point, such as  $\omega$ , can in principle also be computed within our approaches, but are left for future work.

Figure 7.6 shows our results for  $1/\nu$ ,  $\eta_\phi$ , and  $\eta_\psi$  as a function of space-time dimension  $2 < d < 4$  for  $N = 3$  flavors of two-component Dirac fermions, which is the case relevant for the spin-orbital models. For the results from the  $(4 - \epsilon)$  and large- $N$  expansions, we have employed different Padé approximants, marked as “[ $m/n$ ]” with integer  $m$  and  $n$  in the plots. The difference between the different approximants provides a simple estimate for the systematic error of the extrapolation to finite  $\epsilon$  and  $1/N$ , respectively. For the same purpose, in the FRG calculation, we have applied two different regularization schemes, marked as “lin” for the linear cutoff and “sh” for the sharp cutoff. We note that in the sharp-cutoff scheme, there is no stable fixed point for  $2.104 < d < 2.366$  as a consequence of fixed-point collisions at the lower and upper bound of this interval. In this cutoff scheme, the fixed point near  $d = 2 + \epsilon$  dimensions is therefore *not* adiabatically connected to the fixed point at  $d = 4 - \epsilon$  dimensions. We also note that in both cutoff schemes, the FRG fixed point for  $N = 3$  is located in the symmetric regime for  $d = 2 + \epsilon$  and  $d = 4 - \epsilon$ , but in the symmetry-broken regime for  $d = 3$ . This leads to discontinuities in  $1/\nu$  at those values of  $d$ , at which the minimum of the fixed-point potential becomes finite, see Fig. 7.6(a). Reassuringly, we observe that all curves approach each other near the upper critical space-time dimension  $d_{\text{up}} = 4$ , as it should be [140].

Figure 7.7 shows the critical exponents for the physical dimension  $d = 2 + 1$  as a function of the flavor number  $N$ . For  $N$  sufficiently large and increasing, the deviations between the different approaches decrease for increasing  $N$  and vanish in the limit  $N \rightarrow \infty$  as expected. Note that for large  $N$ , the fixed point in the FRG calculation is again located in the symmetric regime, in analogy to the behavior of the Gross-Neveu- $\mathbb{Z}_2$  model [320, 322]. The transition from symmetry-broken to symmetric regime upon increasing  $N$

$N = 6$		$1/\nu$	$\eta_\phi$	$\eta_\psi$
$4 - \epsilon$ expansion	[2/1]	0.96700	0.61484	0.12551
	[1/2]	0.81514	0.60023	0.10216
	[3/0]	0.86069	0.61414	0.09720
	[0/3]	1.01291	n.-e.	n.-e.
$1/N$ expansion	[1/1]	0.91136	0.70076	—
	[2/0]	1.28320	0.70572	—
	[0/2]	1.26614	0.71005	n.-e.
	[2/1]	—	—	0.09317
	[1/2]	—	—	0.08341
	[3/0]	—	—	0.09275
	[0/3]	—	—	n.-e.
	FRG Taylor	linear	0.9294(6)	0.66947(6)
	sharp	0.926(3)	0.6598(4)	0.08257(16)
pseudospectral	linear	0.92961	0.66948	0.073165
	sharp	0.93245	0.65980	0.082570

Table 7.2: Same as Table 7.1, but for  $N = 6$ .

is accompanied by a jump in  $1/\nu$ , similar to the transition as a function of  $d$  at fixed  $d$  discussed above.

The numerical estimates for the physical dimension  $d = 2 + 1$  are given in Table 7.1 for  $N = 3$  and in Tables 7.2–7.3 for larger values of  $N$ . Overall, we observe a fair agreement of the estimates from the three different approaches. In order to obtain final estimates for the three exponents from the combination of the three different approaches we first average over the values of the different Padé approximant and regularization schemes, respectively, within a given approach and then average over the mean values of the three approaches. The spread of the three mean values yield a rough estimate for the accuracy of our final result. This way, we obtain the critical exponents for the physically relevant case of  $N = 3$  flavors of two-component Dirac fermions in  $d = 2 + 1$  space-time dimensions as

$$N = 3 : \quad 1/\nu = 1.03(15), \quad \eta_\phi = 0.42(7), \quad \eta_\psi = 0.180(10). \quad (7.54)$$

Equation (7.54) represents the main result of this work. As there appears to be no dangerously irrelevant coupling in the theory, we expect hyperscaling to be satisfied. The critical exponents  $\alpha$ ,  $\beta$ ,  $\gamma$ , and  $\delta$  can then be obtained from  $\nu$  and  $\eta_\phi$  with the help of the usual hyperscaling relations [61]. For completeness, we also quote the estimates obtained for larger values of  $N$ , which may be relevant for models with microscopic fermionic degrees of freedom,

$$N = 6 : \quad 1/\nu = 1.00(13), \quad \eta_\phi = 0.66(5), \quad \eta_\psi = 0.091(15), \quad (7.55)$$

$$N = 12 : \quad 1/\nu = 0.93(4), \quad \eta_\phi = 0.83(4), \quad \eta_\psi = 0.039(9). \quad (7.56)$$

**Table 7.3:** Same as Table 7.1, but for  $N = 12$ . For the FRG results, we have omitted the error bars corresponding to the uncertainty in the extrapolation of the Taylor expansion of the effective potential, as they are smaller than  $2 \times 10^{-5}$ .

$N = 12$			$1/\nu$	$\eta_\phi$	$\eta_\psi$
$(4 - \epsilon)$ expansion	[2/1]		0.91427	0.80775	sing.
	[1/2]		0.82616	0.80659	0.05391
	[3/0]		0.84820	0.80614	0.04095
	[0/3]		0.99001	n.-e.	n.-e.
$1/N$ expansion	[1/1]		0.93326	0.84134	—
	[2/0]		1.00325	0.84199	—
	[0/2]		0.98522	0.84280	n.-e.
	[2/1]		—	—	0.04056
	[1/2]		—	—	0.03995
	[3/0]		—	—	0.04054
	[0/3]		—	—	n.-e.
FRG	Taylor	linear	0.93660	0.85180	0.02992
		sharp	0.93282	0.85700	0.02941
	pseudospectral	linear	0.93660	0.85180	0.02992
		sharp	0.93282	0.85700	0.02941

## 7.7 Summary and outlook

In this work, we have investigated the critical behavior of the  $(2 + 1)$ -dimensional Gross-Neveu-SO(3) universality class in terms of the universal critical exponents  $\nu$ ,  $\eta_\phi$ , and  $\eta_\psi$  by means of different sophisticated field-theoretical techniques. The fractionalized counterpart of the Gross-Neveu-SO(3) universality class, dubbed Gross-Neveu-SO(3)\*, may be realized in spin-orbital magnets with strong exchange frustration [54]. In contrast to the fractionalized bosonic universality classes [52], in the fractionalized fermionic universality classes, not only the correlation-length exponent  $\nu$ , but also the order-parameter anomalous dimension  $\eta_\phi$  agrees with the value of the corresponding conventional fermionic universality class. This allows us to obtain estimates for both Gross-Neveu-SO(3) and Gross-Neveu-SO(3)\* from the same calculation. We emphasize, however, that the fermionic correlator is not gauge invariant in the spin-orbital model. Our estimate for the fermion anomalous dimension  $\eta_\psi$  therefore applies only to the conventional Gross-Neveu-SO(3) universality class.

The Gross-Neveu-SO(3) theory is different from the previously studied Gross-Neveu-type models, as it features a symmetry-breaking transition between two semimetallic phases, with only a partial gap opening in the ordered phase. This leads to values for the critical exponents that strongly differ from those of the semimetal-to-insulator Gross-Neveu transitions [55, 113] as we discussed them in Chapter 3<sup>4</sup>. In particular, the order-parameter anomalous dimension  $\eta_\phi$  in the Gross-Neveu-SO(3) model is significantly smaller than  $\eta_\phi$  in any of the other Gross-Neveu-type models for the same number of fermion flavors. These difference may be readily observable in numerical simulations of suitable lattice models.

For the future, it would be interesting to study further properties of the Gross-Neveu-SO(3) universality class. In particular, the finite-size spectrum on the torus, which was recently investigated in the conventional Gross-Neveu universality class [180], might be worthwhile to be examined, both in the

4: Unfortunately, the resummation by interpolation to a  $(2 + \epsilon)$  expansion is much more difficult in this model. In fact, we are lacking the epsilon expansions because the corresponding Gross-Neveu model is not closed under RG. A careful analysis would be needed to take all terms in to account which are generated under RG transformations.

conventional Gross-Neveu-SO(3) and the fractionalized Gross-Neveu-SO(3)\* case.





In this thesis, we investigated the critical behavior of Dirac systems at three space-time dimensions from the perturbative renormalization group perspective. The originally for high energy theories (in the realm of the Standard Model) developed tools and techniques to compute higher loop renormalization group functions are used to push the quantitative insight on fermionic universality classes which so far are lacking the astonishing agreement across complementary methods as present in their bosonic siblings.

Starting with the chiral Ising Gross-Neveu-Yukawa model which can be derived as the semi-phenomenological theory for phase transitions in the most prominent Dirac material graphene, we extensively studied the  $(4 - \epsilon)$  expansions to the state of the art fourth loop order. Applying sophisticated resummation schemes as well as taking advantage of the  $(2 + \epsilon)$  expansion in the Gross-Neveu model in Chapter 3, we provided concise estimates of the critical exponents of the chiral Ising Gross-Neveu universality class at  $d = 3$ . Especially, the elaborated interpolations between these two models in the same universality class has proven to maintain the asymptotic divergent behavior of both epsilon expansions. We contributed to the substantial progress on the precision of critical exponents across all methods ranging from non-perturbative RG, (quantum) Monte-Carlo simulations to the conformal bootstrap and the numbers are closing in on to each other, such that the striking agreement seen in the  $O(N)$ -universality seems to be in reach.

With these insights and experiences at hand, we turned to quantum field theories for deconfined quantum critical points. The latter explain the continuous phase transitions between two ordered phases of completely different symmetry by fractionalized spinons which are liberated exclusively at the critical point and drive the transition [40]. For perturbatively RG analysis, we generalized the theory to the Abelian Higgs model which exhibits a critical point only above  $n_c \sim 183$  complex scalars in one-loop order. To improve this number towards  $d = 3$  dimensions, we refined the RG analysis of the critical behavior in Chapter 5 by means of a four loop expansion. The resummed predictions for  $n_c \approx 12 \pm 4$  narrow the previous calculations by multiple orders of magnitude. Nevertheless, it remains to further discussion whether the critical behavior captured by the NCCP<sup>1</sup> model describes a continuous phase transition. Concerning this matter, our findings revealed walking of the RG flow in the vicinity of the fixed point collision which possibly explains the pseudocritical behavior of the NCCP<sup>1</sup> model as found in some numerical simulations [218]. Although a quantitative evaluation of the concomitant Miransky scaling is out of range for the presented perturbative renormalization group analysis, our results motivate future projects using non-perturbative methods as the FRG or possible checks within the numerical simulations.

Partly inspired by the surprising emergent  $SO(5)$  symmetry in the numerical simulations of the deconfined quantum phase transition, an entire web of novel dualities was conjectured [50, 51]. One of the contributing field theories, in a subset of this web connecting deconfined quantum critical points, was

found to exhibit gapless gauged Dirac fermions described by the QED<sub>3</sub>-Gross-Neveu model [50, 279]. In order to check the duality conjectured scaling relations for  $d = 3$ , we performed a three loop perturbative renormalization group analysis in Chapter 6. While for some exponents our predictions are consistent with the duality, especially the anomalous dimension is significantly above unity and therefore out of range of the conjectured dual Néel-VBS transition [50]. The further analysis by a four loop RG, as well as the consideration of Aslamazov-Larkin diagrams at three dimensions, couldn't resolve this issue undoubtedly [303]. Nevertheless, it supports our assessment that the answer may be beyond a perturbative approach. Once again, non-perturbative methods could explore if this proves a violation of the duality or serves as another possible hint for actually pseudo-critical behavior.

In the last part of this thesis, we scrutinized the critical behavior of a recently found fermionic fractionalized critical point [54]. While for bosonic theories already known, the fractionalization of degrees of freedom may shift the transition to a novel universality class. In this project, we perform a comprehensive study of the Gross-Neveu-SO(3) model by means of a three loop perturbative RG, a large- $N$  expansion and a functional RG analysis. The results provide a concise window of confidence on the critical exponents which may be the reference for future comparative Monte-Carlo simulations.

# APPENDIX



# One-loop RG on Gross-Neveu-Yukawa models

# A

In Chapter 2, we discussed the perturbative one-loop renormalization of the Ising model Eq. (2.15) and presented the RG procedure by means of Feynman diagrams and their divergent parts in the dimensional regularization and the subsequent minimal subtraction scheme ( $\overline{\text{MS}}$ ).

A reoccurring Lagrangian, throughout this thesis, is the ungauged Gross-Neveu-Yukawa model. We have seen it emerges as the critical theory for the transition of graphene from a semi-metallic insulator phase to charge density wave ordering or a spin density wave ordering. Additionally, in our last project we extensively discussed another implementation as critical theory for a fractionalized spin-orbital liquid transition. All these models have a relatively simple<sup>1</sup> structure in common, but are distinguished by the spontaneously-broken symmetries. These symmetries are encoded in the generators of the Lie algebra which occur in only one term of the Lagrangian, the Yukawa interaction. By performing the one-loop perturbative renormalization group analysis for a generic Lie algebra, we have the opportunity to unify all these models to limits of generic beta functions.

<b>A.1 Gross-Neveu-Yukawa models</b>	<b>119</b>
<b>A.2 Feynman rules &amp; one loop diagrams</b>	<b>120</b>
<b>A.3 Group theory for Feynman diagrams</b>	<b>121</b>
<b>A.4 Renormalization group procedure</b>	<b>123</b>
<b>A.5 One-loop Calculations</b>	<b>125</b>

1: By “simple”, we mean in comparison to gauged theories with a non-abelian vertex structure like the Lagrangian of QCD.

## A.1 Gross-Neveu-Yukawa models

We start by formulating the Lagrangian of the most general ungauged version of the Gross-Neveu-Yukawa model in  $d = 4 - \epsilon$  dimensions

$$\mathcal{L}_{\text{GNV}} = \bar{\psi}_i (\not{\partial} + g \phi_a T_{ij}^a) \psi_j + \frac{1}{2} \phi_a (m^2 - \partial_\mu^2) \phi_a + \frac{\lambda}{4!} (\phi_a \phi_a)^2. \quad (\text{A.1})$$

In this formulation the fermionic field has  $\psi = (\psi_1, \dots, \psi_N)^T$  components and the bosonic field obtains  $a = 1, \dots, N_A$  components. Besides the global  $U(1)$  symmetry, the discrete chiral symmetry of this model is encoded in the matrices  $T^a$ . These are the the generators of the underlying Lie algebra and couple bosons and fermions by the Yukawa interaction term with coupling  $\sqrt{y}$ . In order to stabilize the RG in four dimensions, we added the usual quartic interaction term with coupling  $\lambda$ . Finally, this model enjoys a full Lorentz symmetry, i.e. the dynamical critical exponent is set to  $z = 1$ .

The renormalizability of this model is easily checked by analyzing the canonical power counting of the mass dimensions of fields and couplings. For a  $d$  dimensional theory like this, they read

$$[\psi] = \frac{d-1}{2}, \quad [\phi] = \frac{d-2}{2}, \quad [\sqrt{y}] = \frac{4-d}{2}, \quad [\lambda] = 4-d. \quad (\text{A.2})$$

Similar to the discussion in Chapter 2 for the Ising model, this ensures that for  $d = 4 - \epsilon$  the couplings of the GNV model scale like

$$[\sqrt{y}] = \epsilon/2 \quad \text{and} \quad [\lambda] = \epsilon. \quad (\text{A.3})$$

At the upper critical dimension, the couplings become marginal and the mean field results apply. However, below four dimension ( $\epsilon > 0$ ), the

Gaussian fixed point becomes unstable and infrared repulsive. In this case, we now ask for other (infrared attractive) fixed points which break the consider symmetry like the ones we dicussed in Chapter 3 and 7.

### A.2 Feynman rules & one loop diagrams

The very first step in any modern (Wilsonian) perturbative renormalization group analysis is deducing the momentum-space Feynman rules from the Lagrangian. How this is done in detail is explained in almost every textbook on quantum field theory<sup>2</sup> and we rush directly to the diagrammatic Feynman rules, also known as tree-level diagrams, which read

2: Once again we refer to the monumental opus by Jean Zinn-Justin [69]. A book which demands more than a life time to be written and yet it's not the only one by Zinn-Justin.

$$\begin{aligned}
 i \xrightarrow{p} j &= \frac{i\delta_{ij}}{\not{p}}, & \begin{array}{c} a \text{---} c \\ \times \\ b \text{---} d \end{array} &= -\lambda(\delta^{ab}\delta^{cd} + \delta^{ac}\delta^{bd} + \delta^{ad}\delta^{bc}), \\
 \begin{array}{c} i \\ \searrow \\ \bullet \\ \nearrow \\ j \end{array} \text{---} a &= \sqrt{y} T_{ij}^a, & a \text{---} \xrightarrow{p} \text{---} b &= \frac{\delta^{ab}}{p^2 + m^2}.
 \end{aligned}
 \tag{A.4}$$

Here, the arrowed line denotes the fermion propagator and the dashed line the boson propagator. The three terms of the quartic interaction stem from the three possible ways to contract the loose ends. At one-loop level, applying these rules we have to compute 13 diagrams as shown in Fig. A.1 from which especially the nasty appearing quartic ones will all contribute equally and it is sufficient to compute only one of them. Each diagram entails one unfixed  $d$ -dimensional *loop momentum*  $k$  which we have to integrate over. This sets the maybe most difficult part of the one-loop RG analysis and we are asked to actually calculate the momentum-loop integrals. Fortunately, many physicists before were challenged by this task and developed several tricks to compute them analytically (see again Ref. [69]). We will perform this calculation in the next section, but first focus on a rather unfamiliar modification. Besides the momentum part, the crucial contributions here are the generators of the Lie algebra  $T_{ij}^a$  in the Yukawa tree-level diagram. In fact, based on the ideas by Pedrag Cvitanovic [327, 328] on so-called birdtrack diagrams, we can separate the momentum part of the diagrams from the *group theoretical part*. Technically, this prescribes a set of additional *color rules* which entail their own ‘‘Feynman rules’’ but for group theoretical part only.

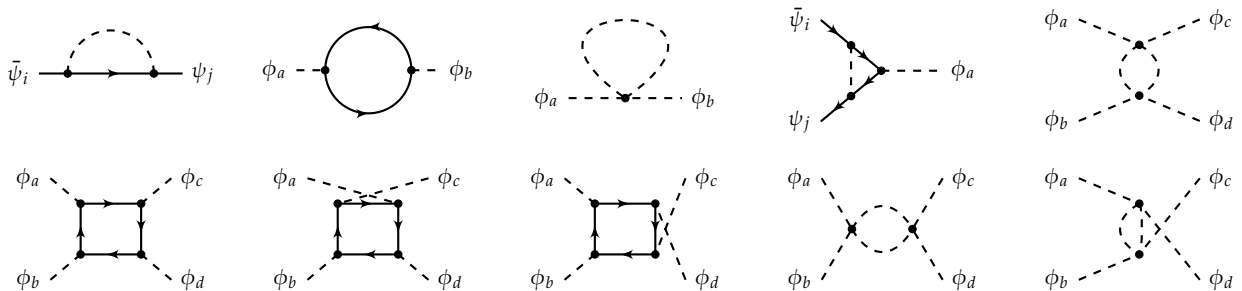


**Figure A.1:** All one-loop diagrams of the ungauged Gross-Neveu-Yukawa model. In total there are 13 diagrams (we omitted three diagrams of the  $\phi^4$ -vertex which just have an anti-clockwise running fermion).

If, for instance, we consider the one-loop diagram of the fermion propagator<sup>3</sup> and explicitly use the Feynman rules in (A.4), we will find that the group theoretical part can be separated in the following way

$$Q, i \text{---} \overset{k}{\curvearrowright} \text{---} Q, j = Q, i \text{---} \overset{k}{\curvearrowright} \text{---} Q, j \times i \text{---} \text{---} j$$

(A.5)

Here,  $Q$  denotes the external momentum and  $k$  again the loop momentum to integrate over. In fact, we are left with a product of the diagram built by the pure momentum-space rules including also the Dirac algebra of the  $\gamma$ -matrices and the *color weight* built by using the color rules. This principle is essential for the computer algebra and offers a generic way to deal with color weights generated by any simple Lie algebra. Since a reduction to invariants is, in general, only possible if all color indices are contracted, we have to apply according projectors as explained next.

### A.3 Group theory for Feynman diagrams

In the general formulation of the Gross-Neveu-Yukawa model Eq. (A.1), we introduced the matrices  $T^a$  in the Yukawa interaction connecting fermionic and bosonic fields. These matrices are the generators of a finite dimensional simple Lie algebra [329]. They satisfy the following commutator relation

$$[T^a, T^b] = T^a T^b - T^b T^a = i f^{abc} T^c, \quad (\text{A.6})$$

where  $f^{abc}$  are called the structure constants. In the following, the generators are conventionally used to be hermitean and the Killing form is chosen to be proportional to  $\delta^{ab}$ , i.e.

$$\text{Tr}[T^a T^b] \propto \delta^{ab}. \quad (\text{A.7})$$

Under these conventions, the structure constants are real and totally anti-symmetric. We further introduce labels where “ $R$ ” denotes a generic representation with dimension  $N_R$  and “ $A$ ” the adjoint representation with dimension  $N_A$ . The generators of the adjoint representation are build from the structure constants by

$$(T_A)_bc^a = -i f^{abc}. \quad (\text{A.8})$$

Since in the calculation of the *color amplitudes* of our Feynman diagrams, traces over products of matrices  $T^a$  play a major role, we can express the entire group theoretical weight by only their invariant tensors. These tensors define Casimir operators from which, in this context, first of all the *quadratic Casimir operator*  $C_R$  is of special interest

$$(T_R^a T_R^a)_{ij} = C_R \delta_{ij}. \quad (\text{A.9})$$

Accordingly, for the adjoint representation using (A.8) follows that

$$f^{acd} f^{bcd} = C_A \delta^{ab}. \quad (\text{A.10})$$

<sup>3</sup>: Because of its appearance, this diagrams is also called “sunrise” diagram. There are also a bunch of other explicitly named diagrams including the “penguin diagram”.

In the Killing form, for a trace over two generators in the representation  $R$ , we can additionally define the coefficient  $I_2(R)$  as

$$\text{Tr} [T_R^a T_R^b] = I_2(R) \delta^{ab}. \tag{A.11}$$

This is related to the quadratic Casimir operator via the dimensions of the representations as

$$I_2(R) = \frac{N_R}{N_A} C_R. \tag{A.12}$$

At the moment, it may seem over-engineered to worry this much about the group theoretical weight and how to express it by their invariants. But it enables us to compute the beta functions for a generic symmetry group and only subsequently fix it by setting the invariants to simple numbers of the wanted version of our model.

Additionally, it provides us with a very perceptive formalized procedure to compute the arising color amplitudes (a.k.a. group theoretical weights) by means of the above mentioned color rules. For the Gross-Neveu-Yukawa model as defined in (A.1), we assign the representation  $R$  to the fermion fields and the adjoint representation  $A$  to the boson fields. Note that we intentionally already chose the bosonic field to have  $N_A$  components. In accordance with the full momentum-space Feynman rules above, the corresponding diagrammatic *color rules* read

$$\begin{aligned}
 i \longrightarrow j &= \delta_{ij}, & a \text{---} b &= \delta^{ab}, & \begin{array}{c} i \\ \searrow \\ \bullet \\ \nearrow \\ j \end{array} \text{---} a &= T_{ij}^a, \\
 \begin{array}{c} a \quad c \\ \diagdown \quad \diagup \\ \bullet \\ \diagup \quad \diagdown \\ b \quad d \end{array} &= \begin{array}{c} a \\ | \\ b \end{array} \begin{array}{c} c \\ | \\ d \end{array} + \begin{array}{c} c \quad a \\ | \quad | \\ d \quad b \end{array} + \begin{array}{c} a \quad c \\ \diagup \quad \diagdown \\ \bullet \\ \diagdown \quad \diagup \\ b \quad d \end{array} \\
 &= \delta^{ab} \delta^{cd} + \delta^{ac} \delta^{bd} + \delta^{ad} \delta^{bc}.
 \end{aligned} \tag{A.13}$$

Again, the three terms of the quartic vertex account for the three possible ways to contract the indices. As a first simple application of these rules, we can depict the dimensions of both representations as well as the quadratic Casimir operator and the  $I_2(R)$  invariant by the following diagrammatic calculations

$$\begin{array}{c} \circlearrowleft \\ \circlearrowright \end{array} = \delta_{ii} = N_R, \quad \begin{array}{c} \circlearrowleft \\ \circlearrowright \end{array} = \delta^{aa} = N_A, \tag{A.14}$$

$$i \text{---} \begin{array}{c} \circlearrowleft \\ \circlearrowright \end{array} \text{---} j = T_{il}^a T_{lj}^a = C_R \delta_{ij}, \tag{A.15}$$

$$a \text{---} \begin{array}{c} \circlearrowleft \\ \circlearrowright \end{array} \text{---} b = T_{ij}^a T_{ji}^b = \text{Tr} [T_R^a T_R^b] = I_2(R) \delta^{ab}. \tag{A.16}$$

Note that connecting loose ends for the color diagrams means that we contract the respecting indices. The presented application of the ideas by Cvitanovic give only a glimpse of the powerful language he developed in Ref. [327, 328].



## A.4 Renormalization group procedure

We begin our renormalization group procedure on the same track as in Section 2.3.2. At first, we write down the *bare* Lagrangian upon replacing the fields and couplings by their bare counterparts  $\{\psi_0, \phi_0, g_0, \lambda_0, m_0\}$ , i.e.

$$\mathcal{L}_{\text{bare}} = \bar{\psi}_0 \not{\partial} \psi_0 + \frac{1}{2} \phi_0 (m_0^2 - \partial_\mu^2) \phi_0 + g_0 \phi_{0,a} \bar{\psi}_0 T^a \psi_0 + \frac{\lambda_0^4}{4!} \phi_0^4, \quad (\text{A.17})$$

where we omitted most of the indices in Eq. (A.1) for a better readability. Note that the bare quantities independent of any cutoff or energy scale  $\mu$ . Although these are of no use for measurable correlation functions, they are related to the renormalized physical quantities by the renormalization constants  $Z_x$

$$\psi_0 = Z_\psi^{1/2} \psi, \quad \phi_0 = Z_\phi^{1/2} \phi, \quad g_0 = Z_g g, \quad \lambda_0 = Z_\lambda \lambda, \quad m_0^2 = Z_m m^2. \quad (\text{A.18})$$

The renormalized quantities are now scale dependent on the energy scale  $\mu$ . For a renormalizable field theory, any divergence or infinity occurring in correlation functions of the renormalized fields  $\bar{\psi}, \psi$  and  $\phi$  is absorbed by the renormalization constants. The renormalized Lagrangian then reads

$$\begin{aligned} \mathcal{L}_{\text{ren}} = Z_\psi \bar{\psi} \not{\partial} \psi + \frac{1}{2} \phi (Z_m Z_\phi m^2 - Z_\phi \partial_\mu^2) \phi + Z_g Z_\phi^{1/2} Z_\psi g \phi_a \bar{\psi} T^a \psi \\ + Z_\lambda Z_\phi^2 \frac{\lambda}{4!} \phi^4. \end{aligned} \quad (\text{A.19})$$

For a better overview and the calculation of the critical exponents and anomalous dimensions, it is worth to summarize the products of renormalization constants in the following definitions

$$Z_{\phi^2} \equiv Z_m Z_\phi, \quad Z_{\phi \bar{\psi} \psi} \equiv Z_g Z_\phi^{1/2} Z_\psi, \quad Z_{\phi^4} \equiv Z_\lambda Z_\phi^2. \quad (\text{A.20})$$

Since for the epsilon expansion, the appearing infinities are regularized within a dimensional regularization (DREG) around  $d = 4 - \epsilon$  dimensions, we have to rescale all quantities regarding their mass dimension in (A.2). The new renormalization mass scale  $\mu$  is attached to render them massless

$$\sqrt{y} \rightarrow \sqrt{y} \mu^{\epsilon/2}, \quad \lambda \rightarrow \lambda \mu^\epsilon, \quad m^2 \rightarrow m^2 \mu^{-2}. \quad (\text{A.21})$$

### A.4.1 Renormalization constants

In the minimal subtraction scheme  $\overline{\text{MS}}$ , the renormalization constants are determined by computing the one-particle-irreducible (1PI) corrections to the propagators and vertices. For this purpose, we demands them to absorb only the divergent part of the Feynman diagrams loop-by-loop. By replacing  $Z_x = 1 + \delta Z_x$  in the renormalized Lagrangian (A.19), we split the Lagrangian in two parts

$$\begin{aligned} \mathcal{L}_{\text{ren}} = (1 + \delta Z_\psi) \bar{\psi} \not{\partial} \psi + \frac{1}{2} \phi ((1 + \delta Z_{\phi^2}) m^2 + (1 + \delta Z_\phi) \partial_\mu^2) \phi \\ + (1 + \delta Z_{\phi \bar{\psi} \psi}) g \phi_a \bar{\psi} T^a \psi + (1 + \delta Z_{\phi^4}) \frac{\lambda}{4!} \phi^4. \end{aligned} \quad (\text{A.22})$$

As before, in Section 2.3.2, the first part provides the physics of the renormalized fields, while the second one generates the counterterms which has to absorb the emerging divergent diagrams

$$\begin{aligned}\mathcal{L}_{\text{ren}} = \mathcal{L} + \mathcal{L}_{\text{ct}} = & \bar{\psi} \not{\partial} \psi + \frac{1}{2} \phi (m^2 - \partial_{\mu}^2) \phi + g \phi_a \bar{\psi} T^a \psi + \frac{\lambda^4}{4!} \phi^4 \\ & + \delta Z_{\psi} \bar{\psi} \not{\partial} \psi + \frac{1}{2} \phi (\delta Z_{\phi^2} m^2 - \delta Z_{\phi} \partial_{\mu}^2) \phi \\ & + \delta Z_{\phi \bar{\psi} \psi} g \phi_a \bar{\psi} T^a \psi + \delta Z_{\phi^4} \frac{\lambda^4}{4!} \phi^4.\end{aligned}\quad (\text{A.23})$$

Therefore, the counterterm Lagrangian  $\mathcal{L}_{\text{ct}}$  gives rise to additional counterterm Feynman rules reading. As a result, we are left with in total eight Feynman rules. While  $\epsilon \ll 1$  is assumed to be small enough for the dimension regularization, the couplings scale with  $\mathcal{O}(\epsilon\lambda)$  even smaller such that for  $\delta Z_i$  we can write  $(1 + \delta Z_i)^s \approx 1 + s\delta Z_i$ . We obtain the following relations between the renormalization constants

$$\delta Z_{\phi^2} = \delta Z_m + \delta Z_{\phi}, \quad (\text{A.24})$$

$$\delta Z_{\phi \bar{\psi} \psi} = \delta Z_g + \frac{1}{2} \delta Z_{\phi} + \delta Z_{\psi}, \quad (\text{A.25})$$

$$\delta Z_{\phi^4} = \delta Z_{\lambda} + 2\delta Z_{\phi}. \quad (\text{A.26})$$

Then, the divergent parts of the according correlation functions define the renormalization constants by the following equations

$$i\not{p}(\delta Z_{\psi} + \langle \bar{\psi} \psi \rangle_{\text{div.}}) = \text{finite}, \quad (\text{A.27})$$

$$p^2 \cdot \delta Z_{\phi} + m^2 \cdot \delta Z_{\phi^2} + \langle \phi \phi \rangle_{\text{div.}} = \text{finite}, \quad (\text{A.28})$$

$$g \cdot \delta Z_{\phi \bar{\psi} \psi} + \langle \phi \bar{\psi} \psi \rangle_{\text{div.}} = \text{finite}, \quad (\text{A.29})$$

$$\lambda \cdot \delta Z_{\phi^4} + \langle \phi \phi \phi \phi \rangle_{\text{div.}} = \text{finite}. \quad (\text{A.30})$$

In particular, the renormalization constants collect all divergent contributions of of the loop momentum integrals after the dimensional regularization.

## A.4.2 Group theoretical weights

Each 1PI Feynman diagrams, we drew so far, comes with loose ends which means there are also non-contracted group indices left. Their handling can become quite challenging for a computer algebra. In order to obtain the group theoretic weight which contributes to a certain vertex or propagator, we therefore use proper projectors  $P_x$  in color space. These are multiplied to the respecting diagram and contract all free indices, such that we are left with a scalar which is proportional to the tensor structure of the corresponding vertex or propagator in the color rules above. For the correct results, we finally have to normalize the projector by a group theoretical factor by demanding the correct result on tree-level. Explicitly, we make the following ansatz

$$(P_{\bar{\psi} \psi})_{ij} = C_{\bar{\psi} \psi} \delta_{ij}, \quad (\text{A.31})$$

$$(P_{\phi \phi})^{ab} = C_{\phi \phi} \delta^{ab}, \quad (\text{A.32})$$

$$(P_{\phi \bar{\psi} \psi})_{ij}^a = C_{\phi \bar{\psi} \psi} T_{ij}^a, \quad (\text{A.33})$$

$$(P_{\phi^4})^{abcd} = C_{1,\phi^4} \delta^{ab} \delta^{cd} + C_{2,\phi^4} \delta^{ac} \delta^{bd} + C_{3,\phi^4} \delta^{ad} \delta^{bc}. \quad (\text{A.34})$$

The normalization constants  $C_x$  are determined by multiplying these projectors with the corresponding propagator or vertex Feynmanrule and demanding the resulting contracted diagrams to be unity

$$\delta_{ij} \cdot (P_{\bar{\psi}\psi})_{ji} = C_{\bar{\psi}\psi} \delta_{ii} = C_{\bar{\psi}\psi} N_R \stackrel{!}{=} 1 \quad (\text{A.35})$$

$$\delta^{ab} \cdot (P_{\phi\phi})^{ba} = C_{\phi\phi} \delta^{aa} = C_{\phi\phi} N_A \stackrel{!}{=} 1 \quad (\text{A.36})$$

$$T_{ij}^a \cdot (P_{\phi\bar{\psi}\psi})_{ji}^a = C_{\phi\bar{\psi}\psi} T_{ij}^a T_{ji}^a = C_{\phi\bar{\psi}\psi} C_R \delta_{ii} = C_{\phi\bar{\psi}\psi} C_R N_R \stackrel{!}{=} 1 \quad (\text{A.37})$$

$$(\delta^{ab} \delta^{cd} + \delta^{ac} \delta^{bd} + \delta^{ad} \delta^{bc}) \cdot (P_{\phi^4})^{abcd} = (N_A^2 + 2N_A)(C_{1,\phi^4} + C_{2,\phi^4} + C_{3,\phi^4}) \stackrel{!}{=} 1. \quad (\text{A.38})$$

Note that for the last projector of the quartic coupling, we are free to choose one of the constants and neglect the other two.

## A.5 One-loop Calculations

At one-loop level, the number of diagrams is still manageable and its worth to do the calculation by hand in order to get a notion of the procedure necessary also in higher loop orders. We will now go through the evaluation of the single diagram contributing to the fermion propagator will be presented in full detail. For the calculation of all other diagrams we can essentially follow the same steps and leave this task to the reader<sup>4</sup>. However, we present how the nontrivial group theoretical weights are calculated in detail.

*Fermion Propagator.* For the fermion propagator, there is only one diagram which contributes on one-loop level. By applying the Feynman rules derived in Section A.2, we obtain the following integral

$$\begin{aligned} Q, i \text{ --- } \overset{k}{\text{---}} \text{---} Q, j &\equiv I_\psi = \int \frac{d^D k}{(2\pi)^D} \left[ T_{im}^a \frac{\delta_{ab}}{k^2 + m^2} T_{lj}^b \frac{i\delta_{lm}}{k + Q} \right] \\ &= i(T^a T^a)_{ij} \int \frac{d^D k}{(2\pi)^D} \frac{1}{(k - Q)^2 + m^2} \frac{\not{k}}{k^2}, \quad (\text{A.39}) \end{aligned}$$

where in the second line the integral was shifted by  $k \rightarrow k - Q$ . Note that, as explained above, the group theoretical weight naturally appears as a factor in front of the momentum integral. We use the Feynman parameter technique to introduce another integral

$$I_\psi = iC_R \delta_{ij} \int \frac{d^d k}{(2\pi)^d} \int_0^1 dx \frac{\not{k}}{[x((Q - k)^2 + m^2) + (1 - x)k^2]^2}. \quad (\text{A.40})$$

By another shift from  $k - xQ \rightarrow k$  and integrating over  $k$ , we obtain

$$I_\psi = iQ C_R \delta_{ij} \frac{\Gamma(2 - d/2)}{(4\pi)^{d/2}} \int_0^1 dx x^{d/2-1} [m^2 + (1 - x)Q^2]^{d/2-2}. \quad (\text{A.41})$$

Expanding this to the first order in  $\epsilon = 4 - d$  and evaluating the integral over  $x$ , the wanted  $1/\epsilon$  pole is given as

$$I_\psi = \frac{iQ}{2} m^{-\epsilon} \frac{N_d}{\epsilon} C_R \delta_{ij} + \text{finite}. \quad (\text{A.42})$$

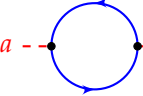
4: A small hint for lazy minds like the author's: take a look at Ref. [69].

The factor  $N_d = (4\pi)^{-d/2}/\Gamma(d/2)$  appears in all orders to the power of the respecting loop level (as here at one loop level) and can be absorbed by a suitable re-scaling of the couplings

$$N_d y \rightarrow y \quad \text{and} \quad N_d \lambda \rightarrow \lambda. \quad (\text{A.43})$$

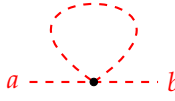
This re-scaling also applies to the following calculations as well as in the computer algebra.

*Boson Propagator.* The Boson propagator has two one-loop diagrams: The fermion-loop diagram and the massive tadpole diagram. For the former the group theoretical weight was already given in (A.16) as



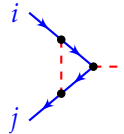
$$\cdot (P_{\phi\phi})^{ba} = \frac{1}{N_A} T_{ij}^a T_{ji}^a = I_2(R). \quad (\text{A.44})$$

The group theoretical weight of the massive tadpole is calculated by applying the projector (A.32) to



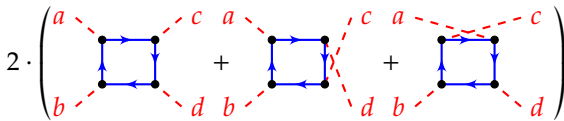
$$\begin{aligned} \cdot (P_{\phi\phi})^{ab} &= (\delta^{ab} \delta^{cc} + \delta^{ac} \delta^{bc} + \delta^{ac} \delta^{cb}) C_{\phi\phi} \delta^{ab} \\ &= (N_A + 2) \delta^{ab} \frac{1}{N_A} \delta^{ab} = N_A + 2. \end{aligned} \quad (\text{A.45})$$

*Yukawa Vertex.* For the calculation of the group theoretical weight of the Yukawa vertex, we have to carefully apply all relations given in Section A.3. The final result of the occurring trace is



$$\cdot (P_{\phi\bar{\psi}\psi})_{ji}^a = C_{\phi\bar{\psi}\psi} \text{Tr} [T_R^b T_R^a T_R^b T_R^a] = C_R + \frac{1}{2} C_A. \quad (\text{A.46})$$

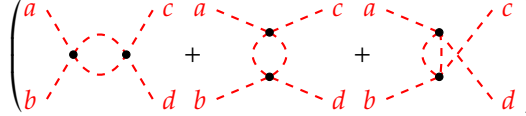
$\phi^4$  Vertex. The computation of the quartic boson vertex follows straightforwardly again by applying the corresponding projector. In fact, there are two types of diagrams. In the first only the Yukawa coupling appears



$$\begin{aligned} 2 \cdot \left( \text{Diagram 1} + \text{Diagram 2} + \text{Diagram 3} \right) \cdot (P_{\phi^4})^{abcd} \\ = \frac{4C_A - 24C_R}{N_A^2 + 2N_A} I_2(R) N_A. \end{aligned} \quad (\text{A.47})$$

Here, the factor two in front accounts for the possible inverse arrow direction in each of the diagrams which has no effect on the color weights. The second

type is constructed by using only the quartic coupling itself

$$\left( \begin{array}{c} \text{diagram 1} \\ + \\ \text{diagram 2} \\ + \\ \text{diagram 3} \end{array} \right) \cdot (P_{\phi^4})^{abcd} = \frac{16N_A + 10N_A^2 + N_A^3}{N_A^2 + 2N_A}. \quad (\text{A.48})$$


Collecting all results, the beta functions can be deduced for an arbitrary simple Lie algebra in the representation matrices  $T^a$  in the GNY model.

### A.5.1 One-loop RG functions

We now have all results at hand to finally compute the renormalization constants and subsequently all renormalization group functions including, most importantly, the beta functions. Remember, the beta functions are computed directly from the renormalization constants by

$$\beta_y^{(1\ell)} = \frac{-\epsilon y}{1 + \alpha \frac{\partial \ln Z_y^{(1\ell)}}{\partial y}} \quad \text{and} \quad \beta_\lambda^{(1\ell)} = \frac{-\epsilon \lambda}{1 + \lambda \frac{\partial \ln Z_\lambda^{(1\ell)}}{\partial \lambda}}, \quad (\text{A.49})$$

where  $Z^{(i\ell)}$  denotes all  $i$ -loop contributions. Therefore, by collecting all the results from the diagrams above, we obtain for the beta functions at one-loop level

$$\beta_y^{(1\ell)} = -\epsilon y + \left( 3C_R + \frac{I_2(R)}{2} - C_A \right) y^2, \quad (\text{A.50})$$

$$\beta_\lambda^{(1\ell)} = -\epsilon \lambda + \frac{(C_A - 6C_R)I_2(R)}{N_A + 2} y^2 + I_2(R)y\lambda + \frac{N_A + 8}{2} \lambda^2, \quad (\text{A.51})$$

and for the other renormalization group functions

$$\gamma_\psi = \frac{d \ln Z_\psi}{d \ln \mu} = \frac{1}{2} C_R y, \quad (\text{A.52})$$

$$\gamma_\phi = \frac{d \ln Z_\phi}{d \ln \mu} = \frac{1}{2} I_2(R) y, \quad (\text{A.53})$$

$$\gamma_{\phi^2} = \frac{d \ln Z_{\phi^2}}{d \ln \mu} = - \left( 1 + \frac{N_A}{2} \right) \lambda. \quad (\text{A.54})$$

By setting the invariants to a certain group and upon a convenient re-scaling of the couplings, we are able to recover the functions for chiral Ising GNY model in Chapter 3 and the Gross-Neveu-SO(3) model in Chapter 7. Beware that for both models the invariants have to involve the number of components of the fermionic field. For many groups, one can find the invariants in the literature [327, 330].



Throughout this thesis, we calculated the perturbative renormalization group functions in higher-loop order multiple times. In the previous Chapter, we also presented that already at one-loop level this can be a tedious but nevertheless straightforward task. All these calculations have in common that they are performed using dimensional regularization (DREG) within the modified minimal subtraction scheme ( $\overline{\text{MS}}$ ) – a method with several advantages for further formalization as we will explore in the first part of this Chapter.

Since the amount of diagrams to compute grows at least factorially with the loop level we rely on computer-aided algebra. In fact, we employ a whole chain of computer algebra tools. These tools emerged from decades long development in the realm of high energy physics and especially the Standard Model. Unfortunately, due to the long development and the large number of software used, some gaps have appeared in the documentation. In the second part of this chapter, we will try to give a tour on the map of these tools and how they are applied on the projects of this thesis.

## B.1 Fundamentals of Feynman diagram computation

In the dimensional regularization within the modified minimal subtraction scheme, the divergent parts relevant to the renormalization occur as  $1/\epsilon$ -poles. As we have shown in Section 2.3.2, for a renormalizable theory these can be absorbed in a finite number of renormalization constants also known as the  $Z$  factors of specific correlators. If we follow our previous procedure, as in Chapter A, this means especially for the more complicated theories that we have to analytically solve millions of integrals. An enormous challenge, which fortunately can be cut short by taking advantage of the DREG.

### B.1.1 Integration by parts

The major advantage of the dimensional regularization for our purpose lies in the Integration-by-Parts (IBP) algorithm. Since the number of integrals at first sight might be scary, this method accomplishes a reduction to only a small amount of tabulated *master integrals*<sup>1</sup> [331]. For this method, we use the special feature of  $d$  dimensional boundary integrals over a total derivative, which have to be zero

$$\int \frac{d^d k}{(2\pi)^d} \frac{\partial}{\partial k_\mu} f(k, \dots) = 0. \quad (\text{B.1})$$

By explicitly evaluating the derivatives, we obtain a number of recurrence relations which relate Feynman integrals of different complexity [334]. Solving a proper system of recurrence relations provides a reduction of any Feynman integral to the mentioned master integrals.

<b>B.1 Fundamentals of Feynman diagram computation</b> . . . . .	129
<b>B.2 Tool Chain</b> . . . . .	132
<b>B.3 Programs for higher loops</b> . . . . .	133

1: In fact, the master integrals have to be computed numerically for most cases. It occurs that certain types precisely approximate magic numbers like  $\pi$  or the Riemann zeta function  $\zeta(n)$  for instance [331]. What could be confused with a coincidence might be a deeper connection between quantum field theory and pure number theory [332, 333].

But let us take a look at an example for a better notion of this procedure. We consider the following simple example of a loop integral

$$F(n) = \int \frac{d^d k}{(2\pi)^d} \frac{1}{(k^2 + m^2)^n}. \quad (\text{B.2})$$

For  $n = 1$ , for instance, this resembles a massive boson propagator. Starting from the boundary integral and explicitly performing the derivative, we obtain

$$\begin{aligned} 0 &= \int \frac{d^d k}{(2\pi)^d} \frac{\partial}{\partial k^\mu} k^\mu \frac{1}{(k^2 + m^2)^n} \\ &= \int \frac{d^d k}{(2\pi)^d} \frac{\delta_\mu^\mu}{(k^2 + m^2)^n} + \int \frac{d^d k}{(2\pi)^d} k^\mu \frac{-2k^\mu n}{(k^2 + m^2)^{n+1}} \\ &= \int \frac{d^d k}{(2\pi)^d} \frac{d - 2n}{(k^2 + m^2)^n} + \int \frac{d^d k}{(2\pi)^d} \frac{2nm^2}{(k^2 + m^2)^{n+1}} \\ &= (d - 2n)F(n) + 2nm^2F(n + 1). \end{aligned} \quad (\text{B.3})$$

Crucially, this relates the integral  $F(n)$  to  $F(n - 1)$  by

$$F(n) = -\frac{d - 2n + 2}{(2n - 2)m^2} F(n - 1). \quad (\text{B.4})$$

Note that by this any integral for  $n > 1$  can be reduced using this integration by parts relation to the master integral  $F(1)$ .

While this gives only a small peak on the method, it generalizes to more complicated integrals. Finally, a system of recurrence relations is constructed which has to be solved by a computer algebra [334–336]<sup>2</sup>. While it is also possible to derive a system of equations for multi-scale-integrals it is much more difficult and worth to reduce them to one-scale-integrals by an asymptotic expansion in the first step.

2: Still a hard task to do, but in a finite amount of time and disk space.

## B.1.2 Asymptotic expansion

Most of the diagrams we are confronted with, especially in higher loop orders, depend on more than one mass or external momentum. These multi-scale integrals has to be factorized before they can be processed in the IBP relations. Strictly speaking, we need to break the diagrams down to products of so-called one-scale-integrals. In case that we can impose a certain hierarchy of the involved scales (or it can at least be assumed a priori) this is achieved by an *asymptotic expansion*.

The goal of this algorithm is to expand certain subdiagrams of a Feynman diagram in several applications until one is left with the wanted products of simpler one-scale-integrals. Depending on the hierarchy, this leaves two major procedures which both are used in this thesis to verify the calculations. There are the

1. marge-momentum procedure with a momentum dominated hierarchy:  $Q \gg q, m$
2. hard-mass procedure with the mass dominated hierarchy:  $M \gg q, m$

Here,  $Q$  denotes the external momentum,  $M$  the leading mass and  $q, m$  smaller momenta or lighter masses. Both procedures are based on the same



principles, but we restrict the following discussion to the large-momentum. From this the hard-mass procedure can easily be adapted.

Let us denote by  $\Gamma(Q, \{m, q\})$  an arbitrary Feynman diagram. Then, the asymptotic expansion is described by the following abstract formular [336, 337]

$$\Gamma(Q, \{m, q\}) \stackrel{Q \rightarrow \infty}{\approx} \sum_{\gamma} \Gamma/\gamma(\{q, m\}) \circ \mathcal{F}_{\{q_{\gamma}, m_{\gamma}\}} \gamma(Q, \{q_{\gamma}, m_{\gamma}\}), \quad (\text{B.5})$$

where  $Q$  denotes the large momentum. The sum runs over all *subgraphs* (or subdiagrams)  $\gamma$  with the collection of smaller scales  $\{q_{\gamma}, m_{\gamma}\}$  which have to fulfill some extra conditions as explained below. We can think of this formula as cutting out parts of the diagram  $\Gamma$  as a whole and expand them individually. Strictly speaking, each subgraph  $\gamma$  will be extracted of the diagram  $\Gamma$  such that only the so-called *co-subgraph*  $\Gamma/\gamma$  is left. Next,  $\gamma$  is expanded in a Taylor series  $\mathcal{F}_{\{q_{\gamma}, m_{\gamma}\}}$  with respect to the small mass scales  $\{q_{\gamma}, m_{\gamma}\}$  of  $\gamma$ , i.e. also internal loop momenta that do not belong to the subgraph are treated as external and consequently considered as small. Finally, in the last step the result is reinserted ( $\circ$ ) into the co-subgraph  $\Gamma/\gamma$ . For this procedure to work, we have to require that we only expand subgraphs  $\gamma$  which are 1PI *and* contain all vertices where a large external momentum  $Q$  is running through [336, 337].

In order to get a better notion and also introduce a diagrammatic representation of the large-momentum procedure, it is worth to consider a simple one-loop example. Not to get confused by a Clifford algebra, we consider a one-loop propagator diagram in a purely bosonic theory with a massive boson (dashed line) and a massless boson (solid line) reading as

$$Q \text{ --- } \begin{array}{c} \text{---} \text{---} \text{---} \\ \text{---} \text{---} \text{---} \\ \text{---} \text{---} \text{---} \end{array} \text{---} Q = \Gamma(Q, m) = \int \frac{d^d k}{(2\pi)^d} \frac{1}{(k^2 + m^2)} \frac{1}{(Q - k)^2}. \quad (\text{B.6})$$

Following (B.5) and the rules for the subgraphs, we identify three terms in the expansion. At first, we consider the contribution of  $\gamma = \Gamma$  and only expand in the single boson mass  $m$

$$\begin{aligned} \mathcal{F}_m \Gamma(Q, m) &= \int \frac{d^s k}{(2\pi)^s} \frac{1}{(Q - k)^2} \mathcal{F}_m \frac{1}{k^2 + m^2} \\ &= \int \frac{d^d k}{(2\pi)^d} \frac{1}{(Q - k)^2} \left( \frac{1}{k^2} - \frac{m^2}{k^4} + \frac{m^4}{k^6} - \dots \right). \end{aligned} \quad (\text{B.7})$$

We are left with two subgraphs which fulfill the conditions explained above: The first one is the contraction of the Boson propagator to a vacuum bubble, i.e.

$$\Gamma/\gamma \circ \mathcal{F}_{q_{\gamma}} \gamma = \int \frac{d^d k}{(2\pi)^d} \frac{1}{k^2 + m^2} \mathcal{F}_{q_{\gamma}} \frac{1}{(Q - k)^2}, \quad (\text{B.8})$$

where the only small momentum is the loop momentum  $q_{\gamma} = k$ . By explicitly expanding, we obtain

$$\mathcal{F}_k \frac{1}{(Q - k)^2} = \mathcal{F}_k \frac{1}{Q^2 - (2Qk - k^2)} = \sum_{n=0}^{\infty} (Q^2)^{-n-1} (2Qk - k^2)^n. \quad (\text{B.9})$$

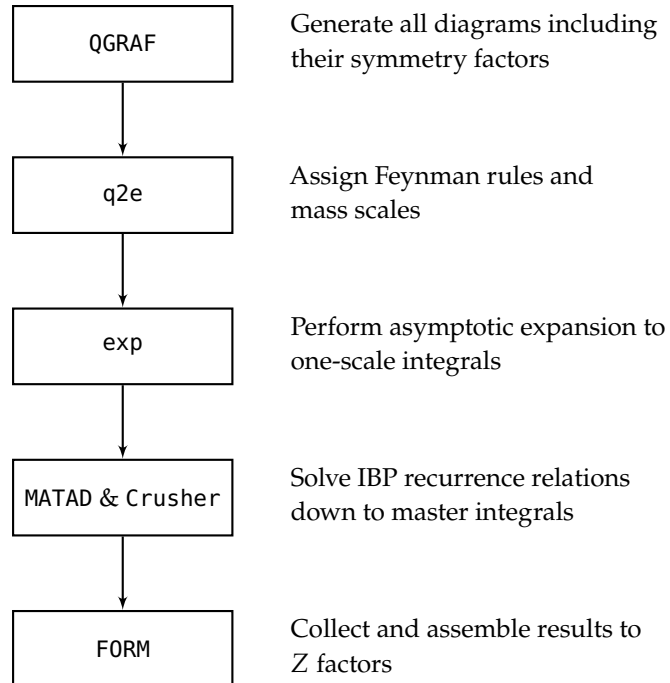
The remaining integral is found to be the Feynman integral of the massive vacuum bubble and the massless propagator (see e.g. in Ref. [69]). To be precise, there is a third subgraph, which fits to the requirements but as vacuum bubble vanishes in DREG. Finally, collecting all contribution the asymptotic expansion of the one-loop diagram in DREG [337] reads

$$\Gamma(Q, m) \stackrel{Q \rightarrow \infty}{\sim} \sum_{\gamma} \dots = \frac{1}{(4\pi)^{D/2}} \left( \frac{\mu^2}{Q^2} \right)^{\epsilon} \left[ \frac{\Gamma^2(1-\epsilon)\Gamma(\epsilon)}{\Gamma(2-2\epsilon)} {}_1F_0(2\epsilon-1; -m^2/Q^2) + \left( \frac{m^2}{Q^2} \right)^{1-\epsilon} \Gamma(1-\epsilon) {}_2F_1(1, \epsilon; 2-\epsilon; -m^2/Q^2) \right]. \quad (\text{B.10})$$

Note that the result not only involves Gamma functions we are familiar with from the DREG but also hypergeometrical functions  ${}_iF_j$ . These functions always depend on  $m^2/Q^2$  such that for an expression extracting the  $1/\epsilon$  poles, we can expand the expression in this ratio. The final results may seem obnoxious but in fact describes a very formal procedure to reduce the multi-scale integral to a product of one-scale integrals like Eq. (B.2).

## B.2 Tool Chain

For the higher-loop calculations throughout this thesis, a whole chain of tools was used. In this section, we want to briefly present the major parts and the order in which they are employed.



## B.3 Programs for higher loops

In this section, we present the different parts of the tool chain in more detail. A pivotal role therein plays the computer algebra language FORM which itself is worth mentioning.

### B.3.1 The Symbolic Manipulation System FORM

The symbolic manipulation system FORM was developed by Jos Vermaseren in 1989 [338–340] to manipulate large scale formulas which appear in perturbative calculations of high energy physics. Its predecessor SCHOONSHIP already offered fast algebraic computations but was hard to program. With the new programming techniques FORM became even faster and more flexible than that.

While other computer algebra systems like Wolfram's Mathematica or Maple offer a large amount of functions including integration, differentiation and even solve ODEs, FORM has very limited features. Actually, it works in a completely different way. While Mathematica and co are processing a formula as a tree, where each bracket is a branch of the level it contains, FORM creates a so-called *queue* and processes the formulas as a sequence of terms. This is the reason why, FORM provides much faster computation and can handle large amount of data (far beyond the RAM space) since the queue is stored on the hard disk. For processing the terms, the user has to learn to implement his code by using the powerful *pattern matching* abilities of FORM. After each step the terms can be "sorted" (i.e. written to the hard disk). Additionally, the program allows to divide the algorithm in so-called FORM -folds which define code segments, for which FORM decides during the runtime to put them in its input stream.

Since FORM was mainly developed for complicated calculations in high energy physics (especially in QCD), several packages were added over the years. One of the most important for loop calculations as done here is the color-package added by Ritbergen, Schellekens, and Vermaseren [329] and follows the concept of [327]. It accomplishes what we discussed in the previous Appendix for the group theoretical weights. For this it contracts all indices of the generators and structure constants for any simple Lie algebra and repeatedly uses the pattern matching function to express the group theoretical weight by the invariants presented in Section A.3.

### B.3.2 Generating Feynman Diagrams with QGRAF

The program QGRAF, originally implemented in Fortran, was written by Nogueira [341, 342] and is used here to generate the wanted Feynman diagrams. By "generating", we mean QGRAF draws each diagram by only knowing about the topologies of the given propagators and vertices. Besides this, it also assigns the all important symmetry factors to each diagram. As input the program needs the basic structure of the Lagrangian, i.e. the different propagators and how they are connected by vertices. At this stage, QGRAF does not ask for the underlying Feynman or color rules. For the Gross-Neveu-Yukawa models discussed in the previous Chapter, the input would look like this

```

1| * propagators *
2|
3| [fq, fQ, -]
4| [phi, phi, +]
5|
6| * vertices *
7|
8| [fQ, fq, phi]
9| [phi, phi, phi, phi]

```

**Figure B.1:** Input file for QGRAF which specifies the “Lagrangian”, i.e. all propagators and vertices from the topological point of view. The identifiers for this are

$fq \rightarrow \bar{\psi}$  (ingoing fermion line)

$fQ \rightarrow \psi$  (outgoing fermion line)

$phi \rightarrow \phi$  (boson line)

Lines which start with an asterisk sign (\*) are only commentary.

Here,  $fq \rightarrow \bar{\psi}$  denotes the ingoing fermion and  $fQ \rightarrow \psi$  the outgoing one, while for the bosonic field we have no momentum direction and thus only one identifier is needed  $phi \rightarrow \phi$ . In contrast to other diagram generators, as e.g. FeynArts, QGRAF does not use lower loop diagrams to compose higher-loop order diagrams. Employing the pseudodiagram technique, it avoids the comparison to other diagrams such that each diagram is “traced out” individually [341].

Since we are searching for all contributing diagrams for a specific choice of external legs up to a certain number of loops, this has to be passed to QGRAF in the file `qgraf.conf`. It contains, besides the in- and outgoing external legs (using again the identifiers specified in the `.lag` Lagrangian file), the number of loops and the path to the `.lag` Lagrangian file. It also allows for some extra options. First of all, the name of the output file has to be given, where QGRAF lists the generated diagrams and assigns momentum labels to each line. The style of this output can be modified freely by a style-file to bring it in a human-readable form and process it in the next step of the tool chain. For example, one of the two-loop diagrams of the boson propagator is generated by QGRAF in the following style (where the diagram itself is drawn right next to it with the labels as assigned by QGRAF)

```

1| diagram          4
2| pre_factor      (-1)*1
3|
4| number_propagators 5
5| number_loops    2
6| number_legs_in  1
7| number_legs_out  1
8|
9| external_leg    q1|1|phi
10| external_leg    q2|2|phi
11|
12| momentum        p1|3,1|fQ,fq
13| momentum        p2|1,4|fQ,fq
14| momentum        p3|2,3|fQ,fq
15| momentum        p4|4,2|fQ,fq
16| momentum        p5|4,3|phi,phi

```

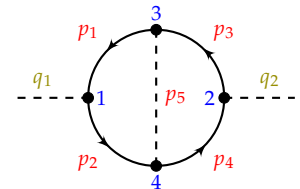


**Figure B.2:** Output of the example diagram by QGRAF which also assigns already labels for the momenta. Note that QGRAF also compute the symmetry factor here called `pre_factor`.

### B.3.3 Interface to Asymptotic Expansion

The program `q2e` was designed by R. Harlander, T. Seidensticker and M. Steinhauser as an interface between QGRAF and `exp` [343], the latter used for the asymptotic expansion. While QGRAF is extremely efficient in generating diagrams, the actual task, i.e. evaluating the corresponding integrals, is left to a computer algebra system like FORM. This link is established by `q2e`. It reads the QGRAF output as shown for the example diagram in Fig. B.2 and assigns FORM-functions to the propagators and vertices. These have to be specified with their momentum space rules and the group theoretical

structure of the underlying simple Lie algebra, similar to the discussion in Appendix A. For the two loop example diagram of the boson propagator as shown on the right of Fig B.2, q2e creates two FORM -folds. The first one includes only the momentum space functions where  $FT(p_i)$  denotes a fermion with momentum  $p_i$  and  $Den(p_i)$  denotes the boson one. The couplings are simple FORM -variables in this language and we use  $g := gffp$  for the Yukawa coupling because the character  $g$  in FORM is already reserved for the  $\gamma$ -matrices. Using the momentum labels assigned by QGRAF in listing B.2 the first fold reads

```

1 | *--#[ d2l4 :
2 |
3 | (-1)*1
4 | *gffp
5 | *FT1(p3)
6 | *gffp
7 | *FT1(p4)
8 | *gffp
9 | *FT1(p2)
10 | *gffp
11 | *FT1(p1)
12 | *Den(p5);
13 |
14 | #define TOPOLOGY "arb"
15 | #define INT1 "arb"
16 |
17 | *--#[ d2l4 :

```

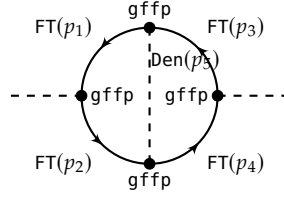


**Figure B.3:** The program q2e already assigns FORM -functions for the propagators and vertices as they are defined in the respecting files. For this it uses the momentum labels assigned by QGRAF as shown in Fig. B.2.

The preprocessor variables TOPOLOGY and INT1 are set to “arbitrary” (arb), since the next program in the tool chain exp will determine the topology itself in order to proceed with the asymptotic expansion. For the color weight, the program creates another fold

```

1 | *--#[ fqcd2l4 :
2 |
3 | 1
4 | *T(j5, j10, ij14)
5 | *d_(j10, j9)
6 | *T(j9, j12, ii2)
7 | *d_(j12, j11)
8 | *T(j11, j8, ij13)
9 | *d_(j8, j7)
10 | *T(j7, j6, ii1)
11 | *d_(j6, j5)
12 | *d_(ij13, ij14)
13 | *1*Numfq
14 | ;
15 |
16 | *--#[ fqcd2l4 :

```

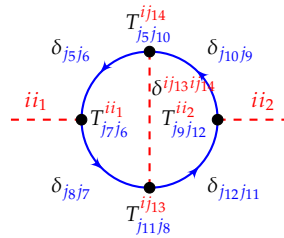


**Figure B.4:** The program q2e also creates a FORM -fold which contains the group theoretical part of the diagram using the color rules. Note here that the indices in the flavor space start with an  $j$  (i.e. for example  $j5$ ) while indices in the adjoint representation of the Bosonic field have an extra  $i$  in front (i.e. for example  $ij13$ )

Finally, q2e needs to know about the hierarchy of the scales for the asymptotic expansion as explained above. This is modified in a configuration file named .conf as shown in listing B.5.

```

1 | * q2e.propagator_file path/to/GN.v0.
   |   prop
2 | * q2e.vertex_file path/to/GN.v0.vrtx
3 |
4 | * q2e.scales q1,M1
5 | * q2e.mass phi:M1
6 |
7 | * q2e.anti_fermion fq:fq

```

**Figure B.5:** Configuration file `.conf` for `q2e`. Here the user has to give the paths to the files for propagators and vertices and also defines the hierarchy of scales. For this scales to the left are considered to be largest, i.e.  $q1 \gg M1$  where the former is the external momentum and the latter the Boson mass as specified in the next line. Depending on this exp will use the large-momentum procedure. In the last line the user tells the program that `fq:fQ` is the anti Fermion to `fQ:fq`.

As output `q2e` produces two files. The first one, with ending `.dia`, is organized in FORM -folds as shown in the listing above and contains the diagrams with the assigned FORM -functions in order to be processed by the FORM programs MATAD , MINCER or Crusher [344]. The second file with the ending `.edia` is prepared for the program `exp`, contains the information about the topology as found by QGRAF in listing B.2) and additionally adds which propagator is massive.

### B.3.4 IBP reduction in FORM

After successfully reducing the multi-scale integrals to one-scale-integrals of certain topologies using the asymptotic expansion, the programs MINCER , MATAD (up to three loop order) and Crusher (up to four loop order) further process the output. All these codes rewrite the amplitudes from the diagram source files in terms of massive tadpole integrals of the following type

$$\int \frac{d^D k}{(2\pi)^D} \frac{1}{(k^2 + M^2)^n} \quad (\text{B.11})$$

$$\int \frac{d^D k_1}{(2\pi)^D} \frac{d^D k_2}{(2\pi)^D} \frac{1}{(p_1^2 + M_1^2)^{n_1} (p_2^2 + M_2^2)^{n_2} (p_3^2 + M_3^2)^{n_3}} \quad (\text{B.12})$$

$$\int \frac{d^D k_1}{(2\pi)^D} \frac{d^D k_2}{(2\pi)^D} \frac{d^D k_3}{(2\pi)^D} \frac{1}{(p_1^2 + M_1^2)^{n_1}} \frac{1}{(p_2^2 + M_2^2)^{n_2}} \cdots \frac{1}{(p_6^2 + M_6^2)^{n_6}} \quad (\text{B.13})$$

In fact, these three integrals are sufficient to describe all possible cases of (up to) three-loop vacuum diagrams [345]. For this, the diagrams are firstly fully contracted by using the proper projectors as derived in Sec. A.4.2.

While MINCER [346, 347] was first developed for diagrams with massless propagators only with a small external momentum, MATAD [345]<sup>3</sup> can also deal with massive lines but for vacuum diagrams up to three loops. For computing the diagrams in the present work, MATAD works as an interface to MINCER and supports also Taylor expansions in small masses or momenta. In particular, this means for a massive diagram with one small external momentum a Taylor expansion provides a vacuum diagram which can be processed by MATAD . At this point, the program has to finally solve the IBP recurrence relations down to a finite number master integrals [331]. Since during this process, there are appearing artificial  $\epsilon$  poles one has to keep for the four loop results terms up to  $\mathcal{O}(\epsilon^8)$  which will drop out in the end. For four loops, this framework was extended by Crusher [344] which solves the system of equations with the Laporta algorithm [348].

3: MATAD stands for MAssiveTADpole.

# Higher-loop RG results

# C

In this appendix, we supplement all higher loop results which are too lengthy for presentation in the main text. In the beginning of each section we shortly give the used Lagrangian. For details on the models see

- ▶ Chapter 3: chiral Ising Gross-Neveu-Yukawa model [55]
- ▶ Chapter 5: Abelian Higgs model [56]
- ▶ Chapter 6: QED<sub>3</sub>-Gross-Neveu model [57]
- ▶ Chapter 7: Gross-Neveu-SO(3) model [58]

or the respective publications and references therein.

C.1 Chiral Ising of Gross-Neveu-Yukawa model .	137
C.2 Abelian Higgs model . . . . .	140
C.3 QED <sub>3</sub> -Gross-Neveu model ...	143
C.4 Gross-Neveu-SO(3) model ...	145

## C.1 Chiral Ising of Gross-Neveu-Yukawa model

In this section we give the four loop contributions to the RG functions of the chiral Ising Gross-Neveu-Yukawa model with the Lagrangian (cf. (3.18))

$$\mathcal{L}_{\text{GN Y}} = \bar{\psi} \not{\partial} \psi - \frac{1}{2} (\partial_\mu \phi)^2 + \frac{m^2}{2} \phi^2 + \sqrt{y} \phi \bar{\psi} \psi + \lambda \phi^4. \quad (\text{C.1})$$

where  $y$  denotes the Yukawa coupling of the of the order parameter field  $\phi$  to the massless fermion  $\psi$  with  $N_f$  flavors of  $d_\gamma$ -component spinors.

### C.1.1 Four loop RG functions

For the convenience of the reader, we give below the analytic expressions for the RG functions that we used in the numerical analysis. Here, and in the following, we use  $N_f = N/d_\gamma$  to display the RG functions. For the Ising GNY model, the beta function contributions to the Yukawa coupling explicitly read [113]

$$\beta_y^{(1\text{L})} = (3 + 2N_f)y^2, \quad (\text{C.2})$$

$$\beta_y^{(2\text{L})} = 24y\lambda(\lambda - y) - \left(\frac{9}{8} + 6N_f\right)y^3, \quad (\text{C.3})$$

$$\beta_y^{(3\text{L})} = \frac{y}{64} \left( 1152(7 + 5N_f)y^2\lambda + 192(91 - 30N_f)y\lambda^2 + (912\zeta_3 - 697 + 2N_f(67 + 112N_f + 432\zeta_3))y^3 - 13824\lambda^3 \right). \quad (\text{C.4})$$

Here  $\zeta_z$  is the Riemann zeta function. The four-loop contribution is listed below, together with all the other four-loop contributions. Accordingly, the

beta function for the quartic scalar coupling are composed of

$$\beta_\lambda^{(1L)} = 36\lambda^2 + 4N_f y \lambda - N_f y^2, \quad (C.5)$$

$$\beta_\lambda^{(2L)} = 4N_f y^3 + 7N_f y^2 \lambda - 72N_f y \lambda^2 - 816\lambda^3, \quad (C.6)$$

$$\begin{aligned} \beta_\lambda^{(3L)} = & \frac{1}{32} \left( 6912(145 + 96\zeta_3)\lambda^4 + 49536N_f y \lambda^3 \right. \\ & - 48N_f(72N_f - 361 - 648\zeta_3)y^2 \lambda^2 + N_f(5 - 628N_f - 384\zeta_3)y^4 \\ & \left. + 2N_f(1736N_f - 4395 - 1872\zeta_3)y^3 \lambda \right). \end{aligned} \quad (C.7)$$

For the contributions to the RG gamma function corresponding to wave function renormalization of the fermion derivative term, we find

$$\gamma_\psi^{(1L)} = \frac{y}{2}, \quad (C.8)$$

$$\gamma_\psi^{(2L)} = -\frac{y^2}{16}(12N_f + 1), \quad (C.9)$$

$$\gamma_\psi^{(3L)} = \frac{y^3}{128} (48\zeta_3 + 4N_f(47 - 12N_f) - 15) + 6\lambda y^2 - \frac{33\lambda^2 y}{2}. \quad (C.10)$$

The gamma function corresponding to the wave function renormalization of the derivative term of the scalar order parameter reads

$$\gamma_\phi^{(1L)} = 2N_f y, \quad (C.11)$$

$$\gamma_\phi^{(2L)} = 24\lambda^2 - \frac{5N_f y^2}{2}, \quad (C.12)$$

$$\gamma_\phi^{(3L)} = -216\lambda^3 + \frac{1}{32} N_f y^3 (48\zeta_3 + 200N_f + 21) + 30\lambda N_f y^2 - 90\lambda^2 N_f y. \quad (C.13)$$

Finally, the scaling of the quadratic scalar operator is given by the following contributions to the RG gamma function  $\gamma_{\phi^2}$ ,

$$\gamma_{\phi^2}^{(1L)} = -12\lambda, \quad (C.14)$$

$$\gamma_{\phi^2}^{(2L)} = 144\lambda^2 - 2N_f y(y - 12\lambda), \quad (C.15)$$

$$\begin{aligned} \gamma_{\phi^2}^{(3L)} = & \frac{3}{2} N_f y^2 \lambda (24N_f - 120\zeta_3 - 11) - 6264\lambda^3 \\ & - 4N_f y^3 (4N_f - 9 + 3\zeta_3) - 288N_f y \lambda^2. \end{aligned} \quad (C.16)$$

To complete the set of RG beta and gamma functions at the available order, we now also display the four-loop contributions,

$$\begin{aligned} \beta_y^{(4L)} = & -\frac{5}{2}\zeta_5(42N_f + 43)y^5 + \frac{(32\pi^4(2N_f + 3)(18N_f + 19) + 40N_f(8N_f(44N_f - 899) + 29721) + 457935) y^5}{7680} \\ & + \frac{\lambda}{8}(8N_f(12N_f - 683) - 2829)y^4 - \frac{1}{2}\lambda^2(4N_f(6N_f + 635) + 4455)y^3 + 36\lambda^3(8N_f - 455)y^2 \\ & - \frac{1}{8}\zeta_3 y^2 (-41472\lambda^3 + (4N_f(125N_f + 331) - 5)y^3 + 432\lambda(12N_f + 7)y^2 - 864\lambda^2(6N_f - 25)y) + 14040\lambda^4 y, \\ & + \Delta_3 N_f(1 + 107\zeta_3 - 125\zeta_5)y^5, \end{aligned} \quad (C.17)$$



$$\begin{aligned}
\beta_\lambda^{(4L)} = & 41472 \left( -39\zeta_3 - 60\zeta_5 + \frac{\pi^4}{10} - \frac{3499}{96} \right) \lambda^5 + \frac{1}{240} \lambda N_f y^4 (-60\zeta_3 (912N_f^2 - 4156N_f - 4677) \\
& + 1200\zeta_5 (157 - 168N_f) - 4\pi^4 (450N_f + 41) + 25(4N_f(337N_f + 3461) + 5847)) \\
& + \frac{N_f y^5 (480\zeta_3 (12N_f(14N_f - 15) + 277) + 2400\zeta_5 (128N_f + 65) + 8\pi^4 (64N_f - 77) + 160N_f(1289 - 386N_f) - 67095)}{1920} \\
& + \frac{1}{80} \lambda^2 N_f y^3 (835200\zeta_5 + 1920\zeta_3 (3N_f(4N_f - 61) + 19) + 72\pi^4 (24N_f + 31) - 40N_f(288N_f + 15649) + 1057825) \\
& + \frac{4}{5} \lambda^3 N_f y^2 (-86400\zeta_5 + 540\zeta_3 (4N_f - 69) + 7890N_f - 288\pi^4 - 72605) + \frac{36}{5} (-17280\zeta_3 + 96\pi^4 - 6775) \lambda^4 N_f y.
\end{aligned} \tag{C.18}$$

The symbol  $\Delta_3$  should be set to  $\Delta_3 = 1$ , see Ref. [112] for more details on the dimensional regularization scheme. The four-loop contributions to the gamma functions read

$$\begin{aligned}
\gamma_\psi^{(4L)} = & \frac{y}{393216} \left( 134479872\lambda^3 + y^3 \left( -884736\zeta_3 - 5 \left( 384 (256\zeta_5 - 893) + \frac{377339\pi^4}{90} \right) \right. \right. \\
& + 16N_f \left( -164352\zeta_3 + N_f (1536 (16\zeta_3 - 3) N_f - 74752) - \frac{1536\pi^4}{5} + 53440 \right) + \frac{303611\pi^4}{18} \\
& - 288\lambda y^2 \left( 512 (93 - 32\zeta_3) + 8 \left( 7424 + \frac{927\pi^4}{4} \right) N_f - \frac{1}{18} \pi^4 (33372N_f + 7079) + \frac{7079\pi^4}{18} \right) \\
& \left. \left. + 96\lambda^2 y (221184\zeta_3 + 344064N_f - 656384) \right) \right),
\end{aligned} \tag{C.19}$$

$$\begin{aligned}
\gamma_\phi^{(4L)} = & 14040\lambda^4 + \frac{\lambda N_f y^3}{256} (768 (16\zeta_3 - 83) - 19456N_f) + \frac{1}{32} \lambda^2 N_f y^2 (256 (81\zeta_3 - 91) - 384N_f) + 288\lambda^3 N_f y \\
& - \frac{N_f y^4 \left( 377856\zeta_3 + 15360 (8\zeta_5 - 29) + 4N_f \left( 162816\zeta_3 + 256 (144\zeta_3 - 101) N_f + \frac{1536\pi^4}{5} - 54016 \right) + 1024\pi^4 \right)}{24576},
\end{aligned} \tag{C.20}$$

$$\begin{aligned}
\gamma_{\phi^2}^{(4L)} = & 1728 \left( 18\zeta_3 + \frac{2\pi^4}{5} + 187 \right) \lambda^4 + \frac{3}{2} \lambda^2 N_f y^2 \left( 5760\zeta_3 + 4(-48\zeta_3 - 176) N_f + \frac{48\pi^4}{5} + 3796 \right) \\
& + \frac{1}{64} N_f y^4 \left( -5376\zeta_3 + 10080\zeta_5 + 2N_f \left( 320\zeta_3 + 4480\zeta_5 + 64(18\zeta_3 - 11) N_f + \frac{48\pi^4}{5} - 5208 \right) - \frac{224\pi^4}{5} - 2846 \right) \\
& - \frac{3}{16} \lambda N_f y^3 \left( -5120\zeta_3 - 5760\zeta_5 + 4N_f \left( -672\zeta_3 + 64(2\zeta_3 - 1) N_f + \frac{16\pi^4}{3} - 1618 \right) + \frac{184\pi^4}{5} + 12989 \right) \\
& + 36(96\zeta_3 + 313) \lambda^3 N_f y.
\end{aligned} \tag{C.21}$$

### C.1.2 GN critical exponents

From the four-loop RG beta and gamma functions of the GN model in Ref. [111] we have extracted the critical exponents as a function of general  $N$ . They read

$$\frac{1}{\nu} = \epsilon + \frac{1}{2-N}\epsilon^2 - \frac{(N-3)}{2(N-2)^2}\epsilon^3 + \frac{6\zeta_3(11N-34) + (N-1)(N+12)}{4(N-2)^3}\epsilon^4 + \mathcal{O}(\epsilon^5), \quad (\text{C.22})$$

$$\eta_\phi = 2 - \frac{N}{N-2}\epsilon + \frac{1-N}{(N-2)^2}\epsilon^2 + \frac{(N-1)N}{2(N-2)^3}\epsilon^3 + \frac{(N-1)(2\zeta_3(N(N+7)-42) - (N-9)N+5)}{4(N-2)^4}\epsilon^4 + \mathcal{O}(\epsilon^5), \quad (\text{C.23})$$

$$\eta_\psi = \frac{N-1}{2(N-2)^2}\epsilon^2 - \frac{(N-6)(N-1)}{4(N-2)^3}\epsilon^3 + \frac{(N-1)((N-11)N+25)}{8(N-2)^4}\epsilon^4 + \mathcal{O}(\epsilon^5). \quad (\text{C.24})$$

We note that these critical exponents have a pole at  $N = 2$ , which is due to a factor of  $(N-2)$  appearing in each loop order of the RG functions, cf. Ref. [111].

## C.2 Abelian Higgs model

In this section we give the four loop contributions to the RG functions of the Abelian Higgs model with the Lagrangian (cf. (5.1))

$$\mathcal{L} = |D_\mu\phi|^2 + \frac{1}{4}F_{\mu\nu}^2 + r|\phi|^2 + \lambda(|\phi|^2)^2. \quad (\text{C.25})$$

Here,  $\phi = (\phi_1, \dots, \phi_n)$  describes the  $n$ -component complex scalar field with mass term  $r$  and quartic interaction  $\lambda$ . It is minimally coupled to the dynamical non-compact U(1) gauge field  $A_\mu$  via the covariant derivative  $D_\mu = \partial_\mu - ieA_\mu$  with charge  $e$  and indices  $\mu, \nu$  run from 0 to  $d-1$ . Common summation convention over repeated indices is implied. The gauge field comes with the field strength tensor  $F_{\mu\nu} = \partial_\mu A_\nu - \partial_\nu A_\mu$  and we add a gauge fixing term  $\mathcal{L}_{\text{gf}} = -\frac{1}{2\xi}(\partial_\mu A_\mu)^2$  where  $\xi$  denotes the gauge fixing parameter.

### C.2.1 Four loop RG functions

The beta functions up to three loops are given in Sec. 5.3. Here, we provide the missing terms at four loops and give the full expressions for the anomalous dimensions and the flow of the gauge fixing parameter. The four-loop contributions to the beta functions read

$$\beta_\alpha^{(4\ell)} = \left( -\frac{323}{3888}n^3 + \left[ \frac{451}{54} - \frac{38\zeta_3}{9} \right]n^2 + \frac{3}{16}n \right) \alpha^5 + \left( \frac{5}{72}n^3 - \frac{41}{9}n^2 - \frac{37}{8}n \right) \alpha^4 \lambda + \left( \frac{1}{24}n^3 + \frac{139}{48}n^2 + \frac{137}{48}n \right) \alpha^3 \lambda^2 \quad (\text{C.26})$$

$$+ \left( -\frac{5}{48}n^3 - \frac{7}{16}n^2 - \frac{1}{3}n \right) \alpha^2 \lambda^3$$

$$\beta_\lambda^{(4\ell)} = \left( \left[ 40\zeta_5 - \frac{27\zeta_3}{2} - \frac{6145}{48} - \frac{\pi^4}{180} \right]n^2 - \left[ \frac{3157\zeta_3}{6} + 80\zeta_5 + \frac{25123}{24} + \frac{143\pi^4}{180} \right]n - \frac{12\pi^4}{5} - \frac{18503}{16} - 768\zeta_3 - 960\zeta_5 \right) \alpha^2 \lambda^3 \quad (\text{C.27})$$

$$+ \left( \left[ \frac{29\zeta_3}{2} - \frac{\pi^4}{60} - \frac{377}{96} \right]n^2 + \left[ -\frac{269\zeta_3}{2} + 50\zeta_5 + \frac{7\pi^4}{10} - \frac{1403}{32} \right]n + \frac{103\pi^4}{60} - \frac{185}{12} + 150\zeta_5 - 435\zeta_3 \right) \alpha \lambda^4$$

$$+ \left( \left[ \frac{1}{81} - \frac{2\zeta_3}{9} \right]n^3 + \left[ 28\zeta_3 - \frac{\pi^4}{10} - \frac{55709}{1296} \right]n^2 + \left[ 310\zeta_5 - \frac{578\zeta_3}{3} - \frac{13987}{36} - \frac{19\pi^4}{60} \right]n - \frac{12751}{16} - \frac{33\pi^4}{20} + 504\zeta_3 - 390\zeta_5 \right) \alpha^5$$

$$+ \left( \left[ \frac{19\zeta_3}{18} + \frac{67}{2592} \right]n^3 + \left[ 20\zeta_5 - \frac{77\zeta_3}{2} + \frac{\pi^4}{5} + \frac{12779}{162} \right]n^2 + \left[ \frac{431\zeta_3}{2} + 305\zeta_5 + \frac{13\pi^4}{10} + \frac{209}{12} \right]n + \frac{26\pi^4}{5} - \frac{19127}{96} + 2095\zeta_5 - \frac{1191\zeta_3}{2} \right) \alpha^4 \lambda$$

$$- \left( \left[ \frac{7\zeta_3}{6} + \frac{139}{1944} \right]n^3 - \left[ 40\zeta_5 - \frac{157\zeta_3}{3} - \frac{\pi^4}{60} + \frac{289817}{7776} \right]n^2 - \left[ 1080\zeta_5 - \frac{1813\zeta_3}{2} - \frac{5\pi^4}{12} + \frac{88871}{96} \right]n + \frac{6\pi^4}{5} - \frac{66851}{48} + 725\zeta_3 - 1520\zeta_5 \right) \alpha^3 \lambda^2$$

$$+ \left( -\frac{5}{96}n^3 + \left[ \frac{63\zeta_3}{2} + 20\zeta_5 - \frac{\pi^4}{12} + \frac{395}{12} \right]n^2 + \left[ 191\zeta_3 + 275\zeta_5 + \frac{10057}{48} - \frac{31\pi^4}{60} \right]n - \frac{11\pi^4}{15} + \frac{24581}{96} + \frac{583\zeta_3}{2} + 465\zeta_5 \right) \lambda^5$$

The field anomalous dimensions are defined through the relation  $\gamma_x = \frac{d \ln Z_x}{d \ln b}$ , for  $x \in \{\phi, \phi^2, A_\mu\}$ . Schematically, order by order, they can be written as  $\gamma_x = \sum_{i=1}^L \gamma_x^{(i\ell)}$ . Up to three loops, the contributions to  $\gamma_{\phi^2}$  read

$$\gamma_{\phi^2}^{(1\ell)} = (1 - \xi)\alpha - (n+1)\lambda, \quad (\text{C.28})$$

$$\gamma_{\phi^2}^{(2\ell)} = \frac{3}{2}(n+1)\lambda^2 - \left( 5n + \frac{1}{2} \right) \alpha^2 - 4(n+1)\alpha\lambda, \quad (\text{C.29})$$

$$\gamma_{\phi^2}^{(3\ell)} = \left( 6\zeta_3(3n+2) - \frac{167n}{4} - \frac{51}{2} \right) \alpha^3 + \frac{1}{16}(n+1)(144\zeta_3 + 43n + 299) \alpha^2 \lambda$$

$$+ 3(\zeta_3 + 1)(n+1)\alpha\lambda^2 - \frac{(n+1)}{16}(31n + 115)\lambda^3. \quad (\text{C.30})$$

The contributions to  $\gamma_\phi$  are

$$\gamma_\phi^{(1\ell)} = -(\xi + 2)\alpha, \quad (\text{C.31})$$

$$\gamma_\phi^{(2\ell)} = \frac{1}{12}(11n+9)\alpha^2 + \frac{1}{4}(n+1)\lambda^2, \quad (\text{C.32})$$

$$\gamma_\phi^{(3\ell)} = \left( \frac{1}{432}n(5n+3267) + \frac{1}{8} - 3\zeta_3(n-1) \right) \alpha^3 - \frac{1}{8}(24\zeta_3 - 13)(n+1)\alpha^2 \lambda$$

$$+ \frac{5}{4}(n+1)\alpha\lambda^2 - \frac{1}{16}(n+1)(n+4)\lambda^3, \quad (\text{C.33})$$

and for  $\gamma_A$  we obtain

$$\gamma_A^{(1\ell)} = \frac{n}{3}\alpha, \quad (\text{C.34})$$

$$\gamma_A^{(2\ell)} = 2n\alpha^2, \quad (\text{C.35})$$

$$\gamma_A^{(3\ell)} = \frac{n}{72}(261 - 49n)\alpha^3 + \frac{n}{2}(n+1)\alpha^2\lambda - \frac{n}{8}(n+1)\alpha\lambda^2. \quad (\text{C.36})$$

The contributions at four loops to these field anomalous dimensions are, again, more lengthy. They read

$$\begin{aligned} \gamma_{\phi^2}^{(4\ell)} = & \left( \left[ -\frac{127\zeta_3}{6} + 40\zeta_5 - \frac{1889}{36} - \frac{\pi^4}{45} \right] n^2 + \left[ -\frac{368\zeta_3}{3} + 70\zeta_5 - \frac{5249}{36} - \frac{67\pi^4}{180} \right] n - \frac{280}{3} - \frac{7\pi^4}{20} + 30\zeta_5 - \frac{203\zeta_3}{2} \right) \alpha^2 \lambda^2 \\ & + \left( -\frac{55\zeta_3}{2} + \left[ -\frac{9\zeta_3}{2} + \frac{\pi^4}{30} - \frac{775}{96} \right] n^2 + \left[ -32\zeta_3 + \frac{\pi^4}{12} - \frac{369}{16} \right] n + \frac{\pi^4}{20} - \frac{1439}{96} \right) \alpha \lambda^3 \\ & + \left( \frac{49\zeta_3}{4} + 70\zeta_5 + \left[ \frac{\zeta_3}{2} + \frac{5}{324} \right] n^3 + \left[ -\frac{145\zeta_3}{6} + \frac{\pi^4}{8} + \frac{42545}{1296} \right] n^2 + \left[ 77\zeta_3 - \frac{285\zeta_5}{4} + \frac{23\pi^4}{60} + \frac{97}{24} \right] n + \frac{11\pi^4}{40} - \frac{1283}{48} \right) \alpha^4 \\ & + \left( 120\zeta_5 - \frac{327\zeta_3}{2} - \left[ \frac{7\zeta_3}{6} + \frac{139}{1944} \right] n^3 + \left[ \frac{273683}{7776} - \frac{119\zeta_3}{6} - \frac{\pi^4}{30} \right] n^2 + \left[ 120\zeta_5 + \frac{\pi^4}{15} + \frac{23665}{144} - \frac{1093\zeta_3}{6} \right] n + \frac{\pi^4}{10} + \frac{12391}{96} \right) \alpha^3 \lambda \\ & + \left( \frac{17\zeta_3}{4} + \left[ \frac{3\zeta_3}{4} - \frac{1}{12} \right] n^3 + \left[ 2\zeta_3 + \frac{\pi^4}{24} + \frac{977}{48} \right] n^2 + \left[ \frac{11\zeta_3}{2} + \frac{2\pi^4}{15} + \frac{377}{6} \right] n + \frac{11\pi^4}{120} + \frac{2035}{48} \right) \lambda^4, \quad (\text{C.37}) \end{aligned}$$

$$\begin{aligned} \gamma_{\phi}^{(4\ell)} = & \left( -4\zeta_3 - 20\zeta_5 + \left[ \frac{5\zeta_3}{3} + \frac{199}{144} - \frac{\pi^4}{180} \right] n^2 + \left[ -\frac{7\zeta_3}{3} - 20\zeta_5 + \frac{2\pi^4}{45} + \frac{413}{18} \right] n + \frac{\pi^4}{20} + \frac{345}{16} \right) \alpha^3 \lambda \\ & + \left( \frac{11\zeta_3}{2} + 5\zeta_5 + \left[ \frac{19\zeta_3}{12} - \frac{\pi^4}{120} - \frac{641}{288} \right] n^2 + \left[ \frac{85\zeta_3}{12} + 5\zeta_5 - \frac{179}{18} - \frac{\pi^4}{24} \right] n - \frac{\pi^4}{30} - \frac{247}{32} \right) \alpha^2 \lambda^2 \\ & + \left( -\zeta_3 + \left[ \frac{\zeta_3}{2} - \frac{19}{96} \right] n^2 + \left[ \frac{61}{96} - \frac{\zeta_3}{2} \right] n + \frac{5}{6} \right) \alpha \lambda^3 + \left( -\frac{5}{64}n^3 + \frac{5}{8}n^2 + \frac{85}{32}n + \frac{125}{64} \right) \lambda^4 \\ & + \left( \frac{63\zeta_3}{2} - 45\zeta_5 + \left[ \frac{13}{5184} - \frac{\zeta_3}{36} \right] n^3 + \left[ \frac{9\zeta_3}{4} - \frac{\pi^4}{120} - \frac{1505}{432} \right] n^2 + \left[ -\frac{49\zeta_3}{4} - \frac{25\zeta_5}{4} + \frac{231}{16} - \frac{\pi^4}{24} \right] n - \frac{\pi^4}{20} + \frac{133}{64} \right) \alpha^4, \quad (\text{C.38}) \end{aligned}$$

$$\begin{aligned} \gamma_A^{(4\ell)} = & \left( \frac{323}{3888}n^3 + \left[ \frac{38\zeta_3}{9} - \frac{451}{54} \right] n^2 - \frac{3}{16}n \right) \alpha^4 + \left( -\frac{5}{72}n^3 + \frac{41}{9}n^2 + \frac{37}{8}n \right) \alpha^3 \lambda + \left( -\frac{1}{24}n^3 - \frac{139}{48}n^2 - \frac{137}{48}n \right) \alpha^2 \lambda^2 \\ & + \left( \frac{5}{48}n^3 + \frac{7}{16}n^2 + \frac{1}{3}n \right) \alpha \lambda^3. \quad (\text{C.39}) \end{aligned}$$

Finally, we also give the corresponding expression for the renormalization group flow of the gauge fixing parameter

$$\beta_{\xi}^{(1\ell)} = \frac{8}{3}n\alpha\xi, \quad (\text{C.40})$$

$$\beta_{\xi}^{(2\ell)} = 16n\alpha^2\xi, \quad (\text{C.41})$$

$$\beta_{\xi}^{(3\ell)} = \left( 29 - \frac{49n}{9} \right) n\alpha^3\xi + \left( \frac{17}{6}\alpha - \frac{5}{12}\lambda \right) n(n+1)\alpha\lambda\xi, \quad (\text{C.42})$$

$$\begin{aligned} \beta_{\xi}^{(4\ell)} = & \xi \left( \frac{11}{192}n(5n^2 + 21n + 16)\alpha\lambda^3 \right. \\ & - \frac{25}{288}n(5n^2 - 328n - 333)\alpha^3\lambda - \frac{3}{32}n(2n^2 + 139n + 137)\alpha^2\lambda^2 \\ & \left. + \frac{n}{486}(323n^2 + 72n(228\zeta_3 - 451) - 729)\alpha^4 \right). \quad (\text{C.43}) \end{aligned}$$

### C.3 QED<sub>3</sub>-Gross-Neveu model

In this section, we give further three loop RG functions of the QED<sub>3</sub>-Gross-Neveu model with the Lagrangian (cf. (6.1))

$$\mathcal{L} = \bar{\psi}_i (\not{D} + g\phi) \psi_i + \frac{1}{4} F_{\mu\nu}^2 + \frac{1}{2} \phi (r - \partial_\mu^2) \phi + \lambda \phi^4, \quad (\text{C.44})$$

with  $\psi_i$  and  $\bar{\psi}_i$  being  $2N$  flavors of two-component gapless Dirac spinors,  $i = 1, \dots, 2N$ , which interact with each other through the real scalar field  $\phi$ . Here, we have abbreviated the covariant derivative  $\not{D} \equiv (\partial_\mu - ieA_\mu) \sigma_\mu$ , with the  $2 \times 2$  matrices  $\sigma_\mu$  serving as a two-dimensional representation of the Clifford algebra,  $\{\sigma_\mu, \sigma_\nu\} = 2\delta_{\mu\nu} \mathbf{1}$ . The summation convention over repeated indices is implicitly assumed.  $F_{\mu\nu} = \partial_\mu A_\nu - \partial_\nu A_\mu$  is the field strength tensor of the U(1) gauge field  $A_\mu$ ,  $\mu, \nu \in \{0, 1, 2\}$ . In our calculations, we will also add a gauge-fixing term

$$\mathcal{L}_{\text{gf}} = -\frac{1}{2\xi} (\partial_\mu A_\mu)^2, \quad (\text{C.45})$$

to the Lagrangian with gauge fixing parameter  $\xi$ .

#### C.3.1 Further three loop RG functions

Here, we display the RG functions that have been omitted in the main text. For the fermion anomalous dimension the corresponding loop contributions read

$$\gamma_\Psi^{(1L)} = \alpha\xi + \frac{y}{2}, \quad (\text{C.46})$$

$$\gamma_\Psi^{(2L)} = \frac{1}{4} \alpha^2 (-4N - 3) - \frac{3}{4} N y^2 - \frac{y^2}{16} - \alpha y, \quad (\text{C.47})$$

$$\begin{aligned} \gamma_\Psi^{(3L)} &= \frac{1}{72} \alpha^3 (40N^2 + 54N + 27) + \frac{1}{128} (188N - 48N^2 - 15) y^3 + \frac{5}{16} \alpha N y^2 \\ &\quad + \frac{3}{8} \zeta_3 y [4\alpha^2 + 4y(\alpha + 2\alpha N) + y^2] + 6\lambda y^2 \\ &\quad + \frac{3}{32} y [\alpha^2(4N - 17) - 176\lambda^2] + \frac{\alpha y^2}{2}. \end{aligned} \quad (\text{C.48})$$

We note that only the one-loop term depends on the gauge-fixing parameter  $\xi$ , cf. also Refs. [292]. The beta function of the gauge fixing parameter follows the form  $\beta_\xi = \sum_{k=1}^3 \beta_\xi^{(kL)}$  and reads

$$\beta_\xi^{(1L)} = -\frac{2}{3} N \alpha \xi \quad (\text{C.49})$$

$$\beta_\xi^{(2L)} = -\frac{1}{2} N \alpha (2\alpha - y) \xi \quad (\text{C.50})$$

$$\beta_\xi^{(3L)} = -\frac{1}{72} N \alpha \xi [-2\alpha^2(22N + 9) + 9(7N + 6)y^2 - 27\alpha y]. \quad (\text{C.51})$$

These beta functions agree in the limit  $y = \lambda \rightarrow 0$  with the QED calculations [292]. To explicitly verify the Ward identity associated with the local U(1) symmetry in our calculations, we also compute the gauge anomalous

dimension. We obtain

$$\gamma_A^{(1L)} = \frac{4}{3}N\alpha, \quad (\text{C.52})$$

$$\gamma_A^{(2L)} = (2\alpha - y)N\alpha, \quad (\text{C.53})$$

$$\gamma_A^{(3L)} = \frac{\alpha}{36}N [9(6 + 7N)y^2 - 27y\alpha - 2(9 + 22N)\alpha^2]. \quad (\text{C.54})$$

Gauge invariance requires  $\gamma_A = 4 - D$  exactly at the critical fixed point [279].

### C.3.2 Critical exponents for arbitrary $N$

We display the critical exponents for general  $N$ . It is convenient to abbreviate  $s \equiv s(N) = \sqrt{4N^4 + 204N^3 + 1521N^2 + 2916N}$ . The inverse of the correlation-length exponent then reads

$$\begin{aligned} 1/\nu = & 2 - \frac{10N^2 + 39N + s}{6N(2N + 3)}\epsilon - \frac{1}{108N(2N + 3)^3s^2} (192N^8 + 10672N^7 - 96N^6s + 131232N^6 - 8936N^5s \\ & + 1196856N^5 - 141660N^4s + 7872660N^4 - 835326N^3s + 27080487N^3 \\ & - 2230713N^2s + 41504886N^2 - 2985255Ns + 21257640N - 2125764s)\epsilon^2 \\ & + \frac{1}{15552N^3(2N + 3)^5s^3} (294912N^{14}\zeta_3 - 453120N^{14} + 37380096N^{13}\zeta_3 - 42546688N^{13} - 147456N^{12}s\zeta_3 \\ & + 917760N^{12}s + 1706655744N^{12}\zeta_3 - 1248153088N^{12} - 14929920N^{11}s\zeta_3 + 35954979840N^{11}\zeta_3 \\ & + 66756224N^{11}s - 11880201600N^{11} + 228480N^{10}s^2 - 582100992N^{10}s\zeta_3 + 1536213056N^{10}s \\ & + 414397472256N^{10}\zeta_3 + 7521785280N^{10} + 12064128N^9s^2 - 11530874880N^9s\zeta_3 + 17570258400N^9s \\ & + 2913244123392N^9\zeta_3 + 939273904800N^9 - 234624N^8s^3 + 152479584N^8s^2 - 118782816768N^8s\zeta_3 \\ & + 113751808560N^8s + 13271427877248N^8\zeta_3 + 7692596085888N^8 - 4509312N^7s^3 + 748856448N^7s^2 \\ & - 689855242752N^7s\zeta_3 + 432301897800N^7s + 40165847835840N^7\zeta_3 + 30916853322552N^7 - 21600N^6s^4 \\ & - 32667552N^6s^3 + 893187000N^6s^2 - 2383905022848N^6s\zeta_3 + 943060541292N^6s + 80251526970144N^6\zeta_3 \\ & + 68128907003406N^6 - 233280N^5s^4 - 103418208N^5s^3 - 5311161576N^5s^2 - 4991366935296N^5s\zeta_3 \\ & + 1056628909674N^5s + 101314839073104N^5\zeta_3 + 72296243742564N^5 - 2160N^4s^5 - 882576N^4s^4 \\ & - 102824640N^4s^3 - 22336611030N^4s^2 - 6205207152672N^4s\zeta_3 + 397375835472N^4s + 72105783082632N^4\zeta_3 \\ & + 991212929622N^4 - 14904N^3s^5 - 1364688N^3s^4 + 149467356N^3s^3 - 32684093892N^3s^2 \\ & - 4220721428112N^3s\zeta_3 - 73196963253N^3s + 20189256522768N^3\zeta_3 - 73287042502500N^3 - 72N^2s^6 \\ & - 30132N^2s^5 - 739206N^2s^4 + 362560860N^2s^3 - 17065633392N^2s^2 - 1214950653504N^2s\zeta_3 - 18954Ns^5 \\ & + 74901294540N^2s - 2008387814976N^2\zeta_3 - 53054911445616N^2 - 216Ns^6 + 183347145Ns^3 - 162s^6)\epsilon^3. \end{aligned} \quad (\text{C.55})$$

The order-parameter anomalous dimension is

$$\begin{aligned} \eta_\phi = & \frac{2N+9}{2N+3}\epsilon - \frac{332N^3 + 1200N^2 - 22Ns + 2205N - 93s + 5103}{36N(2N+3)^3}\epsilon^2 \\ & - \frac{1}{2592N^2(2N+3)^5s} (12224N^8 + 1145920N^7 + 56096N^6s + 24748032N^6 - 2115072N^5s\zeta_3 + 1119952N^5s \\ & + 223255440N^5 - 16625088N^4s\zeta_3 + 5031576N^4s + 1031152788N^4 - 46422720N^3s\zeta_3 + 2559276N^3s \\ & + 2651693112N^3 - 55427328N^2s\zeta_3 - 27824040N^2s + 3828763404N^2 - 25509168Ns\zeta_3 - 56551446Ns \\ & + 2593432080N - 2125764s\zeta_3 - 34897959s)\epsilon^3. \end{aligned} \quad (\text{C.56})$$

The scaling dimension of the flavor-symmetry-breaking bilinear at the critical point reads

$$\begin{aligned} [\bar{\Psi}\sigma_z\Psi] = & 3 - \frac{2(N+3)}{2N+3}\epsilon + \frac{284N^4 + 552N^3 + 2N^2s - 279N^2 + 51Ns + 2673N + 162s}{72N^2(2N+3)^3}\epsilon^2 \\ & - \frac{1}{5184N^2(2N+3)^5s} (2112N^8 + 234944N^7 - 63264N^6s + 8115072N^6 + 559872N^5s\zeta_3 - 559696N^5s \\ & + 111458160N^5 + 1041984N^4s\zeta_3 + 545256N^4s + 750279564N^4 - 8724672N^3s\zeta_3 + 14256756N^3s \\ & + 2710445976N^3 - 31492800N^2s\zeta_3 + 42085224N^2s + 5432779188N^2 - 34012224Ns\zeta_3 + 41551542Ns \\ & + 6081810804N - 10628820s\zeta_3 + 13167927s + 3443737680)\epsilon^3. \end{aligned} \quad (\text{C.57})$$

In the above equations,  $\zeta_z \equiv \zeta(z)$  denotes Riemann's zeta function.

## C.4 Gross-Neveu-SO(3) model

In this section, we give the three loop epsilon expansion and the full large- $N$  expressions of the Gross-Neveu-SO(3) model with the Lagrangian (cf. (7.2))

$$\mathcal{L} = \bar{\psi}\gamma^\mu\partial_\mu\psi + \frac{1}{2}\phi_a\left(-\partial_\mu^2 + m^2\right)\phi_a + \lambda(\phi_a\phi_a)^2 - g\phi_a\bar{\psi}\left(\mathbb{1}_{2N/3} \otimes L_a\right)\psi. \quad (\text{C.58})$$

### C.4.1 Epsilon expansions

The full expressions for the critical exponents from the  $(4 - \epsilon)$  expansion at three-loop order for arbitrary  $N \geq 3$  are quite lengthy. They are available electronically in the supplemental material of Ref. [58]. We also print the full expressions here

$$\begin{aligned}
\frac{1}{\nu} = & 2 - \frac{17N + 5(s+6)}{22(N+6)} \epsilon + \frac{820N^4 - N^3(820s - 172050) - N^2(19032s - 65745) - 18N(7417s - 111450) - 179280(s+6)}{10648(N+6)^3 s} \epsilon^2 \\
& + \frac{3}{10307264(N+6)^5 s^3} \left( 130160N^8 - 40N^7(3254s - 792723) - 42N^6(615046s - 62828375) \right. \\
& + N^5(38744100900 - 1283135016s) - 90N^4(76274956s + 4047257499) - 27N^3(650749372s + 61741071045) \\
& + 324N^2(690975808s - 10686990915) - 972N(39813404s + 2231925285) - 32313945600(s+6) \\
& + 88(N^3 + 126N^2 + 756N + 216) \left( 2960N^5 + N^4(417300 - 2960s) - 150N^3(1598s - 31167) \right. \\
& \left. \left. - 9N^2(181016s - 2657505) - 162N(15058s - 43965) + 3836160(s+6) \right) \zeta_3 \right) \epsilon^3 + \mathcal{O}(\epsilon^4), \tag{C.59}
\end{aligned}$$

$$\begin{aligned}
\eta_\phi = & \frac{N}{N+6} \epsilon + \frac{3}{968(N+6)^3} (1010N^2 + N(200s - 867) + 120(s+6)) \epsilon^2 \\
& + \frac{3}{468512(N+6)^5 s} \left( -44590N^5 + 6N^4(41594s - 1353735) + 15N^3(494903s + 858426) + 72N^2(342319s - 6404430) \right. \\
& \left. + 27N(829517s + 593640) + 11171520(s+6) - 3162456(N^2 + 9N + 18) N s \zeta_3 \right) \epsilon^3 + \mathcal{O}(\epsilon^4), \tag{C.60}
\end{aligned}$$

$$\begin{aligned}
\eta_\psi = & \frac{3}{2(N+6)} \epsilon + \frac{3}{1936(N+6)^3} (-736N^2 + 5N(2s + 123) + 600s + 9045) \epsilon^2 \\
& - \frac{9}{937024(N+6)^5 s} \left( 1570N^5 + 32N^4(866s + 13605) + 3N^3(457279s + 9071670) + N^2(65284110 - 55782s) \right. \\
& \left. + N(330505920 - 39115413s) + 81(339000 - 719473s) + 3162456(N^2 + 9N + 18) s \zeta_3 \right) \epsilon^3 + \mathcal{O}(\epsilon^4). \tag{C.61}
\end{aligned}$$

with  $s = \sqrt{N^2 + 120N + 36}$ .

#### C.4.2 Critical exponents for $2 < d < 4$ from $1/N$ expansion

In this appendix, we record the full  $d$ -dimensional expressions for the various critical exponents that have been computed. These are also provided electronically in the ancillary file of the supplemental material of Ref. [58]. We denote the numerical coefficients of the  $1/N$  series as

$$\chi = \sum_{n=0}^{\infty} \chi_n \left( \frac{1}{N} \right)^n, \quad \lambda = \sum_{n=0}^{\infty} \lambda_n \left( \frac{1}{N} \right)^n, \quad \eta_\psi = \sum_{n=0}^{\infty} \eta_n \left( \frac{1}{N} \right)^n, \tag{C.62}$$

The leading-order terms are identical in all Gross-Neveu-like universality classes,

$$\chi_0 = 0, \quad \lambda_0 = \mu - 1, \quad \eta_0 = 0. \tag{C.63}$$

To order  $\mathcal{O}(1/N)$ , we recover the expressions that were originally determined in Ref. [54],

$$\chi_1 = \frac{\mu}{2(\mu-1)} \eta_1, \quad \lambda_1 = -(2\mu-1)\eta_1, \tag{C.64}$$

where

$$\eta_1 = - \frac{3\Gamma(2\mu-1)}{\mu\Gamma(1-\mu)\Gamma(\mu-1)\Gamma^2(\mu)}. \tag{C.65}$$



At next order, we have

$$\eta_2 = \left[ \frac{(3\mu - 2)}{2(\mu - 1)} \Psi(\mu) + \frac{13\mu^2 - 12\mu + 2}{4\mu(\mu - 1)^2} \right] \eta_1^2, \quad (\text{C.66})$$

$$\chi_2 = \left[ \frac{\mu(3\mu - 2)}{4(\mu - 1)^2} \Psi(\mu) - \frac{\mu(4\mu^2 - 3\mu - 2)}{4(\mu - 1)^2} + \frac{9\mu^2 \Theta(\mu)}{8(\mu - 1)} \right] \eta_1^2, \quad (\text{C.67})$$

for the field anomalous dimensions, while the correction to the exponent relating to  $\nu$  is

$$\begin{aligned} \lambda_2 = & \left\{ \frac{3\mu(\mu^2 - 2\mu + 4)}{4(\mu - 1)(\mu - 2)^2 \eta_1} - \frac{32\mu^6 - 178\mu^5 + 349\mu^4 - 265\mu^3 - 14\mu^2 + 128\mu - 32}{8(\mu - 1)^2(\mu - 2)^2} \Psi(\mu) \right. \\ & - \frac{7\mu^2(2\mu - 3)}{8(\mu - 1)(\mu - 2)} [\Psi^2(\mu) + \Phi(\mu)] - \frac{3\mu^2(4\mu^2 - 27\mu + 28)}{8(\mu - 1)(\mu - 2)} \Theta(\mu) \\ & \left. + \frac{64\mu^8 - 528\mu^7 + 1650\mu^6 - 2375\mu^5 + 1367\mu^4 + 218\mu^3 - 632\mu^2 + 256\mu - 32}{16\mu(\mu - 1)^3(\mu - 2)^2} \right\} \eta_1^2. \end{aligned} \quad (\text{C.68})$$

At this order, derivatives of the Euler  $\Gamma$  function arise, which is apparent in the functions

$$\Psi(\mu) = \psi(2\mu - 1) - \psi(1) + \psi(2 - \mu) - \psi(\mu), \quad \Theta(\mu) = \psi'(\mu) - \psi'(1), \quad (\text{C.69})$$

where  $\psi(z) = d \ln \Gamma(z)/(dz)$  is the Euler  $\psi$  function. Finally, the large- $N$  conformal bootstrap formalism produced

$$\begin{aligned} \eta_3 = & \left\{ \frac{3(3\mu - 2)^2}{8(\mu - 1)^2} \Psi^2(\mu) + \frac{(3\mu - 2)^2}{8(\mu - 1)^2} \Phi(\mu) - \frac{8\mu^7 - 5\mu^6 - 8\mu^5 - 182\mu^4 + 414\mu^3 - 288\mu^2 + 80\mu - 8}{16\mu^2(\mu - 1)^4} \right. \\ & - \frac{4\mu^5 - 7\mu^4 - 101\mu^3 + 178\mu^2 - 88\mu + 12}{8\mu(\mu - 1)^3} \Psi(\mu) + \frac{3\mu^3 + 24\mu^2 + 12\mu - 8}{32(\mu - 1)^2} \left[ \Theta(\mu) + \frac{1}{(\mu - 1)^2} \right] \\ & \left. + \frac{9\mu^2}{8(\mu - 1)} \left[ \Theta(\mu) + \frac{1}{(\mu - 1)^2} \right] \Psi(\mu) + \frac{9\mu^2}{16(\mu - 1)} \Xi(\mu) \left[ \Theta(\mu) + \frac{1}{(\mu - 1)^2} \right] \right\} \eta_1^3, \end{aligned} \quad (\text{C.70})$$

where an additional function  $\Xi(\mu)$  appears. It is related to a particular two-loop self-energy diagram that was defined as  $I(\mu)$  in Eq. (16) of Ref. [314] and is connected to  $\Xi(\mu)$  by

$$I(\mu) = -\frac{2}{3(\mu - 1)} + \Xi(\mu). \quad (\text{C.71})$$

In Ref. [349] it was shown to be related to derivatives with respect to the parameter dependence of an  ${}_4F_3$  hypergeometric function and its  $\epsilon$  expansion was given to very high orders near two and four space-time dimensions. The three-dimensional value was given in Ref. [314] as

$$I\left(\frac{3}{2}\right) = 2 \ln 2 - \frac{21}{\pi^2} \zeta_3. \quad (\text{C.72})$$



# Bibliography

Here are the references in citation order.

- [1] Lev Davidovich Landau. 'On the theory of phase transitions'. In: *Zh. Eksp. Teor. Fiz.* 7 (1937), p. 19 (cited on pages 1, 7).
- [2] V. L. Ginzburg. 'Some Remarks on Phase Transitions of the Second Kind and the Microscopic theory of Ferroelectric Materials'. In: *Sov. Phys. Solid State* 2 (1961), pp. 1824–1834 (cited on pages 1, 7).
- [3] Lars Onsager. 'Crystal statistics. I. A two-dimensional model with an order-disorder transition'. In: *Phys. Rev.* 65 (1944), pp. 117–149. doi: 10.1103/PhysRev.65.117 (cited on page 1).
- [4] Pierre Cladé, Estefania De Mirandes, Malo Cadoret, Saïda Guellati-Khélifa, Catherine Schwob, François Nez, Lucile Julien, and François Biraben. 'Determination of the fine structure constant based on bloch oscillations of ultracold atoms in a vertical optical lattice'. In: *Phys. Rev. Lett.* 96 (2006), p. 033001. doi: 10.1103/PhysRevLett.96.033001 (cited on page 1).
- [5] G. Gabrielse, D. Hanneke, T. Kinoshita, M. Nio, and B. Odom. 'New determination of the fine structure constant from the electron  $g$  value and QED'. In: *Phys. Rev. Lett.* 97 (2006), p. 030802. doi: 10.1103/PhysRevLett.97.030802 (cited on page 1).
- [6] Leo P. Kadanoff. 'Scaling laws for Ising models near  $T_c$ '. In: *Phys. Publ. Co.* 2 (1966), pp. 263–272 (cited on pages 1, 10).
- [7] Kenneth G. Wilson. 'Renormalization group and critical phenomena. I. Renormalization group and the Kadanoff scaling picture'. In: *Phys. Rev. B* 4 (1971), pp. 3174–3183. issn: 01631829. doi: 10.1103/PhysRevB.4.3174. url: <https://journals.aps.org/prb/abstract/10.1103/PhysRevB.4.3174>; Kenneth G. Wilson. 'Renormalization group and critical phenomena. II. Phase-space cell analysis of critical behavior'. In: *Phys. Rev. B* 4 (1971), pp. 3184–3205. issn: 01631829. doi: 10.1103/PhysRevB.4.3184. url: <https://journals.aps.org/prb/abstract/10.1103/PhysRevB.4.3184>. Cited on pages 1, 10.
- [8] Kenneth G. Wilson and Michael E. Fisher. 'Critical exponents in 3.99 dimensions'. In: *Phys. Rev. Lett.* 28 (1972), pp. 240–243. doi: 10.1103/PhysRevLett.28.240 (cited on pages 1, 10).
- [9] Kenneth G. Wilson and John B. Kogut. 'The renormalization group and the  $\epsilon$  expansion'. In: *Phys. Rep.* 12 (1974), pp. 75–199. doi: 10.1016/0370-1573(74)90023-4 (cited on pages 1, 10).
- [10] Kenneth G. Wilson. 'The renormalization group: Critical phenomena and the Kondo problem'. In: *Rev. Mod. Phys.* 47 (1975), pp. 773–840. doi: 10.1103/RevModPhys.47.773 (cited on pages 1, 10).
- [11] Kenneth G. Wilson. 'The renormalization group and critical phenomena'. In: *Rev. Mod. Phys.* 55 (1983), pp. 583–600. doi: 10.1103/RevModPhys.55.583 (cited on pages 1, 10).
- [12] Christof Wetterich. 'Exact evolution equation for the effective potential'. In: *Phys. Lett.* B301 (1993), pp. 90–94. doi: 10.1016/0370-2693(93)90726-X (cited on page 1).
- [13] David Simmons-Duffin. 'TASI Lectures on the Conformal Bootstrap'. In: (Sept. 2016) (cited on pages 1, 20).
- [14] Slava Rychkov. 'EPFL Lectures on Conformal Field Theory in  $D \geq 3$  Dimensions'. In: (2016) (cited on pages 1, 20).
- [15] Rufus Boyack, Hennadii Yerzhakov, and Joseph Maciejko. 'Quantum phase transitions in Dirac fermion systems'. In: *arXiv* (Apr. 2020) (cited on pages 2, 23, 27, 91).
- [16] Eduardo C. Marino. *Quantum field theory approach to condensed matter physics*. Cambridge University Press, 2017, pp. 1–516 (cited on pages 2, 5).
- [17] Alexander Altland and Ben D. Simons. *Condensed Matter Field Theory*. Cambridge: Cambridge University Press, 2010, p. 786 (cited on pages 2, 59).

- [18] E. Y. Loh, J. E. Gubernatis, R. T. Scalettar, S. R. White, D. J. Scalapino, and R. L. Sugar. ‘Sign problem in the numerical simulation of many-electron systems’. In: *Phys. Rev. B* 41.13 (May 1990), pp. 9301–9307. doi: 10.1103/PhysRevB.41.9301 (cited on page 2).
- [19] Matthias Troyer and Uwe Jens Wiese. ‘Computational complexity and fundamental limitations to fermionic quantum Monte Carlo simulations’. In: *Phys. Rev. Lett.* 94.17 (May 2005), p. 170201. doi: 10.1103/PhysRevLett.94.170201 (cited on page 2).
- [20] Zi-Xiang Li, Yi-Fan Jiang, and Hong Yao. ‘Fermion-sign-free Majorana-quantum-Monte-Carlo studies of quantum critical phenomena of Dirac fermions in two dimensions’. In: *New J. Phys.* 17 (2015). doi: 10.1088/1367-2630/17/8/085003 (cited on pages 2, 20, 29, 34, 43, 44).
- [21] Zi-Xiang Li and Hong Yao. ‘Sign-Problem-Free Fermionic Quantum Monte Carlo: Developments and Applications’. In: (2018), pp. 1–20. doi: 10.1146/annurev-conmatphys-033117-054307 (cited on pages 2, 20, 29).
- [22] Konstantin S. Novoselov, A. K. Geim, S. V. Morozov, D. Jiang, Y. Zhang, S. V. Dubonos, I. V. Grigorieva, and A. A. Firsov. ‘Electric Field Effect in Atomically Thin Carbon Films’. In: *Science* 306 (2004), pp. 666–669. doi: 10.1126/science.1102896 (cited on pages 2, 24).
- [23] Konstantin S. Novoselov, A. K. Geim, S. V. Morozov, D. Jiang, M. I. Katsnelson, I. V. Grigorieva, S. V. Dubonos, and A. A. Firsov. ‘Two-dimensional gas of massless Dirac fermions in graphene’. In: *Nature* 438 (2005), pp. 197–200. doi: 10.1038/nature04233 (cited on pages 2, 24).
- [24] A. K. Geim and Konstantin S. Novoselov. ‘The rise of graphene.’ In: *Nature Material* 6 (2007), pp. 183–91. doi: 10.1038/nmat1849 (cited on pages 2, 24).
- [25] A. H. Castro Neto, F. Guinea, N. M. R. Peres, Konstantin S. Novoselov, and A. K. Geim. ‘The electronic properties of graphene’. In: *Rev. Mod. Phys.* 81 (2007), pp. 109–162. doi: 10.1103/RevModPhys.81.109 (cited on pages 2, 24).
- [26] N. M. R. Peres. ‘Colloquium: The transport properties of graphene: An introduction’. In: *Rev. Mod. Phys.* 82 (2010), pp. 2673–2700. doi: 10.1103/RevModPhys.82.2673 (cited on page 2).
- [27] T. O. Wehling, A. M. Black-Schaffer, and A. V. Balatsky. ‘Dirac materials’. In: *Adv. Phys.* 63 (2014), pp. 1–76. doi: 10.1080/00018732.2014.927109 (cited on pages 2, 24).
- [28] Shuai Ren, Ping Rong, and Qi Yu. *Preparations, properties and applications of graphene in functional devices: A concise review*. 2018. doi: 10.1016/j.ceramint.2018.04.089 (cited on pages 2, 24, 25).
- [29] Michael M. Scherer and Igor F. Herbut. ‘Gauge-field-assisted Kekulé quantum criticality’. In: *Phys. Rev. B* 94 (20 Nov. 2016), p. 205136. doi: 10.1103/PhysRevB.94.205136 (cited on page 2).
- [30] Laura Classen, Igor F. Herbut, and Michael M. Scherer. ‘Fluctuation-induced continuous transition and quantum criticality in Dirac semimetals’. In: *Phys. Rev. B* 96 (11 Sept. 2017), p. 115132. doi: 10.1103/PhysRevB.96.115132 (cited on pages 2, 104).
- [31] Emilio Torres, Lukas Weber, Lukas Janssen, Stefan Wessel, and Michael M. Scherer. ‘Emergent symmetries and coexisting orders in Dirac fermion systems’. In: *Phys. Rev. Res.* 2 (2020), p. 022005. doi: 10.1103/PhysRevResearch.2.022005 (cited on pages 2, 50, 104).
- [32] Yuan Cao, Valla Fatemi, Shiang Fang, Kenji Watanabe, Takashi Taniguchi, Efthimios Kaxiras, and Pablo Jarillo-Herrero. ‘Unconventional superconductivity in magic-angle graphene superlattices’. In: *Nature* 556 (2018), pp. 43–50. doi: 10.1038/nature26160 (cited on pages 2, 47).
- [33] Yuan Cao, Valla Fatemi, Ahmet Demir, Shiang Fang, Spencer L. Tomarken, Jason Y. Luo, Javier D. Sanchez-Yamagishi, Kenji Watanabe, Takashi Taniguchi, Efthimios Kaxiras, Ray C. Ashoori, and Pablo Jarillo-Herrero. ‘Correlated insulator behaviour at half-filling in magic-angle graphene superlattices’. In: *Nature* 556 (2018), pp. 80–84. doi: 10.1038/nature26154 (cited on pages 2, 47).
- [34] Xiao Yan Xu, K T Law, and Patrick A Lee. ‘Kekulé valence bond order in an extended Hubbard model on the honeycomb lattice with possible applications to twisted bilayer graphene’. In: *Phys. Rev. B* 98 (2018), p. 121406. doi: 10.1103/PhysRevB.98.121406 (cited on pages 2, 47).
- [35] J. M. Kosterlitz. ‘The critical properties of the two-dimensional xy model’. In: *J. Phys. C: Solid State Phys.* 7 (1974), pp. 1046–1060. doi: 10.1088/0022-3719/7/6/005 (cited on page 2).

- [36] A. W. Sandvik, S. Daul, R. R.P. Singh, and D. J. Scalapino. ‘Striped Phase in a Quantum [Formula presented] Model with Ring Exchange’. In: *Phys. Rev. Lett.* 89 (2002), p. 247201. doi: 10.1103/PhysRevLett.89.247201 (cited on pages 2, 49, 51, 52).
- [37] Toshihiro Sato, Martin Hohenadler, and Fakher F. Assaad. ‘Dirac Fermions with Competing Orders: Non-Landau Transition with Emergent Symmetry’. In: *Phys. Rev. Lett.* 119 (2017), p. 197203. doi: 10.1103/PhysRevLett.119.197203 (cited on pages 2, 52).
- [38] T. Senthil, Ashvin Vishwanath, Leon Balents, Subir Sachdev, and Matthew P.A. Fisher. ‘Deconfined Quantum Critical Points’. In: *Science* 303 (2004), pp. 1490–1494. doi: 10.1126/science.1091806 (cited on pages 2, 49, 50, 52–55, 60).
- [39] Todadri Senthil, Leon Balents, Subir Sachdev, Ashvin Vishwanath, and Matthew P. A. Fisher. ‘Deconfined Criticality Critically Defined’. In: *J. Phys. Soc. Japan* 74 (2005), pp. 1–9. doi: 10.1143/JPSJS.74S.1 (cited on pages 2, 10, 49, 52, 56, 60).
- [40] T. Senthil, Leon Balents, Subir Sachdev, Ashvin Vishwanath, and Matthew P. A. Fisher. ‘Quantum criticality beyond the Landau-Ginzburg-Wilson paradigm’. In: *Phys. Rev. B* 70 (2004), p. 144407. doi: 10.1103/PhysRevB.70.144407 (cited on pages 2, 49, 52–55, 57, 60, 115).
- [41] Anders W. Sandvik. ‘Evidence for deconfined quantum criticality in a two-dimensional Heisenberg model with four-spin interactions’. In: *Phys. Rev. Lett.* 98 (2007), p. 227202. doi: 10.1103/PhysRevLett.98.227202 (cited on pages 2, 50, 51, 89).
- [42] Roger G. Melko and Ribhu K. Kaul. ‘Scaling in the fan of an unconventional quantum critical point’. In: *Phys. Rev. Lett.* 100 (2008), p. 017203. doi: 10.1103/PhysRevLett.100.017203 (cited on pages 2, 51, 52, 89).
- [43] Hui Shao, Wenan Guo, and Anders W. Sandvik. ‘Quantum criticality with two length scales’. In: *Science* 352 (2016), pp. 213–216. doi: 10.1126/science.aad5007 (cited on pages 2, 52, 89, 91).
- [44] Adam Nahum, P. Serna, J. T. Chalker, M. Ortuño, and A. M. Somoza. ‘Emergent SO(5) Symmetry at the Néel to Valence-Bond-Solid Transition’. In: *Phys. Rev. Lett.* 115 (2015), p. 267203. doi: 10.1103/PhysRevLett.115.267203 (cited on pages 2, 52, 73, 78, 91).
- [45] Chong Wang and T. Senthil. ‘Dual Dirac Liquid on the Surface of the Electron Topological Insulator’. In: *Phys. Rev. X* 5 (2015), p. 041031. doi: 10.1103/PhysRevX.5.041031 (cited on pages 2, 57).
- [46] Max A. Metlitski and Ashvin Vishwanath. ‘Particle-vortex duality of two-dimensional Dirac fermion from electric-magnetic duality of three-dimensional topological insulators’. In: *Phys. Rev. B* 93 (2016), p. 245151. doi: 10.1103/PhysRevB.93.245151 (cited on pages 2, 57).
- [47] David F. Mross, Jason Alicea, and Olexei I. Motrunich. ‘Explicit Derivation of Duality between a Free Dirac Cone and Quantum Electrodynamics in (2+1) Dimensions’. In: *Phys. Rev. Lett.* 117 (2016), p. 016802. doi: 10.1103/PhysRevLett.117.016802 (cited on pages 2, 57).
- [48] C. Dasgupta and B. I. Halperin. ‘Phase Transition in a Lattice Model of Superconductivity’. In: *Phys. Rev. Lett.* 47 (1981), pp. 1556–1560. doi: 10.1103/PhysRevLett.47.1556 (cited on pages 2, 55–57, 59, 67).
- [49] Nathan Seiberg, T. Senthil, Chong Wang, and Edward Witten. ‘A duality web in 2+1 dimensions and condensed matter physics’. In: *Ann. Phys.* 374 (2016), pp. 395–433. doi: 10.1016/j.aop.2016.08.007 (cited on pages 2, 57).
- [50] Chong Wang, Adam Nahum, Max A. Metlitski, Cenke Xu, and T. Senthil. ‘Deconfined Quantum Critical Points: Symmetries and Dualities’. In: *Phys. Rev. X* 7 (Sept. 2017), p. 031051. doi: 10.1103/PhysRevX.7.031051 (cited on pages 2, 52, 57, 60, 73, 74, 76–78, 84, 90, 91, 115, 116).
- [51] T. Senthil, Dam Thanh Son, Chong Wang, and Cenke Xu. ‘Duality between (2+1)d quantum critical points’. In: *Phys. Rep.* 827 (2019), pp. 1–48. doi: 10.1016/j.physrep.2019.09.001 (cited on pages 2, 52, 56, 57, 115).
- [52] Sergei V. Isakov, Roger G. Melko, and Matthew B. Hastings. ‘Universal signatures of fractionalized quantum critical points’. In: *Science* 335 (2012), pp. 193–195. doi: 10.1126/science.1212207 (cited on pages 2, 93, 112).

- [53] Matthias Vojta. ‘Frustration and quantum criticality’. In: *Reports Prog. Phys.* 81 (2018), p. 064501. doi: 10.1088/1361-6633/aab6be (cited on pages 2, 49).
- [54] Urban F. P. Seifert, Xiao-Yu Dong, Sreejith Chulliparambil, Matthias Vojta, Hong-Hao Tu, and Lukas Janssen. ‘Fractionalized fermionic quantum criticality in spin-orbital Mott insulators’. In: *Phys. Rev. Lett.* 125 (2020), p. 257202. doi: 10.1103/PhysRevLett.125.257202 (cited on pages 2, 49, 93–96, 98, 99, 108, 110, 112, 116, 146).
- [55] Bernhard Ihrig, Luminita N. Mihaila, and Michael M. Scherer. ‘Critical behavior of Dirac fermions from perturbative renormalization’. In: *Phys. Rev. B* 98 (2018), p. 125109. doi: 10.1103/PhysRevB.98.125109 (cited on pages 3, 23, 33, 34, 37, 40–42, 45, 46, 88, 112, 137, 171).
- [56] Bernhard Ihrig, Nikolai Zerf, Peter Marquard, Igor F. Herbut, and Michael M. Scherer. ‘Abelian Higgs model at four loops, fixed-point collision, and deconfined criticality’. In: *Phys. Rev. B* 100 (2019), p. 134507. doi: 10.1103/PhysRevB.100.134507 (cited on pages 3, 59, 63, 66, 68, 69, 137, 171).
- [57] Bernhard Ihrig, Lukas Janssen, Luminita N. Mihaila, and Michael M. Scherer. ‘Deconfined criticality from the QED<sub>3</sub>-Gross-Neveu model at three loops’. In: *Phys. Rev. B* 98 (2018), p. 115163. doi: 10.1103/PhysRevB.98.115163 (cited on pages 3, 73, 88, 137, 171).
- [58] Shouryya Ray, Bernhard Ihrig, Daniel Kruti, John A. Gracey, Michael M. Scherer, and Lukas Janssen. ‘Fractionalized quantum criticality in spin-orbital liquids from field theory beyond the leading order’. In: *Phys. Rev. B* 103 (2021), p. 155160. doi: 10.1103/PhysRevB.103.155160 (cited on pages 3, 94, 95, 98, 102, 137, 145, 146, 171).
- [59] Gregor Wentzel. ‘Zur Quantenoptik’. In: *Zeitschrift für Phys.* 22 (1924), pp. 193–199. doi: 10.1007/BF01328122 (cited on page 6).
- [60] Paul Adrien Maurice Dirac. ‘The Lagrangian in Quantum Mechanics’. In: *Phys. Zeitschrift der Sowjetunion* 3 (1933), pp. 64–72 (cited on page 6).
- [61] Igor F. Herbut. *A Modern Approach to Critical Phenomena*. Cambridge: Cambridge University Press, 2007, p. 224 (cited on pages 6, 7, 19, 59, 63, 111).
- [62] Gregg Jaeger. ‘The Ehrenfest Classification of Phase Transitions: Introduction and Evolution’. In: *Arch. Hist. Exact Sci.* 53 (1998), pp. 51–81. doi: 10.1007/s004070050021 (cited on page 6).
- [63] James P Sethna. *Entropy, Order Parameters, and Complexity*. Vol. 2. Oxford University Press, 2016, p. 376 (cited on page 7).
- [64] Aron Beekman, Louk Rademaker, and Jasper van Wezel. ‘An introduction to spontaneous symmetry breaking’. In: *SciPost Phys. Lect. Notes* (2019). doi: 10.21468/SciPostPhysLectNotes.11 (cited on page 7).
- [65] Douglas Ashton. *Kinetically Constrained: Critical Point*. URL: <http://www.kineticallyconstrained.com/2009/05/critical-point.html> (visited on 02/13/2020) (cited on pages 8, 9).
- [66] Subir Sachdev. *Quantum Phase Transitions*. Cambridge University Press, 2011 (cited on pages 9, 85).
- [67] Subir Sachdev and Bernhard Keimer. ‘Quantum criticality’. In: *Phys. Today* 64 (2011), pp. 29–35. doi: 10.1063/1.3554314 (cited on page 9).
- [68] Matthias Vojta. ‘Quantum phase transitions’. In: *Reports Prog. Phys.* 66 (2003), pp. 2069–2110. doi: 10.1088/0034-4885/66/12/R01 (cited on pages 9, 10).
- [69] Jean Zinn-Justin. ‘Quantum field theory and critical phenomena’. In: *Int. Ser. Monogr. Phys.* 113 (2002), pp. 1–1054 (cited on pages 11, 38, 59, 120, 125, 132).
- [70] P. V. Dong, L. T. Hue, H. T. Hung, H. N. Long, and N. H. Thao. ‘Symmetry factors of Feynman diagrams for scalar fields’. In: *Theor. Math. Phys.* 165 (2010), pp. 1500–1511. doi: 10.1007/s11232-010-0124-1 (cited on page 12).
- [71] A. N. Vasil’ev, Yu M. Pis’mak, and Yu R. Khonkonen. ‘Simple method of calculating the critical indices in the  $1/n$  expansion’. In: *Theor. Math. Phys.* 46 (1981), pp. 104–113. doi: 10.1007/BF01030844 (cited on pages 15, 95, 100).

- [72] John A. Gracey. 'Large  $N_f$  quantum field theory'. In: *Int. J. Mod. Phys. A* 33 (2018), p. 1830032. doi: 10.1142/S0217751X18300326 (cited on pages 15, 95, 100, 102, 103).
- [73] Matthew D. Schwartz. *Quantum Field Theory and the Standard Model*. Cambridge University Press, 2013, p. 863 (cited on page 15).
- [74] Juergen Berges, Nikolaos Tetradis, and Christof Wetterich. 'Nonperturbative renormalization flow in quantum field theory and statistical physics'. In: *Phys. Rept.* 363 (2002), pp. 223–386. doi: 10.1016/S0370-1573(01)00098-9 (cited on pages 15, 17, 104, 107, 108).
- [75] Jan M. Pawłowski. 'Aspects of the functional renormalisation group'. In: *Annals of Physics* 322 (2007), pp. 2831–2915. doi: <https://doi.org/10.1016/j.aop.2007.01.007> (cited on page 15).
- [76] Andreas Wipf. 'Functional Renormalization Group'. In: *Statistical Approach to Quantum Field Theory*. Springer, 2013, pp. 257–293. doi: [https://doi.org/10.1007/978-3-642-33105-3\\_12](https://doi.org/10.1007/978-3-642-33105-3_12) (cited on pages 15, 104).
- [77] Peter Kopietz, Lorenz Bartosch, and Florian Schütz. *Introduction to the functional renormalization group*. Springer, 2010 (cited on pages 15, 104).
- [78] Walter Metzner, Manfred Salmhofer, Carsten Honerkamp, Volker Meden, and Kurt Schönhammer. 'Functional renormalization group approach to correlated fermion systems'. In: *Rev. Mod. Phys.* 84 (2012), pp. 299–352. doi: 10.1103/RevModPhys.84.299 (cited on pages 15, 104).
- [79] Jens Braun. *Fermion interactions and universal behavior in strongly interacting theories*. 2012. doi: 10.1088/0954-3899/39/3/033001. URL: <https://iopscience.iop.org/article/10.1088/0954-3899/39/3/033001>. URL: <https://iopscience.iop.org/article/10.1088/0954-3899/39/3/033001/meta> (cited on pages 15, 104).
- [80] Bertrand Delamotte. 'An introduction to the nonperturbative renormalization group'. In: *Lect. Notes Phys.* 852 (2012), pp. 49–132. doi: 10.1007/978-3-642-27320-9\_2 (cited on pages 15, 17).
- [81] Holger Gies, Tobias Hellwig, Andreas Wipf, and Omar Zanusso. 'A functional perspective on emergent supersymmetry'. In: *J. High Energy Phys.* 2017 (2017), pp. 1–26. doi: 10.1007/JHEP12(2017)132 (cited on pages 15, 29, 33, 44).
- [82] Daniel F. Litim. 'Optimized renormalization group flows'. In: *Phys. Rev. D* 64 (2001), p. 17. doi: 10.1103/PhysRevD.64.105007 (cited on pages 16, 17, 108, 109).
- [83] Holger Gies. 'Introduction to the Functional RG and Applications to Gauge Theories'. In: *Lect. Notes Phys.* Vol. 852. 2012, pp. 287–348. doi: 10.1007/978-3-642-27320-9\_6 (cited on pages 16, 17, 71, 104).
- [84] N. Dupuis, L. Canet, A. Eichhorn, W. Metzner, J. M. Pawłowski, M. Tissier, and N. Wschebor. 'The nonperturbative functional renormalization group and its applications'. In: *arXiv* (2020) (cited on pages 16, 17, 104).
- [85] John P Boyd. *Chebyshev and Fourier spectral methods*. Courier Corporation, 2001 (cited on pages 17, 106).
- [86] Julia Borchardt and Benjamin Knorr. 'Global solutions of functional fixed point equations via pseudospectral methods'. In: *Phys. Rev. D* 91 (2015). doi: 10.1103/PhysRevD.91.105011 (cited on pages 17, 106).
- [87] Julia Borchardt, Holger Gies, and René Sondenheimer. 'Global flow of the Higgs potential in a Yukawa model'. In: *Eur. Phys. J. C* 76 (2016), p. 472. doi: 10.1140/epjc/s10052-016-4300-9 (cited on pages 17, 106).
- [88] Julia Borchardt and Benjamin Knorr. 'Solving functional flow equations with pseudospectral methods'. In: *Phys. Rev. D* 94 (2016), p. 025027. doi: 10.1103/PhysRevD.94.025027 (cited on pages 17, 106).
- [89] Julia Borchardt and Astrid Eichhorn. 'Universal behavior of coupled order parameters below three dimensions'. In: *Phys. Rev. E* 94 (2016). doi: 10.1103/PhysRevE.94.042105 (cited on pages 17, 106).
- [90] Benjamin Knorr. 'Ising and Gross-Neveu model in next-to-leading order'. In: *Phys. Rev. B* 94 (24 Dec. 2016), p. 245102. doi: 10.1103/PhysRevB.94.245102 (cited on pages 17, 29, 33, 37, 42, 43, 105, 106).
- [91] Slava Rychkov. 'Conformal bootstrap and the  $\lambda$ -point specific heat experimental anomaly'. In: *J. Club Condens. Matter Phys.* (2020). doi: 10.36471/JCCM (cited on pages 20, 21).

- [92] Shai M. Chester, Walter Landry, Junyu Liu, David Poland, David Simmons-Duffin, Ning Su, and Alessandro Vichi. ‘Carving out OPE space and precise  $O(2)$  model critical exponents’. In: *J. High Energy Phys.* 2020 (2020), p. 142. doi: 10.1007/JHEP06(2020)142 (cited on pages 20, 21).
- [93] David Poland and David Simmons-Duffin. ‘The conformal bootstrap’. In: *Nature Phys.* 12 (2016), pp. 535–539. doi: 10.1038/nphys3761 (cited on page 20).
- [94] David Poland, Slava Rychkov, and Alessandro Vichi. ‘The conformal bootstrap: Theory, numerical techniques, and applications’. In: *Rev. Mod. Phys.* 91 (2019), p. 015002. doi: 10.1103/RevModPhys.91.015002 (cited on pages 20, 60).
- [95] Yu Nakayama. ‘Scale invariance vs conformal invariance’. In: *Phys. Rep.* 569 (2015). doi: 10.1016/j.physrep.2014.12.003 (cited on page 20).
- [96] Sheer El-Showk, Miguel F. Paulos, David Poland, Slava Rychkov, David Simmons-Duffin, and Alessandro Vichi. ‘Solving the 3d ising model with the conformal bootstrap II. c-Minimization and precise critical exponents’. In: *J. Stat. Phys.* 157 (2014), pp. 869–914. doi: 10.1007/s10955-014-1042-7 (cited on page 20).
- [97] Mikhail V. Kompaniets and Erik Panzer. ‘Minimally subtracted six loop renormalization of  $O(n)$ -symmetric  $\phi^4$  theory and critical exponents’. In: *Phys. Rev. D* 96 (2017), p. 036016. doi: 10.1103/PhysRevD.96.036016 (cited on pages 20, 21, 31, 38–41, 98).
- [98] Abouzeid M. Shalaby. ‘Precise critical exponents of the  $O(N)$ -symmetric quantum field model using hypergeometric-Meijer resummation’. In: *Phys. Rev. D* 101 (2020), p. 105006. doi: 10.1103/PhysRevD.101.105006 (cited on pages 20, 21).
- [99] Gonzalo De Polsi, Ivan Balog, Matthieu Tissier, and Nicolás Wschebor. ‘Precision calculation of critical exponents in the  $O(N)$  universality classes with the nonperturbative renormalization group’. In: *Phys. Rev. E* 101 (2020), p. 042113. doi: 10.1103/PhysRevE.101.042113 (cited on page 21).
- [100] J. A. Lipa, J. A. Nissen, D. A. Stricker, D. R. Swanson, and T. C. P. Chui. ‘Specific heat of liquid helium in zero gravity very near the lambda point’. In: *Phys. Rev. B* 68 (2003), p. 174518. doi: 10.1103/PhysRevB.68.174518 (cited on page 21).
- [101] Martin Hasenbusch. ‘Monte Carlo study of an improved clock model in three dimensions’. In: *Phys. Rev. B* 100 (2019), p. 224517. doi: 10.1103/PhysRevB.100.224517 (cited on page 21).
- [102] Wanwan Xu, Yanan Sun, Jian-Ping Lv, and Youjin Deng. ‘High-precision Monte Carlo study of several models in the three-dimensional  $U(1)$  universality class’. In: *Phys. Rev. B* 100 (2019), p. 064525. doi: 10.1103/PhysRevB.100.064525 (cited on page 21).
- [103] R. Reisser, R.K. Kremer, and A. Simon. ‘3d-XY critical behavior of the layered metal-rich halides  $Gd_2IFe_2$ ,  $Gd_2ICo_2$  and  $Gd_2BrFe_2$ ’. In: *Phys. B Condens. Matter* 204 (1995), pp. 265–273. doi: 10.1016/0921-4526(94)00273-X (cited on page 21).
- [104] David J. Gross and André Neveu. *Dynamical symmetry breaking in asymptotically free field theories*. 1974. doi: 10.1103/PhysRevD.10.3235. url: [http://prd.aps.org/abstract/PRD/v10/i10/p3235%7B%5C\\_%7D1](http://prd.aps.org/abstract/PRD/v10/i10/p3235%7B%5C_%7D1) (cited on pages 23, 27).
- [105] Y. Nambu and G. Jona-Lasinio. ‘Dynamical model of elementary particles based on an analogy with superconductivity. II’. In: *Phys. Rev.* 124 (1961), pp. 246–254. issn: 0031899X. doi: 10.1103/PhysRev.124.246. url: <https://journals.aps.org/pr/abstract/10.1103/PhysRev.124.246>; Y. Nambu and G. Jona-Lasinio. ‘Dynamical model of elementary particles based on an analogy with superconductivity. I’. In: *Phys. Rev.* 122 (1961), pp. 345–358. issn: 0031899X. doi: 10.1103/PhysRev.122.345. url: <https://journals.aps.org/pr/abstract/10.1103/PhysRev.122.345>. Cited on page 23.
- [106] Igor F. Herbut, Vladimir Juričić, and Bitan Roy. ‘Theory of interacting electrons on the honeycomb lattice’. In: *Phys. Rev. B* 79 (2009), p. 085116. doi: 10.1103/PhysRevB.79.085116 (cited on pages 23, 26, 27, 43, 75, 95).
- [107] Walter E. Thirring. ‘A soluble relativistic field theory’. In: *Ann. Phys. (N. Y.)* 3 (1958), pp. 91–112. doi: 10.1016/0003-4916(58)90015-0 (cited on page 23).



- [108] Shailesh Chandrasekharan and Anyi Li. ‘Quantum critical behavior in three dimensional lattice Gross-Neveu models’. In: *Phys. Rev. D* 88 (2013), p. 021701. doi: 10.1103/PhysRevD.88.021701 (cited on pages 23, 29, 34, 37, 42, 43, 46).
- [109] Igor F. Herbut. ‘“Interactions and Phase Transitions on Graphene’s Honeycomb Lattice”’. In: *Phys. Rev. Lett.* 97 (Oct. 2006), p. 146401. doi: 10.1103/PhysRevLett.97.146401 (cited on pages 23, 25, 26, 29, 42, 43).
- [110] Igor F. Herbut, Vladimir Juričić, and Oskar Vafek. ‘Relativistic Mott criticality in graphene’. In: *Phys. Rev. B* 80 (2009), p. 075432. doi: 10.1103/PhysRevB.80.075432 (cited on pages 23, 26).
- [111] J. A. Gracey, T. Luthe, and Y. Schroder. ‘Four loop renormalization of the Gross-Neveu model’. In: *Phys. Rev. D* 94 (2016), p. 125028. doi: 10.1103/PhysRevD.94.125028 (cited on pages 23, 27, 32, 42, 140).
- [112] Luminita N. Mihaila, Nikolai Zerf, Bernhard Ihrig, Igor F. Herbut, and Michael M. Scherer. ‘Gross-Neveu-Yukawa model at three loops and Ising critical behavior of Dirac systems’. In: *Phys. Rev. B* 96 (2017), p. 165133. doi: 10.1103/PhysRevB.96.165133 (cited on pages 23, 29, 35, 44, 81, 82, 139).
- [113] Nikolai Zerf, Luminita N. Mihaila, Peter Marquard, Igor F. Herbut, and Michael M. Scherer. ‘Four-loop critical exponents for the Gross-Neveu-Yukawa models’. In: *Phys. Rev. D* 96 (2017), p. 096010. doi: 10.1103/PhysRevD.96.096010 (cited on pages 23, 29–32, 35, 42, 44, 47, 81, 82, 88, 112, 137).
- [114] J. A. Gracey. ‘Large  $N$  critical exponents for the chiral Heisenberg Gross-Neveu universality class’. In: *Phys. Rev. D* 97 (2018), p. 105009. doi: 10.1103/PhysRevD.97.105009 (cited on pages 23, 47).
- [115] R. Peierls. ‘Quelques propriétés typiques des corps solides’. In: *Ann. l’institut Henri Poincaré* 5 (1935), pp. 177–222 (cited on page 24).
- [116] N. D. Mermin. ‘Crystalline order in two dimensions’. In: *Phys. Rev.* 176 (1968), pp. 250–254. doi: 10.1103/PhysRev.176.250 (cited on page 24).
- [117] N. D. Mermin and H. Wagner. ‘Absence of ferromagnetism or antiferromagnetism in one- or two-dimensional isotropic Heisenberg models’. In: *Phys. Rev. Lett.* 17 (1966), pp. 1133–1136. issn: 00319007. doi: 10.1103/PhysRevLett.17.1133. url: <https://journals.aps.org/prl/abstract/10.1103/PhysRevLett.17.1133>; P. C. Hohenberg. ‘Existence of long-range order in one and two dimensions’. In: *Phys. Rev.* 158 (1967), pp. 383–386. issn: 0031899X. doi: 10.1103/PhysRev.158.383. url: <https://journals.aps.org/pr/abstract/10.1103/PhysRev.158.383>. Cited on page 24.
- [118] Mikhail I. Katsnelson. ‘Graphene: carbon in two dimensions’. In: *Materials Today* 10 (2007), pp. 20–27. doi: 10.1016/S1369-7021(06)71788-6 (cited on page 24).
- [119] Anthony Leggett. *Lecture 5: Graphene: Electronic band structure and Dirac fermions*. Tech. rep. 2010, p. 12 (cited on page 24).
- [120] Paul Adrien Maurice Dirac. ‘The quantum theory of the electron’. In: *Proc. R. Soc. London* 117 (1928), pp. 610–624. doi: 10.1098/rspa.1928.0023 (cited on page 25).
- [121] S. Raghu, Xiao-Liang Qi, C. Honerkamp, and Shou-Cheng Zhang. ‘Topological Mott Insulators’. In: *Phys. Rev. Lett.* 100 (15 Apr. 2008), p. 156401. doi: 10.1103/PhysRevLett.100.156401 (cited on pages 26, 29).
- [122] Chuang Chen, Xiao Yan Xu, Zi Yang Meng, and Martin Hohenadler. ‘Charge-Density-Wave Transitions of Dirac Fermions Coupled to Phonons’. In: *Phys. Rev. Lett.* 122 (2019), p. 077601. doi: 10.1103/PhysRevLett.122.077601 (cited on page 27).
- [123] Yuan Yao He, Xiao Yan Xu, Kai Sun, Fakher F. Assaad, Zi Yang Meng, and Zhong Yi Lu. ‘Dynamical generation of topological masses in Dirac fermions’. In: *Phys. Rev. B* 97 (2018), p. 081110. doi: 10.1103/PhysRevB.97.081110 (cited on page 27).
- [124] Pavel Buividovich, Dominik Smith, Maksim Ulybyshev, and Lorenz Von Smekal. ‘Hybrid Monte Carlo study of competing order in the extended fermionic Hubbard model on the hexagonal lattice’. In: *Phys. Rev. B* 98 (2018), p. 235129. doi: 10.1103/PhysRevB.98.235129 (cited on page 27).

- [125] Thomas C. Lang and Andreas M. Läuchli. ‘Quantum Monte Carlo Simulation of the Chiral Heisenberg Gross-Neveu-Yukawa Phase Transition with a Single Dirac Cone’. In: *Phys. Rev. Lett.* 123 (2019), p. 137602. doi: 10.1103/PhysRevLett.123.137602 (cited on pages 27, 47).
- [126] Laura Classen, Igor F. Herbut, Lukas Janssen, and Michael M. Scherer. ‘Competition of density waves and quantum multicritical behavior in Dirac materials from functional renormalization’. In: *Phys. Rev. B* 93 (2016), p. 125119. doi: 10.1103/PhysRevB.93.125119 (cited on pages 28, 104).
- [127] Jean Zinn-Justin. ‘Four-fermion interaction near four dimensions’. In: *Nucl. Phys. B* 367 (Dec. 1991), pp. 105–122. doi: 10.1016/0550-3213(91)90043-W (cited on pages 28, 29, 34, 73, 75, 90).
- [128] Bitan Roy, Vladimir Juričić, and Igor F. Herbut. ‘Emergent Lorentz symmetry near fermionic quantum critical points in two and three dimensions’. In: *J. High Energy Phys.* 2016 (2016). doi: 10.1007/JHEP04(2016)018 (cited on page 28).
- [129] Lei Wang, Philippe Corboz, and Matthias Troyer. ‘Fermionic quantum critical point of spinless fermions on a honeycomb lattice’. In: *New J. Phys.* 16 (2014). doi: 10.1088/1367-2630/16/10/103008 (cited on pages 29, 34, 44).
- [130] Emilie Huffman and Shailesh Chandrasekharan. ‘Fermion bag approach to Hamiltonian lattice field theories in continuous time’. In: *Phys. Rev. D* 96 (11 Dec. 2017), p. 114502. doi: 10.1103/PhysRevD.96.114502 (cited on pages 29, 34, 37, 43, 44, 46).
- [131] S. Hesselmann and S. Wessel. ‘Thermal Ising transitions in the vicinity of two-dimensional quantum critical points’. In: *Phys. Rev. B* 93 (2016), p. 155157. doi: 10.1103/PhysRevB.93.155157 (cited on pages 29, 34, 37, 44).
- [132] Yuichi Otsuka, Seiji Yunoki, and Sandro Sorella. ‘Universal Quantum Criticality in the Metal-Insulator Transition of Two-Dimensional Interacting Dirac Electrons’. In: *Phys. Rev. X* 6 (1 Mar. 2016), p. 011029. doi: 10.1103/PhysRevX.6.011029 (cited on pages 29, 47).
- [133] Zi-Xiang Li, Abolhassan Vaezi, Christian B. Mendl, and Hong Yao. ‘Numerical observation of emergent spacetime supersymmetry at quantum criticality’. In: *Sci. Adv.* 4 (2018), eaau1463. doi: 10.1126/sciadv.aau1463 (cited on pages 29, 47).
- [134] Zi Xiang Li, Yi Fan Jiang, Shao Kai Jian, and Hong Yao. ‘Fermion-induced quantum critical points’. In: *Nature Commun.* 8 (2017), p. 314. doi: 10.1038/s41467-017-00167-6 (cited on pages 29, 47, 49, 52).
- [135] Yuichi Otsuka, Kazuhiro Seki, Sandro Sorella, and Seiji Yunoki. ‘Quantum criticality in the metal-superconductor transition of interacting Dirac fermions on a triangular lattice’. In: *Phys. Rev. B* 98 (2018), p. 035126. doi: 10.1103/PhysRevB.98.035126 (cited on pages 29, 47).
- [136] Denis Bashkirov. ‘Bootstrapping the  $\mathcal{N} = 1$  SCFT in three dimensions’. In: *ArXiv eprints* (2013) (cited on page 29).
- [137] Nikolay Bobev, Sheer El-Showk, Dalimil Mazac, and Miguel F. Paulos. ‘Bootstrapping the Three-Dimensional Supersymmetric Ising Model’. In: *Phys. Rev. Lett.* 115 (2015), p. 051601. doi: 10.1103/PhysRevLett.115.051601 (cited on pages 29, 47).
- [138] Luca Iliesiu, Filip Kos, David Poland, Silviu S. Pufu, David Simmons-Duffin, and Ran Yacoby. ‘Bootstrapping 3D Fermions’. In: *JHEP* 03 (2016), p. 120. doi: 10.1007/JHEP03(2016)120 (cited on page 29).
- [139] Luca Iliesiu, Filip Kos, David Poland, Silviu S. Pufu, and David Simmons-Duffin. ‘Bootstrapping 3D Fermions with Global Symmetries’. In: *JHEP* 01 (2018), p. 036. doi: 10.1007/JHEP01(2018)036 (cited on pages 29, 34, 37, 42–46).
- [140] Lukas Janssen and Igor F. Herbut. ‘Antiferromagnetic critical point on graphene’s honeycomb lattice: A functional renormalization group approach’. In: *Phys. Rev. B* 89 (2014), p. 205403. doi: 10.1103/PhysRevB.89.205403 (cited on pages 29, 34, 95, 105, 107–110).
- [141] Gian Paolo Vacca and Luca Zambelli. ‘Multimeson Yukawa interactions at criticality’. In: *Phys. Rev. D* 91 (June 2015), p. 125003. doi: 10.1103/PhysRevD.91.125003 (cited on pages 29, 33, 45, 105).
- [142] Benjamin Knorr. ‘Critical chiral Heisenberg model with the functional renormalization group’. In: *Phys. Rev. B* 97 (2018), p. 075129. doi: 10.1103/PhysRevB.97.075129 (cited on pages 29, 105, 106).

- [143] Polina Feldmann, Andreas Wipf, and Luca Zambelli. ‘Critical Wess-Zumino models with four supercharges from the functional renormalization group’. In: *Phys. Rev. D* 98 (2017). doi: 10.1103/PhysRevD.98.096005 (cited on page 29).
- [144] B. Rosenstein, Hoi-Lai Yu, and A. Kovner. ‘Critical exponents of new universality classes’. In: *Phys. Lett.* B314 (1993), pp. 381–386. doi: 10.1016/0370-2693(93)91253-J (cited on pages 29, 47).
- [145] Anna Hasenfratz, Peter Hasenfratz, Karl Jansen, Julius Kuti, and Yue Shen. ‘The equivalence of the top quark condensate and the elementary Higgs field’. In: *Nuclear Physics B* 365 (1991), pp. 79–97. doi: [https://doi.org/10.1016/0550-3213\(91\)90607-Y](https://doi.org/10.1016/0550-3213(91)90607-Y) (cited on page 29).
- [146] Lin Fei, Simone Giombi, Igor R. Klebanov, and Grigory Tarnopolsky. ‘Yukawa conformal field theories and emergent supersymmetry’. In: *Prog. Theor. Exp. Phys.* 2016 (2016), p. 12C105. doi: 10.1093/ptep/ptw120 (cited on pages 29, 44).
- [147] Tarun Grover, D. N. Sheng, and Ashvin Vishwanath. ‘Emergent Space-Time Supersymmetry at the Boundary of a Topological Phase’. In: *Science* 344 (2014), pp. 280–283. doi: 10.1126/science.1248253 (cited on pages 29, 44).
- [148] Hagen Kleinert and Verena Schulte-Frohlinde. *Critical Properties of  $\phi^4$ -Theories*. Vol. 2729503230. World Scientific Publishing Co. Pte. Ltd., 1991 (cited on pages 32, 33, 38, 63, 81, 82, 86, 87).
- [149] George A. Baker. *Essentials of Padé approximants*. Academic Press, 1975 (cited on page 33).
- [150] Emilie Huffman and Shailesh Chandrasekharan. ‘Fermion-bag inspired Hamiltonian lattice field theory for fermionic quantum criticality’. In: *Phys. Rev. D* 101 (2020), p. 074501. doi: 10.1103/PhysRevD.101.074501 (cited on pages 33, 37, 43–47).
- [151] Yuzhi Liu, Wei Wang, Kai Sun, and Zi Yang Meng. ‘Designer Monte Carlo simulation for the Gross-Neveu-Yukawa transition’. In: *Phys. Rev. B* 101 (2020), p. 064308. doi: 10.1103/PhysRevB.101.064308 (cited on pages 33, 34, 37, 42, 45, 46).
- [152] F. Benitez, J.-P. Blaizot, H. Chaté, B. Delamotte, R. Méndez-Galain, and N. Wschebor. ‘Solutions of renormalization-group flow equations with full momentum dependence’. In: *Phys. Rev. E* 80 (3 Sept. 2009), p. 030103. doi: 10.1103/PhysRevE.80.030103 (cited on page 34).
- [153] F. Benitez, J.-P. Blaizot, H. Chaté, B. Delamotte, R. Méndez-Galain, and N. Wschebor. ‘Nonperturbative renormalization group preserving full-momentum dependence: Implementation and quantitative evaluation’. In: *Phys. Rev. E* 85 (2 Feb. 2012), p. 026707. doi: 10.1103/PhysRevE.85.026707 (cited on page 34).
- [154] Daniel Schmidt. ‘Three-dimensional four-Fermi theories with exact chiral symmetry on the lattice’. In: *PhD thesis, Jena University* (Nov. 2017) (cited on pages 34, 37, 42–44).
- [155] Yuan-Yao He, Xiao Yan Xu, Kai Sun, Fakher F. Assaad, Zi Yang Meng, and Zhong-Yi Lu. ‘Dynamical generation of topological masses in Dirac fermions’. In: *Phys. Rev. B* 97 (8 Feb. 2018), p. 081110. doi: 10.1103/PhysRevB.97.081110 (cited on page 34).
- [156] Leo Karkkainen, R. Lacaze, P. Lacock, and B. Petersson. ‘Critical behavior of the three-dimensional Gross-Neveu and Higgs-Yukawa models’. In: *Nucl. Phys.* B415 (1994). [Erratum: *Nucl. Phys.* B438,650(1995)], pp. 781–796. doi: 10.1016/0550-3213(94)90309-3, 10.1016/0550-3213(95)00055-W (cited on pages 34, 42, 43, 45, 73, 75).
- [157] J. A. Gracey. ‘Calculation of exponent  $\eta$  to  $\mathcal{O}(1/N^2)$  in the  $O(N)$  Gross-Neveu model’. In: *Int. J. Mod. Phys.* A6 (1991). [Erratum: *Int. J. Mod. Phys.* A6,2755(1991)], pp. 395–408. doi: 10.1142/S0217751X91000241 (cited on pages 34, 95, 100–102).
- [158] J. A. Gracey. ‘Anomalous mass dimension at  $\mathcal{O}(1/N^2)$  in the  $O(N)$  Gross-Neveu model’. In: *Phys. Lett.* B297 (1992), pp. 293–297. doi: 10.1016/0370-2693(92)91265-B (cited on pages 34, 42, 43, 45).
- [159] A. N. Vasiliev, Sergey E. Derkachov, N. A. Kivel, and A. S. Stepanenko. ‘The  $1/n$  expansion in the Gross-Neveu model: Conformal bootstrap calculation of the index  $\eta$  in order  $1/n^3$ ’. In: *Theor. Math. Phys.* 94 (1993). [Teor. Mat. Fiz.94,179(1993)], pp. 127–136. doi: 10.1007/BF01019324 (cited on pages 34, 86, 100, 102).

- [160] A. N. Vasiliev and A. S. Stepanenko. ‘The  $1/n$  expansion in the Gross-Neveu model: Conformal bootstrap calculation of the exponent  $1/\nu$  to the order  $1/n^2$ ’. In: *Theor. Math. Phys.* 97 (1993). [Teor. Mat. Fiz.97,364(1993)], pp. 1349–1354. doi: 10.1007/BF01015764 (cited on pages 34, 100, 102).
- [161] J. A. Gracey. ‘Computation of  $\beta'(g_c)$  at  $\mathcal{O}(1/N^2)$  in the  $O(N)$  Gross-Neveu model in arbitrary dimensions’. In: *Int. J. Mod. Phys. A* 9 (1994), pp. 567–590. doi: 10.1142/S0217751X94000285 (cited on pages 34, 42, 43, 45, 100, 102).
- [162] J. A. Gracey. ‘Computation of critical exponent  $\eta$  at  $\mathcal{O}(1/N^3)$  in the four Fermi model in arbitrary dimensions’. In: *Int. J. Mod. Phys. A* 9 (1994), pp. 727–744. doi: 10.1142/S0217751X94000340 (cited on pages 34, 42, 43, 45, 86, 95, 100, 102).
- [163] Sergey E. Derkachov, N. A. Kivel, A. S. Stepanenko, and A. N. Vasiliev. ‘On calculation in  $1/n$  expansions of critical exponents in the Gross-Neveu model with the conformal technique’. In: *ArXiv eprints* (1993) (cited on pages 34, 95, 100, 102).
- [164] J. A. Gracey. ‘Critical exponent  $\omega$  in the Gross-Neveu-Yukawa model at  $\mathcal{O}(1/N)$ ’. In: *Phys. Rev. D* 96 (2017), p. 065015. doi: 10.1103/PhysRevD.96.065015 (cited on page 34).
- [165] Alexander N. Manashov and Matthias Strohmaier. ‘Correction exponents in the Gross - Neveu - Yukawa model at  $1/N^2$ ’. In: (2017) (cited on page 34).
- [166] A J McKane, D J Wallace, and O F de Alcantara Bonfim. ‘Non-perturbative renormalisation using dimensional regularisation: applications to the epsilon expansion’. In: *Journal of Physics A: Mathematical and General* 17 (1984), p. 1861 (cited on page 38).
- [167] A J McKane and D J Wallace. ‘Instanton calculations using dimensional regularisation’. In: *Journal of Physics A: Mathematical and General* 11 (1978), p. 2285 (cited on page 38).
- [168] J. -P. Eckmann, J. Magnen, and R. Sénéor. ‘Decay properties and Borel summability for the Schwinger functions in  $P(\Phi)_2$  theories’. In: *Communications in Mathematical Physics* 39 (Dec. 1975), pp. 251–271. doi: 10.1007/BF01705374 (cited on page 38).
- [169] J. Magnen and R. Sénéor. ‘Phase space cell expansion and Borel summability for the Euclidean  $\phi_3^4$  theory’. In: *Communications in Mathematical Physics* 56 (Oct. 1977), pp. 237–276. doi: 10.1007/BF01614211 (cited on page 38).
- [170] A A Vladimirov, D I Kazakov, and V Tarasov. ‘Calculation of critical exponents by quantum field theory methods’. In: *Sov. Phys. JETP* 50 (1979), pp. 521–526 (cited on pages 38, 39).
- [171] E. Brézin, J. C. Le Guillou, and J. Zinn-Justin. ‘Perturbation theory at large order. I. The  $\varphi^{2N}$  interaction’. In: *Phys. Rev. D* 15 (6 Mar. 1977), pp. 1544–1557. doi: 10.1103/PhysRevD.15.1544 (cited on page 40).
- [172] R Guida and J Zinn-Justin. ‘Critical exponents of the  $N$  -vector model’. In: *Journal of Physics A: Mathematical and General* 31 (1998), p. 8103 (cited on page 41).
- [173] Sylvain Capponi. ‘Phase diagram of interacting spinless fermions on the honeycomb lattice’. In: *Journal of Physics: Condensed Matter* 29 (2017), p. 043002 (cited on page 43).
- [174] Marianne Heilmann, Tobias Hellwig, Benjamin Knorr, Marcus Ansorg, and Andreas Wipf. ‘Convergence of Derivative Expansion in Supersymmetric Functional RG Flows’. In: *JHEP* 02 (2015), p. 109. doi: 10.1007/JHEP02(2015)109 (cited on page 44).
- [175] Holger Gies, Franziska Synatschke, and Andreas Wipf. ‘Supersymmetry breaking as a quantum phase transition’. In: *Phys. Rev. D* 80 (2009), p. 101701. doi: 10.1103/PhysRevD.80.101701 (cited on page 44).
- [176] Filip Kos, David Poland, David Simmons-Duffin, and Alessandro Vichi. ‘Precision Islands in the Ising and  $O(N)$  Models’. In: *JHEP* 08 (2016), p. 036. doi: 10.1007/JHEP08(2016)036 (cited on page 45).
- [177] Francesco Parisen Toldin, Martin Hohenadler, Fakhher F. Assaad, and Igor F. Herbut. ‘Fermionic quantum criticality in honeycomb and  $\pi$ -flux Hubbard models: Finite-size scaling of renormalization-group-invariant observables from quantum Monte Carlo’. In: *Phys. Rev. B* 91 (16 Apr. 2015), p. 165108. doi: 10.1103/PhysRevB.91.165108 (cited on page 47).
- [178] Yi-Fan Jiang, Zi-Xiang Li, Steven A. Kivelson, and Hong Yao. ‘Charge- $4e$  superconductors: A Majorana quantum Monte Carlo study’. In: *Phys. Rev. B* 95 (24 June 2017), p. 241103. doi: 10.1103/PhysRevB.95.241103 (cited on page 47).

- [179] Shuai Yin and Zhi Yao Zuo. ‘Fermion-induced quantum critical point in the Landau-Devonshire model’. In: *Phys. Rev. B* 101 (2020), p. 155136. doi: 10.1103/PhysRevB.101.155136 (cited on page 47).
- [180] Michael Schuler, Stephan Hesselmann, Seth Whitsitt, Thomas C. Lang, Stefan Wessel, and Andreas M. Läuchli. ‘Torus Spectroscopy of the Gross-Neveu-Yukawa Quantum Field Theory: Free Dirac versus Chiral Ising Fixed Point’. In: *arXiv* (2019) (cited on pages 47, 112).
- [181] Michael Schuler, Seth Whitsitt, Louis-Paul Henry, Subir Sachdev, and Andreas M. Läuchli. ‘Universal Signatures of Quantum Critical Points from Finite-Size Torus Spectra: A Window into the Operator Content of Higher-Dimensional Conformal Field Theories’. In: *Phys. Rev. Lett.* 117 (21 Nov. 2016), p. 210401. doi: 10.1103/PhysRevLett.117.210401 (cited on page 47).
- [182] Seth Whitsitt, Michael Schuler, Louis-Paul Henry, Andreas M. Läuchli, and Subir Sachdev. ‘Spectrum of the Wilson-Fisher conformal field theory on the torus’. In: *Phys. Rev. B* 96 (3 July 2017), p. 035142. doi: 10.1103/PhysRevB.96.035142 (cited on page 47).
- [183] Cenke Xu and Leon Balents. ‘Topological Superconductivity in Twisted Multilayer Graphene’. In: *Phys. Rev. Lett.* 121 (2018), p. 087001. doi: 10.1103/PhysRevLett.121.087001 (cited on page 47).
- [184] Noah F.Q. Yuan and Liang Fu. ‘Model for the metal-insulator transition in graphene superlattices and beyond’. In: *Phys. Rev. B* 98 (2018), p. 045103. doi: 10.1103/PhysRevB.98.045103 (cited on page 47).
- [185] Hoi Chun Po, Liujun Zou, Ashvin Vishwanath, and T. Senthil. ‘Origin of Mott Insulating Behavior and Superconductivity in Twisted Bilayer Graphene’. In: *Phys. Rev. X* 8 (2018), p. 031089. doi: 10.1103/PhysRevX.8.031089 (cited on page 47).
- [186] Huaiming Guo, Xingchuan Zhu, Shiping Feng, and Richard T. Scalettar. ‘Pairing symmetry of interacting fermions on a twisted bilayer graphene superlattice’. In: *Phys. Rev. B* 97 (2018), p. 235453. doi: 10.1103/PhysRevB.97.235453 (cited on page 47).
- [187] J. F. Dodaro, S. A. Kivelson, Y. Schattner, X. Q. Sun, and C. Wang. ‘Phases of a phenomenological model of twisted bilayer graphene’. In: 98 (2018), p. 075154. doi: 10.1103/PhysRevB.98.075154 (cited on page 47).
- [188] Emilio Torres, Laura Classen, Igor F. Herbut, and Michael M. Scherer. ‘Fermion-induced quantum criticality with two length scales in Dirac systems’. In: *Phys. Rev. B* 97 (12 Mar. 2018), p. 125137. doi: 10.1103/PhysRevB.97.125137 (cited on pages 49, 105).
- [189] Lucile Savary and Leon Balents. ‘Quantum spin liquids: A review’. In: *Reports Prog. Phys.* 80 (2017), p. 016502. doi: 10.1088/0034-4885/80/1/016502 (cited on page 49).
- [190] Lukas Janssen, Igor F. Herbut, and Michael M. Scherer. ‘Compatible orders and fermion-induced emergent symmetry in Dirac systems’. In: *Phys. Rev. B* 97 (2018), p. 041117. doi: 10.1103/PhysRevB.97.041117 (cited on page 50).
- [191] C. Lacroix, P. Mendels, and F. Mila. *Introduction to Frustrated Magnetism*. Ed. by Claudine Lacroix, Philippe Mendels, and Frédéric Mila. Vol. 164. Springer Series in Solid-State Sciences. Berlin, Heidelberg: Springer Berlin Heidelberg, 2011, pp. 293–326 (cited on page 50).
- [192] Tom Kennedy, Elliott H. Lieb, and Hal Tasaki. ‘A Two-Dimensional Isotropic Quantum Antiferromagnet with Unique Disordered Ground State’. In: *J. Stat. Phys.* 53 (1988), pp. 383–415. doi: 10.1007/BF01011563 (cited on page 50).
- [193] Tom Kennedy, Elliott H. Lieb, and B. Sriram Shastry. ‘Existence of Néel order in some spin-1/2 Heisenberg antiferromagnets’. In: *J. Stat. Phys.* 53 (1988), pp. 1019–1030. doi: 10.1007/BF01023854 (cited on page 50).
- [194] David A. Huse and Veit Elser. ‘Simple Variational Wave Functions for Two-Dimensional Heisenberg Spin-1/2 Antiferromagnets’. In: *Phys. Rev. Lett.* 60 (1988), pp. 2531–2534. doi: 10.1103/PhysRevLett.60.2531 (cited on page 50).
- [195] Ute Löw. ‘Néel order in the two-dimensional  $S = 1/2$  Heisenberg model’. In: *Phys. Rev. B* 76 (2007), p. 220409. doi: 10.1103/PhysRevB.76.220409 (cited on page 50).

- [196] Jie Lou, Anders W. Sandvik, and Naoki Kawashima. ‘Antiferromagnetic to valence-bond-solid transitions in two-dimensional  $SU(N)$  Heisenberg models with multispin interactions’. In: *Phys. Rev. B* 80 (2009), p. 180414. doi: 10.1103/PhysRevB.80.180414 (cited on pages 51, 52, 60, 70).
- [197] Anders W. Sandvik. ‘Finite-size scaling and boundary effects in two-dimensional valence-bond solids’. In: *Phys. Rev. B* 85 (2012), p. 134407. doi: 10.1103/PhysRevB.85.134407 (cited on page 51).
- [198] Bowen Zhao, Jun Takahashi, and Anders W. Sandvik. ‘Multicritical Deconfined Quantum Criticality and Lifshitz Point of a Helical Valence-Bond Phase’. In: *Phys. Rev. Lett.* 125 (2020), p. 257204. doi: 10.1103/PhysRevLett.125.257204 (cited on pages 51, 52, 60).
- [199] Jun Takahashi and Anders W. Sandvik. *Valence-bond solids, vestigial order, and emergent  $SO(5)$  symmetry in a two-dimensional quantum magnet*. 2020. doi: 10.1103/physrevresearch.2.033459. URL: <https://journals.aps.org/prresearch/abstract/10.1103/PhysRevResearch.2.033459> (cited on pages 51, 52, 73).
- [200] Michael Levin and T. Senthil. ‘Deconfined quantum criticality and Néel order via dimer disorder’. In: *Phys. Rev. B* 70 (2004), p. 220403. doi: 10.1103/PhysRevB.70.220403 (cited on pages 51, 54, 55).
- [201] Elliott Lieb, Theodore Schultz, and Daniel Mattis. ‘Two soluble models of an antiferromagnetic chain’. In: *Ann. Phys. (N. Y.)* 16 (1961), pp. 407–466. doi: 10.1016/0003-4916(61)90115-4 (cited on page 51).
- [202] M. B. Hastings. ‘Lieb-Schultz-Mattis in higher dimensions’. In: *Phys. Rev. B* 69 (2004), p. 104431. doi: 10.1103/PhysRevB.69.104431 (cited on page 51).
- [203] Dominik Kiese, Finn Lasse Buessen, Ciarán Hickey, Simon Trebst, and Michael M. Scherer. ‘Emergence and stability of spin-valley entangled quantum liquids in moiré heterostructures’. In: *Phys. Rev. Res.* 2 (2020), p. 013370. doi: 10.1103/PhysRevResearch.2.013370 (cited on page 51).
- [204] Ribhu K. Kaul and Anders W. Sandvik. ‘Lattice model for the  $SU(N)$  Néel to valence-bond solid quantum phase transition at large  $N$ ’. In: *Phys. Rev. Lett.* 108 (2012), p. 137201. doi: 10.1103/PhysRevLett.108.137201 (cited on pages 51, 52, 60, 77).
- [205] Yuhai Liu, Zhenjiu Wang, Toshihiro Sato, Martin Hohenadler, Chong Wang, Wenan Guo, and Fakhre F. Assaad. ‘Superconductivity from the condensation of topological defects in a quantum spin-Hall insulator’. In: *Nature Commun.* 10 (2019). doi: 10.1038/s41467-019-10372-0 (cited on page 51).
- [206] Ribhu K. Kaul. ‘Quantum criticality in  $SU(3)$  and  $SU(4)$  antiferromagnets’. In: *Phys. Rev. B* 84 (2011), p. 054407. doi: 10.1103/PhysRevB.84.054407 (cited on pages 52, 60, 70).
- [207] Sumiran Pujari, Kedar Damle, and Fabien Alet. ‘Néel-state to valence-bond-solid transition on the honeycomb lattice: Evidence for deconfined criticality’. In: *Phys. Rev. Lett.* 111 (2013), p. 087203. doi: 10.1103/PhysRevLett.111.087203 (cited on pages 52, 60, 70, 89).
- [208] Matthew S. Block, Roger G. Melko, and Ribhu K. Kaul. ‘Fate of  $\mathbb{C}P^{N-1}$  fixed points with  $q$  monopoles’. In: *Phys. Rev. Lett.* 111 (2013), p. 137202. doi: 10.1103/PhysRevLett.111.137202 (cited on pages 52, 60, 70).
- [209] Sumiran Pujari, Fabien Alet, and Kedar Damle. ‘Transitions to valence-bond solid order in a honeycomb lattice antiferromagnet’. In: *Phys. Rev. B* 91 (2015). doi: 10.1103/PhysRevB.91.104411 (cited on page 52).
- [210] Xue-Feng Zhang, Yin-Chen He, Sebastian Eggert, Roderich Moessner, and Frank Pollmann. ‘Continuous Easy-Plane Deconfined Phase Transition on the Kagome Lattice’. In: *Phys. Rev. Lett.* 120 (2018), p. 115702. doi: 10.1103/PhysRevLett.120.115702 (cited on pages 52, 57).
- [211] Anders W. Sandvik and Bowen Zhao. ‘Consistent Scaling Exponents at the Deconfined Quantum-Critical Point’. In: *Chinese Phys. Lett.* 37 (2020), p. 057502. doi: 10.1088/0256-307X/37/5/057502 (cited on pages 52, 89).
- [212] Kenji Harada, Takafumi Suzuki, Tsuyoshi Okubo, Haruhiko Matsuo, Jie Lou, Hiroshi Watanabe, Synge Todo, and Naoki Kawashima. ‘Possibility of deconfined criticality in  $SU(N)$  Heisenberg models at small  $N$ ’. In: *Phys. Rev. B* 88 (2013), p. 220408. doi: 10.1103/PhysRevB.88.220408 (cited on pages 52, 60, 70).

- [213] Stephen Powell and J. T. Chalker. ‘SU(2)-Invariant Continuum Theory for an Unconventional Phase Transition in a Three-Dimensional Classical Dimer Model’. In: *Phys. Rev. Lett.* 101 (2008), p. 155702. doi: 10.1103/PhysRevLett.101.155702 (cited on pages 52, 60, 70).
- [214] Gang Chen, Jan Gukelberger, Simon Trebst, Fabien Alet, and Leon Balents. ‘Coulomb gas transitions in three-dimensional classical dimer models’. In: *Phys. Rev. B* 80 (2009), p. 045112. doi: 10.1103/PhysRevB.80.045112 (cited on pages 52, 60, 70).
- [215] Yan Qi Qin, Yuan Yao He, Yi Zhuang You, Zhong Yi Lu, Arnab Sen, Anders W. Sandvik, Cenke Xu, and Zi Yang Meng. ‘Duality between the deconfined quantum-critical point and the bosonic topological transition’. In: *Phys. Rev. X* 7 (2017), p. 031052. doi: 10.1103/PhysRevX.7.031052 (cited on pages 52, 57).
- [216] Anders W. Sandvik. ‘Continuous quantum phase transition between an antiferromagnet and a valence-bond solid in two dimensions: Evidence for logarithmic corrections to scaling’. In: *Phys. Rev. Lett.* 104 (2010), p. 177201. doi: 10.1103/PhysRevLett.104.177201 (cited on page 52).
- [217] Nvsen Ma, Phillip Weinberg, Hui Shao, Wenan Guo, Dao-Xin Yao, and Anders W. Sandvik. ‘Anomalous Quantum-Critical Scaling Corrections in Two-Dimensional Antiferromagnets’. In: *Phys. Rev. Lett.* 121 (2018), p. 117202. doi: 10.1103/PhysRevLett.121.117202 (cited on page 52).
- [218] Adam Nahum, J. T. Chalker, P. Serna, M. Ortuño, and A. M. Somoza. ‘Deconfined Quantum Criticality, Scaling Violations, and Classical Loop Models’. In: *Phys. Rev. X* 5 (2015), p. 041048. doi: 10.1103/PhysRevX.5.041048 (cited on pages 52, 60, 68, 69, 78, 89, 90, 115).
- [219] Pablo Serna and Adam Nahum. ‘Emergence and spontaneous breaking of approximate O(4) symmetry at a weakly first-order deconfined phase transition’. In: *Phys. Rev. B* 99 (2019), p. 195110. doi: 10.1103/PhysRevB.99.195110 (cited on pages 52, 60, 90, 91).
- [220] Zi Xiang Li, Shao Kai Jian, and Hong Yao. *Deconfined quantum criticality and emergent SO(5) symmetry in fermionic systems*. 2019. URL: <http://arxiv.org/abs/1904.10975> (cited on pages 52, 73).
- [221] G. J. Sreejith, Stephen Powell, and Adam Nahum. ‘Emergent SO(5) Symmetry at the Columnar Ordering Transition in the Classical Cubic Dimer Model’. In: *Phys. Rev. Lett.* 122 (2019), p. 080601. doi: 10.1103/PhysRevLett.122.080601 (cited on pages 52, 73).
- [222] Arnab Sen. ‘Deconfined quantum critical points’. PhD thesis. 2007. doi: 10.1142/9789814704410\_0018 (cited on pages 53–55).
- [223] *The synchronized dance of skyrmion spins*. URL: <https://phys.org/news/2017-05-synchronized-skyrmion.html> (visited on 01/24/2021) (cited on page 53).
- [224] F. D.M. Haldane. ‘O(3) nonlinear model and the topological distinction between integer- and half-integer-spin antiferromagnets in two dimensions’. In: *Phys. Rev. Lett.* 61 (1988), pp. 1029–1032. doi: 10.1103/PhysRevLett.61.1029 (cited on page 53).
- [225] N. Read and Subir Sachdev. ‘Valence-bond and spin-Peierls ground states of low-dimensional quantum antiferromagnets’. In: *Phys. Rev. Lett.* 62 (1989), pp. 1694–1697. doi: 10.1103/PhysRevLett.62.1694 (cited on page 53).
- [226] N. Read and Subir Sachdev. ‘Spin-Peierls, valence-bond solid, and Néel ground states of low-dimensional quantum antiferromagnets’. In: *Phys. Rev. B* 42 (1990), pp. 4568–4589. doi: 10.1103/PhysRevB.42.4568 (cited on page 53).
- [227] Jie Lou, Anders W. Sandvik, and Leon Balents. ‘Emergence of U(1) symmetry in the 3D XY model with  $Z_q$  anisotropy’. In: *Phys. Rev. Lett.* 99 (2007), p. 207203. doi: 10.1103/PhysRevLett.99.207203 (cited on page 55).
- [228] Michael Kiometzis, Hagen Kleinert, and Adriaan M. J. Schakel. ‘Critical Exponents of the Superconducting Phase Transition’. In: *Phys. Rev. Lett.* 73 (1994), pp. 1975–1977. doi: 10.1103/PhysRevLett.73.1975 (cited on pages 55, 57, 59).
- [229] Ganpathy Murthy and Subir Sachdev. ‘Action of hedgehog instantons in the disordered phase of the (2 + 1)-dimensional CPN-1 model’. In: *Nucl. Physics, Sect. B* 344 (1990), pp. 557–595. doi: 10.1016/0550-3213(90)90670-9 (cited on page 55).

- [230] F. S. Nogueira, S. Kragset, and Asle Sudbø. ‘Quantum critical scaling behavior of deconfined spinons’. In: *Phys. Rev. B* 76 (2007), p. 220403. doi: 10.1103/PhysRevB.76.220403 (cited on pages 55, 60).
- [231] Michael E. Peskin. ‘Mandelstam-’t Hooft duality in abelian lattice models’. In: *Ann. Phys. (N. Y.)* 113 (1978), pp. 122–152. doi: 10.1016/0003-4916(78)90252-X (cited on page 57).
- [232] A. K. Nguyen and A. Sudbø. ‘Topological phase fluctuations, amplitude fluctuations, and criticality in extreme type-II superconductors’. In: *Phys. Rev. B* 60 (1999), pp. 15307–15331. doi: 10.1103/PhysRevB.60.15307 (cited on pages 57, 59).
- [233] Olexei I. Motrunich and Ashvin Vishwanath. ‘Emergent photons and transitions in the O(3) sigma model with hedgehog suppression’. In: *Phys. Rev. B - Condens. Matter Mater. Phys.* 70 (2004), p. 075104. doi: 10.1103/PhysRevB.70.075104 (cited on pages 57, 60).
- [234] Dam Thanh Son. ‘Is the composite fermion a dirac particle?’ In: *Phys. Rev. X* 5 (2015), p. 031027. doi: 10.1103/PhysRevX.5.031027 (cited on page 57).
- [235] Jason Alicea, Olexei I. Motrunich, Michael Hermele, and Matthew P.A. Fisher. ‘Criticality in quantum triangular antiferromagnets via fermionized vortices’. In: *Phys. Rev. B* 72 (2005), p. 064407. doi: 10.1103/PhysRevB.72.064407 (cited on page 57).
- [236] Andreas Karch and David Tong. ‘Particle-Vortex Duality from 3D Bosonization’. In: *Phys. Rev. X* 6 (2016), p. 031043. doi: 10.1103/PhysRevX.6.031043 (cited on page 57).
- [237] Jing Yuan Chen, Jun Ho Son, Chao Wang, and S. Raghu. ‘Exact Boson-Fermion Duality on a 3D Euclidean Lattice’. In: *Phys. Rev. Lett.* 120 (2018), p. 016602. doi: 10.1103/PhysRevLett.120.016602 (cited on page 57).
- [238] Shamit Kachru, Michael Mulligan, Gonzalo Torroba, and Huajia Wang. ‘Nonsupersymmetric Dualities from Mirror Symmetry’. In: *Phys. Rev. Lett.* 118 (2017), p. 011602. doi: 10.1103/PhysRevLett.118.011602 (cited on page 57).
- [239] Ofer Aharony. ‘Baryons, monopoles and dualities in Chern-Simons-matter theories’. In: *J. High Energy Phys.* 2016 (2016), pp. 1–16. doi: 10.1007/JHEP02(2016)093 (cited on page 57).
- [240] Michael E. Peskin and Daniel V. Schroeder. *An Introduction to Quantum Field Theory*. CRC Press, 2018 (cited on page 59).
- [241] P. W. Anderson. ‘Plasmons, gauge invariance, and mass’. In: *Phys. Rev.* 130 (1963), pp. 439–442. doi: 10.1103/PhysRev.130.439 (cited on page 59).
- [242] F. Englert and R. Brout. ‘Broken Symmetry and the Mass of Gauge Vector Mesons’. In: *Phys. Rev. Lett.* 13 (1964), pp. 321–323. doi: 10.1103/PhysRevLett.13.321 (cited on page 59).
- [243] Peter W. Higgs. ‘Broken symmetries and the masses of gauge bosons’. In: *Phys. Rev. Lett.* 13 (1964), pp. 508–509. doi: 10.1103/PhysRevLett.13.508 (cited on page 59).
- [244] G. S. Guralnik, C. R. Hagen, and T. W.B. Kibble. ‘Global conservation laws and massless particles’. In: *Phys. Rev. Lett.* 13 (1964), pp. 585–587. doi: 10.1103/PhysRevLett.13.585 (cited on page 59).
- [245] John Bartholomew. ‘Phase structure of a lattice superconductor’. In: *Phys. Rev. B* 28 (1983), pp. 5378–5381. doi: 10.1103/PhysRevB.28.5378 (cited on page 59).
- [246] B. I. Halperin, T. C. Lubensky, and Shang-keng Ma. ‘First-Order Phase Transitions in Superconductors and Smectic- A Liquid Crystals’. In: *Phys. Rev. Lett.* 32 (1974), pp. 292–295. doi: 10.1103/PhysRevLett.32.292 (cited on pages 59–61, 65, 76, 90).
- [247] S. Kolnberger and R. Folk. ‘Critical fluctuations in superconductors’. In: *Phys. Rev. B* 41 (1990), pp. 4083–4088. doi: 10.1103/PhysRevB.41.4083 (cited on pages 59, 63).
- [248] L. Radzihovsky. ‘Self-consistent theory of normal-to-superconducting transition’. In: *EPL* 29 (1995), pp. 227–232. doi: 10.1209/0295-5075/29/3/007 (cited on page 59).
- [249] Igor F. Herbut and Zlatko Tešanović. ‘Critical Fluctuations in Superconductors and the Magnetic Field Penetration Depth’. In: *Phys. Rev. Lett.* 76 (1996), p. 4588. doi: 10.1103/PhysRevLett.76.4588 (cited on pages 59, 60).



- [250] Igor F. Herbut and Zlatko Tešanović. ‘Herbut and Tešanović Reply’. In: *Phys. Rev. Lett.* 78 (1997), p. 980. doi: 10.1103/PhysRevLett.78.980 (cited on pages 59, 60).
- [251] Ian D. Lawrie and C. Athrone. ‘Phase transitions in nonlinear Abelian Higgs models’. In: *J. Phys. A. Math. Gen.* 16 (1983), pp. L587–L590. doi: 10.1088/0305-4470/16/15/007 (cited on page 59).
- [252] Ian D. Lawrie. ‘Comment on “Critical Fluctuations in Superconductors and the Magnetic Field Penetration Depth”’. In: *Phys. Rev. Lett.* 78 (1997), pp. 979–979. doi: 10.1103/PhysRevLett.78.979 (cited on page 59).
- [253] B. Bergerhoff, F. Freire, D. F. Litim, S. Lola, and C. Wetterich. ‘Phase diagram of superconductors from nonperturbative flow equations’. In: *Phys. Rev. B* 53 (1996), pp. 5734–5757. doi: 10.1103/PhysRevB.53.5734 (cited on pages 59, 71).
- [254] Lorenz Bartosch. ‘Corrections to scaling in the critical theory of deconfined criticality’. In: *Phys. Rev. B* 88 (2013), p. 195140. doi: 10.1103/PhysRevB.88.195140 (cited on pages 59, 71, 89).
- [255] G. Fejos and T. Hatsuda. ‘Renormalization group flows of the N-component Abelian Higgs model’. In: *Phys. Rev. D* 96 (2017), p. 056018. doi: 10.1103/PhysRevD.96.056018 (cited on pages 59, 71).
- [256] Yu Nakayama and Tomoki Ohtsuki. ‘Necessary Condition for Emergent Symmetry from the Conformal Bootstrap’. In: *Phys. Rev. Lett.* 117 (2016). doi: 10.1103/PhysRevLett.117.131601 (cited on page 60).
- [257] D. Charrier, F. Alet, and P. Pujol. ‘Gauge Theory Picture of an Ordering Transition in a Dimer Model’. In: *Phys. Rev. Lett.* 101 (2008), p. 167205. doi: 10.1103/PhysRevLett.101.167205 (cited on pages 60, 70).
- [258] Victor Gorbenko, Slava Rychkov, and Bernardo Zan. ‘Walking, weak first-order transitions, and complex CFTs’. In: *J. High Energy Phys.* 2018 (2018), p. 108. doi: 10.1007/JHEP10(2018)108 (cited on page 60).
- [259] K.-I. Kubota and H. Terao. ‘Dynamical Symmetry Breaking in QED3 from the Wilson RG Point of View’. In: *Prog. Theor. Phys.* 105 (2001), pp. 809–825. doi: 10.1143/PTP.105.809 (cited on page 60).
- [260] Kamran Kaveh and Igor F. Herbut. ‘Chiral symmetry breaking in three-dimensional quantum electrodynamics in the presence of irrelevant interactions: A renormalization group study’. In: *Phys. Rev. B* 71 (2005), p. 184519. doi: 10.1103/PhysRevB.71.184519 (cited on page 60).
- [261] David B Kaplan, Jong-Wan Lee, Dam T Son, and Mikhail A Stephanov. ‘Conformality lost’. In: *Phys. Rev. D* 80 (2009), p. 125005. doi: 10.1103/PhysRevD.80.125005 (cited on pages 60, 69, 90).
- [262] Holger Gies and Jörg Jaeckel. ‘Chiral phase structure of QCD with many flavors’. In: *Eur. Phys. J. C* 46 (2006), pp. 433–438. doi: 10.1140/epj c/s2006-02475-0 (cited on pages 60, 69, 90).
- [263] Igor F. Herbut and Lukas Janssen. ‘Topological Mott Insulator in Three-Dimensional Systems with Quadratic Band Touching’. In: *Phys. Rev. Lett.* 113 (2014), p. 106401. doi: 10.1103/PhysRevLett.113.106401 (cited on page 60).
- [264] Igor F. Herbut. ‘Chiral symmetry breaking in three-dimensional quantum electrodynamics as fixed point annihilation’. In: *Phys. Rev. D* 94 (2016), p. 025036. doi: 10.1103/PhysRevD.94.025036 (cited on pages 60, 90).
- [265] John A. Gracey, Igor F. Herbut, and Dietrich Roscher. ‘Tensor  $O(N)$  model near six dimensions: Fixed points and conformal windows from four loops’. In: *Phys. Rev. D* 98 (2018), p. 096014. doi: 10.1103/PhysRevD.98.096014 (cited on page 60).
- [266] Lev Davidovich Landau and V L Ginzburg. ‘On the theory of superconductivity’. In: *Zh. Eksp. Teor. Fiz.* 20 (1950), p. 1064 (cited on page 61).
- [267] S. Hikami. ‘Renormalization Group Functions of  $CP^{N-1}$  Non-Linear-Model and  $N$ -Component Scalar QED Model’. In: *Prog. Theor. Phys.* 62 (1979), pp. 226–233. doi: 10.1143/ptp.62.226 (cited on pages 61, 67).
- [268] John March-Russell. ‘On the possibility of second-order phase transitions in spontaneously broken gauge theories’. In: *Phys. Lett. B* 296 (1992), pp. 364–370. doi: 10.1016/0370-2693(92)91333-5 (cited on pages 61, 62, 67).

- [269] S. Hikami. ‘Three-loop  $\beta$ -functions of non-linear  $\sigma$  models on symmetric spaces’. In: *Phys. Lett. B* 98 (1981), pp. 208–210. doi: 10.1016/0370-2693(81)90989-8 (cited on page 61).
- [270] S. Hikami. ‘Isomorphism and the  $\beta$ -function of the non-linear  $\sigma$  model in symmetric spaces’. In: *Nucl. Physics, Sect. B* 215 (1983), pp. 555–565. doi: 10.1016/0550-3213(83)90260-2 (cited on page 61).
- [271] Franz Wegner. ‘Four-loop-order  $\beta$ -function of nonlinear  $\sigma$ -models in symmetric spaces’. In: *Nucl. Physics, Sect. B* 316 (1989), pp. 663–678. doi: 10.1016/0550-3213(89)90063-1 (cited on page 61).
- [272] S. Hikami. ‘Non-Linear Model of Grassmann Manifold and Non-Abelian Gauge Field with Scalar Coupling’. In: *Prog. Theor. Phys.* 64 (1980), pp. 1425–1434. doi: 10.1143/PTP.64.1425 (cited on page 62).
- [273] Igor V. Lerner and Franz Wegner. ‘High-gradient operators of the unitary matrix-model’. In: *Zeitschrift für Phys. B Condens. Matter* 81 (1990), pp. 95–97. doi: 10.1007/BF01454219 (cited on page 67).
- [274] Guillermo E. Castilla and Sudip Chakravarty. ‘Instability of the fixed point of the  $O(N)$  nonlinear  $\sigma$ -model in  $(2 + \epsilon)$  dimensions’. In: *Phys. Rev. Lett.* 71 (1993), pp. 384–387. doi: 10.1103/PhysRevLett.71.384 (cited on page 67).
- [275] E. Brézin and S. Hikami. ‘Irrelevance in the  $(d - 2)$  expansion of nonlinear  $\sigma$  and Heisenberg models’. In: *Phys. Rev. B* 55 (1997), R10169–R10172. doi: 10.1103/PhysRevB.55.R10169 (cited on page 67).
- [276] Jens Braun, Christian S. Fischer, and Holger Gies. ‘Beyond Miransky scaling’. In: *Phys. Rev. D* 84 (2011), p. 034045. doi: 10.1103/PhysRevD.84.034045 (cited on page 70).
- [277] R. Folk and Yu. Holovatch. ‘Critical Fluctuations in Normal-to-Superconducting Transition’. In: *Correl. Coherence, Order*. Boston, MA: Springer US, 1999, pp. 83–116. doi: 10.1007/978-1-4615-4727-3\_3 (cited on page 71).
- [278] G. Fejos and T. Hatsuda. ‘Fixed point structure of the Abelian Higgs model’. In: *Phys. Rev. D* 93 (2016), pp. 1–5. doi: 10.1103/PhysRevD.93.121701 (cited on page 71).
- [279] Lukas Janssen and Yin-Chen He. ‘Critical behavior of the QED<sub>3</sub>-Gross-Neveu model: duality and deconfined criticality’. In: *Phys. Rev. B* 96 (Nov. 2017), p. 205113. doi: 10.1103/PhysRevB.96.205113 (cited on pages 73, 75, 81–83, 89, 116, 144).
- [280] F. D. M. Haldane. ‘Model for a quantum hall effect without landau levels: Condensed-matter realization of the “Parity Anomaly”’. In: *Phys. Rev. Lett.* 61 (1988), pp. 2015–2018. doi: 10.1103/PhysRevLett.61.2015 (cited on page 74).
- [281] Friedrich Gehring, Holger Gies, and Lukas Janssen. ‘Fixed-point structure of low-dimensional relativistic fermion field theories: Universality classes and emergent symmetry’. In: *Phys. Rev. D* 92 (2015), p. 085046. doi: 10.1103/PhysRevD.92.085046 (cited on pages 75, 96).
- [282] Holger Gies and Lukas Janssen. ‘UV fixed-point structure of the three-dimensional Thirring model’. In: *Phys. Rev. D* 82 (Oct. 2010), p. 085018. doi: 10.1103/PhysRevD.82.085018 (cited on page 75).
- [283] Lorenzo Di Pietro, Zohar Komargodski, Itamar Shamir, and Emmanuel Stamou. ‘Quantum electrodynamics in  $d = 3$  from the  $\epsilon$  expansion’. In: *Phys. Rev. Lett.* 116 (Apr. 2016), p. 131601. doi: 10.1103/PhysRevLett.116.131601 (cited on pages 75, 82).
- [284] John A. Gracey. ‘Critical point analysis of various fermionic field theories in the large  $N$  expansion’. In: *J. Phys. A. Math. Gen.* 25 (1992), pp. 109–122. doi: 10.1088/0305-4470/25/3/005 (cited on pages 76, 86).
- [285] John A. Gracey. ‘Gauge independent critical exponents for QED coupled to a four fermi interaction with and without a chern simons term’. In: *Ann. Phys.* 224 (June 1993), pp. 275–300. doi: 10.1006/aphy.1993.1047 (cited on pages 76, 86, 87, 90).
- [286] John A. Gracey. ‘Analysis of Abelian gauge theory with four-Fermi interaction at  $\mathcal{O}(1/N^2)$  in arbitrary dimensions’. In: *J. Phys. A Gen. Phys.* 26 (1993), pp. 1431–1440. doi: 10.1088/0305-4470/26/6/024 (cited on pages 76, 86).
- [287] V. Yu Irkhin, A. Katanin, and M. Katsnelson. ‘ $1/N$  expansion for critical exponents of magnetic phase transitions in the model for  $2 < d < 4$ ’. In: *Phys. Rev. B* 54 (Nov. 1996), pp. 11953–11956. doi: 10.1103/PhysRevB.54.11953 (cited on page 76).

- [288] Ribhu K. Kaul and Subir Sachdev. ‘Quantum criticality of U(1) gauge theories with fermionic and bosonic matter in two spatial dimensions’. In: *Phys. Rev. B* 77 (2008), pp. 1–14. doi: 10.1103/PhysRevB.77.155105 (cited on pages 76, 77).
- [289] Ethan Dyer, Márk Mezei, Silviu S. Pufu, and Subir Sachdev. ‘Scaling dimensions of monopole operators in the  $CP^{N_b-1}$  theory in 2 + 1 dimensions’. In: *J. High Energy Phys.* 6 (June 2015). [Erratum: *ibid.* 03 (2016) 111], p. 37. doi: 10.1007/JHEP06(2015)037 (cited on page 77).
- [290] N. K. Nielsen and Bert Schroer. ‘Axial anomaly and Atiyah-Singer theorem’. In: *Nucl. Phys. B* 127 (1977), pp. 493–508. doi: 10.1016/0550-3213(77)90453-9 (cited on page 77).
- [291] S.G. Gorishny, A.L. Kataev, and S.A. Larin. ‘The three-loop QED photon vacuum polarization function in the  $\overline{MS}$ -scheme and the four-loop QED  $\beta$ -function in the on-shell scheme’. In: *Phys. Lett. B* 273 (1991), pp. 141–144. doi: 10.1016/0370-2693(91)90568-B (cited on pages 81, 82).
- [292] John A. Gracey. ‘Three-loop  $\overline{MS}$  renormalization of QED in the ‘t Hooft–Veltman gauge’. In: *J. Phys. A* 40 (2007), pp. 13989–13996. doi: 10.1088/1751-8113/40/46/011 (cited on pages 81, 82, 143).
- [293] Nikolai Zerf, Chien-Hung Lin, and Joseph Maciejko. ‘Superconducting quantum criticality of topological surface states at three loops’. In: *Phys. Rev. B* 94 (2016), p. 205106. doi: 10.1103/PhysRevB.94.205106 (cited on page 81).
- [294] John A. Gracey. ‘Three loop  $\overline{MS}$  tensor current anomalous dimension in QCD’. In: *Phys. Lett. B* 488 (2000), pp. 175–181. doi: 10.1016/S0370-2693(00)00859-5 (cited on page 82).
- [295] Robert D. Pisarski. ‘Chiral-symmetry breaking in three-dimensional electrodynamics’. In: *Phys. Rev. D* 29 (1984), pp. 2423–2426. doi: 10.1103/PhysRevD.29.2423 (cited on page 86).
- [296] Lukas Janssen. ‘Spontaneous breaking of Lorentz symmetry in  $(2 + \epsilon)$ -dimensional QED’. In: *Phys. Rev. D* 94 (2016), p. 094013. doi: 10.1103/PhysRevD.94.094013 (cited on pages 86, 90).
- [297] V P Gusynin and P K Pyatkovskiy. ‘Critical number of fermions in three-dimensional QED’. In: *Phys. Rev. D* 94 (2016), p. 125009. doi: 10.1103/PhysRevD.94.125009 (cited on page 86).
- [298] Nikolai Zerf, Peter Marquard, Rufus Boyack, and Joseph Maciejko. ‘Critical behavior of the QED<sub>3</sub>-Gross-Neveu-Yukawa model at four loops’. In: *Phys. Rev. B* 98 (2018), p. 165125. doi: 10.1103/PhysRevB.98.165125 (cited on pages 89, 91).
- [299] Jens Braun, Holger Gies, Lukas Janssen, and Dietrich Roscher. ‘Phase structure of many-flavor QED<sub>3</sub>’. In: *Phys. Rev. D* 90 (2014), p. 036002. doi: 10.1103/PhysRevD.90.036002 (cited on page 90).
- [300] Lukas Janssen and Igor F Herbut. ‘Phase diagram of electronic systems with quadratic Fermi nodes in  $2 < d < 4$ :  $2 + \epsilon$  expansion,  $4 - \epsilon$  expansion, and functional renormalization group’. In: *Phys. Rev. B* 95 (2017), p. 075101. doi: 10.1103/PhysRevB.95.075101 (cited on pages 90, 105).
- [301] Dietrich Roscher and Igor F Herbut. ‘Critical O(2) field theory near six dimensions beyond one loop’. In: *Phys. Rev. D* 97 (2018), p. 116019. doi: 10.1103/PhysRevD.97.116019 (cited on page 90).
- [302] Héctor Mera, Thomas G. Pedersen, and Branislav K. Nikolić. ‘Fast summation of divergent series and resurgent transseries from Meijer-G approximants’. In: *Phys. Rev. D* 97 (2018), p. 105027. doi: 10.1103/PhysRevD.97.105027 (cited on page 91).
- [303] Rufus Boyack, Ahmed Rayyan, and Joseph Maciejko. ‘Deconfined criticality in the QED<sub>3</sub>-Gross-Neveu-Yukawa model: The  $1/N$  expansion revisited’. In: *Phys. Rev. B* 99 (2019), p. 195135. doi: 10.1103/PhysRevB.99.195135 (cited on pages 91, 96, 116).
- [304] Rufus Boyack and Joseph Maciejko. ‘Critical exponents for the valence-bond-solid transition in lattice quantum electrodynamics’. In: (Nov. 2019) (cited on page 91).
- [305] Lukas Janssen, Wei Wang, Michael M. Scherer, Zi Yang Meng, and Xiao Yan Xu. ‘Confinement transition in the QED<sub>3</sub>-Gross-Neveu-XY universality class’. In: *Phys. Rev. B* 101 (2020), p. 235118. doi: 10.1103/PhysRevB.101.235118 (cited on page 91).
- [306] Nikolai Zerf, Rufus Boyack, Peter Marquard, John A. Gracey, and Joseph Maciejko. ‘Critical properties of the valence-bond-solid transition in lattice quantum electrodynamics’. In: *Phys. Rev. D* 101 (2020), p. 094505. doi: 10.1103/PhysRevD.101.094505 (cited on page 91).

- [307] Nikolai Zerf, Rufus Boyack, Peter Marquard, John A. Gracey, and Joseph Maciejko. ‘Critical properties of the Néel–algebraic-spin-liquid transition’. In: *Phys. Rev. B* 100 (2019), p. 235130. doi: 10.1103/PhysRevB.100.235130 (cited on page 91).
- [308] Michael Schuler, Seth Whitsitt, Louis Paul Henry, Subir Sachdev, and Andreas M. Läuchli. ‘Universal signatures of quantum critical points from finite-size torus spectra: A window into the operator content of higher-dimensional conformal field theories’. In: *Phys. Rev. Lett.* 117 (2016), p. 210401. doi: 10.1103/PhysRevLett.117.210401 (cited on page 93).
- [309] Andrey V. Chubukov, Subir Sachdev, and T. Senthil. ‘Quantum phase transitions in frustrated quantum antiferromagnets’. In: *Nucl. Physics, Sect. B* 426 (1994), pp. 601–643. doi: 10.1016/0550-3213(94)90023-X (cited on page 93).
- [310] Alexei Kitaev. ‘Anyons in an exactly solved model and beyond’. In: *Ann. Phys. (N. Y.)* 321 (2006), pp. 2–111. doi: 10.1016/j.aop.2005.10.005 (cited on page 94).
- [311] Sreejith Chulliparambil, Urban F. P. Seifert, Matthias Vojta, Lukas Janssen, and Hong-Hao Tu. ‘Microscopic models for Kitaev’s sixteenfold way of anyon theories’. In: *Phys. Rev. B* 102 (2020), p. 201111. doi: 10.1103/PhysRevB.102.201111 (cited on page 94).
- [312] A. N. Vasil’ev, Yu. M. Pis’mak, and Yu. R. Khonkonen. ‘ $1/n$  Expansion: Calculation of the exponents  $\eta$  and  $\nu$  in the order  $1/n^2$  for arbitrary number of dimensions’. In: *Theor. Math. Phys.* 47 (1981), pp. 465–475. doi: 10.1007/BF01019296 (cited on pages 95, 100, 101).
- [313] G. Parisi. ‘On self-consistency conditions in conformal covariant field theory’. In: *Lett. Al Nuovo Cim.* 4 (1972), pp. 777–780. doi: 10.1007/BF02757039 (cited on pages 95, 102).
- [314] A. N. Vasil’ev, Yu M. Pis’mak, and Yu R. Khonkonen. ‘ $1/n$  Expansion: Calculation of the exponent  $\nu$  in the order  $1/n^3$  by the Conformal Bootstrap Method’. In: *Theor. Math. Phys.* 50 (1982), pp. 127–134. doi: 10.1007/BF01015292 (cited on pages 95, 100, 102, 147).
- [315] Simon Hands, Aleksandar Kocić, and John B. Kogut. ‘Four-fermi theories in fewer than four dimensions’. In: *Ann. Phys.* 224 (1993), pp. 29–89. doi: 10.1006/aphy.1993.1039 (cited on page 95).
- [316] Anna Hasenfratz and Peter Hasenfratz. ‘The equivalence of the SU(N) Yang-Mills theory with a purely fermionic model’. In: *Phys. Lett. B* 297 (1992), pp. 166–170. doi: 10.1016/0370-2693(92)91086-0 (cited on page 100).
- [317] A.M. Polyakov. ‘Conformal Symmetry of Critical Fluctuations’. In: *JETP Lett.* 12 (1970), p. 381 (cited on page 102).
- [318] M. D’eramo, L. Peliti, and G. Parisi. ‘Theoretical predictions for critical exponents at the  $\lambda$ -point of bose liquids’. In: *Lett. Al Nuovo Cim.* 2 (1971), pp. 878–880. doi: 10.1007/BF02774121 (cited on page 102).
- [319] L. Rosa, P. Vitale, and C. Wetterich. ‘Critical exponents of the Gross-Neveu model from the effective average action’. In: *Phys. Rev. Lett.* 86 (2001), pp. 958–961. doi: 10.1103/PhysRevLett.86.958 (cited on page 105).
- [320] F. Hofling, C. Nowak, and C. Wetterich. ‘Phase transition and critical behavior of the  $D = 3$  Gross-Neveu model’. In: *Phys. Rev. B* 66 (2002), p. 205111. doi: 10.1103/PhysRevB.66.205111 (cited on pages 105, 110).
- [321] Holger Gies, Lukas Janssen, Stefan Rechenberger, and Michael M. Scherer. ‘Phase transition and critical behavior of  $d=3$  chiral fermion models with left-right asymmetry’. In: *Phys. Rev. D* 81 (2010), p. 025009. doi: 10.1103/PhysRevD.81.025009 (cited on page 105).
- [322] Jens Braun, Holger Gies, and Daniel D. Scherer. ‘Asymptotic safety: A simple example’. In: *Phys. Rev. D* 83 (2011), pp. 1–15. doi: 10.1103/PhysRevD.83.085012 (cited on pages 105, 110).
- [323] Daniel D. Scherer, Jens Braun, and Holger Gies. ‘Many-flavor phase diagram of the  $(2 + 1)d$  Gross-Neveu model at finite temperature’. In: *J. Phys. A Math. Theor.* 46 (2013), p. 23. doi: 10.1088/1751-8113/46/28/285002 (cited on page 105).
- [324] Lukas Janssen and Holger Gies. ‘Critical behavior of the  $(2+1)$ -dimensional Thirring model’. In: *Phys. Rev. D* 86 (2012), p. 105007. doi: 10.1103/PhysRevD.86.105007 (cited on pages 105, 108, 109).

- [325] Daniel F. Litim and Lautaro Vergara. ‘Subleading critical exponents from the renormalisation group’. In: *Phys. Lett. Sect. B* 581 (2004), pp. 263–269. doi: 10.1016/j.physletb.2003.11.047 (cited on page 106).
- [326] Christian S. Fischer and Holger Gies. ‘Renormalization flow of Yang-Mills propagators’. In: *J. High Energy Phys.* 8 (2004), pp. 1043–1073. doi: 10.1088/1126-6708/2004/10/048 (cited on page 106).
- [327] Pedrag Cvitanovic. ‘Group theory for Feynman diagrams in non-Abelian gauge theories’. In: *Phys. Rev. D* 14 (1976) (cited on pages 120, 122, 127, 133).
- [328] Pedrag Cvitanovic. *Group Theory - Birdtracks, Lie’s and Exceptional Groups*. 2008 (cited on pages 120, 122).
- [329] T. van Ritbergen, A. N. Schellekens, and J. A. M. Vermaseren. ‘Group theory factors for Feynman diagrams’. In: *Int. J. Mod. Phys. A* 14 (1999), pp. 41–96. doi: 10.1142/S0217751X99000038 (cited on pages 121, 133).
- [330] T. van Ritbergen, J. A. M. Vermaseren, and S. A. Larin. ‘The four-loop beta-function in Quantum Chromodynamics’. In: *Phys. Lett. B* 400 (1997), pp. 379–384. doi: 10.1016/S0370-2693(97)00370-5 (cited on page 127).
- [331] M Czakon. ‘The four-loop QCD  $\beta$ -function and anomalous dimensions’. In: *Nucl. Phys. B* 710 (2005), pp. 485–498. doi: 10.1016/j.nuclphysb.2005.01.012 (cited on pages 129, 136).
- [332] J. G. D. Luna. ‘Aspects of Quantum Field Theory and Number Theory’. PhD thesis. 2015 (cited on page 129).
- [333] Ivan Todorov. ‘Perturbative Quantum Field Theory Meets Number Theory’. In: *Springer Proc. Math. Stat.* Vol. 314. 2020, pp. 1–28. doi: 10.1007/978-3-030-37031-2\_1 (cited on page 129).
- [334] K. G. Chetyrkin and F. V. Tkachov. ‘Integration by parts: The algorithm to calculate  $\beta$ -functions in 4 loops’. In: *Nucl. Physics, Sect. B* 192 (1981), pp. 159–204. doi: 10.1016/0550-3213(81)90199-1 (cited on pages 129, 130).
- [335] T. Seidensticker. ‘Automatic application of successive asymptotic expansions of Feynman diagrams’. In: *arXiv hep-ph/9905298* (1999), p. 5 (cited on page 130).
- [336] R. Harlander and Matthias Steinhauser. ‘Automatic computation of Feynman diagrams’. In: *Prog. Part. Nucl. Phys.* 43 (1999), pp. 167–228. doi: 10.1016/S0146-6410(99)00095-2 (cited on pages 130, 131).
- [337] V.A. Smirnov. ‘Asymptotic Expansions in Momenta and Masses and Calculation of Feynman Diagrams’. In: *Mod. Phys. Lett. A* 10 (1995), pp. 1485–1499. doi: 10.1142/s0217732395001617 (cited on pages 131, 132).
- [338] J. A. M. Vermaseren. ‘New features of FORM’. In: *arXiv math-ph/0010025* (Oct. 2000), p. 23 (cited on page 133).
- [339] J. Kuipers, T. Ueda, J. A. M. Vermaseren, and J. Vollinga. ‘FORM version 4.0’. In: *Comput. Phys. Commun.* 184 (2013), pp. 1453–1467. doi: 10.1016/j.cpc.2012.12.028 (cited on page 133).
- [340] Ben Ruijl, Takahiro Ueda, and Jos Vermaseren. ‘FORM version 4.2’. In: *arXiv 1707.06453* (July 2017) (cited on page 133).
- [341] P. Nogueira. ‘Automatic Feynman Graph Generation’. In: *J. Comput. Phys.* 105 (1993), pp. 279–289. doi: 10.1006/jcph.1993.1074 (cited on pages 133, 134).
- [342] P. Nogueira. ‘Abusing QGRAF’. In: *Nucl. Instruments Methods Phys. Res. Sect. A Accel. Spectrometers, Detect. Assoc. Equip.* 559 (2006), pp. 220–223. doi: 10.1016/j.nima.2005.11.151 (cited on page 133).
- [343] R. Harlander, T. Seidensticker, and M. Steinhauser. ‘Complete Corrections of  $O(\alpha_s)$  to the Decay of the Z Boson into Bottom Quarks’. In: December (1997). doi: 10.1016/S0370-2693(98)00220-2 (cited on page 134).
- [344] P. Marquard and D. Seidel. ‘unpublished’. In: () (cited on page 136).
- [345] Matthias Steinhauser. ‘MATAD: a program package for the computation of MAssive TADpoles’. In: *Comput. Phys. Commun.* 134 (2001), pp. 335–364. doi: 10.1016/S0010-4655(00)00204-6 (cited on page 136).

- [346] S. G. Gorishny, S. A. Larin, L. R. Surguladze, and F. V. Tkachov. 'Mincer: Program for multiloop calculations in quantum field theory for the Schoonschip system'. In: *Comput. Phys. Commun.* 55 (1989), pp. 381–408. doi: 10.1016/0010-4655(89)90134-3 (cited on page 136).
- [347] S. A. Larin, F. V. Tkachov, and J. A. M. Vermaseren. 'The FORM version of MINCER'. In: NIKHEF-H-91-18 (1991) (cited on page 136).
- [348] S. Laporta. 'High-precision calculation of multi-loop Feynman integrals by difference equations'. In: *Int. J. Mod. Phys. A* 15 (2001), p. 5087. doi: 10.1016/S0217-751X(00)00215-7 (cited on page 136).
- [349] D. J. Broadhurst, J. A. Gracey, and D. Kreimer. 'Beyond the triangle and uniqueness relations: Non-zeta counterterms at large N from positive knots'. In: *Zeitschrift fur Phys. C-Particles Fields* 75 (1997), pp. 559–574. doi: 10.1007/s002880050500 (cited on page 147).

# Acknowledgments

An dieser Stelle möchte ich mich bei all den Menschen bedanken, die meine Weg die letzten Jahre begleitet, geprägt und mit viel Freude gefüllt haben.

Zuallererst möchte ich meinem Betreuer PD Dr. Michael Scherer danken, der diese Arbeit nicht nur ermöglicht hat, sondern mir auch stets mit Rat und Tat bei allen Fragen zur Seite stand. Nur durch seine organisatorische Unterstützung waren die vielen Konferenzteilnahmen und ganz besonders der Forschungsaufenthalt in Paris überhaupt möglich. Doch ich möchte mich an dieser Stelle nicht nur für die professionelle Betreuung sondern auch für alles darüber hinaus, wie die gemeinsamen Cocktail-Abende und Renormierbar-Aktionen, bedanken, die uns zu mehr als einer Arbeitsgruppe geformt haben.

Dank gebührt auch Prof. Dr. Igor Herbut, PD Dr. Lukas Janssen, Shouryya Ray und Prof. Dr. John Gracey für die immer erhellende und äußerst fruchtbare Zusammenarbeit. Besonders möchte ich außerdem Dr. Luminita Mihail und Dr. Nikolai Zerf für ihre Mentorschaft zu dem Framework für die Loop-Rechnungen bedanken. Ohne ihren Rat wäre es nicht in dieser Zeit möglich gewesen. Für die freundliche Übernahme der Zweitbegutachtung möchte ich mich bei Prof. Dr. Simon Trebst bedanken. Außerdem möchte ich Mariela Boevska und Clara Berthet vom Institut für theoretische Physik und dem SFB1238, sowie Frau Gotzmann im Dekanat für die unkomplizierte Hilfe bei allen organisatorischen Dingen danken.

Für meinen dreimonatigen Forschungsaufenthalt in Paris bedanke ich mich ganz herzlich bei Prof. Dr. Slava Rychkov für die Gastfreundschaft in seiner Arbeitsgruppe. Besonders die beiden Post-Docs der Gruppe, Emilio Trevisani und Apratim Kaviraj, haben mir diese Zeit mit fachlichem Rat und freundschaftlicher Feierabendgestaltung versüßt.

Ganz besonderer Dank geht an meine Arbeits- und Bürokollegen, Nico, Björn, Oriana, Paula, Carl, Passant, David, Emilio und Fabian, die ich jetzt nach unserer gemeinsamen Zeit zu meinen besten Freunden zählen darf. Die gemeinsamen Grillparties auf dem Dach des Instituts bleiben unvergessen. Nico und Björn sei an dieser Stelle noch einmal für die zahlreichen hilfreichen Anmerkungen zu dieser Arbeit gedankt.

Mein größter Dank geht an Lara. Danke für Deine bedingungslose Liebe, unermüdliche Motivation und das Aushalten meiner Eigenheiten an den schlechten Tagen.

Dank geht an dieser Stelle auch an meine Eltern, die mir durch ihre unerschöpfliche Unterstützung diesen Weg bis zur Promotion überhaupt erst ermöglicht haben, und meinem Bruder, für die vielen unbeschwerten Stunden und Gespräche während meines gesamten Studiums.





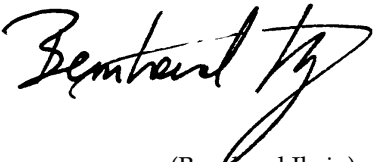
# Erklärung zur Dissertation

Hiermit versichere ich an Eides statt, dass ich die vorliegende Dissertation selbstständig und ohne die Benutzung anderer als der angegebenen Hilfsmittel und Literatur angefertigt habe. Alle Stellen, die wörtlich oder sinngemäß aus veröffentlichten und nicht veröffentlichten Werken dem Wortlaut oder dem Sinn nach entnommen wurden, sind als solche kenntlich gemacht. Ich versichere an Eides statt, dass diese Dissertation noch keiner anderen Fakultät oder Universität zur Prüfung vorgelegen hat; dass sie - abgesehen von unten angegebenen Teilpublikationen und eingebundenen Artikeln und Manuskripten - noch nicht veröffentlicht worden ist sowie, dass ich eine Veröffentlichung der Dissertation vor Abschluss der Promotion nicht ohne Genehmigung des Promotionsausschusses vornehmen werde. Die Bestimmungen dieser Ordnung sind mir bekannt. Darüber hinaus erkläre ich hiermit, dass ich die Ordnung zur Sicherung guter wissenschaftlicher Praxis und zum Umgang mit wissenschaftlichem Fehlverhalten der Universität zu Köln gelesen und sie bei der Durchführung der Dissertation zugrundeliegenden Arbeiten und der schriftlich verfassten Dissertation beachtet habe und verpflichte mich hiermit, die dort genannten Vorgaben bei allen wissenschaftlichen Tätigkeiten zu beachten und umzusetzen. Ich versichere, dass die eingereichte elektronische Fassung der eingereichten Druckfassung vollständig entspricht.

Teilpublikationen:

- ▶ Bernhard Ihrig, Luminita N. Mihaila, and Michael M. Scherer. 'Critical behavior of Dirac fermions from perturbative renormalization'. In: *Phys. Rev. B* 98 (2018). arXiv: 1806.04977
- ▶ Bernhard Ihrig, Lukas Janssen, Luminita N. Mihaila, and Michael M. Scherer. 'Deconfined criticality from the QED<sub>3</sub>-Gross-Neveu model at three loops'. In: *Phys. Rev. B* 98 (2018). arXiv: 1807.04958
- ▶ Bernhard Ihrig, Nikolai Zerf, Peter Marquard, Igor F. Herbut, and Michael M. Scherer. 'Abelian Higgs model at four loops, fixed-point collision, and deconfined criticality'. In: *Phys. Rev. B* 100 (2019). arXiv: 1907.08140
- ▶ Shouryya Ray, Bernhard Ihrig, Daniel Kruti, John A. Gracey, Michael M. Scherer, and Lukas Janssen. 'Fractionalized quantum criticality in spin-orbital liquids from field theory beyond the leading order'. In: *Phys. Rev. B* 103 (2021). arXiv: 2101.10335

Köln, den 28.01.2021



(Bernhard Ihrig)